

**THE EFFECT OF
MATERIAL AND PROCESS PARAMETERS
ON THE FRICTIONAL CONDITIONS
IN HOT FLAT ROLLING OF STEELS**

by

Per A. Munther

A thesis
presented to the University of Waterloo
in the fulfilment of the
thesis requirement for the degree of
Doctor of Philosophy
in
Mechanical Engineering

Waterloo, Ontario, Canada, 1997

© Per A. Munther, 1997



National Library
of Canada

Acquisitions and
Bibliographic Services

395 Wellington Street
Ottawa ON K1A 0N4
Canada

Bibliothèque nationale
du Canada

Acquisitions et
services bibliographiques

395, rue Wellington
Ottawa ON K1A 0N4
Canada

Your file Votre référence

Our file Notre référence

The author has granted a non-exclusive licence allowing the National Library of Canada to reproduce, loan, distribute or sell copies of this thesis in microform, paper or electronic formats.

The author retains ownership of the copyright in this thesis. Neither the thesis nor substantial extracts from it may be printed or otherwise reproduced without the author's permission.

L'auteur a accordé une licence non exclusive permettant à la Bibliothèque nationale du Canada de reproduire, prêter, distribuer ou vendre des copies de cette thèse sous la forme de microfiche/film, de reproduction sur papier ou sur format électronique.

L'auteur conserve la propriété du droit d'auteur qui protège cette thèse. Ni la thèse ni des extraits substantiels de celle-ci ne doivent être imprimés ou autrement reproduits sans son autorisation.

0-612-30633-X

The University of Waterloo requires the signatures of all persons using or photocopying this thesis. Please sign below, and give address and date.

Abstract

An extensive investigation on the frictional conditions in laboratory and industry is undertaken due to increased demands on accuracy in roll separating force predictions, as well as demands on understanding of roll wear.

In an attempt to clarify the role of process and material parameters, including the role of scale, on the frictional conditions in hot flat rolling, a large set of controlled laboratory investigations is undertaken. Two steels, one low-carbon and one Nb-treated micro-alloyed steel are investigated. The experimental findings from the laboratory are compared to findings obtained by an analysis of hot strip mill logbooks.

In calculating the coefficient of friction, the laboratory investigations are analysed in a unique manner, as a simultaneous match in measured and calculated roll separating force, roll torque, and forward slip is achieved. The effect of scale on the coefficient of friction is investigated after a scale growth kinetics study, which results in an equation relating scale thickness to time, temperature, and environment. The laboratory rolling experiments show that the coefficient of friction increases with decreasing rolling temperatures, decreasing roll velocities, decreasing scale thickness, and to a lesser degree, increasing reductions. Most of these cause increased material flow stress, increased adhesive bond strength and increased number of adhesive bonds.

Similarities are found in the analysis of the mill logbook data, in which the measured and calculated roll separating forces are matched. It is shown that the coefficient of friction increases with decreasing temperature, increasing amount of alloying elements, increasing relative velocity, as well as increasing material flow stress. Moreover, it is shown that the coefficient of friction is low in the first stands, increases stand by stand, and results in sticking friction in F7. The introduction of a dimensionless

parameter, λ , a function of the properties of the interface, the strip, and the work rolls, successfully describes the general frictional conditions throughout the finishing train. It is shown that the predominant wear mechanism in the first 4 stands is thermal fatigue, whereas abrasive wear is more severe in the last 3 stands of a 7 stand finishing train. A study on the non-steady-state condition of rolling with freshly ground rolls indicates that high-speed steel work rolls in stand F3 initially produce a low coefficient of friction. As a thin chromium oxide layer develops on the surface, the coefficient of friction increases, reaches a plateau, and then drops to a steady-state value after a total contact time of 200 s.

In comparing the findings from laboratory and industry it is shown that laboratory hot rolling experiments may be compared to data from industry by correcting for the most obvious difference in geometry - the roll radius. Furthermore, it is shown that, by the use of the λ - parameter, tribology of hot rolling can be considered in terms of regions of different modes of lubrication. These are boundary, mixed, and quasi-hydrodynamic lubrication. Previously, this theory has been limited to the tribology of cold rolling. It is shown that although the temperature has an effect, two parameters, the scale thickness and the relative velocity, appear to control the mode of lubrication.

Keywords: Steel, hot rolling, friction

Acknowledgements

I would like to express my sincere gratitude to the following people and organisations:

Dr. John G. Lenard, for suggestions, guidance, and encouragement throughout the course of this research.

Jernkontoret of Sweden for financial support.

Ron Webber and John Tiley of Dofasco Inc. for supplying mill logbook data as well as for helpful discussions.

Richard Gordon for his help in preparing samples and with the laboratory equipment.

Pia Segal Munther for help and support along the way.

In memory of Mauritz Munther

Table of Contents

	Page
Title Page	i
Author's Declaration	ii
Borrower's Page	iii
Abstract	iv
Acknowledgements	vi
Dedication	vii
Table of Contents	viii
List of Tables	xiii
List of Figures	xiv
Nomenclature	xvii
1. Introduction	1
1.1 Introduction to the Hot Strip Mill	2
1.1.1 The Equipment	2
1.1.2 The Process	5
1.2 Definition of the Problems	10
1.3 Possible Solutions to the Problems	11

2. Literature Review and Objectives	13
2.1 Mechanics of Hot Rolling	13
2.2 Mathematical Modeling of Hot Rolling	17
2.3 Roll Wear and Friction	19
2.3.1 Wear Modes in a Hot Strip Mill	19
2.3.2 Roll Damage and Wear in an Industrial Hot Strip Mill	19
2.3.3 Measurements of Friction in Rolling	20
2.3.4 Relationships between Friction and Wear	22
2.3.5 Relating the Coefficient of Friction to Roll Wear	23
2.3.6 The Effect of Process and Material Parameters on Friction	25
2.4 Metallurgy in Hot Rolling	27
2.4.1 Hardening Mechanisms	27
2.4.2 Kinetics of Oxidation / Composition of Scale	28
2.4.2.1 Growth Kinetics	29
2.4.2.2 Effect of Alloying Elements and Environment on Scale Growth	29
2.4.3 Methods of Evaluating Growth Kinetics	32
2.4.4 Mechanical Properties of Iron Oxides	32
2.5 Metallurgy of Roll Materials	34
2.5.1 High Speed Steel Work Rolls - A new Technology	34
2.5.2 Metallurgy of High Speed Steel Work Rolls	35
2.6 The Interface in Hot Rolling	40
2.6.1 Effect of Oxides on Friction and Wear	40
2.6.2 The Effect of Scale on Heat Transfer	43

2.6.3 The Effect of Scale on Surface Quality	45
2.7 Objectives	47
3. Organisation and Methodology	53
3.1 Methods to Calculate the Coefficient of Friction	55
3.2 Dimensional Analysis	57
3.3 Experimental Work	59
4. Equipment, Materials, and Procedure	63
4.1 Full Scale Finishing Train	63
4.1.1 Equipment and Conditions	63
4.1.2 Material Parameters	64
4.2 Laboratory	66
4.2.1 Stanat Rolling Mill and Barstaed/Thermolyne Furnace	66
4.2.2 Instron Testing Machine	67
4.2.3 Material	67
4.3 Experimental Matrices	69
4.3.1 Hot Oxidation Experiments	69
4.3.2 Hot Rolling Experiments	70
4.3.3 Hot Compression Tests	71

5. Material Behaviour	73
5.1 Hot Oxidation - Scale Formation	73
5.1.1 Predicting Scale Thickness	73
5.1.2 Results and Discussion	77
5.1.2.1. Kinetics of Hot Oxidation in Air	77
5.1.2.2 Effect of the Steels' Chemical Composition on Kinetics	82
5.1.2.3 Kinetics of Hot Oxidation in Nitrogen	82
5.1.2.4 Calculated Scale Thickness	85
5.2 Modelling Material Flow Stress	91
5.2.1 Empirical Formulas	91
5.2.2 Results and Discussion	93
5.3 Conclusions	99
6. Hot Rolling - Laboratory	100
6.1 The Effect of the Temperature on the Coefficient of Friction	105
6.2 The Effect of the Velocity on the Coefficient of Friction	111
6.3 The Effect of the Reduction on the Coefficient of Friction	117
6.4 The Effect of the Steel's Chemical Composition on the Coefficient of Friction	123
6.5 The Effect of the Scale Thickness on the Coefficient of Friction	130
6.6 Experimental Error	148
6.7 Conclusions	150

7. Hot Rolling - Industry	151
7.1 Break-in Time of Freshly Ground Rolls	153
7.2 The Coefficient of Friction in the Various Stand	155
7.3 The Effect of the Temperature on the Coefficient of Friction	158
7.4 The Effect of the Steels' Chemical Composition on the Coefficient of Friction	161
7.5 The Effect of the Velocity on the Coefficient of Friction	164
7.6 Introducing Dimensionless Groups	168
7.7 Experimental Error	177
7.8 Relating the Coefficient of Friction to Roll Wear	179
7.9 Conclusions	181
8. Tribology in Hot Rolling - A Comparison between Laboratory and Industry	182
8.1 Relating Results from Laboratory to Conditions in Industry	182
8.2 Interpreting Results from Laboratory and Industry	188
8.3 Conclusions	195
9. Summary	196
9.1 Summary and Conclusions	197
9.2 Recommendations for Future Work	203
References	206

List of Tables

Table	Page
2.1 Chemical composition of high-speed steels	36
2.2 Mechanical and physical properties of roll materials	38
4.1 Typical conditions in Dofasco's No. 2 hot strip mill	64
4.2 Steel chemical composition (industry)	65
4.3 Steel chemical composition (laboratory)	67
4.4 Experimental matrix for scale growth investigations	69
4.5 Laboratory hot rolling process parameter targets	71
4.6 Experimental matrix for hot compression tests	72
5.1 Calculated scale thickness	88
6.1 Typical Procedure of Determining the Coefficient of Friction	104
7.1 Average interface conditions including roll pressure and scale thickness	157
7.2 Average conditions for analysis of various grades in F3	161

List of Figures

Figure	Page
1.1 The layout of the mechanical equipment of a hot strip mill	2
1.2 Schematic illustration of a horizontal mill stand	12
2.1 Diagram showing material being rolled	16
2.2 Layers of oxides	28
3.1 Flow of information - connecting the various chapters	62
5.1 Scale index as a function of time	78
5.2 Scale index as a function of time	79
5.3 Scale index as a function of temperature	81
5.4 The effect of chemical composition on growth kinetics	83
5.5 The effect of oxygen-free nitrogen on growth kinetics	84
5.6 Calculated and measured scale index	86
5.7 Calculated scale thickness at various temperatures	87
5.8 Calculated scale thickness for various environments	90
5.9 Experimental flow stress for AISI 1018	94
5.10 Experimental flow stress for Nb-HSLA	96
5.11 Experimental and calculated flow stresses	97
5.12 Modelling flow stress according to Shida	98
6.1 Roll separating force as a function of temperature	106
6.2 Roll torque as a function of temperature	107
6.3 Forward slip as a function of temperature	108
6.4 The coefficient of friction a function of temperature	109
6.5 Roll separating force as a function of velocity	112
6.6 Roll torque as a function of velocity	113
6.7 Forward slip as a function of velocity	114
6.8 The coefficient of friction a function of velocity	115
6.9 Roll separating force as a function of reduction	118

Figure	Page
6.10 Roll torque as a function of reduction	119
6.11 Forward slip as a function of reduction	120
6.12 The coefficient of friction a function of reduction	121
6.13 Roll separating force as a function of velocity for two different steels	124
6.14 Roll torque as a function of velocity for two different steels	125
6.15 Forward slip as a function of velocity for two different steels	126
6.16 The coefficient of friction a function of velocity for two different steels	128
6.17 Roll separating force as a function of scale thickness	131
6.18 Roll torque as a function of scale thickness	132
6.19 Forward slip as a function of scale thickness	133
6.20 The coefficient of friction a function of scale thickness	134
6.21 Roll separating force as a function of temperature for various scale thickness	135
6.22 Roll torque as a function of temperature for various scale thickness	136
6.23 Forward slip as a function of temperature for various scale thickness	137
6.24 The coefficient of friction a function of temperature for Various scale thickness	138
6.25 Roll separating force as a function of scale index and roll roughness	139
6.26 Roll torque as a function of scale index and roll roughness	140
6.27 Forward slip as a function of scale index and roll roughness	141
6.28 The coefficient of friction a function of scale index and roll roughness	143
6.29 Scale layer after deformation	145
6.30 A comparison between calculated and predicted effect of scale on friction	147
6.31 Experimental errors	149
7.1 Break-in time of freshly ground HSS rolls	154
7.2 Frictional conditions in F1-F6	156
7.3 The effect of the temperature on the coefficient of friction	159
7.4 The effect of the steels' chemical composition on the frictional conditions	162
7.5 The effect of roll velocity on the coefficient of friction	165

Figure	Page
7.6 The effect of roll velocity on the coefficient of friction - A comparison of methods of solution	166
7.7 The effect of the arc of contact - mean thickness ratio on the coefficient of friction	169
7.8 The combined effect of various parameters on the coefficient of friction	171
7.9 The effect of the viscosity of the interface on the coefficient of friction	174
7.10 The coefficient of friction as a function of λ	175
7.11 Experimental error - Dofasco data	178
7.12 The roll wear in F1 - F6	180
8.1 The Pawelski curve	184
8.2 The effect of draft and flow stress on the coefficient of friction	185
8.3 The effect of $p/2k$ on the coefficient of friction	187
8.4 The Stribeck Curve	189
8.5 The coefficient of friction in industry and laboratory as a function of λ	190
8.6 The three lubrication modes in hot rolling	193

Nomenclature

A	: area
A_a	: apparent area
A_r	: real area
A_{r1}	: finishing transformation temperature from austenite to ferrite
A_{r3}	: starting transformation temperature from austenite to ferrite
C_{eq}	: carbon equivalency
C_p	: specific heat
dR	: decrease in roll radius due to abrasive wear
D	: work roll diameter
E	: Young's modulus
h_0	: entry thickness of strip
h_f	: exit thickness
h_m	: mean thickness of strip in roll gap
h	: coefficient of heat transfer
k	: shear flow strength
k_e	: exponential scale growth constant
k_p	: parabolic scale growth constant
k_w	: wear constant
K	: thermal conductivity
K_w	: modified wear constant
l	: rolled length
L	: projected arc of contact
L'	: projected arc of contact (corrected for roll flattening)
m	: friction factor
m_i	: mass of element i
M	: roll torque

M_i	: molecular weight of element i
n_i	: mole of element i
p	: average roll pressure
P	: roll separating force
Q	: activation energy of rate-controlling process in scale formation
r	: reduction as a decimal fraction
R	: work roll radius
R'	: flattened work roll radius
R_a	: surface roughness
R_{gas}	: universal gas constant
Red	: reduction
s	: sliding length
S_f	: forward slip
t	: time
t_1	: dimensionless temperature
t_c	: contact time
t_d	: dimensionless temperature reflecting a steel's chemical composition
T	: temperature
T_0	: strip entry temperature
T_C	: instantaneous contact temperature
T_f	: strip exit temperature
T_{nr}	: non-recrystallisation temperature
V	: volume
v	: roll velocity
v_f	: strip exit velocity
w	: width of strip
w_D	: power required for plastic deformation
x	: scale thickness
X	: dimensionless group, combining the effects of h , T , σ_{fm} , Δv

α	: angle of contact
α_{\min}	: minimum angle of contact
ϵ	: true strain
$\dot{\epsilon}$: strain rate
$\bar{\dot{\epsilon}}$: mean strain rate
$\bar{\dot{\epsilon}}_{sl}$: mean strain rate for sliding friction
$\bar{\dot{\epsilon}}_{st}$: mean strain rate for sticking friction
γ	: scale index
η	: viscosity
λ	: dimensionless group describing the interface between the rolls and the strip
μ	: coefficient of friction
ρ	: density
σ_{cs}	: compressive strength of roll material
σ_f	: stress function in Shida's equations
σ_{fs}	: flow stress
σ_{fm}	: mean flow stress
σ_x	: stress in x-direction
σ_{yss}	: yield strength of the scale layer
τ	: shear stress
ν	: Poisson's ratio
ξ	: roll material constant
Δh	: draft
Δm	: increase in weight
ΔT	: temperature drop
ΔT_K	: temperature drop due to conduction
ΔT_D	: adiabatic temperature rise
Δv	: relative velocity

Chapter 1

Introduction to Hot Flat Rolling of Steel

Flat rolled steel products are important in modern society. Steel strips and plates are widely used in areas ranging from automotive to household goods, tools, and construction. Over the last 30 years, extensive advancements in the fields of material science and control systems have led to the introduction of new steel grades as well as improvements in productivity, mechanical properties, gauge accuracy, and surface quality. Steel today is still a very cheap and competitive alternative to other materials such as aluminium and polymers.

Today most flat rolled products are produced from continuous-cast slabs. Only a few ingot based flat rolling mills remain, whose life span is limited due to the increased demands in productivity and savings in power consumption. The recent introduction of the latest generation mills, i.e. mini mills and especially thin strip casters, will make these redundant as well. They have already started to infringe on the markets previously monopolised by all traditional steel companies.

The slabs are reduced in thickness first by hot rolling and then, in cases where tolerances and mechanical properties are crucial, by cold rolling. Today's advancements have reduced the proportion cold rolled, as better properties may be achieved in the hot rolling stage.

1.1 Introduction to the Hot Strip Mill

1.1.1 The Equipment

Before hot rolling, the slabs are reheated to approximately 1250°C in a reheating furnace. This is done in order to remove the as-cast dendrite structure and to dissolve most of the alloying elements, as well as to ensure uniform temperatures before rolling into strips. The most common furnace type today is the walking beam furnace, in which moveable beams raise the slab and transport it onward from the entry side to the exit side. These furnaces may utilise oil, natural gas, or gas by-products from the blast furnace. Their dimensions are typically 10 -12 m wide and 30 - 65 m long. The placement of the reheating furnace and the layout of a modern hot strip mill can be seen in Figure 1.1. below.

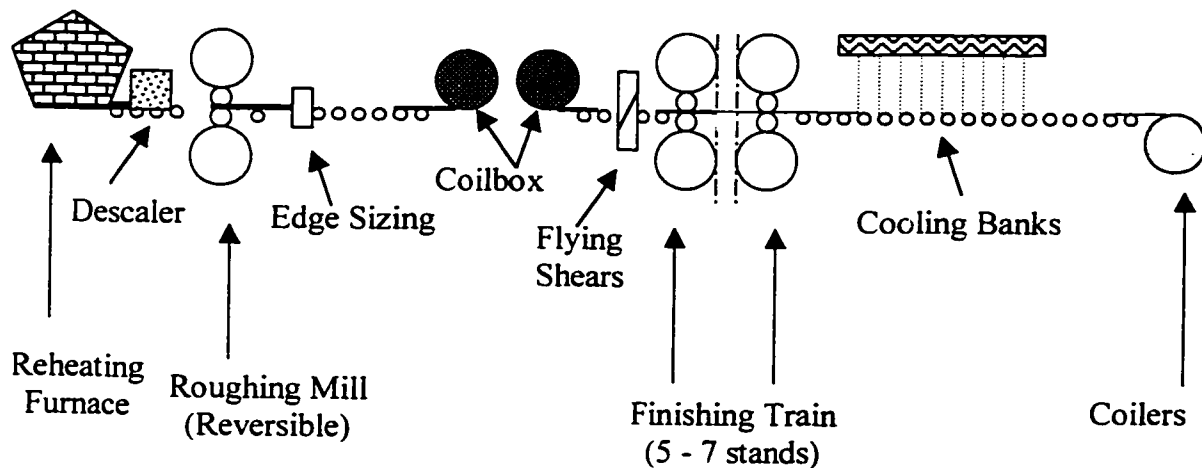


Figure 1.1. The Layout of the Mechanical Equipment of a Hot Strip Mill

With the help of descalers, primary oxides that have formed upon reheating are removed prior to rough rolling. These descalers are typically high-pressure water jets. It is crucial that all scale is removed, since it causes a poor surface quality of the final product. If the descaling is not done properly at this stage, the final product will be scrapped. Since scale forms immediately on the surface of the hot steel, this process is repeated prior to entry into the finishing train as well.

The slabs are initially reduced in thickness from about 220 - 250 mm to 30 - 50 mm in the roughing mill. This is done throughout 5 passes. The length increases at the same time from 10 to 40 m. Roughing mills can be duo or quarto type mills, i.e. with or without backup rolls. Duo types are less expensive due to their simplicity, but do not offer the same gauge consistency as quarto type mills. One or several stands may be used. Today most mills strive to use one powerful reversible stand of the quarto type.

Since only a limited number of widths are cast, the desired width of the bar is obtained by sizing the edges. This is done by either rolling or forging. The advantage of edge rolling is the relatively low investment cost of the equipment. The disadvantage is that the low penetration of deformation causes the sides to be thicker than the centre. This results in an increased fishtail effect that ultimately leads to more waste. Although edge-forging equipment is more expensive, the losses due to fishtailing are drastically reduced. In this case, tools may be used to control the deformation geometry.

After rougher rolling and edge sizing, the bar enters the transfer table. Some mills have installed a coilbox in between the roughing mill and the finishing train. The bar is coiled up in the coilbox, allowing the tail end of the transfer bar to become the head end in the finishing train. There are several advantages with the coilbox: (1) The productivity of the mill is increased. (2) The temperature drop is not as severe in the finishing train, removing the need to accelerate the bar. (3) Better and thinner gauge accuracy may be

achieved as a result of the even temperature. (4) The marks from the walking beam furnace may be reduced.

Before entering the finishing train, the uneven head-end and the fishtail of the transfer bar are cut off by a flying shear. A pyrometer takes a surface temperature reading, which is used by the control algorithm of the finishing train to predict roll separating forces, roll gap settings, etc.

In the finishing train, the thickness of the bar is successively reduced from 30 - 50 mm down to about 1 - 2 mm in 5 - 7 stands, usually 5 meters apart. Most finishing trains today handle widths of more than 2000 mm. Loopers between the stands help control the speed and provide a tension of 5 - 15 MPa. The most common configuration in the finishing train is the quarto type mill, which also is known as four-high (see Figure 1.2). However, some Japanese mills utilise a six-high configuration. A control algorithm provides the initial roll gap settings, which are adjusted as a gauge meter positioned immediately after the finishing train sends a feedback signal to the automatic gauge control. A pyrometer located at the exit provides another surface temperature measurement, which is used to accelerate the speed throughout some mills (zooming). This is also important information for controlled rolling.

As the strip exits the finishing train, it enters a run out table, where it is cooled by a laminar water curtain. A final temperature reading is taken at the end of the run out table. A feedback signal is used to control the cooling rates. This is another important step as much of the microstructure may be controlled by this and the final step, coiling.

Two to three coilers are placed at the end of the mill. Different steel grades are coiled at different temperatures. A low coiling temperature results in the precipitation of fine carbides, whereas a higher coiling temperature produces coarser carbides.

1.1.2 The Process

Today's high demands have made the steel companies to spend great efforts to ensure that high quality in terms of gauge and mechanical properties is met. The gauge is controlled by the mechanical equipment described above. The metallurgy of the process defines the mechanical properties that are obtained. Controlling the deformation schedule in the finishing train, the cooling on the run out table, and coiling temperature as a whole is often referred to as thermal-mechanical treatment. The objective is to control the grain size and the volume fraction of second phase particles in such a way that desired mechanical properties are obtained and may be reproduced with minimal deviation.

In obtaining the final mechanical properties of the product, many important metallurgical events are encountered. These can all be controlled by selecting appropriate processing parameters such as slab reheating temperatures, rough and finishing rolling temperatures, rolling speed, amount of deformation, cooling rates, and coiling temperatures.

Two phenomena balance the selection of slab reheating temperature, as well as the selection of many other parameters in the hot strip mill. The first phenomenon is related to the austenite grain size. High slab reheating temperatures produce an increase in austenite grain growth, resulting in a coarse austenite grain size, which upon phase transformation gives a coarse ferrite grain size of the final product. It is desirable to obtain as fine austenite grain size as possible, since the ferrite grain size determines the mechanical properties of the product. This phenomenon is called grain refinement and determines the upper limit of the reheating temperature. A second phenomenon determines the lower range of the slab reheating temperature. As the slabs are cooled after casting, various carbides and nitrides precipitate. These precipitates are coarse and

provide little increase in strength. Optimum strength is obtained when these precipitates are fine and evenly distributed. This is done by first dissolving all precipitates upon reheating and then letting the precipitation proceed once again during controlled conditions.

The rougher rolling stage is generally carried out in the conventional hot rolling regime, i.e. above the high non-recrystallisation and the upper transformation temperature, T_{nr} and A_{r3} , respectively. This, along with the relatively low speeds and the build-up of a dislocation density that the heavy reductions provide, allows the austenite grains to recrystallise dynamically in each pass. The grains thereby become smaller as the transfer bar is repeatedly reduced in thickness. However, this is not the most effective way to achieve a fine and uniform grain size.

Depending on the temperature, reduction, and rolling speed, the steel may either recrystallise dynamically, statically, or metadynamically in the finishing train. This can happen fully, partly, or not at all. For process conditions when this does not happen the steel may either dynamically or statically recover or in some cases even cause strain hardening upon deformation. Today most finishing rolling is carried out in the austenitic one-phase region. However, some mills finish the rolling schedule in the intercritical austenite-ferrite two-phase region, in which case the transfer bar enters at a temperature higher than A_{r3} and exits at a temperature in between the upper and lower austenite to ferrite phase transformation temperatures.

The most significant reduction in grain size is obtained in the finishing rolling stage, and results in a pancaked microstructure, meaning the grains become elongated in the rolling direction. Moreover, as the deformation progresses, deformation bands are produced in the pancaked unrecrystallised austenite grains. This resulting substructure plays an important role since the ferrite grains will nucleate not only in the austenite grain

boundaries, but also along these deformation bands, thereby enabling a finer ferrite structure. When the rolling schedule is carried out above A_{r3} , but below T_{nr} , small uniform equiaxed ferrite grains are formed as the steel is cooled. When the rolling schedule is finished in the austenite-ferrite two-phase region, existing ferrite grains develop subgrains, whereas existing austenite is transformed upon cooling on the run out table. This leaves a mixed structure consisting of equiaxed grains and subgrains.

Alloying with certain elements strongly affects both the non-recrystallisation temperature and the continuous cooling transformation diagram. High-strength low-alloy (HSLA) steels gain strength by effective retardation of the recrystallisation, which is caused by suppression of grain boundary migration. This may be achieved by alloying with elements such as Nb, which increases the material strength both by grain refinement and precipitation hardening. Other common alloying elements such as Ti and V have a modest effect on grain refinement, but later increase the steel's strength by precipitation hardening.

By controlling the cooling on the run out table according to the continuous cooling transformation diagram, the total volume fraction of ferrite is determined. Depending on the steel's chemical composition, accelerated cooling permits transformation of the remaining austenite to pearlite, bainite, or martensite.

The final stage in the hot strip mill, coiling, determines the amount and distribution of second phase particles and thereby the amount precipitation strengthening. A high coiling temperature results in coarse second phase particles, whereas a low coiling temperature gives an evenly distributed dispersion of second phase particles. The coiling temperature affects mechanical properties such as elongation and tensile strength. A higher coiling temperature causes a drop in both elongation and tensile strength.

Controlling the rolling temperature, reduction, speed, and cooling rates in combination achieves the goal of the desired mechanical properties. However, the path to these properties is, in practise, dictated by the limitations in the equipment of a hot strip mill. Lack of available power may not allow for heavy reductions or low rolling temperatures. The same goes for insufficient cooling capabilities at the run out table.

The accuracy of the mill control algorithm used in controlled rolling, which calculates the roll separating forces and thereafter sets the reduction so that desired gauge may be obtained, is highly dependent on the process and the feedback information it provides. In addition to the metallurgical events described above, also the interface between the work rolls and the rolled material affect the magnitude of the roll separating forces. The boundary conditions are here described by heat transfer and friction. The process parameters, i.e. different contact times, temperatures, and pressures, affect both the heat transfer and the frictional conditions. Factors, such as the work roll material, also affect it, as the physical properties may vary. Moreover, as Section 1.1.1 indicated, a thin scale layer is more or less always separating the rolls and the transfer bar. The behaviour of this layer is also important since it affects not only the frictional conditions, but also the surface quality of the final product.

Friction is always present in metal forming. In hot rolling, friction results in increased roll-separating forces and excessive roll wear. Both factors are associated with an increase in the cost of production. An increase in friction can be caused by material strength or an increasing amount or strengthening of adhesive bonds between the rolls and the rolled material as well as by abrasion if one hard surface or particle scratches the softer surface. A hard particle may even scratch both surfaces at the same time.

Process parameters such as velocity, temperature, and reduction all affect the frictional conditions as they dictate the properties of the adhesive bonds and the interface.

Materials parameters such as chemical composition and metallurgical history also affect the interface and the bonding between the two metals.

The interface may consist of oxides on either one of the metals, worn off particles, lubricants, water from roll cooling and scale breaking operations, etc. Primary oxides are formed when the steel is reheated at elevated temperatures. Secondary, ternary, and tertiary oxides are formed randomly on the steel surface in the mill when the primary (secondary, etc) oxide is removed. The roles these oxides play have not been investigated in sufficient detail so far.

Surprisingly little work has been devoted to these specific problems, since the hot strip mill research over the last five decades in majority has concentrated on the mechanical properties of the product. However, the fact that all steel companies today strive to produce better surface quality as well as improvements in gauge accuracy along with the recent introduction of new work roll materials has called for clarification of the effects on the process and materials parameters on the events in the interface.

1.2 Definition of the Problems

In the competition for high quality and low price between competing materials and companies, further advancements on productivity, mechanical properties, gauge accuracy, and surface issues of hot rolled products have been called for. As a result, a number of questions have arisen over the last few years:

1. *What are the effects of the process and materials parameters on the frictional conditions in hot rolling?*

In order to achieve optimum gauge consistency, accurate predictions on roll separating forces is vital. Friction in hot rolling affects the roll separating forces as well as the costly wear of the work rolls. Little is known about the individual effects of various process parameters on the frictional conditions. The same goes for information on the effect of the steel's chemical composition.

2. *What is the effect of scale on the frictional conditions?*

The presence of scale on the surface of the bar affects not only the surface quality of the finished product, but also the interface between the rolls and the bar. Anything that affects this interface causes changes in the frictional conditions.

3. *What is the performance of HSS work rolls?*

Wear of work rolls make up about 10% of total rolling cost today. This has recently led to the introduction of high-speed steelwork roll materials. Some signals from industry have indicated that the use of these rolls affects the roll separating force, i.e. in terms of friction. Another question is their behaviour as they are broken in.

1.3 Possible Solutions to the Problems

The question of the effects of process and material parameters on the frictional conditions is easiest handled by controlled laboratory experiments in which one parameter at a time is varied. The coefficient of friction is then back calculated from experimentally measured roll separating forces, roll torques, etc. The material parameter of interest is the steel's chemical composition. The relevant process parameters are, in this case, sample temperature, reduction, and roll velocity.

Scale thickness effects the frictional conditions and may be seen as either a process or a material parameter. After all, it is a function of the steel's chemical composition, immediate environment, temperature, and oxidation time. In order to enable modelling of the scale thickness, the kinetics of scale formation must first be known. The kinetics may be determined from separate laboratory hot oxidation experiments in which the effects of temperature, time, chemical composition, and environment are investigated separately.

Although laboratory investigations will clarify the effects of the various parameters, the work would be incomplete without studying the genuine conditions of a full-scale hot strip mill. Since higher velocities are seen for the full-scale conditions, laboratory and industrial investigations complement each other. Together, they also help to unravel the true effects of process and materials parameters on the frictional conditions in hot rolling, as they overlap and corroborate each other in some cases.

Break-in behaviour of freshly ground rolls is an interesting non steady-state phenomenon that might further enhance the understanding of the frictional conditions in hot rolling. Since the interface changes for every bar that is being rolled, the build-up of an oxide layer on the roll surface is well suited to be studied in terms of the coefficient of friction.

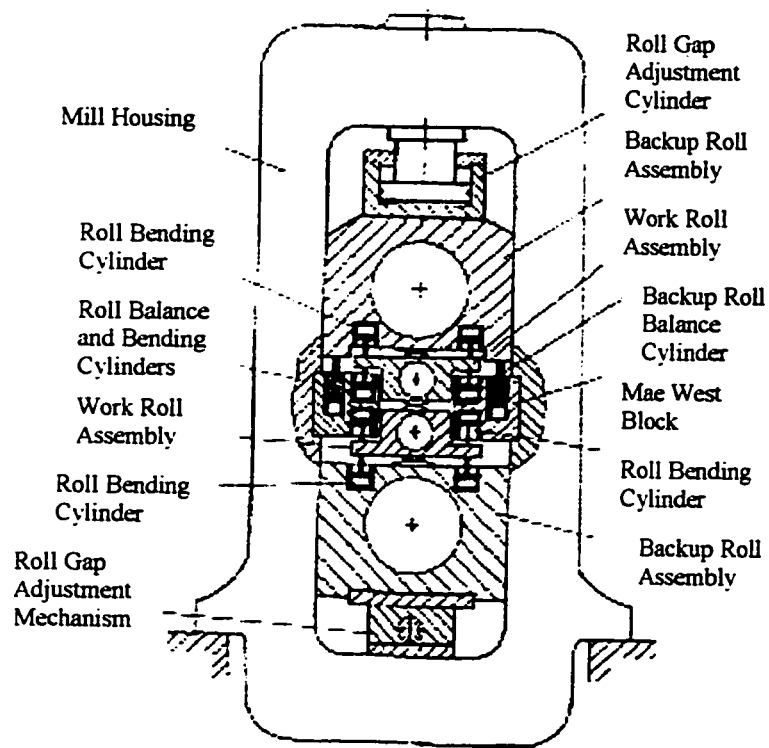


Figure 1.2. Schematic Illustration of a Horizontal Mill Stand (Ginzburg, 1989)

Chapter 2

Literature Review and Objectives

In what follows, the technical literature is reviewed in terms of modelling of the hot rolling process, friction and wear, and metallurgy, including the kinetics of oxidation. This is followed by a statement of objectives of research.

2.1 Mechanics of Hot Rolling

Figure 2.1 depicts a workpiece being rolled between two rolls. It also defines the geometry of rolling as the material is reduced in thickness from the initial height, h_0 , to the final, h_f . R is the roll radius, and R' is the larger, deformed or flattened roll radius, which can be described by Hitchcock's formula. P is the normal force acting on the rolls. Other common basic definitions include:

$$\text{Reduction:} \quad \text{Red} = \frac{h_0 - h_f}{h_0} 100 (\%) \quad (2.1)$$

$$\text{Forward slip:} \quad \frac{v_f - v}{v_f} 100 (\%) \quad (2.2)$$

$$\text{Contact length:} \quad L = \sqrt{R\Delta h} \quad (2.3)$$

Roll pressure:
$$p = \frac{P}{wL} \quad (2.4)$$

Draft:
$$\Delta h = h_0 - h_f \quad (2.5)$$

Deformed roll radius:
$$R' = R \left(1 + \frac{16(1-\nu^2)P}{\pi E \Delta h} \right) \quad (2.6)$$

Mean strain rate:
$$\dot{\epsilon}_{sl} = \frac{v}{h_0} \sqrt{\frac{h_0 - h_f}{R}} \quad \text{for sliding friction} \quad (2.7)$$

$$\dot{\epsilon}_{st} = \frac{v}{\sqrt{R(h_0 - h_f)}} \ln \frac{h_0}{h_f} \quad \text{for sticking friction} \quad (2.8)$$

where w is the strip width, E is Young's modulus and ν is Poisson's ratio for the roll material. R' is used to correct the contact length as R is substituted by R' . L then becomes L' and v is the roll velocity.

Assuming that planes remain planes and the plane strain conditions exist, the geometry of flat rolling allows for the definition of an equation based on the equilibrium of forces:

$$(\sigma_x + d\sigma_x)(h + dh) - \sigma_x h \pm 2\tau R' \cos \alpha d\alpha + 2pR' \sin \alpha d\alpha = 0 \quad (2.9)$$

where α is the angular coordinate or angle of contact, p is the roll pressure, σ_x is the stress in the x -direction, h is the current thickness of the strip, and τ is the shear stress between the roll and the strip, defined as $\tau = \mu p$. The algebraic sign refers to regions on either side of the neutral plane. Simplification leads to:

$$\frac{d(\sigma h)}{d\alpha} = 2R'(p \sin \alpha \pm \tau \cos \alpha) \quad (2.10)$$

which, along with the Huber-Mises criterion of plastic flow, flow stress description, and further assumptions regarding the boundary conditions, leads to the classical one-dimensional solutions.

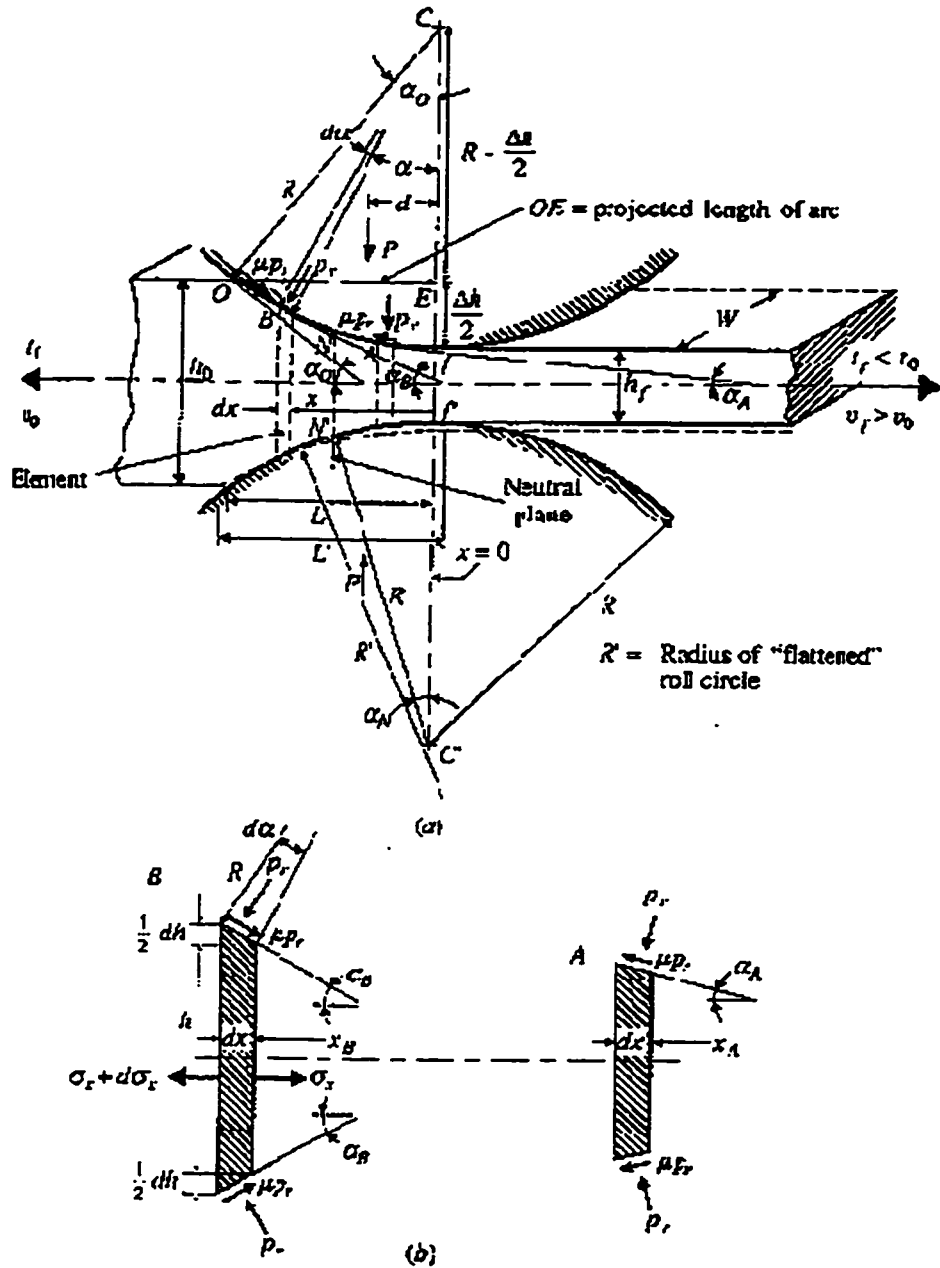


Figure 2.1. (a) Diagram showing material being rolled, including some definitions and nomenclature. Tension, in either forward, t_f , or backward, t_0 , direction may or may not be applied. If applied, the neutral plane will be shifted in opposite direction of the applied tension. Note that the frictional stress, μp , changes direction at the neutral plane. (b) Freebody slices taken on either side of the neutral plane. These are used in the classical slab method (Mielnik, 1991).

2.2 Mathematical Modelling of Hot Rolling

Bland and Ford (1948) derived a formula for the calculation of the required roll force for conditions of sliding friction, based on the hypothesis of the friction hill. The roll force for sticking friction can be calculated with a formula derived by Sims (1954). However, as el Kalay and Sparling (1968) pointed out, actual conditions can be expected to be found in between these two extremes.

Wusatowski (1969), Tselikov *et al.* (1981), and Pietrzyk and Lenard (1991) have reviewed the flat rolling models of Ekelund, Geleji, Bakhtinov, Shternov, Get, Golovin, Samarin, Tselikov, Orovan, Siebel, Cook-McCrum, Sims, Alexander, Jortner, Schey, and Bland-Ford. These models have all been derived from the equation of equilibrium under certain assumptions about geometry, friction, and material behaviour, making them applicable for rough estimation of the required rolling forces. However, they are not accurate enough to deal with sensitive computations such as inverse calculations of the coefficient of friction using experimentally measured rolling forces and if used, would result in inaccurate data. After all, they all have their foundation in either the classical slab method or in simplified slip-line field solutions.

A finite element approach, allowing the matching of the roll torque, the forward slip, and the roll separating forces, would reduce these inaccuracies. Finite-element techniques have been used successfully to model rolling since the mid 1980's. There are currently several commercial packages available on the market. Some, like Abaqus, are general finite-element codes that may be applied to flat or shape rolling. Others, like Elroll, are specifically written for flat rolling.

Elroll is based on the rigid-plastic finite-element approach and allows for coupled analyses of plastic deformation and heat transfer. The rigid-plastic approach means that the deformation is always referred to the current configuration. The unknown is the

velocity field and the analysis is achieved by means of many small steady-state deformation steps. The advantage with special codes, like Elroll, is their proven performance and the relatively fast computing times. The disadvantage, on the other hand, is a limited degree of freedom when it comes to geometry, mesh size, and overall complexity.

2.3 Roll Wear and Friction

2.3.1 Wear Modes in a Hot Strip Mill

The wear modes in metalforming can be divided into abrasion, thermal and mechanical fatigue, adhesion, and corrosion. Schey (1983) considered two types of roll wear: uniform wear caused by abrasion in combination with thermal fatigue and localised wear caused by accumulation of secondary scale on the roll surface. Material pick-up, as in localised wear, is caused by adhesion of contacting surfaces (Rabinowicz, 1965). Williams and Boxall (1965) studied roll defects in a full-scale mill where they identified the most severe mechanisms as those of thermal fatigue and abrasion of hard oxides. More recently, Collins (1994) and Caillaud and Delaitre (1994) have proposed that the major wear mechanisms in the finishing train of a seven-stand mill would be thermal fatigue in the first 4 stands (F1-F4), and abrasive wear in the last 3 stands (F5-F7). This was attributed to the differences in relative velocities at the various stands.

2.3.2 Roll Damage and Wear in an Industrial Hot Strip Mill

The damage that work rolls are likely to experience are, as stated previously, thermal fatigue in the first stands and abrasive wear in the middle and higher stands of the finishing train. The wear and damage resistance of a roll material is dictated by its mechanical and physical properties.

A phenomenon associated with thermal fatigue is fire-cracking resulting in fine cracks on the roll surface. This is caused by cyclic heating and cooling where upon contact the hot strip heats up the rolls, which experience circumferential compression as their expansion is limited by the adjoining cold metal. A crack may nucleate when the

material's compressive yield strength is exceeded, which is easily done when subjected to combined thermal and mechanical loads. Cooling may have the same effect, since the material is subjected to tensile stresses upon its recovery to its original dimensions, especially when the back-up rolls produce further stresses on the surface when in contact (Innse Cilindri, 1995). When the material's tensile yield strength is exceeded, a crack will also nucleate due to this mechanism. Due to the repeated thermal cycle in every revolution, the rolls may experience a more severe damage, known as banding. This is when the previously nucleated fire-cracks grow into a network causing a reduced abrasive wear resistance of the surface. When oxides form inside the network of fire-cracks a failure known as spalling may result from the notch-effect the oxides have on the fire-cracks. Both physical and thermal properties are therefore of great importance at the early stands.

The mechanical properties are of great importance in the later stands where abrasive wear is predominant. The mechanical properties are defined by the roll material's microstructure. In fact, carbide hardness, their homogeneous distribution, and matrix capacity to hold these carbides determine the abrasive wear resistance.

The overall wear resistance may be improved further by the formation of hard, adhesive, and continuous chromium oxide layers, which form an interface between the rolls and the strip. These layers take up some of the friction stresses, but they also insulate the rolls thereby reducing the overall risk of spalling of the surface (Innse Cilindri, 1995).

2.3.3 Measurements of Friction in Rolling

The coefficient of friction in hot rolling can be measured using several

experimental methods. These were reviewed by Schey (1983), Ginzburg (1989), and Underwood (1950). The techniques include:

- (1) Normal and inclined force transducers and pins inserted into the work roll: the measured forces give the roll pressure and the interfacial shear stress in the deformation zone. Their ratio, the coefficient of friction, has been shown to vary over the contact surface.
- (2) Method of forced skidding: the workpiece is prevented from entering the roll gap by an increase in back tension.
- (3) Method of limiting gauge: the reduction is increased gradually until the rolls start skidding and no bite is possible.
- (4) Friction from forward slip: geometry provides relationships between the coefficient of friction and the forward slip.
- (5) Friction from roll force: the coefficient of friction is back calculated from roll force formulae. This method can also be applied to roll torque.

All methods listed involve certain difficulties (Underwood, 1950; Sparling, 1977). The problem with the first is that the workpiece material can extrude into the clearance in between the pins and their holes, potentially resulting in inaccurate measurements. An additional difficulty is caused by the different stiffness of the pin-transducer combination and the roll material. Methods (2) and (3) are not comparable to steady-state rolling conditions, since the rolling process is altered to extremes. Methods (4) and (5) take for granted that mathematical models, derived under several restrictive assumptions, predict the correct values. However, methods (4) and (5) have recently been successfully

combined in analyses utilising a finite-element technique (Munther and Lenard, 1995a and 1995b).

2.3.4 Relationships between Friction and Wear

Wear in hot rolling is hard to measure and monitor on the spot, since the various mechanisms result in different effects: abrasive wear results in removal of material, thermal and mechanical fatigue in cracks, adhesion in material pick-up or removal, and corrosion in oxidation. All but the two types of fatigue result in changes in the coefficient of friction as surface conditions are altered. This makes the coefficient of friction suitable for detection of changes in wear conditions. Forward slip is a measurement of the slippage in the roll gap, defined as the relative increase in speed the strip experiences upon exiting the roll gap. A high forward slip is believed to indicate a high coefficient of friction and a high wear rate (Ekelund, 1927).

Friction in hot rolling can be classified into sliding friction and sticking friction (Schey, 1983). Sliding friction is an indication of low friction and occurs as a result of sliding of the workpiece surface relative to the roll surface. Sticking friction can occur either partially over a zone near the neutral plane, which is the case for an intermediate friction, or, as for a high friction, over the whole roll gap. Roberts (1977) proposed an equation that relates the coefficient of friction to roll wear. In his work only the contribution of abrasive wear is taken into account, since the volume removed from the roll surface defines the roll wear in his equation. The equation would thus be applicable to the last stands where abrasive wear prevails.

Ekelund (1927) proposed a relationship between forward slip and the coefficient of friction by assuming that the rolls were cylindrical and that the roll pressure was

constant in the roll gap:

$$\mu = \left(\frac{\alpha}{2}\right)^2 \left[\frac{\alpha}{2} - \sqrt{\frac{2S_f}{\left(\frac{2R}{h_f} - 1\right)}} \right] \quad (2.11)$$

where α is the angle of contact and S_f is the forward slip.

Jarl (1988) compared a numerical solution of von Karman's equation to Ekelund's equation, thereby relating forward slip to the coefficient of friction. von Karman's equation is dependent on the model of friction, the geometry of rolling, the deformation of the rolls, the elastic entrance and exit regions, as well as the flow stress. Jarl concluded that it is unreliable to evaluate the coefficient of friction from measurements of forward slip in hot rolling by the application of a simple equation like Ekelund's.

2.3.5 Relating the Coefficient of Friction to Roll Wear

As stated previously, Caillaud and Delaitre (1994) found that abrasive wear is of considerable significance for stand F4 and beyond. It is therefore of interest to model the abrasive wear and its dependency on the coefficient of friction. Abrasive wear effectively removes material from the rolls. Following Archard (1953), this volume, V , can fundamentally be defined per unit width as:

$$V = \frac{k_w \mu P s}{3\sigma_{cs}} \quad (2.12)$$

where k_w is a wear constant depending on the hard asperity angle (Kato, 1997) and roll material, μ is the coefficient of friction, P is the total roll separating force in N/mm, s is the sliding length in mm, and σ_{cs} is the compressive strength of the roll material in N/mm². The sliding length, or the slippage, was defined by Roberts (1977) as:

$$s = \frac{lLr}{4\pi D} \quad (2.13)$$

where L is the arc of contact in mm, l is the rolled length in mm, D is the work roll diameter in mm, and r is the reduction as decimal fraction. The removed volume can also be described in terms of unit width as:

$$V = \pi D dR \quad (2.14)$$

where D is the roll diameter in mm and dR is the decrease in roll radius caused by the abrasive wear in mm. Equations (2.12), (2.13), and (2.14) may now be combined to give:

$$\frac{dR}{l} = \frac{K_w \mu L r P}{D^2 \sigma_{cs}} \quad (2.15)$$

where K_w is a modified wear constant, defined as: $K = k / 12\pi^2$.

Equation (2.15) may be used to determine the wear constant from industrial measurements.

2.3.6 The Effect of Process and Material Parameters on Friction

Hot rolling is generally carried out in the austenitic region with a few exceptions for rolling in the intercritical two-phase region and rolling in the ferritic region. The latter is a new commercial technique described in (Sander, 1995). The strength of the workpiece material and its scale has an effect on the frictional conditions. Hot strength depends directly on the process parameters, reduction, strain rate, and temperature. Altering the process parameters results in a change in microstructure and thus, in hot strength. A change in material parameters, such as the chemical composition, affects both the material's hot strength and its oxidation characteristics.

The immediate subsurface of the workpiece experiences an extreme drop in temperature due to heat transferred to the rolls, resulting in a local increase in strength. v. Kortzfleisch *et al.* (1967) estimated that the surface temperature drops to 600° from 1125°C in industrial flat rolling. This trend has been corroborated by several researchers. Pietrzyk and Lenard (1990), and Chen *et al.* (1992) carried out both experimental laboratory work and finite element simulations. However, these researchers reported results that indicate that the temperature drop is lower and highly dependent on experimental conditions, as well as process and material parameters.

Inhomogeneous deformation would also result in a variation in hot strength over the cross section of the workpiece. Variations in chemical composition make certain strengthening mechanisms more or less active, the result being that certain steel grades have higher hot strength than others.

The effect of the workpiece hot strength has seldom been related to friction and wear behaviour in the mill. Ekelund (1927) pointed out that workpiece composition seemed to have an effect on friction conditions.

Wallquist (1955, 1950, and 1962) published an impressive amount of data on roll force, power consumption, and forward slip at various temperatures for 16 steel grades ranging from mild carbon to stainless steel. He investigated the differences that material parameters, such as the chemical composition, can have on the forward slip and torque arm and examined how these differed from grade to grade. While not considering the frictional conditions explicitly, the published values of the forward slip may be seen as indicative of the frictional conditions. He found that the parameter that had the strongest effect after the reduction was that of the temperature. The reported forward slip typically increased from 4 to 10% as the reduction was increased from 10 to 50%.

Wusatowski (1969) quoted experimental findings by Pavlov and Kuprin, who investigated the frictional behaviour of several steels. These varied in chemistry from low carbon to stainless steels. Rolling speeds ranging from 0.5 to 4.0 m/s and temperatures from 735 to 1212°C were studied. It was reported that the coefficient of friction decreased, from a high of 0.49 to a low of 0.17, with increasing rolling speed and increasing temperatures. However, when the temperature was considered, the coefficient of friction reached a plateau, where the highest numbers were found. This point appears, in some cases, to coincide with A_{r3} for the chosen steels, and it is not evident from the information given how the data was treated nor is the plateau phenomenon itself explained. There is, furthermore, no evident relationship between the various steel's chemical compositions and their corresponding coefficients of friction. Nor is it stated whether rolling actually was carried out in the intercritical austenite-ferrite two-phase region.

2.4 Metallurgy in Hot Rolling

2.4.1 Hardening Mechanisms

Rabinowicz (1965) made it clear that material parameters such as elastic and plastic strength play a significant role in friction behaviour. A material's plastic strength in the case of hot rolling primarily means its flow stress. The workpiece material's flow stress can increase during processing due to various strengthening mechanisms (Tamura *et al.*, 1988). The strengthening mechanisms that are of interest in hot rolling of various low carbon and micro-alloyed grades are those of:

- Grain refinement
- Solid solution strengthening
- Increase in dislocation density / strain hardening
- Precipitation hardening

The largest single contribution is the effect of grain refinement, which is a result of a number of recrystallisation cycles. The other acting mechanisms, in decreasing order of contribution (Majta *et al.*, 1996), are those of solid solution strengthening, increase in dislocation density, and precipitation hardening. Solid solution strengthening is caused by interstitially or substitutionally dissolved atoms that hinder the movement of dislocations. An increase in dislocation density can be a result of either partial or full retardation of recrystallisation. Precipitation strengthening can be achieved by alloying elements that form carbides, nitrides, or carbonitrides, which in turn hinder the movement of dislocations. These mechanisms are all very sensitive to changes in the process parameters.

2.4.2 Kinetics of Oxidation / Composition of Scale

Three types of iron oxide phases may make up the scale on the steel surface. These are, with increasing oxygen content:

Wüstite, FeO

Magnetite, Fe_3O_4

Haematite, Fe_2O_3

In some cases a scale with all three types of oxide phases is present on the steel surface with wüstite being closest to the steel matrix followed by the intermediate magnetite layer and the outermost haematite layer (Figure 2.2).

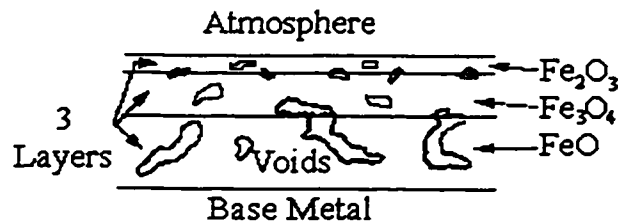


Figure 2.2. Layers of Oxides (after Roberts, 1983)

Unlike laboratory conditions, the surface temperature of a descaled strip in industrial hot rolling differs from the internal strip temperature depending on contact with cooling work rolls, roll cooling water (temperature and flow rate) and lubricants, descaling spray cooling, as well as ambient temperature. The strip surface temperature in a laboratory is only affected by the cooling of the work rolls and ambient temperature. These events on the surface all affect the scale growth. Low strip temperatures or lower surface temperatures caused by chilling of the work rolls, roll cooling water, or descaling spray cooling retard the scale growth, whereas higher temperatures accelerate the scale growth.

2.4.2.1 Growth Kinetics

In order for an oxide to grow, it must overcome kinetic barriers. These energy barriers are consequences of not only temperature and pressure, but also of the environment, available space, and the steel's chemical composition. As oxidation starts, the oxide layer is discontinuous and begins by lateral extension of discrete nuclei. The mass transportation of ions occurs in a direction normal to the surface when the nuclei are interwoven. The iron diffuses as cations and electrons through the oxide film. At the gas-oxide interface on the surface, oxygen is reduced to oxygen ions. The zone of the oxide formation is at the gas-oxide interface.

The diffusion of oxygen in oxides is slower than that of iron in oxides (Samsonov, 1973; Sørensen, 1981). Scale growth on steels therefore requires Fe ions from the matrix to diffuse outward through the scale layers. Since there is an abundance of oxygen at the surface, the diffusivity of iron in the oxides determines the growth rate. This means that the temperature and the time control the distance the iron atoms can travel; high temperature in combination with long time will allow the iron atoms to travel far (i.e. the concentration gradient, dc/dx decreases with time). This will aid the growth of the oxide layer, since more iron atoms are made available to react with oxygen and to form oxides. Scale growth is commonly seen as parabolic with regard to time and exponential with regard to temperature (Roberts, 1983).

2.4.2.2 Effect of Alloying and Environment on Scale Growth

Unlike stainless steels, carbon and micro alloyed steels both oxidise heavily at elevated temperatures. There might be some differences in kinetics, provided the differences in the amounts of some elements are great enough. The general effects of the various elements on the scale growth are given below:

Carbon: This element forms carbon monoxide, resulting from a reaction with FeO at the metal/oxide interface at high temperature. The carbon monoxide is a reducing gas, thereby lowering the oxide growth rates for steels with high carbon contents. Ginzburg (1989) points out that the gas may expand in gaps between oxide and metal. This may eventually lead to cracks in the oxide layer. In such a case, the oxidation rates are increased locally. It is believed that the formation of pores in the scale is a result of the decarburisation of the steel surface and a receding iron/wüstite interface (Shaesby *et al.*, 1984). This makes the scale more porous and metal loss, due to re-heating in a furnace, is therefore expected to be less for high carbon steels than for low carbon steels.

Silicon: This element diffuses from the matrix to the metal/oxide interface, where it precipitates as SiO₂. A reaction with FeO results in the formation of fayalite, Fe₂SiO₄. This oxide layer acts as an effective barrier for diffusing Fe ions. However, it melts at 1171-1205°C, above which the protecting effect disappears (E. Schurmann *et al.*, 1973; G.C Wood, 1971; Kiessling and Lange, 1964). The formation of fayalite creates a problem with descaling in Si-added steels (Fukagawa *et al.*, 1994). The eutectic phase has been found to have a hardness that exceeds wüstite's just 60°C below its solidification temperature. The hard fayalite acts as an anchor between the wüstite and the steel, making the descaling incomplete, which may cause surface defects on the strip.

Manganese: According to Sachs and Tuck (1968), the manganese content does not play a significant role in retarding or aiding scale growth.

Chromium: The high chromium amounts in stainless steels provide oxidation resistance. However, the small trace amounts of chromium in carbon and micro alloyed steels do not provide any significant retardation of the scale growth. The relatively high chromium amount in work rolls (2-10%) retards the oxidation of the steel. Further, the addition of chromium aids the formation of an adherent ductile black oxide, Cr₂O₃ that protects the

rolls from abrasive wear (Werquin and Bocquet, 1994). Murata *et al.* (1984) investigated the effect of different interfaces on heat transfer and concluded that a chromium-oxide layer on the roll surface protects it by insulating it from heat transfer and reducing the effects of thermal fatigue.

Environment: An environment in an industrial or laboratory furnace can be either oxidising or reducing. This is linked to the standard free energy of formation for the various phases. If the partial pressure of oxygen or the ratio between carbon dioxide and carbon monoxide is altered not only will the composition of the scale be different, but also its thickness. As a matter of fact, a carbon dioxide to carbon monoxide ratio of 0.2 will be sufficient to establish a reducing environment at 1200°C. Oxidising gases are oxygen, water vapour, and carbon dioxide. Reducing gases are carbon monoxide and hydrogen. Other gases such as nitrogen or inert gases such as argon slow the growth rate, but have little effect on the composition of the scale.

Shaesby *et al.* (1984) investigated the kinetics and morphology of scale growth on steels at 1200°C in oxygen-nitrogen, oxygen-water vapour-nitrogen, and water vapour-nitrogen gas mixtures. It was found that the addition of water to the oxidising gas increased the scale growth on carbon steels. The parabolic rate of oxidation began after ten minutes in air and at the start of oxidation with pure oxygen. It was concluded that the lower rate of oxidation in steels, observed with oxidising gases without water, was due to scale separation. It was also determined that the pores were interconnected near the interfaces and became larger as they migrated away from the interface, forming isolated pores in the scale. It was furthermore said that oxygen is transferred through these pores via the gas phase (Sachs and Tuck, 1968). Shaesby *et al.* (1984) reported FeO : Fe₃O₄ : Fe₂O₃ ratios of 95 : 4 : 1. This is consistent with information reported by Mrowec and Przybylski and quoted by Birks and Meier (1983), who attributed this fact to the greater mobility of defects in wüstite.

Matsuno (1980) studied blistering and hydraulic removal of relatively thin scale films on AISI 1008 steel. Samples were heated in vacuum and were allowed to oxidise for times of no longer than 3 minutes. Comments were made regarding the adhesion of the scale to the steel substrate, but also on the composition of scale and the growth kinetics thereof. It was reported that the scale consisted of wüstite to the greatest extent followed by magnetite and haematite. It was also said that the growth kinetics followed the parabolic rate law with regards to time.

2.4.3 Methods of Evaluating Growth Kinetics

According to Birks and Meier (1983), the growth kinetics can be evaluated by either continuous or discontinuous methods. A continuous method involves uninterrupted monitoring of the sample, but requires sophisticated equipment. There are two types of continuous methods: those that monitor gas consumption and those that monitor mass gain. A discontinuous method involves either mass gain, in which case the mass of oxygen taken in the scale is measured, or mass loss if the oxide layer is stripped from the sample. Another discontinuous method is to measure the scale thickness. However, this may result in inaccuracies if it is carried out at room temperature, since the scale layer is likely to crack and spall upon cooling. The disadvantage with the discontinuous methods is that many specimens are needed along with the fact that the progress cannot be observed between the data points.

2.4.4 Mechanical Properties of Iron Oxides

When oxides are present in hot metal working operations, the stresses in them are generally so high that the deformation of the scale is dominated by dislocation glide.

According to the Huber-Mises criterion, plastic deformation requires dislocation glide on five active and independent slip systems (Robertson and Manning, 1988). Because of the ionic bonding in the oxides, this is only likely to happen at temperatures above $0.5T_m$. This also means that the oxide may behave in a visco-plastic manner and deform with the bulk.

The most important attributes of the scale, at least when metalworking is considered, are its hardness and yield strength, since these indicate whether the oxides are abrasive when in contact with the work rolls. Luong and Heijkoop (1981) have reported room temperature hardness values of 460 H_v for FeO, 540 H_v for Fe_3O_4 , and 1050 H_v for Fe_2O_3 . Funke *et al.* (1978) analysed data obtained by Hirano and Ura (1970) and Stevens *et al.* (1971) and concluded that the hardness of the oxides is temperature dependent. They found the hardness of magnetite exceeding the hardness of cementite (which was the only carbide present in the roll material investigated) at all temperatures. Lundberg and Gustavsson (1994) have reported hardness values at 900°C for FeO, Fe_3O_4 , and Fe_2O_3 . These were 105, 366, and 516 H_v .

2.5 Metallurgy of Roll Materials

2.5.1 High Speed Steel Work Rolls - A new Technology

The increase in demand for better surface quality along with the increase of geometrical accuracy over recent years has made development of work rolls and lubricants a necessity. Another contributing factor is the high cost of roll wear, which has been reported (Lundberg and Gustafsson, 1994) to be in the order of 10% of total rolling cost. The most recent trend in the steel industry is marked by the newly introduced high-speed steel (HSS) work rolls, which are characterised by high hardness and resistance to abrasion. According to Roberts and Cary (1980) HSS grades are, generally, tool steels, classes 610-660. Previously, these grades have primarily been used for cutting tools. However, the roll manufacturers modify both chemical composition and heat treatment in order to satisfy their customers' needs.

According to Kurahashi *et al.* (1992) and Hashimoto *et al.* (1994) HSS rolls offer a wear resistance 3-5 times greater than the currently used high chrome and indefinite chilled rolls. This is corroborated by Arnaud (1996), who reported wear rates for HSS rolls ranging between 2-4 times less than those of Hi-Cr (high chromium iron) rolls in the first stands. At the higher stands, where ICDP rolls (indefinite chilled iron) are used, the wear rates dropped by a factor of 5. Arnaud (1996) pointed out that although the coefficient of friction increased, the wear rates were dramatically reduced. Barzan (1996) reported that one of the problems with the HSS rolls is their poor toughness resulting in cracking and spalling in the middle and higher stands and causing the Hi-Cr and ICDP rolls to be more cost effective than HSS rolls. Webber (1996) has corroborated this to a certain extent, but emphasised that detection of micro cracks is crucial. Webber (1996) reports that the wear resistance has increased threefold on average. He also points out that the incidence of surface breakdown decreased by 10% since the introduction of the HSS

rolls.

Zum Gahr (1987) reviewed the importance of hardness in rolling contact fatigue. The review concluded that high hardness is important for ensuring a high resistance to crack initiation by fatigue and that crack propagation is affected by properties such as ductility and fracture toughness. Due to their microstructure and higher hardness, HSS rolls are more resistant to thermal fatigue than the high chrome and indefinite chilled rolls.

Common HSS work roll defects in Dofasco's No.2 hot strip mill have been classified into pressure and thermal cracks by Hill and Kerr (1996). The pressure cracks include: longitudinal localised stress cracks due to mechanical overloading, longitudinal and circumferential combination slip/stress cracks due to overheating caused by mechanical slippage, and irregular longitudinal and circumferential localised impact cracks caused by the steel, on the roll, by tail end whipping in the later finishing stands. The thermal defects were divided into thermal cracks and roll spalls. Circumferential thermal cracks are originating on longitudinal stress cracks where they are propagated circumferentially by local overheating of the roll. Longitudinal thermal cracks are referred to as bar firecracks and are caused by cobbles or other mill stops that induce a local overheating of the roll surface. Severe unrepaired pressure cracks may cause the rolls to spall. In this case, irregular sizes and shapes of the surface material spalls off the roll surface.

2.5.2 Metallurgy of High Speed Steel Work Rolls

Hot rolling work rolls usually consist of a tough core and a high alloy shell. Work rolls can be manufactured by casting, forging, powder metallurgy, or by the Osprey

process (Hashimoto *et al.*, 1994; Kudo *et al.*, 1992; Hashimoto *et al.*, 1992, Price *et al.*, 1996). The different manufacturing techniques yield different final mechanical and metallurgical properties of the roll. The most common technique of manufacturing the shell is casting (Hashimoto *et al.*, 1992). The core can be produced by either casting or forging (Sano *et al.*, 1992). HSS rolls differ mainly from high chrome and indefinite chilled rolls in that they are steel and not white cast iron rolls. HSS rolls have a microstructure of the outer shell that consists of hard primary carbides embedded in a tempered martensitic matrix (Kurahashi *et al.*, 1992; Hashimoto *et al.*, 1994; Hashimoto *et al.*, 1992; Sano *et al.*, 1992). The primary carbides are mainly of the MC type (Collins, 1994; Kurahashi *et al.*, 1992; Hashimoto *et al.*, 1994; Hashimoto *et al.*, 1992; Sano *et al.*, 1992) with a hardness of 2500 HV (Kurahashi *et al.*, 1991). Typical carbides of conventional indefinite chilled and high chrome rolls are Fe₃C (1000 HV) and M₇C₃ (1400 HV), respectively. The microstructure of the HSS rolls is made possible by alloying additions of C, Cr, Mo, W, V, and in some cases Co. Getting specific information on chemical composition from roll manufacturers is extremely difficult, due to the competitive nature of the industry. However, some experimental data are available (Collins, 1994; Caillaud and Delaitre, 1994; Werquin and Bocquet, 1994; Goto *et al.*, 1994; Kurahashi *et al.*, 1992; Hashimoto *et al.*, 1994; Hashimoto *et al.*, 1992; Sano *et al.*, 1992) and can be seen in Table 2.1.

Element (wt.%)								
	C	Mn	Si	Cr	V	W	Mo	Co
Min	0.8	0.2	0.3	2.0	2.0	2.0	2.0	0.0
Max	3.5	0.3	0.5	10.0	15.0	10.0	10.0	12.0

Table 2.1. Chemical composition of high-speed steels (Roberts and Cary, 1980; Collins, 1994; Caillaud and Delaitre, 1994; Werquin and Bocquet, 1994; Goto *et al.*, 1994; Kurahashi *et al.*, 1992; Hashimoto *et al.*, 1996; Hashimoto *et al.*, 1994; Hashimoto *et al.*, 1992; Sano *et al.*, 1992)

Carbon hardens the matrix and forms carbides. Vanadium forms the desirable carbides of MC type. Molybdenum and tungsten are used for solid solution strengthening of the matrix. The addition of chromium aids the formation of an adherent ductile black oxide, Cr₂O₃ (Werquin and Bocquet, 1994), which protects the rolls from abrasive wear. Cobalt is not a strong carbide former, but tends to reduce the stability of Fe₃C (Roberts and Cary, 1980) and retain the hardness of the roll at elevated temperatures (Hashimoto *et al.*, 1994).

Undesirable eutectic carbides of the type M₆C (Mo and W), M₇C₃ (Cr), and M₃C (Fe), are formed (Collins, 1994; Kudo *et al.*, 1992, Hashimoto *et al.*, 1992) if the carbon content is too high (>2.5%). These carbides form at the austenite grain boundaries and are undesirable because of their networked morphology that is poor for thermal fatigue.

A martensitic matrix is achieved by a thermal treatment where austenite is produced by induction heating of the roll surface followed by quenching to subzero temperatures. This process is repeated a few times, as a great amount of retained austenite would otherwise be present. The diffusionless process of martensite formation results in a highly stressed, brittle, and dimensionally unstable material, an effect of the martensite having a larger volume than the austenite. The inner stresses and the brittleness are removed by tempering.

Tempering of HSS at 500°C for 2.5 hours results in the resolution of undesirable carbides, such as M₂C, and transformation of any retained austenite on cooling (Roberts and Cary, 1980). This gives the matrix the preferred properties: high hardness and certain ductility, as well as the preferred carbides of MC type.

Troeder *et al.* (1985) investigated temperature and thermal stresses during hot rolling. These investigations lead to the conclusion that the roll surface experiences cyclic peaks from 80 to 400°C in every revolution. These temperature peaks make it possible for

the rolls to build up the protective oxide layer. However, a certain break-in period is required for a freshly ground pair of rolls.

Since the fall of 1994, Dofasco has expanded the use of HSS rolls from F3 to F1, F2 and F4. Mill trials in F5 have indicated dramatically reduced wear rates. Today, only HSS and ICDP rolls are in use. The mechanical and physical properties of the three different roll materials can be seen in Table 2.2.

Property		Hi-Cr	HSS	ICDP
Tensile Strength (N/mm ²)		800	900	450
Bending Strength (N/mm ²)		1200	2500	700
Compressive Strength (N/mm ²)		2400	2800	2300
Young's Modulus (kN/mm ²)		230	230	170
Specific Heat @500°C (J/gK)		0.50	0.60	0.47
Heat Conductivity @500°C (W/mK)		14	27.2	18
Coefficient Of Expansion (1/°C)		13x10 ⁻⁶	13x10 ⁻⁶	11x10 ⁻⁶
Primary Carbide	Type	M ₇ C ₃	MC	M ₃ C
	Hardness (Hv)	1400	2500	1000

Table 2.2. Mechanical and Physical Properties of Roll Materials (Innse Cilindri, 1995; Kurahashi *et al.*, 1991)

The reason why the HSS rolls are so effective in the first few stands is due not only to the mechanical properties, but also to the physical, as pointed out previously. Since thermal fatigue is the major cause of wear in these stands, doubling the heat conductivity dramatically reduces the wear caused by this mechanism. In the higher stands where traditionally ICDP rolls are used, the abrasive wear can be reduced due to the better mechanical properties of the HSS rolls. However, caution must be observed at

the highest stands, since the HSS material cannot withstand severe impacts to the same extent as ICDP can, due to its graphite-flake microstructure. HSS rolls have more than twice the bending strength than that of Hi-Cr rolls and more than three times that of ICDP rolls. The compressive strength is also one of the important properties when it comes to abrasive wear resistance. This property is significantly higher for the HSS rolls, as well.

2.6 The Interface in Hot Rolling

2.6.1 Effect of Oxides on Friction and Wear

El-Kalay and Sparling (1968) were the first to investigate the effect of scale on conditions in hot rolling of low carbon steel. Different conditions were studied in a laboratory: light, medium, and heavy scaling with both smooth and rough rolls at various velocities. Load and torque functions, according to Sims' equations, were calculated. They pointed out that the effect of scale comes, in order of importance, after the effects of degree of inhomogeneity during deformation and strain hardening. It was assumed that the scale acts as a poor lubricant and that its effect varies along the arc of contact as it fractures. It was found that the presence of scale could reduce the roll loads by as much as 25%. A thick scale reduced the loads more than a thin scale since the thick scale breaks up into islands that transmit the load from the rolls to the strip. The islands become separated as the strip is elongated. Hot metal then extrudes between the islands and sticks to the rolls while the sliding islands move further apart and promote tensions applied to the sticking portion, thereby reducing the load. It was also found that thin scale promotes sliding friction with smooth rolls, but sticking friction with rough rolls. The load functions increased with temperature in rolling with rough rolls, but decreased with the temperature for smooth rolls.

Roberts (1977, 1983) studied the data obtained by el-Kalay and Sparling (1968). This was used to empirically model the coefficient of friction in terms of scale thickness, roll roughness, and temperature. The model predicts an increase in the coefficient of friction because of an increase in roll surface roughness, decrease in scale thickness or, increased temperature:

$$\mu = 36 \exp\left(\frac{-4810}{T + 459}\right) + 0.063 \ln\left(\frac{\text{roll roughness}}{\text{scale thickness}}\right) \quad (2.16)$$

where the temperature is given in °F. Roberts does not explain the surprising effect of the temperature. After all, a higher temperature yields a lower flow-stress, which in turn has the greatest effect on the frictional conditions. Neither does he explain in detail how the original data were analysed and manipulated: El-Kalay and Sparling's data on its own does not indicate this trend. However, he pointed out that although the scale provides a degree of lubricity it is not desirable to roll a scaled strip as that would result in an unacceptable surface quality.

Luong and Heijkoop (1981) studied the effect of scale on friction in hot forging, using the ring test technique. They were the first to investigate the frictional conditions in terms of the scale composition. Altering furnace atmosphere and heating times varied the scale composition and thickness in the investigations on carbon steel. The furnace atmosphere consisted of CO₂, O₂, or air and the heating times ranged from 8 to 240 minutes. Longer heating times resulted in greater amounts of wüstite. It was found that the friction factor and hence the coefficient of friction decreased with increasing scale thickness. The effect of the composition of the scale could not be related to the overall frictional conditions.

Li and Sellars (1996) found that sticking friction takes place in hot forging of scaled low carbon steel, but a certain degree of forward slipping, indicating partly or completely sliding friction, occurs in rolling of the same material. They found a limited number of cracks on specimens with thin scale. A scale layer can follow a similar reduction and elongation as the steel only if its hot strength is equal to or lower than that of the hot steel. No numbers on the coefficient of friction were reported.

Schunke *et al.* (1988) presented a hypothesis on the effect of oxygen partial pressure on friction coefficients at room temperature, as well as additional information for temperatures below 600°C for various Fe alloys. In analysing data obtained by other researchers, it was found that the coefficient of friction during sliding was dependent on the partial pressure of oxygen as well as the sliding length. Generally, the coefficient of friction decreased with increased oxygen pressure and temperature as these caused an oxide layer to grow more rapidly on the surface. The drop in friction was explained as follows: the oxide particles are fragmented upon deformation and become further oxidised and compacted onto the metal surfaces where they form islands on the next cycle. This causes the total contact area to be reduced. When these islands grow in area a large portion of the shearing will be in the islands. Friction is then lowered because of the brittle nature of the oxide particles that are being sheared.

Shaw *et al.* (1995) determined fracture energies of oxide-metal and oxide-silicide interfaces. It was concluded that the fracture energy depends primarily on interfacial bond strength although roughness of the interface, microstructure of the compounds, and porosity also have some effect.

Ball *et al.* (1993) investigated the role of oxides in hot rolling of aluminium, where material pickup on the roll may result in serious surface defects. Quoting various references, they described the differences in fracture behaviour of thin and thick scales. In thin layers (<100 nm), cracks emerge at slip steps, whereas in thick layers these are replaced by regularly spaced fractures, perpendicular to the applied tensile stresses. It was noted that a tensile strain larger than 2% was needed to fracture thick layers.

Lundberg and Gustavsson (1994) carried out an abrasive wear study at temperatures between 800 and 1000°C, in which the interface conditions in rolling of long products were met. A disc-on-disc technique, described in (Lundberg and Waldén, 1992; Lundberg, 1993), was used in which the disc simulating the rolled material was

heated with a propane burner, giving an environment similar to a reheating furnace. They found that the surface temperature of their simulated tool was lowest for the highest sample temperature. This was attributed to the insulating effect of the scale, the thickness, of which was highest at the highest temperature. It was found that the abrasive wear rate was dependent on the hardness of the abrading oxide particles. The abrasive wear rate reached a maximum at 900°C, above which scale grows more rapidly at the same time as the hardness of the oxides drops. A thermal model showed that the roll temperature indeed was highest at 900°C, causing a drop in roll hardness. The investigations led to the suggestion that temperatures in the range 850-950°C should be avoided if abrasive roll wear is a major concern.

Savage *et al.* (1996) recreated the experiments of Lundberg and Gustavsson (1994) and found similar results in hot wear testing of indefinite chill iron, high chrome iron, and high-speed steel roll alloys. An induction coil was used to heat the simulated work piece. Both friction and wear peaked between 900 and 950°C for all roll materials or steel type. The cause was attributed to a hypothesis that the scale shears internally at temperatures above 950°C. According to their hypothesis the scale remains intact at temperatures below 950°C, thereby causing an increase in wear with temperature up to this temperature.

2.6.2 The Effect of Scale on Heat Transfer

Wüstite has a thermal conductivity of 3.2 W/mK, magnetite 1.5 W/mK, and haematite 1.2 W/mK compared to austenite's 30.5 W/mK at 1000°C (Torres and Colas, 1994a, 1994b). Due to the lower thermal conductivity of the oxide phases compared to steel, they insulate the rolled stock from the chilling effect of the cold work rolls to a certain degree.

Murata *et al.* (1984) found that the heat transfer coefficient in compression of hot steel ranged between 25-30 kW/m²K for oxide free surfaces, and between 7-10 kW/m²K when a 0.01 mm thick oxide covered one surface. The temperature of the hot compression sample was 780°C, whereas the temperature of the tool was 22-30°C.

Chen *et al.* (1993) reported numbers on the heat transfer coefficient that varied between 25 and 50 kW/m²K. The coefficient of heat transfer was back calculated from laboratory hot rolling experiments in which thermocouples were used. These were used both inside and on the surface of low carbon and micro-alloyed steel samples. The samples were soaked in an atmosphere of nitrogen. However, the scale thickness produced was not indicated. It was concluded that temperature, velocity, steel chemical composition, and reduction all affect the coefficient of heat transfer. It was also pointed out that roll pressure was the most significant and that the effect of the other parameters could be related to their influence on the roll pressure.

Li and Sellars (1996) compared heat transfer in hot forging, where sticking friction prevails, and hot rolling, where sliding friction prevails. The integrity of the scale did not change in their forging experiments leading to a low heat transfer coefficient due to the low thermal conductivity of the oxides compared to that of steel's. The values of the heat transfer coefficient were reportedly dependent on the scale thickness. In rolling, the break-up of the scale led to an increase in the heat transfer coefficient caused by the increase in contact with the chilling rolls. The heat transfer coefficient was shown to increase with decreasing scale thickness and increasing reduction, which in turn increases the pressure.

Torres and Colas (1994a, 1994b) developed a heat conduction model capable of predicting the temperature distribution within the scale during rolling. In their model, break-up of the scale was not accounted for. It was determined that a single node model with the properties of wüstite gave satisfactory results on the insulating effects of thin

scale layers.

Lundberg and Gustafsson (1994) derived a model by means of successive stationary solutions of the heat conduction equation, enabling calculation of the thermal stress for various oxide situations. The model was used in the analysis of results obtained in a hot wear test apparatus.

2.6.3 The Effect of Scale on Surface Quality

Blazevic has published a number of articles on the role of scale on surface issues. Earlier work (1983a, 1983b, 1985) covers scaling on steels during re-heating, roughing, finishing, and coiling. A great amount of information on the occurrence of surface defects caused by scale and their location on the strip surface, including their causes and remedies, has also been collected. Ginzburg (1989) has compiled a great deal of this information. A more recent paper (Blazevic, 1996) discusses the role of the tertiary scale. According to Blazevic, the scale layer that enters the finishing train can be considered either thin and hot or thick and cold.

In the first case of thin hot scale, the scale fractures along fine lines as it is being compressed and elongated during deformation in the first stand. Hot metal is then extruded partially up into the fine lines as the deformation proceeds. At the same time, the hot metal deforms in a perpendicular direction (i.e. in the rolling direction). The result is a simultaneous roughening and smoothening of the steel surface.

In the second case of cold thick scale, the scale is less plastic and therefore fractures severely upon elongation. The fractured scale becomes depressed into the steel surface, while hot metal extrudes outwards. This causes a very rough surface creating

problems even after the steel has been pickled. The reason is that the metal that extruded upwards in the early stands will be over-pickled and thereby leaves a mirror image of the prior roughness. This image remains although the cold rolling process creates an elongated and reduced mirror image on the final product.

The presence of a red scale on finished products is another serious surface defect that has been addressed by Fukagawa *et al.* (1994). This defect results in two things. First is an aesthetic defect as stripes of red and black scales are found in the rolling direction. Secondly, it affects the roughness and shape of the strip since the scale is pushed into the surface of the steel. Fukagawa and co-worker's emphasis was on Si-added steels. However, the red oxide scale is a potential problem on other steels as well, especially when the steel is not descaled properly. Consider a scale layer consisting of the three phases (Figure 2.2), where the majority is wüstite: the area of wüstite particles exposed to the air increases considerably as the scale is fractured by hot rolling. Fewer iron atoms are available to these particles, which become completely separated from the wüstite matrix, where there is a ready supply of oxygen. This results in the accelerated reaction of $\text{FeO} \rightarrow \text{Fe}_3\text{O}_4 \rightarrow \text{Fe}_2\text{O}_3$. The colour of the final product is the red haematite.

With these things in mind, it is obvious that scale formation has a great effect on the quality of the rolled surfaces and thereby the commercial value of the product. Modelling of scale formation at the somewhat arbitrary surface temperatures seen in the finishing train along with proper descaling operations is therefore crucial in order to obtain optimum surface quality. The previous works show that it is also important to understand the basic phenomenon of scale formation when modelling friction in hot rolling.

2.7 Objectives

Much progress has been made in hot rolling during the last decades. The main focus has been on the control of mechanical properties and increased accuracy in gauge, as well as overall, productivity. Little interest has been shown in the topic of tribology in hot rolling. It is of great industrial importance to clarify the frictional conditions in hot flat rolling. When improvements in surface quality and productivity are concerned, striving for further understanding of the frictional phenomena is unavoidable.

The literature review made it clear that the available information of the effects of process and material parameters on the conditions at the interface is inconclusive, outdated or filled with contradictions and inconsistencies. For instance, the equation proposed by Roberts predicts that the coefficient of friction increases with increasing temperature, despite the fact that the material hot strength drops as the temperature increases. In this equation, only temperature and scaling affect the coefficient of friction. Wallquist presented information on forward slip, roll separating force, roll torque, power consumption, and spread. He did not use his experimental data to calculate the coefficient of friction, since he was mainly preoccupied with power consumption and geometry. The same goes for el-Kalay and Sparling. Their work resulted in the derivation of new roll force and torque formulas, which did not include the coefficient of friction itself. Although Ekelund and others have derived relationships between forward slip and the coefficient of friction, these are of little practical use as they result in unrealistic predictions. The same may be said about the use of traditional roll force formulas, which often result in values in coefficients of friction that exceed what is physically possible.

There is little information available on the effects of the process parameters, much of which dates back 30-50 years. This information was often produced using methods that have limited accuracy. In industry, inaccurate roll forces may be predicted, since the coefficient of friction is not an input in the General Electric control algorithm, which is

based on Sims' equation and is used in most hot strip mills. Since numbers are missing, it is common to assume that the coefficient of friction is 0.4. Most researchers who have investigated the effect of oxides on the frictional conditions have done so for processes other than hot rolling in attempts to simulate the hot rolling process. Others have investigated metals other than steel. Blazevic investigated the behaviour of the scale layer in terms of surface defects, but not the contributions of the coefficient of friction. No researcher has tried to reproduce the scale thickness in a laboratory that is seen in industrial hot rolling. The ones that indeed have worked on the effects of scale on friction have not modelled the kinetics of scale formation in terms of scale thickness in order to control their experiments and reproduce the actual mill conditions.

The questions that have to be answered are therefore:

- 1. What are the effects of process parameters such as temperature, velocity, and reduction on the frictional conditions in laboratory and industry?*
- 2. What are the effects of material parameters such as steel chemical composition and scale thickness on the frictional conditions?*
- 3. What is the break in time of freshly ground high-speed steel work rolls?*
- 4. Can relationships be found between laboratory and industry results?*

Consequently, the distinct objectives are to:

- 1. Investigate the kinetics of scale formation*

Scale thicknesses corresponding to those in the finishing train are to be reproduced in the laboratory in order to enable physical modelling of a relevant roll/workpiece interface. This is important, since the variation in scale thickness may have a dramatic effect on the frictional conditions. After all, el-Kalay and Sparling's investigations (1968) indicated that there was an effect on roll

separating force and roll torque. Roberts' analysis of their data (1977, 1983) clearly indicated that there is an effect on the coefficient of friction. The question is whether and how it can be related to the process and material parameters.

The effect of scale thickness in hot rolling may be investigated first when the thickness itself is known and may be controlled. Systematic hot oxidation experiments reveal the effects of temperature, time, chemical composition, and furnace environment.

2. Perform and analyse controlled laboratory hot rolling experiments

Systematic investigations are to elucidate the contradictory effects a parameter like temperature has according to the different sources in the literature. The investigated parameters are temperature, roll velocity, reduction, chemical composition, and scale thickness. One parameter is altered at a time and its effect on the coefficient of friction is monitored.

The most accurate analytical technique is chosen since relatively small differences in roll separating force may result in a large difference in the coefficient of friction. A commercial finite-element code, Elroll, is used to obtain a simultaneous match between measured and calculated roll separating force, roll torque, and forward slip. This effectively combines the three techniques of determining the coefficient of friction into one. Nevertheless, the errors in the calculations are minimised since three different techniques are combined. However, a simultaneous perfect match between all three can hardly be expected at all times. The match in order of importance is therefore: (1) roll separating force (2) forward slip, and (3) roll torque.

3. Retrieve and analyse industrial hot rolling data

This project would have little industrial applicability without considering true industrial conditions. Dofasco's No.2 hot strip mill is one of the most modern in North America and makes an excellent candidate for studying today's frictional conditions.

Mill logbooks provide an excellent source of data on process and material parameters. This together with measured roll separating forces permits calculation of the coefficient of friction. Industrial data also provides a source of information where several parameters may interact in their effects on the coefficient of friction. Thus, synergistic effects may be revealed.

The coefficient of friction is to be evaluated from either roll separating force or roll torque or both simultaneously. Roll separating force is preferred, since the unknown losses included in the measured torque are excluded in the force values. The use of Elroll permits a match between measured and calculated roll separating force that results in the retrieval of the coefficient of friction. The effects of the process and material parameters on the frictional conditions are thus revealed and may be compared to trends found in the laboratory.

Of interest are not only the frictional conditions for steady-state rolling conditions, but also the progression of the breaking-in of freshly ground rolls. This information will clarify how the coefficient of friction changes as the oxide builds up on the roll surface and will be helpful in the control algorithm early on in a rolling campaign.

4. Find relationship between friction and roll wear in industrial hot rolling

Roll wear data is also available from Dofasco's logbooks. This, together with the fact that the third objective will provide the coefficient of friction throughout the whole finishing train, will enable modelling of roll wear in terms of process parameters.

The roll wear equations presented in Chapter 2 showed that the input parameters are: coefficient of friction, contact length, reduction, roll diameter, roll material compressive strength, and roll separating force.

This will be beneficial for mill practice as the wear rates can be inferred from the process parameters and the measured roll separating forces, making it a useful tool on-line.

5. Find relationships between results from laboratory and industry

Although there are some similarities between hot rolling in a laboratory and industry, the differences are vast. One significant difference is that of the velocity, which is much higher in industry. There are also differences with regards to the geometry, as greater roll diameters are used in industry. However, the interface may also differ since the process in industry includes roll cooling water, which might act as a lubricant. It is therefore important to compare process conditions that are as alike as possible, or in cases when it is not possible to use a technique that focuses on the synergistic effects.

A dimensional analysis will indicate relationships between the results from laboratory and industry, as it will expose synergistic effects. However, if different frictional mechanisms, mainly due to the vast differences in velocity, control the

frictional behaviour these will be revealed instead.

In conclusion, further understanding of the frictional phenomena in hot flat rolling is to be developed. This will contribute towards improvements in surface quality and productivity. Major financial advantages lie in a better product being produced at a lower price.

Chapter 3

Organisation and Methodology

Oxidation and rolling tests have been carried out in addition to the analysis of industrial mill logbooks. The coefficient of friction has been determined as a function of process and material parameters.

The objective of the hot oxidation experiments was primarily to control and enable predictions of the scale thickness, thereby defining the scale interface. It is therefore important to ensure that:

- A. Samples are of a size that permits accurate measurements of the weight increase.*
- B. Experiments must be carried out under conditions similar to those of the laboratory rolling experiments.*

Several phenomena have to be considered when industrial rolling conditions are to be simulated in a laboratory:

- A. The conditions of geometry and mass flow should be met as closely as possible.*
- B. The interfaces should be similar and be well defined.*
- C. The chosen analytical method must be one that yields minimum error.*

In order to achieve the most accurate results in analysing industrial data the following have to be observed:

- A. *The chosen analytical method must be one that yields minimum error.*
- B. *The data must be treated in such a way that synergistic effects among the process parameters are revealed.*

Since the literature survey clearly indicated that the traditional one-dimensional roll force and torque equations were not sensitive enough to allow for trustworthy numbers on the coefficient of friction, a reliable, commercial finite-element program was chosen as a primary candidate for the calculations. This program is described in Section 3.1. Another benefit with this approach is the possibility to simultaneously match measured and calculated force, torque, and forward slip in cases when all this information is available. This ultimately leads to an evaluation that gives the best possible result. However, early industrial results utilised Ekelund's roll separating force equation. Some of them are retained as a comparison on break-in times of freshly ground work rolls (Chapter 7).

Many experimental cases allow for the change in one parameter to be plotted versus to outcome, which in the present study is the coefficient of friction. However, if several process parameters are altered at the same time, which is the case for industrial conditions, the interactions amongst the various parameters might be severe, and could lead to misguided conclusions. This potential problem can be avoided if dimensionless parameters are introduced. These should have their base in fundamental rolling theory. They are defined in Section 3.2.

3.1 Methods to Calculate the Coefficient of Friction

The finite-element program, Elroll, has been described in detail by Pietrzyk *et al.* (1992). Elroll has been substantiated in a number of publications (Lenard and Pietrzyk, 1990; Lenard *et al.*, 1992; Pietrzyk and Lenard, 1988; 1990; 1991, 1992). It is based on some assumptions: First, the von Mises material law prevails in this rigid plastic finite-element method. The analysis is achieved by many small steady-state deformation steps. An Eulerian reference system is used. This means that the deformation is referred to the current configuration. The unknown is the velocity field. The greatest advantage of this method is that it allows for fast computation times, a necessity in these investigations since a trial and error approach is used. The disadvantage is that elastic deformation is not taken into account (Mielnik, 1991).

The inputs in the finite-element program are: initial temperature profile in the strip, ambient temperature, reduction, roll velocity, coefficient of friction, coefficient of heat transfer, emissivity, geometry including symmetry/asymmetry, as well as the relative size of the mesh. The mesh is limited to 72 elements, which permit relatively short computation times. The outputs are: roll separating force, roll torque, average strain, temperature profiles in both strip and rolls, relative velocity field, strain and strain rates in the individual elements, normal and tangential stresses at the roll/strip interface, as well as average roll pressure and friction stress. The relative velocity field provides the information necessary for the calculation of the forward slip. A coupled heat transfer analysis produces a temperature profile in both strip and roll. Since the coefficient of friction is an input variable, an arbitrary number has to be used as the initial input. Depending on the outcome of this value, i.e. how well the calculated roll separating force, roll torque, and forward slip match the measured numbers, the coefficient of friction is either increased or decreased. This is repeated until a satisfactory simultaneous match is made amongst all three variables. The most important match is that of roll separating

force, followed by forward slip or exit velocity obtained from the velocity field. A significant, but less important match is the roll torque, since the measured numbers will include difficult to predict losses in bearings, gears, and so on.

3.2 Dimensional Analysis

Dimensional analysis is often used as a tool when closed form equations are derived either from experimental findings or from more complex models, such as finite-element models. The advantage with closed form equations derived by dimensional analysis is fast computation. Accuracy may suffer when compared to finite-element models. There is another very useful side of the dimensional analysis: that of tracing symbiotic interactions amongst several process parameters. This is of particular interest when analysing industrial data where several parameters change at once.

Farkas and Lenard (1994) used the dimensional analysis approach when deriving new roll force formulae from data produced by the finite-element code, Elroll. Some basic functions with roots in rolling theory were defined. These were:

$$A = (h_0 - h_f)\sigma_{fs} \quad (3.1a)$$

$$B = \frac{h_0}{R} \quad (3.1b)$$

$$C = \frac{2L}{(h_0 + h_f)} \quad (3.1c)$$

$$D = \frac{hT}{\sigma_{fs}v} \quad (3.1d)$$

where A, although not dimensionless according to definition, describes the combined effect of draft and flow stress, and becomes dimensionless when the roll separating force per unit width is introduced in an equation containing all functions; B may be seen as an

indication of the homogeneity of deformation; C is commonly known as the shape factor and also expresses the homogeneity along with the effects of contact length and reduction; and D the combined effects of heat transfer, temperature, flow stress, and roll velocity. In the equations, h_0 and h_f are initial and final sample thickness, respectively, R is the roll radius, L is the arc of contact, σ_g is the flow stress, v is the roll velocity, and h is the coefficient of heat transfer. S.I units will be used in all calculations.

Roll separating force, P, and roll torque, M, were described in terms of these four functions and the coefficient of friction, μ , as:

$$P = P(A, B, C, D, \mu) \quad (3.2a)$$

$$M = M(A, B, C, D, \mu) \quad (3.2b)$$

in which the dimensionless groups C and especially D are of great interest in the analysis of the industrial data, since combined effects amongst these parameters are expected. The roll velocity will be replaced by the relative velocity, Δv , a parameter related to the abrasive wear mechanism. It is relevant to solve the roll separating force equation for the industrial conditions since it can be used as a means to back calculate the coefficient of friction on-line. This is done by regression analysis of the obtained data with the results from the finite-element calculations.

3.3 Investigations in Laboratory and Industry

Since the scale thickness on the steel samples defines the sample/roll interface and is believed to affect the frictional conditions, a detailed kinetics study will be presented in Chapter 5. Three parameters: time, temperature, and furnace environment characterise the isothermal experiments. For low carbon and micro-alloyed steels, a new model that relates scale thickness to the three parameters is developed. This will enable modelling, including corrections due to changes in sample dimensions, and predictions of the scale interface so that its effects on the frictional behaviour may be investigated.

Another topic of Chapter 5 is the material flow stress. This is also a necessary piece of information that must be obtained before the coefficient of friction can be back calculated from hot rolling experiments. Hot compression tests will enable the flow stress to be inferred from Shida's equation (Shida, 1974a, 1974b), which expresses the flow stress in terms of carbon content, strain, strain-rate, and temperature. By substituting the carbon content with carbon equivalence, the effects of alloying elements, other than carbon, will be taken into account. A match between measured and predicted flow stress will thus be made by choosing a carbon equivalence model that yields the closest agreement between the two.

Laboratory hot rolling experiments will be presented in Chapter 6, where the coefficient of friction will be calculated simultaneously from measured roll separating force, roll torque, and forward slip for different temperatures, roll velocities, percent reductions, and scale thicknesses. Two grades of steel will be investigated, one common low carbon grade (AISI 1018) and one Nb-treated micro-alloyed grade. The effects of both process and material parameters will thus be made clear. The various mechanisms that effect the coefficient of friction will be discussed in the same chapter. To enable this discussion, the chilling effects of the rolls on the sample, i.e. temperature drop due to

conduction, will be approximated along with the adiabatic temperature rise due to deformation and the instantaneous contact temperature. In order to gain insight into the amount of metal-to-metal contact, a relationship between the real and apparent contact areas will be approximated in terms of the coefficient of friction, material shear strength, and roll pressure.

Industrial hot rolling data, obtained from Dofasco's mill logbooks will be investigated in Chapter 7. The break-in time of freshly ground high speed steel work rolls in F3 will be studied in terms of changes in the coefficient of friction, which will be calculated both from Ekelund's equation and from a commercial finite-element code. Furthermore, the effect of temperature will be studied along with the effects of changes in alloy content and work roll material. The temperature and the other process parameters will also be studied by the introduction of dimensionless groups. A study on actual roll wear will also be presented along with the calculated coefficient of friction, as roll wear constants will be calculated based on the information on the frictional conditions along with roll wear data supplied by Dofasco. A discussion on the contributions of various mechanisms that affect the frictional conditions will be done in the same chapter, as real and apparent contact areas are approximated along with instantaneous contact temperatures, temperature drop due to conduction, and temperature rise due to deformation.

Based on the findings in Chapters 6 and 7, an effort will be made to connect the laboratory and industry results in Chapter 8. Since higher velocities are seen for the full-scale conditions, laboratory and industrial investigations complement each other. Together, they will help to unravel the true effects of the process and materials parameters on the frictional conditions in hot rolling. A qualitative comparison will also reveal if and where there are differences in mode of friction in laboratory and industry.

Figure 3.1 illustrates the flow of information, and shows how the various chapters depend on each other. The accuracy of derived models and results are generally discussed in the chapters where they are used. Conclusions relevant to the topics investigated will end each separate experimental chapter. General conclusions are drawn and recommendations for future research are made in Chapter 9.

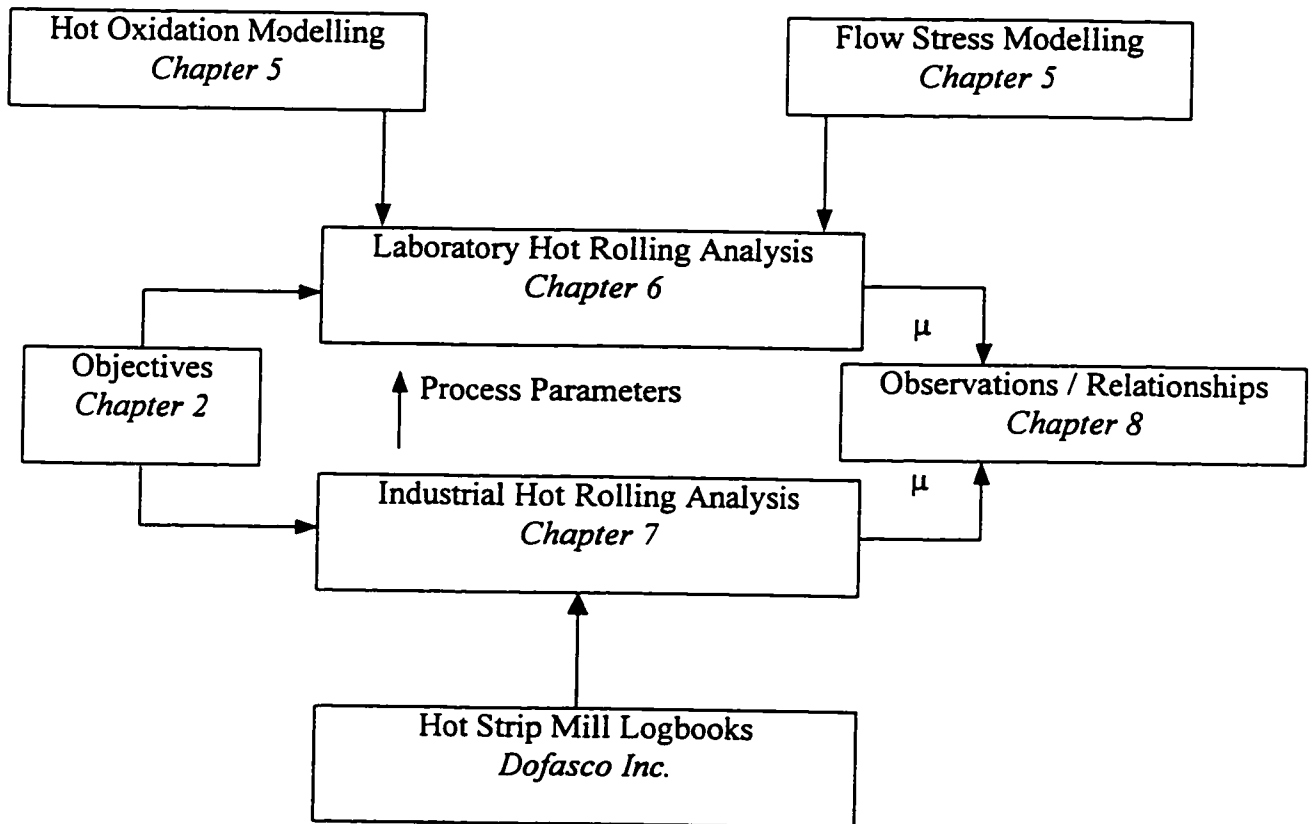


Figure 3.1 Flow of Information - Connecting the Various Chapters

Chapter 4

Equipment, Materials, and Procedure

4.1 Full Scale Finishing Train

4.1.1 Equipment and Conditions

The conditions in the various stands vary with regards to the process parameters; temperature, roll velocity, reduction, and work roll material. Even the interface changes from stand to stand as the tertiary scale grows continuously. Descaled bars enter the finishing train at a thickness of about 30 mm and exit with a thickness of about 2 mm. Meanwhile, the temperature drops from about 1030°C at entry to about 880°C at exit. Throughout the whole process, the velocity increases tenfold. The work roll diameter is commonly about 775 mm. Bars entering the finishing train range in width from 900 to 1000 mm. The work roll material and typical process parameters for campaigns rolled in the fall of 1994 can be seen in Table 4.1.

Dofasco uses a universal hot flat rolling software package designed by General Electric for mill control. The software has been heavily modified over the years as demands on accuracy have increased. The additional data that can be obtained from the mill logbooks include history, estimated flowstress, bars rolled after last roll change, roll separating force and torque, power consumption, and looper angles, all of which are of

interest in evaluating the frictional conditions. Data on forces 2 and 10 seconds after the bar enters are available. The temperature is measured by pyrometers prior to entry and after exiting the finishing train. This makes the temperature estimates the weakest link in the GE package. The reliability of the other parameters is much greater since these, unlike the temperature, are actual measurements. It is obvious that the interaction between the process parameters is strong since they all change from one stand to the next.

Stand	T_0 (°C)	T_f (°C)	v (m/s)	h_0 (mm)	h_f (mm)	Material
F1	1030	975	1.3	30	16.5	Hi-Cr
F2	975	945	2.2	16.5	10.0	Hi-Cr
F3	945	920	3.2	10.0	6.5	HSS
F4	920	910	4.9	6.5	4.5	ICDP
F5	910	900	7.0	4.5	3.25	ICDP
F5	900	890	9.0	3.25	2.5	ICDP
F7	890	880	11.0	2.5	2.0	ICDP
Hi-Cr = high chrome iron, HSS = high speed steel, ICDP = indefinite chilled iron						

Table 4.1: Typical Conditions in Dofasco's No.2 Hot Strip Mill

4.1.2 Material Parameters

A number of different steel grades were investigated. The emphasis, however, was on low carbon steel grades, since the influence of steel chemical composition preferably was to be minimised in the investigations of break-in time of freshly ground rolls as well as the investigations of the effect of process parameters on the frictional conditions. Nevertheless, medium carbon and high-strength low-alloy steel grades were investigated separately in order to clarify the effect of steel chemical composition on the frictional

conditions. Thus, three low carbon, two medium carbon, and two micro-alloyed steel grades were studied. Their typical chemical composition can be seen in Table 4.2. The various steels' flow stresses are obtained from mill logbooks in which they are estimated along with the temperature profile in the finishing train.

Grade	%C	%Mn	%Si	%Al	%Ca	%Nb
CC060	.045-.065	.20-.35	< .030	.02-.06	-	-
CC082	.060-.090	.30-.45	< .025	.02-.06	-	-
CC100	.080-.110	.30-.40	< .025	.01-.03	-	-
CC210	.190-.230	.30-.45	< .040	.02-.06	-	-
CC324	.320-.380	.65-.85	.20-.25	.02-.06	-	-
CC650	.040-.080	.55-.75	.20-.25	.02-.06	.0015-.005	.005-.010
CC762	.120-.160	.55-.75	.20-.25	.02-.06	.0015-.005	.015-.025

Table 4.2: Steel Chemical Composition, weight % (industry)

4.2 Laboratory

4.2.1 Stanat Rolling Mill and Barstaed/Thermolyne Furnace

A 15 kW STANAT laboratory mill with a four-speed transmission was fully instrumented with two load cells, two torque transducers, a SINGER Kearfoot DC tachometer, and three LAND GP112 optical pyrometers, as well as possibilities for temperature measurements with thermocouples. Data was collected using a DASH 16 A/D board and stored in a personal computer. The minimum sampling time was 1 ms over 12 channels. The three pyrometers served two functions, one measuring the surface temperature at the entry and two, placed at the exit, monitor the temperature there. In addition, the time delay in their response gives the necessary information for calculation of the workpiece exit velocity, leading to the forward slip. The sandblasted workrolls, made of D2 tool steel and hardened to $R_c = 55$, had diameters of 150 mm and a surface roughness, R_a , of 0.8 μm . The mill was set-up in a two-high configuration although it can be set-up in a four-high configuration. Its maximum velocity is 100 rpm. A Barstaed/Thermolyne Type 1700 3-phase resistance furnace, rated 208V, 33A, and 6900W, was used in all rolling and oxidation experiments. The furnace was a high temperature model (FA 1748-1) with calcium silicate thermal insulation and heating elements on 4 sides, enabling even heating for temperatures up to 1200°C. The chamber of the furnace measured 216 x 241 x 330 mm. To allow for environments other than air, two stainless steel inlets allowed gas to be purged into the furnace. The temperature was monitored with an R-type thermocouple in the back of the chamber. A temperature feedback control unit made certain that the proper temperature was maintained at all times. The controller was an Omega CN 9121A PID auto-tune microprocessor. A Mettler PC 2000 digital scale with maximum capacity of 2 kg was used to measure the weight of the oxidation samples before and after heating.

4.2.2 Instron Testing Machine

An Instron testing machine, Model 1331, with digital control and data acquisition system was used to perform compression tests for modelling the material flowstress behaviour. Inconel rams were used as compression platens and their temperature was monitored through attached thermocouples. A three-zone resistance furnace was utilised for even heating of specimen and rams. The control software allowed choosing the desired waveform off-line. The generated waveform was used through an 8500 control system to command the ram movement by the servo hydraulic system. The load was measured by an Instron 3116 load cell with maximum capacity of 50 kN and an accuracy of $\pm 1\%$. The crosshead displacement was measured by the master dynamic controller, using signals with a maximum rate of 1000/s. Both displacement and load signals are written to an output file along with calculated true stress and true strain. The machine stiffness correction at different temperatures is considered in the true strain calculations.

4.2.3 Material

Two steel grades were investigated in the laboratory experiments. These were AISI 1018 and a Nb-treated HSLA grade donated by Dofasco Inc. Their chemical composition, in weight %, is given in Table 4.3, below:

Element	C	Si	Mn	Ni	Cr	Mo	V	Nb
HSLA-Nb	0.067	0.345	1.3014	0.0086	0.0253	0.0043	0.0046	0.0764
AISI 1018	0.18	0.21	0.71	-	-	-	-	-

Table 4.3. Steel Chemical Composition, weight % (laboratory)

The hot rolled HSLA grade was obtained in the shape of a 25.4 mm thick plate. The plate was sectioned in half, cut in 50.8 mm wide and 305 mm long flats. These were later milled to a thickness of 12.65 mm. The low carbon grade was delivered as cold-drawn flat bars measuring 50.8 x 12.65 mm or 6.21 mm. These were cut to lengths of 305 mm. All sample dimensions were measured using a digital vernier prior to and after rolling. Samples designated for oxidation experiments were made into pieces weighing 100 g, which corresponded to a surface area of 38.5 cm². Compression samples measured a diameter of 8 mm and a height of 12 mm. HSLA compression samples were machined from the sectioned hot rolled plate, whereas AISI 1018 samples were cut from round cold-drawn bars. All samples were cleaned with n-heptane prior to the experiments.

4.3 Experimental Matrices

4.3.1 Hot Oxidation Experiments

An experimental matrix, given in Table 4.4, consisting of five temperatures and four holding times was established for the scale growth tests. The temperatures were chosen to represent the soaking temperature and the various rolling temperatures. These were 900, 975, 1050, 1125, and 1200°C. The holding times had to provide sufficient time for a scale growth resulting in a weight increase that could be measured accurately, given a sample weight of 100 g. Therefore, holding times of 25, 100, 225, and 400 minutes were selected.

	900°C	975°C	1050°C	1125°C	1200°C
25 min	1	1	1	1, 2, 3	1
100 min	1	1	1	1, 2, 3 ^{&}	1
225 min	1	1	1	1, 2, 3 [#]	1
400 min	1	1	1	1, 2	1

Table 4.4. Experimental Matrix for Scale Growth Investigations. 1 - LC in air, 2 - HSLA in air, 3 - LC in N₂, [&] - 80 min., [#] - 130 min.

In determining the effect of the chemical composition and the environment, it is sufficient to use one temperature. The literature survey showed that it could be assumed that approximately 95% of the oxide layer is wüstite. This means that the activation energy for the scale formation remains independent of the chemical composition of the steel and its environment. These will only affect the growth rate constant, giving a different slope when scale growth is plotted versus the square root of time, assuming a parabolic scale growth behaviour of the iron oxides.

A temperature of 1125°C was selected for the Nb-alloyed HSLA steel. Oxygen-free nitrogen was used as an alternate environment. Three times were investigated for the latter: 25, 80, and 130 minutes.

4.3.2 Hot Rolling Experiments

For the hot rolling experiments, the samples were soaked at 1200°C for 20 minutes to ensure a homogeneous temperature distribution. 2-4 samples were heated at a time (2 in the case of soaking in an atmosphere of nitrogen). They were then taken out of the furnace and held under a pyrometer on the entry side of the mill until the desired temperature was reached.

Four temperatures, representing various stands in the finishing train of a hot strip mill were chosen: 1050, 975, 900, and 825°C. The selected four velocities of 0.2, 0.4, 0.8, and 1.0 m/s could not be chosen to represent the industrial conditions other than at the first stand, due to the limiting velocities of the laboratory mill. The velocities were instead chosen so that maximum engine torque would be achieved at each in order to maximise the drafts at each temperature. Reductions ranging from 15 to 35% were selected. The samples were soaked at 1200°C. The scale thickness was controlled by either purging with oxygen-free nitrogen or by increasing the soaking times from 20 to 100 and 225 minutes, respectively. According to the hot oxidation experiments, the first scenario, purging with nitrogen, minimised scale growth and produced a scale thickness of 0.015 mm. The latter two, increased soaking times, promote scale growth. A soaking time of 20 minutes resulted in a scale thickness of 0.29 mm whereas 100 minutes resulted in a scale thickness of 1.00 mm. Scales 1.59 mm thick were produced by soaking for 225 minutes.

Several experiments were carried out on both grades of steel. Data on roll separating force and roll torques were collected along with surface temperatures, roll velocity and the exit speed of the samples, which allowed the calculation of the forward slip. The investigated process parameters are compiled in Table 4.5.

Temperature (°C)	825*	900	975	1050
Velocity (m/s)	0.2	0.4	0.8*	1.0*
Reduction (%)	15	20	25	30
Thickness (mm)	12.6	6.21 ^x	n/a	n/a
Scale thickness (mm)	0.015 ⁺	0.29 ⁺	1.00 ⁺	1.59 ⁺

Table 4.5. Laboratory Hot Rolling Process Parameter Targets, * indicate parameters that might exceed equipment limitations, ^x indicate series limited to fewer reductions, and ⁺ indicate series limited to fewer velocities.

Due to limitations in the equipment, not all of the intended process parameters could be investigated. Therefore, one process parameter was varied at the time while the others remained constant. Furthermore, a complete matrix would contain 512 experiments for the AISI 1018 steel alone. This number was reduced to about half because of the limitations in equipment. Because of the amount of inhomogeneous deformation for 15 % reductions, this group was restricted to a limited number.

4.3.3 Hot Compression Tests

The compression tests on AISI 1018 were carefully chosen to coincide with of the conditions met in some hot rolling experiments. The HSLA compression tests were carried out over a much wider range with strain rates ranging from 0.2 to 4.0 s⁻¹. In both cases, temperatures between 900 and 1050°C were investigated. The results from the

experiments were then matched with the output from Shida's equations, as discussed earlier. The experimental matrix for the hot compression tests can be seen in Table 4.6.

Material	AISI 1018				Nb-HSLA		
Temperature (°C)	900	975	1050	n/a	900	950	1030
Mean strain-rate (s ⁻¹)	3.6	5.9	7.3	11.8	0.2	4.0	n/a

Table 4.6 Experimental Matrix for Hot Compression Tests

Chapter 5

Material Behaviour

5.1 Hot Oxidation - Scale Formation

The literature review indicated that the thickness of the scale present in the roll gap during hot rolling affects the frictional conditions, including roll wear and heat transfer. The composition of the scale was also said to affect the aforementioned to a certain extent since the different iron-oxide phases have different mechanical and physical properties. This led to a series of investigations on scale growth under laboratory conditions, relevant to the hot rolling experiments. These investigations resulted in growth rate constants as well as a simple predictive model of the scale thickness. In the model, the total scale thickness is described as a function of time, temperature, alloy composition, and furnace environment.

5.1.1 Predicting Scale Thickness

According to most elementary textbooks (Askeland, 1996; Callister, 1997; Smith, 1990) the kinetics of oxidation of iron is parabolic with regard to time and exponential with respect to temperature. It is convenient to describe the kinetics in terms of weight gained per unit surface area. This is a direct reflection on the amount of oxygen involved in the formation of the various oxide phases. Sometimes, the weight gain per unit surface area is referred to as scale index, γ , (Roberts, 1983), and may be written:

$$\gamma = k_p \sqrt{t} \quad (5.1)$$

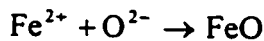
where k_p is a parabolic rate constant for a given temperature, chemical composition, and environment. Its dependency on temperature is, as mentioned, exponential:

$$k_p = k_e \exp\left(\frac{-Q}{R_{\text{gas}} T}\right) \quad (5.2)$$

where the temperature, T , is expressed in K. Q is the activation energy of the rate-controlling process, and R_{gas} is the universal gas constant. The dependency on chemical composition and environment is expressed in the exponential constant, k_e . The scale index, γ , or weight gain per unit surface area can thus be defined as:

$$\gamma = k_e \exp\left(\frac{-Q}{R_{\text{gas}} \cdot T}\right) \sqrt{t} \quad (5.3)$$

The scale index can be measured experimentally by measuring the dimensions and the weights of the sample before and after heating. Assuming that 100% wüstite is formed, consider the following reaction:



Mass balance indicates that 1 mole of iron, n_{Fe} , reacts with one mole of oxygen, n_{O} :

$$n_{\text{Fe}} = n_{\text{O}} = \frac{m_{\text{Fe}}}{M_{\text{Fe}}} = \frac{m_{\text{O}}}{M_{\text{O}}} \quad (5.4)$$

where m is mass and M is molecular weight for the elements, respectively. The measured increase in weight, Δm , is equal to the weight of the oxygen in the wüstite:

$$\Delta m = m_{\text{O}} = \frac{m_{\text{Fe}} \cdot M_{\text{O}}}{M_{\text{Fe}}} \quad (5.5)$$

The total mass of the wüstite can then be expressed as:

$$m_{\text{FeO}} = m_{\text{Fe}} + m_{\text{O}} = m_{\text{O}} \cdot \left(1 + \frac{M_{\text{Fe}}}{M_{\text{O}}}\right) = \Delta m \cdot \left(1 + \frac{M_{\text{Fe}}}{M_{\text{O}}}\right) = 4.491 \cdot \Delta m \quad (5.6)$$

where $M_{\text{Fe}} = 55.85$ g/mole and $M_{\text{O}} = 16.00$ g/mole.

The thickness of the wüstite may be calculated from its density, ρ , mass, and volume, V .

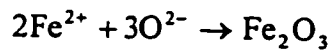
The mass may then be written:

$$m_{\text{FeO}} = \rho_{\text{FeO}} \cdot V_{\text{FeO}} = \rho_{\text{FeO}} \cdot A_{\text{FeO}} \cdot x_{\text{FeO}} \quad (5.7)$$

where A is area and x is thickness. Substitution and re-writing allows the thickness to be expressed as:

$$x_{\text{FeO}} = \frac{\Delta m \cdot \left(1 + \frac{M_{\text{Fe}}}{M_{\text{O}}}\right)}{A_{\text{FeO}} \cdot \rho_{\text{FeO}}} = \frac{4.491 \cdot \Delta m}{A_{\text{FeO}} \cdot \rho_{\text{FeO}}} \quad (5.8)$$

Similarly, the thickness for 100% magnetite or haematite can be calculated. If 100% haematite is formed, consider the reaction:



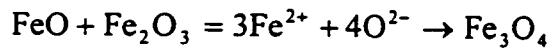
The same reasoning as above gives a haematite weight described by:

$$m_{\text{Fe}_2\text{O}_3} = m_{\text{Fe}} + m_{\text{O}} = m_{\text{O}} \cdot \left(1 + \frac{2}{3} \cdot \frac{M_{\text{Fe}}}{M_{\text{O}}}\right) = \Delta m \cdot \left(1 + \frac{2}{3} \cdot \frac{M_{\text{Fe}}}{M_{\text{O}}}\right) = 3.327 \cdot \Delta m \quad (5.9)$$

resulting in a thickness:

$$x_{\text{Fe}_2\text{O}_3} = \frac{\Delta m \cdot \left(1 + \frac{2}{3} \cdot \frac{M_{\text{Fe}}}{M_{\text{O}}}\right)}{A_{\text{Fe}_2\text{O}_3} \cdot \rho_{\text{Fe}_2\text{O}_3}} = \frac{3.327 \cdot \Delta m}{A_{\text{Fe}_2\text{O}_3} \cdot \rho_{\text{Fe}_2\text{O}_3}} \quad (5.10)$$

The same arguments applied to formation of magnetite from:



which results in a weight described by:

$$m_{\text{Fe}_3\text{O}_4} = m_{\text{Fe}} + m_{\text{O}} = m_{\text{O}} \cdot \left(1 + \frac{3}{4} \cdot \frac{M_{\text{Fe}}}{M_{\text{O}}}\right) = \Delta m \cdot \left(1 + \frac{3}{4} \cdot \frac{M_{\text{Fe}}}{M_{\text{O}}}\right) = 3.618 \cdot \Delta m \quad (5.11)$$

The thickness is similarly described by:

$$x_{\text{Fe}_3\text{O}_4} = \frac{\Delta m \cdot \left(1 + \frac{3}{4} \cdot \frac{M_{\text{Fe}}}{M_{\text{O}}}\right)}{A_{\text{Fe}_3\text{O}_4} \cdot \rho_{\text{Fe}_3\text{O}_4}} = \frac{3.618 \cdot \Delta m}{A_{\text{Fe}_3\text{O}_4} \cdot \rho_{\text{Fe}_3\text{O}_4}} \quad (5.12)$$

These would all be ideal conditions where only one phase exists at the time. This is not the case in the laboratory furnace environments where a scale consisting of 95% wüstite

can be expected, assuming the data presented by Sachs and Tuck (1968) is correct. The relative error in assuming that 100% wüstite is formed will therefore be small, since the densities of magnetite and haematite are less than wüstite's: 5.40 and 5.24 g/cm³ compared to wüstite's 7.75 g/cm³ (Samsonov, 1973). A worst case scenario would be that 100% magnetite is formed. This would result in an underestimation of the thickness by 15.5 % if the equations for wüstite were used instead of the proper equations for magnetite.

5.1.2 Results and Discussion

5.1.2.1. Kinetics of Hot Oxidation in Air

The effects of holding time and temperature on scale growth for the AISI 1018 low carbon steel, presented as scale index in mg/cm², can be seen in Figure 5.1. The scale index was, as described previously, determined from measured weight increase and surface area. The area was calculated from the mean thickness, width, and length, which were measured with a digital micrometer. The weight was measured using a digital scale.

As can be expected, the scale index increases with both time and temperature. For times of 400 minutes, the scale index increases ten times when the temperature is increased from 900°C to 1200°C. Under the assumption of a parabolic growth rate with regards to time, the scale index may be plotted versus the square root of time (see Figure 5.2).

Figure 5.1. Scale Index as a Function of Time

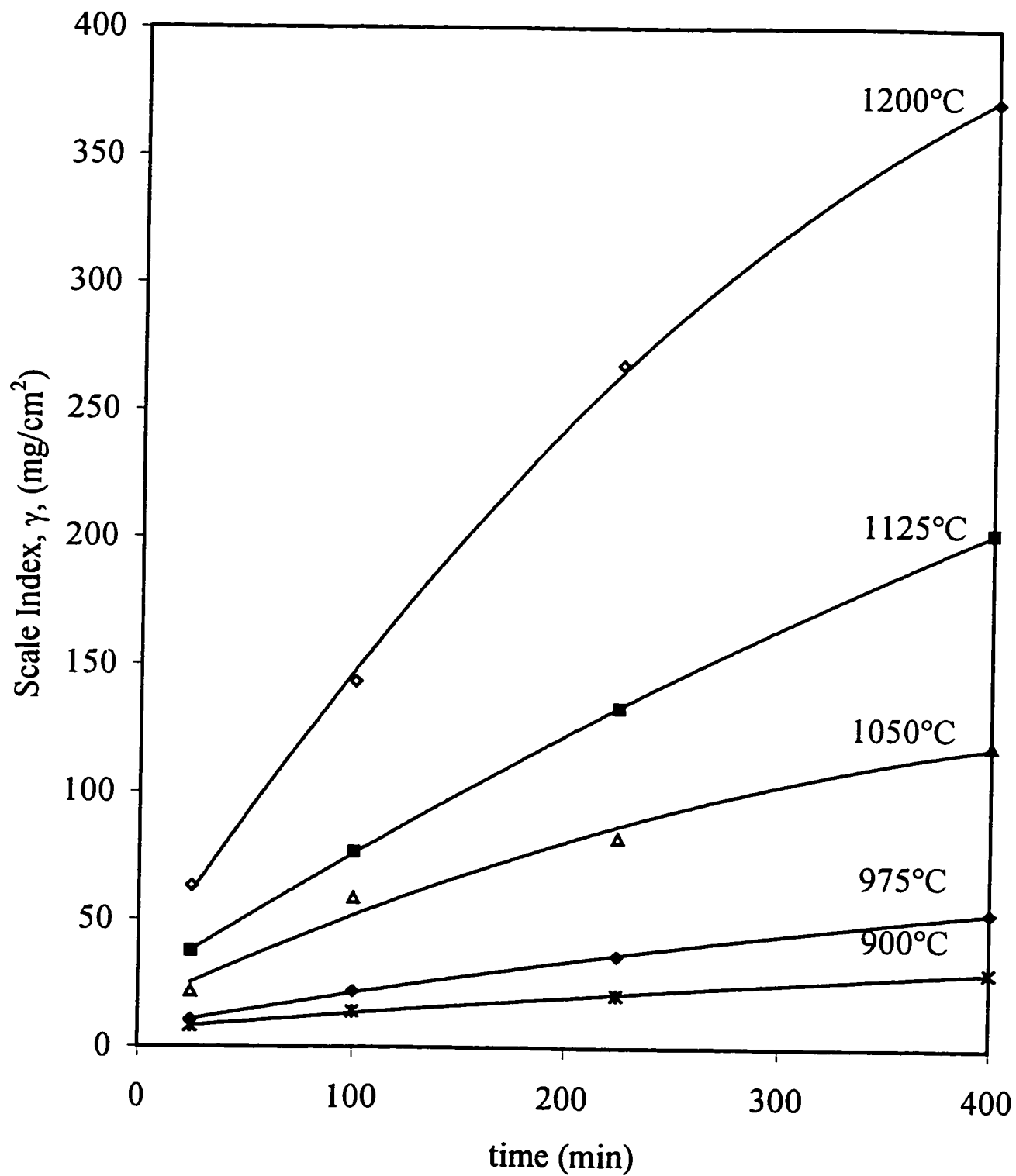
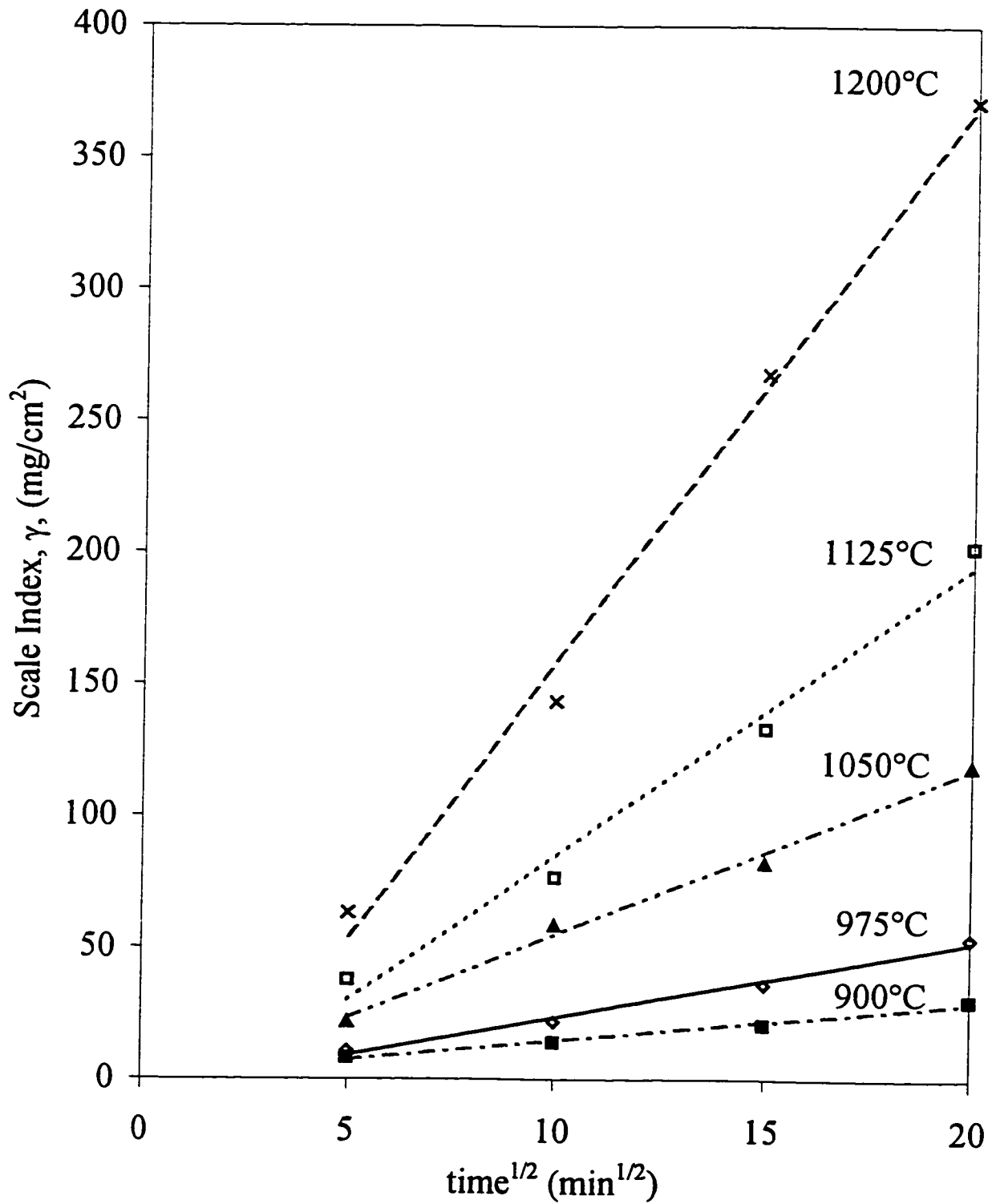


Figure 5.2. Scale Index as a Function of Time



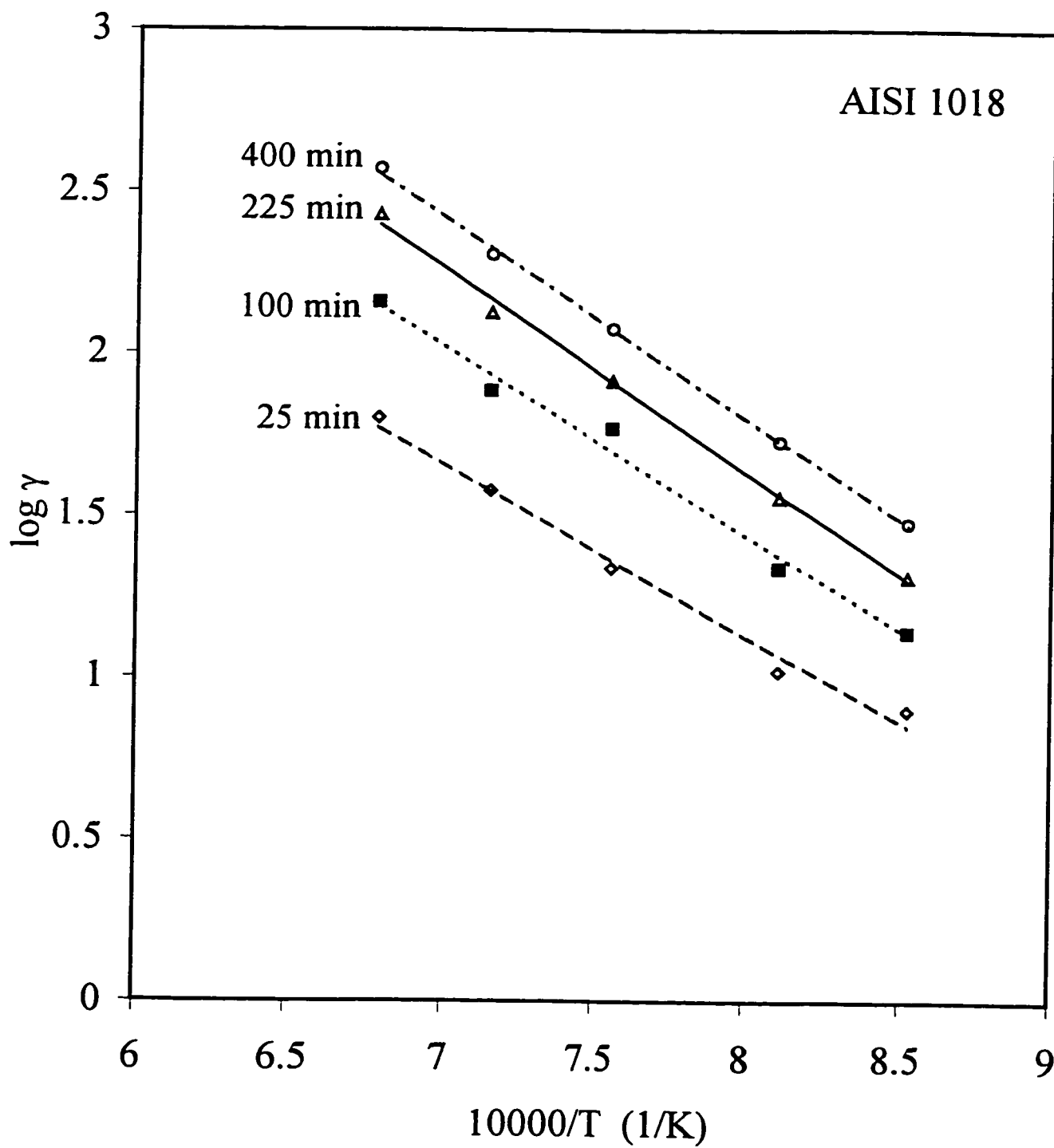
The parabolic growth rate constants, k_p , for the various temperatures are, in fact, the slopes of $\log(\gamma)$ and $1/T$. Assuming an exponential growth rate with regards to temperature, the logarithm of the scale index may be plotted versus the inverse temperature in K^{-1} (Figure 5.3).

The parallel slopes in Figure 5.3 enable the calculation of the activation energy for scale formation as:

$$\frac{-Q}{\ln(10)R_{\text{gas}}} = \frac{d \log(\gamma)}{d\left(\frac{1}{T}\right)} = \text{slope} \quad (5.13)$$

The good fit of the trend lines to the experimental measurements in Figures 5.2 and 5.3 justifies the assumption that the scale growth is parabolic with regards to time and exponential with regards to temperature. The R^2 values of the fit range between 0.987 and 0.999. The activation energy was calculated from a slope, based on the average slopes of the three longer holding times in Figure 5.3. The calculated activation energy for the scale layer was 120 kJ/mole. This is very close to the activation energy of 124 kJ/mole for wüstite found in literature (Samsonov, 1973). The same source reports activation energies for magnetite and haematite of 188 and 419 kJ/mole, respectively. The expected amounts of magnetite and haematite are therefore small, since the presence of a larger amount of either phase would have given a higher experimental activation energy. Visual inspection of the samples also leads to the conclusion that there was practically no haematite and magnetite present. This argument is based on the fact that wüstite is grey or light grey in colour while magnetite and haematite are dark grey and red, respectively. Magnetite also has a mineral lustre to it.

Figure 5.3. Scale Index as a Function of Temperature



5.1.2.2 Effect of the Steel's Chemical Composition on Kinetics

The effect of the chemical composition of the steels is illustrated in Figure 5.4, where the scaling of the low carbon steel is compared to that of the Nb-treated HSLA steel at 1125°C. The two slopes are almost identical for the two different alloys, resulting in a parabolic growth rate constant of 11.00.

Figure 5.4, showing the effect of chemical composition at 1125°C, indicates that the scale kinetics are very similar for the low carbon and the micro-alloyed steels. Although carbon content was expected to have an influence on the kinetics (Roberts, 1983), the observed effect of the slightly higher carbon content in the low carbon steel is small and within experimental error. Since the slope is the same in both cases, it can be concluded that the kinetics are similar for the two steels. The parabolic growth constant is 11.00 for both 1018 and Nb-treated HSLA at 1125°C. The scale on the two steels appears to be of similar composition according to colour.

5.1.2.3 Kinetics of Hot Oxidation in Nitrogen

The effect of an alternate environment, shown in Figure 5.5, is more pronounced than the effect of chemical composition of the steels. Purging with oxygen-free nitrogen gas at a pressure of 7 kPa decreased the parabolic growth rate constant from 11.00 to 0.57 at 1125°C. The reason for this is the lowered oxygen amount in the furnace. It is therefore concluded that oxygen-free nitrogen is a satisfactory medium to reduce the oxygen partial pressure and thus control the scale growth in the hot rolling experiments. These conditions would result in more than 95% wüstite, which was visually corroborated since the scale on the samples was, in all cases, light grey. Purging with nitrogen is therefore a method that can be used not only to control the scale growth prior to hot rolling

Figure 5.4. The Effect of Chemical Composition on Growth Kinetics

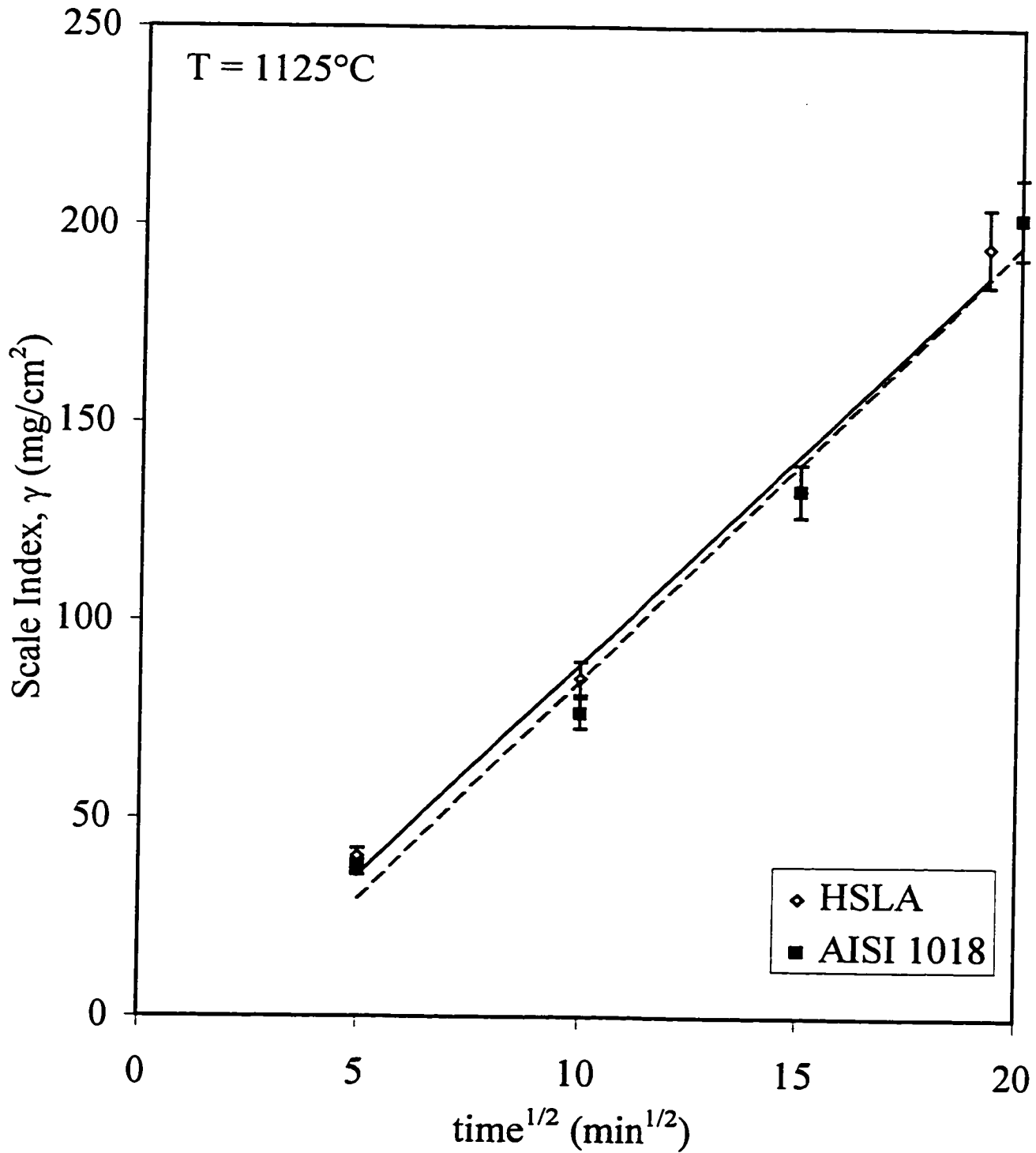
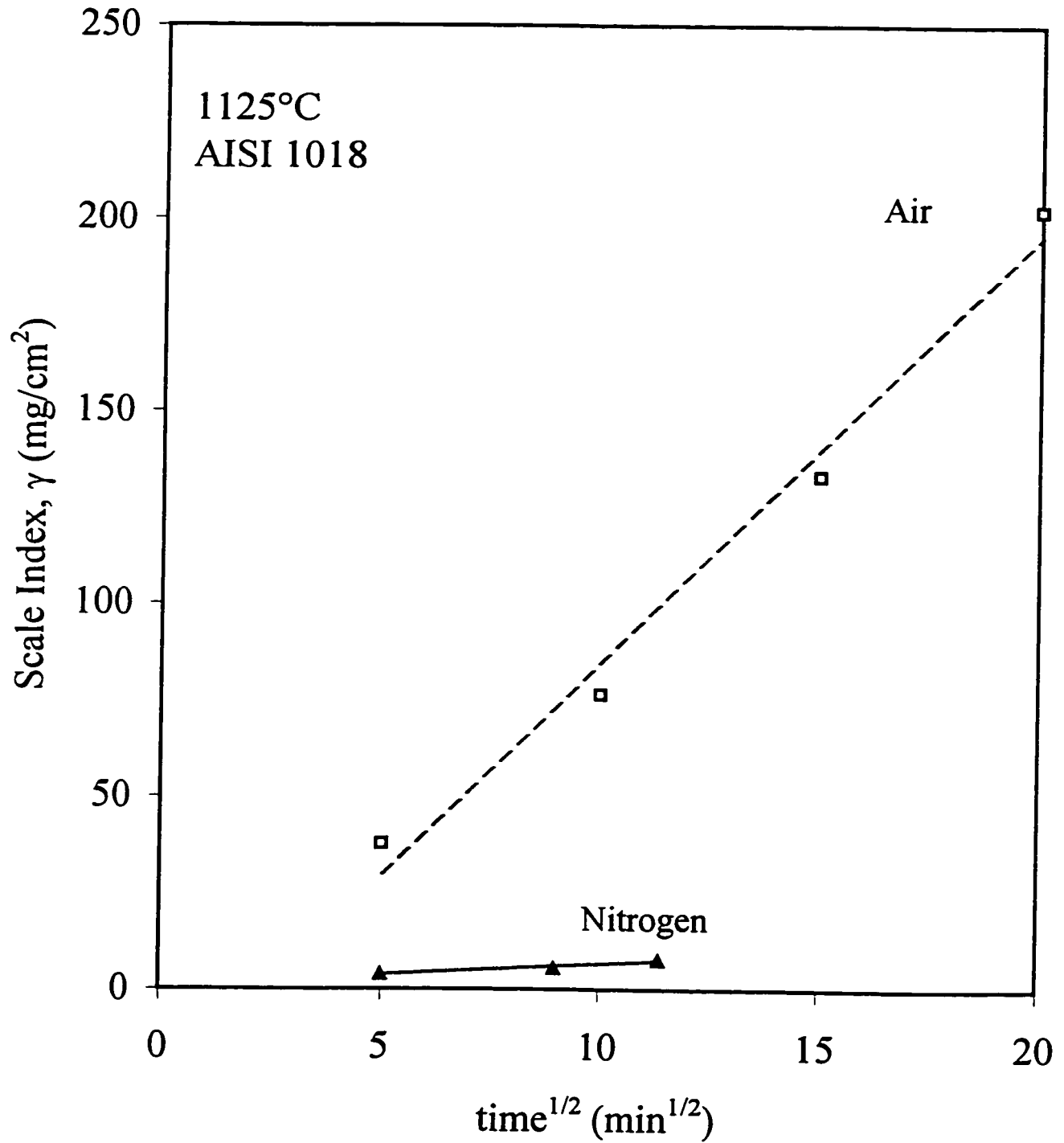


Figure 5.5. The Effect of Oxygen-free Nitrogen on Growth Kinetics



experiments, but it can also bring material losses down while it is providing a mild nitriding effect on the surface of the steel. This is particularly useful for companies that have operations that produce nitrogen as a by-product. However, a thin scale might be more difficult to remove as it adheres better to the steel surface.

5.1.2.4 Calculated Scale Thickness

The capabilities of the simple model, presented previously, are shown in Figures 5.6 and 5.7. Figure 5.6 illustrates the predicted scale index along with the trend lines from Figure 5.2 for three selected temperatures. The margin of error is, in all cases, within 5%. The shortest times were omitted from the data, since they could result in discrepancies due to small differences in environment. After all, these samples experienced an environment consisting of less oxidation and decarburisation exhaust. These samples also took the same amount of time to heat up to the appropriate temperatures.

Information, such as presented in Figure 5.6, was used to calculate the scale thickness, assuming 100% wüstite, at the various temperatures by the use of equations 5.3 and 5.8 together with the fact that the scale index, $\gamma = \Delta m/A$. The scale thickness can then be described:

$$x_{\text{FeO}} = \frac{1 + \frac{M_{\text{Fe}}}{M_{\text{O}}}}{\rho_{\text{FeO}}} k_c \exp\left(\frac{-Q}{R_{\text{gas}} T}\right) \sqrt{t} \quad (5.14)$$

The scale thickness was calculated for all five temperatures and the final results are presented in Figure 5.7. This simple model also allows for the thickness at other, intermediate temperatures to be estimated. Table 5.1 shows the reheating conditions under which four different scale thicknesses have been produced.

Figure 5.6. Calculated and Measured Scale Index

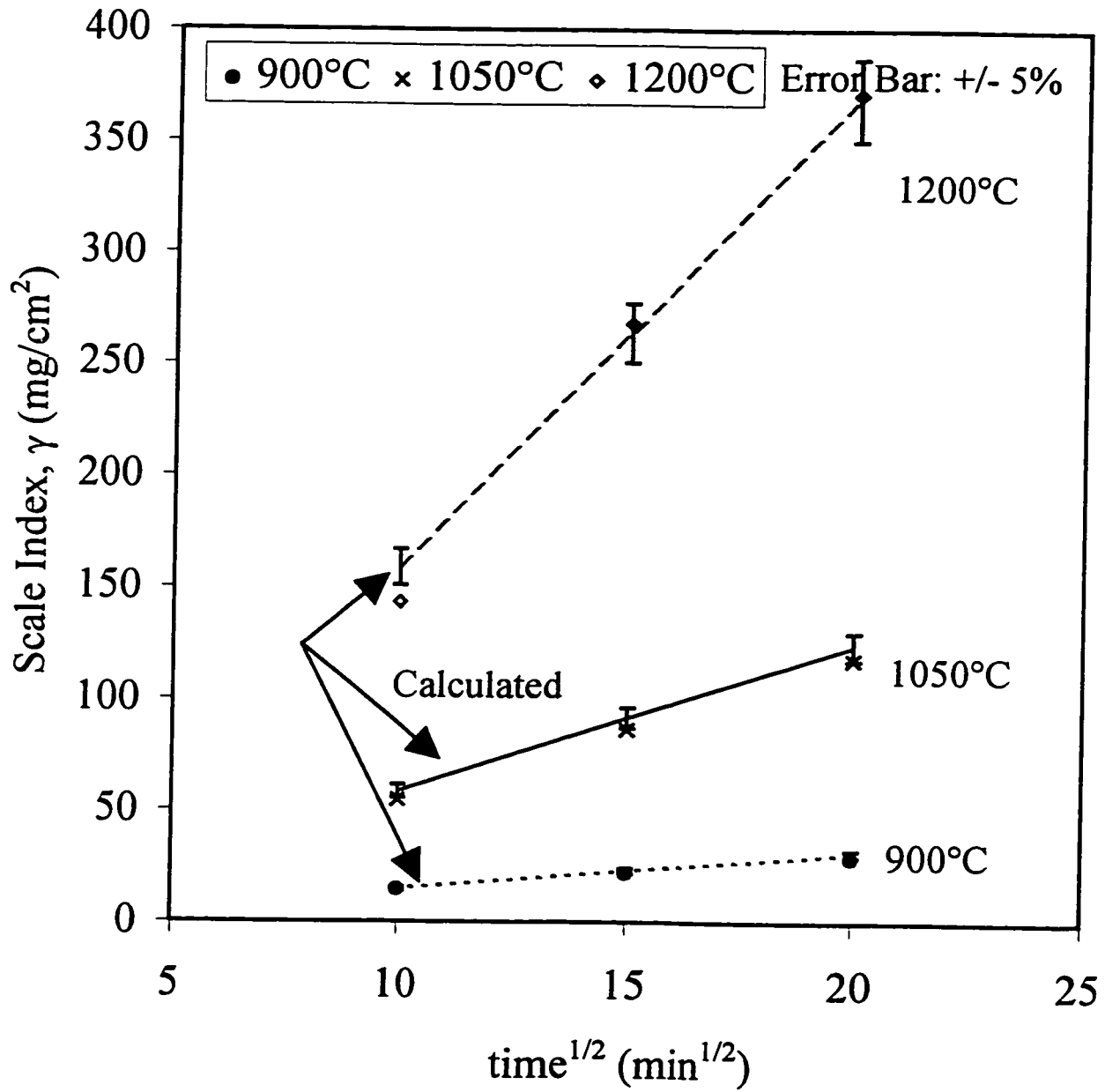
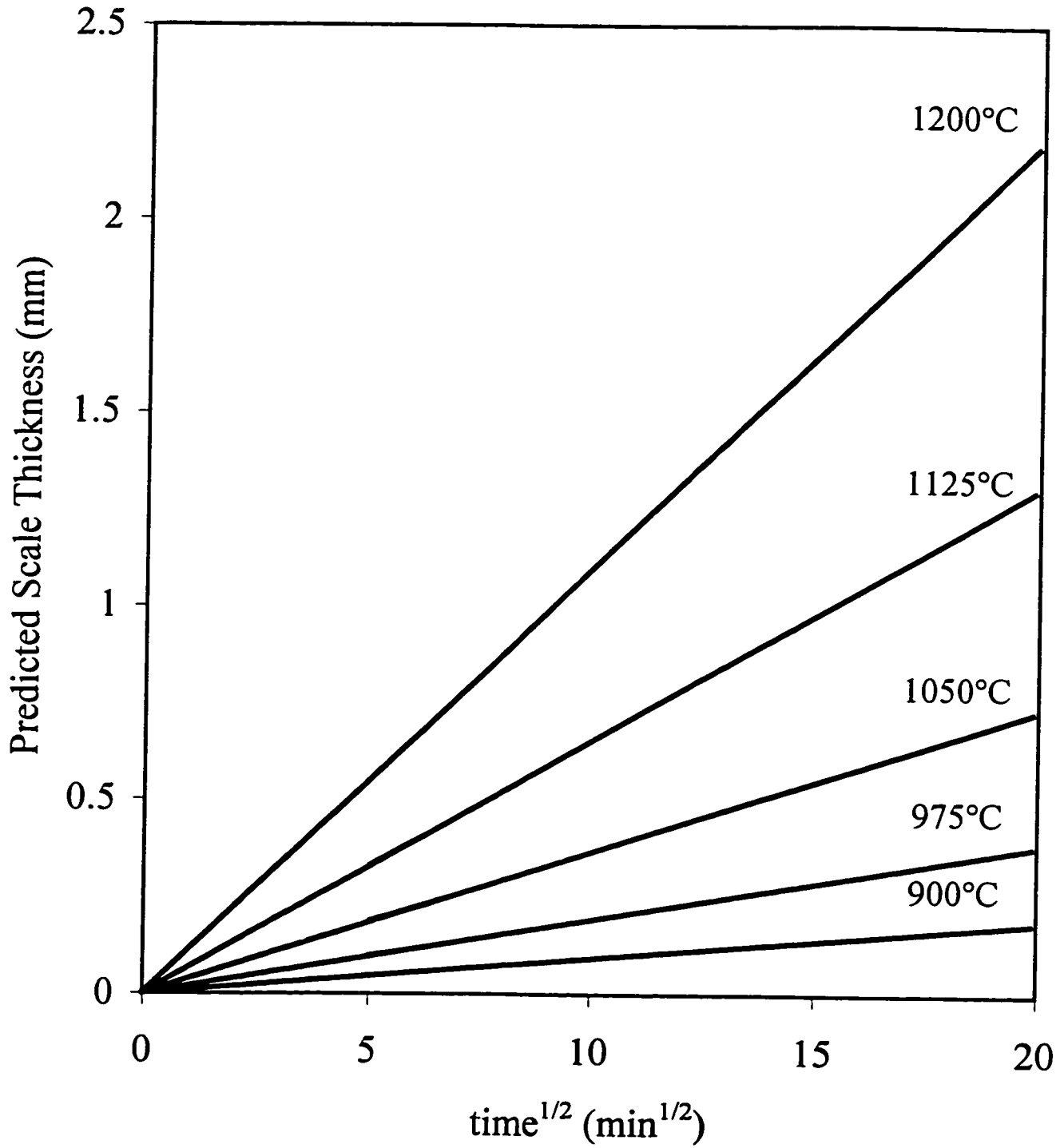


Figure 5.7. Calculated Scale Thickness at Various Temperatures



Temperature (°C)	Time (min)	Environment	Scale Thickness (mm)
1200	20	Nitrogen	0.015
1200	20	Air	0.290
1200	100	Air	1.000
1200	225	Air	1.590

Table 5.1 Calculated Scale Thickness

A scale thickness of 0.015 mm corresponds to the one that develops after the scale breaking operation prior to the entry of the finishing train of a hot strip mill (Tiley, 1997).

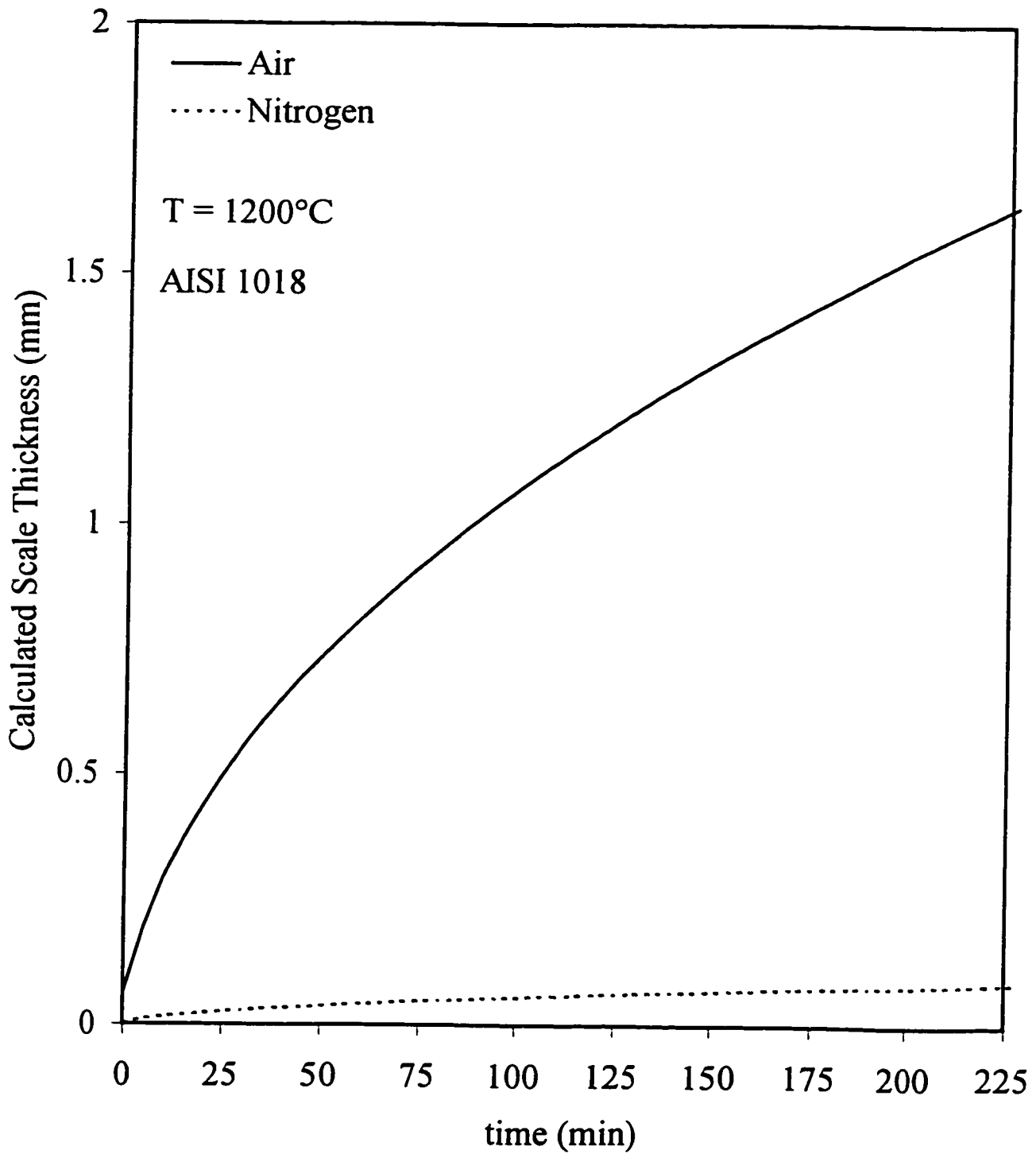
The simple model, whose results are presented in Figures 5.6 and 5.7, gave reasonable estimates of the scale growth in terms of the scale index, all within 5 % of the experimental data taken from Figure 5.2.

It is harder to comment on the accuracy of the predicted scale thickness in Figure 5.7, since scale thickness is more difficult to measure experimentally. However, room temperature measurements on the scale thickness were made on a selected number of samples from which the scale was carefully removed. The result was as might be expected; the measured scale thickness was higher than the calculated. This is explained by the fact that the various oxide phases have a different thermal expansion than steel, causing the scale to blister and flake upon cooling. The porous and blistered scale therefore gains in thickness and was in some cases up to 30% greater at room temperatures than the predictions at the test temperature.

This simple approach, using weight gain, can be used to estimate the thickness of the scale layer formed at various temperatures, times, and environments. Based on the information presented in Figure 5.5, Figure 5.8 shows the results obtained when purging with nitrogen gas at a pressure of 7 kPa. This decreases the growth rate constant in the

calculations from 11.00 to 0.57, corresponding to a scale thickness of 0.290 mm when soaked in air compared to a thickness of 0.015 when soaked in oxygen-free nitrogen. Furthermore, Table 5.1, illustrates the combined effects of the environments and soaking time. These conditions will be used to model the effect of the scale interface on the frictional conditions in Chapter 6.

Figure 5.8. Calculated Scale Thickness for Various Environments



5.2 Modelling Material Flow Stress

When modelling the laboratory hot rolling conditions, not only is scale formation important, but also the material flow stress. This is a crucial part, since the input of material strength in the finite-element program affects both calculated roll separating force and roll torque. Since errors in these calculations strongly affect the outcome of the friction investigations, the flow stress must be described in the best possible manner. One means of doing this is the adaptation of a generic flow stress model, which is calibrated by a limited series of hot compression tests.

5.2.1 Empirical Formulas

Many available empirical formulas describe a material's flow stress. However, a limited number do so in terms of the combined effects of strain, strain-rate, temperature, and chemical composition. The first one to express flow stress in terms of chemical composition, temperature, and velocity was Ekelund (1927). However, this equation is of little relevance today. More recently, Shida (1974a, 1974b) derived empirical formulae describing the flow stress behaviour in terms of dimensionless groups for eight different carbon steels. Based on the simple power law, these formulae are valid for strains up to 0.6, strain-rates ranging from $0.3\text{-}30\text{ s}^{-1}$, and temperatures between $650\text{ and }1200^\circ\text{C}$. After dividing the temperature in K by 1000, thereby making it a dimensionless unit, t_1 , the material flow stress, σ_{fs} , is expressed in MPa as:

$$\sigma_{fs} = \sigma_f f\left(\frac{\dot{\epsilon}}{10}\right)^m \quad (5.15)$$

where f is an expression containing the strain as:

$$f = 1.3 \left(\frac{\varepsilon}{0.2} \right)^n - 0.3 \left(\frac{\varepsilon}{0.2} \right) \quad (5.16)$$

where the strain sensitivity, n , is expressed in terms of carbon content as: $n = 0.41 - 0.07C$. Considering the boundary between the austenite and ferrite regions, Shida introduced a dimensionless temperature expression, t_d , which reflects the chemical composition as:

$$t_d = 0.95 \frac{C + 0.41}{C + 0.32} \quad (5.17)$$

This expression determines which functions are to be used in equation (5.16). σ_f is a function of the temperature and carbon content, defined as:

$$\sigma_f = 2.75 \exp \left(\frac{5.0}{t_1} - \frac{0.01}{C + 0.05} \right) \quad \text{for } t_1 > t_d \quad (5.18a)$$

$$\sigma_f = 2.75g(C, t_1) \exp \left(\frac{5.0}{t_1} - \frac{0.01}{C + 0.05} \right) \quad \text{for } t_1 < t_d \quad (5.18b)$$

$$g(C, t_1) = 30.0(C + 90) \left(t_1 - 0.95 \frac{C + 0.49}{C + 0.42} \right)^2 + \frac{C + 0.06}{C + 0.09}$$

The strain-rate sensitivity, m , in equation (5.16) is expressed as:

$$m = (-0.019C + 0.126)t_1 + (0.075C - 0.050) \quad \text{for } t_1 > t_d \quad (5.19a)$$

$$m = (0.081C - 0.154)t_1 + (-0.019C + 0.207) + \frac{0.027}{C + 0.320} \quad \text{for } t_1 < t_d \quad (5.19b)$$

The advantage of Shida's empirical equations is that relatively accurate flow stresses can easily be calculated. However, this model does not include the effect of grain size and thermal-mechanical history. Another disadvantage is that it does not consider alloying elements other than carbon.

To include the effects of alloying elements other than carbon on a steel's hot strength, carbon equivalency may be introduced. Carbon equivalents, C_{eq} , have traditionally been used to describe weldability, however, they also give a rough estimate of a steel's hot strength. Many relationships have been proposed. Laasraoui and Jonas (1991) proposed the following expression:

$$C_{eq} = C + \frac{Mn}{6} + \frac{Ni + Cu}{15} + \frac{Cr + Mo + V}{5} \quad (5.20)$$

where the elements are given as weight percent. Yurioka et al. (1987) proposed a more complex relationship, which also includes the effects of Nb and B:

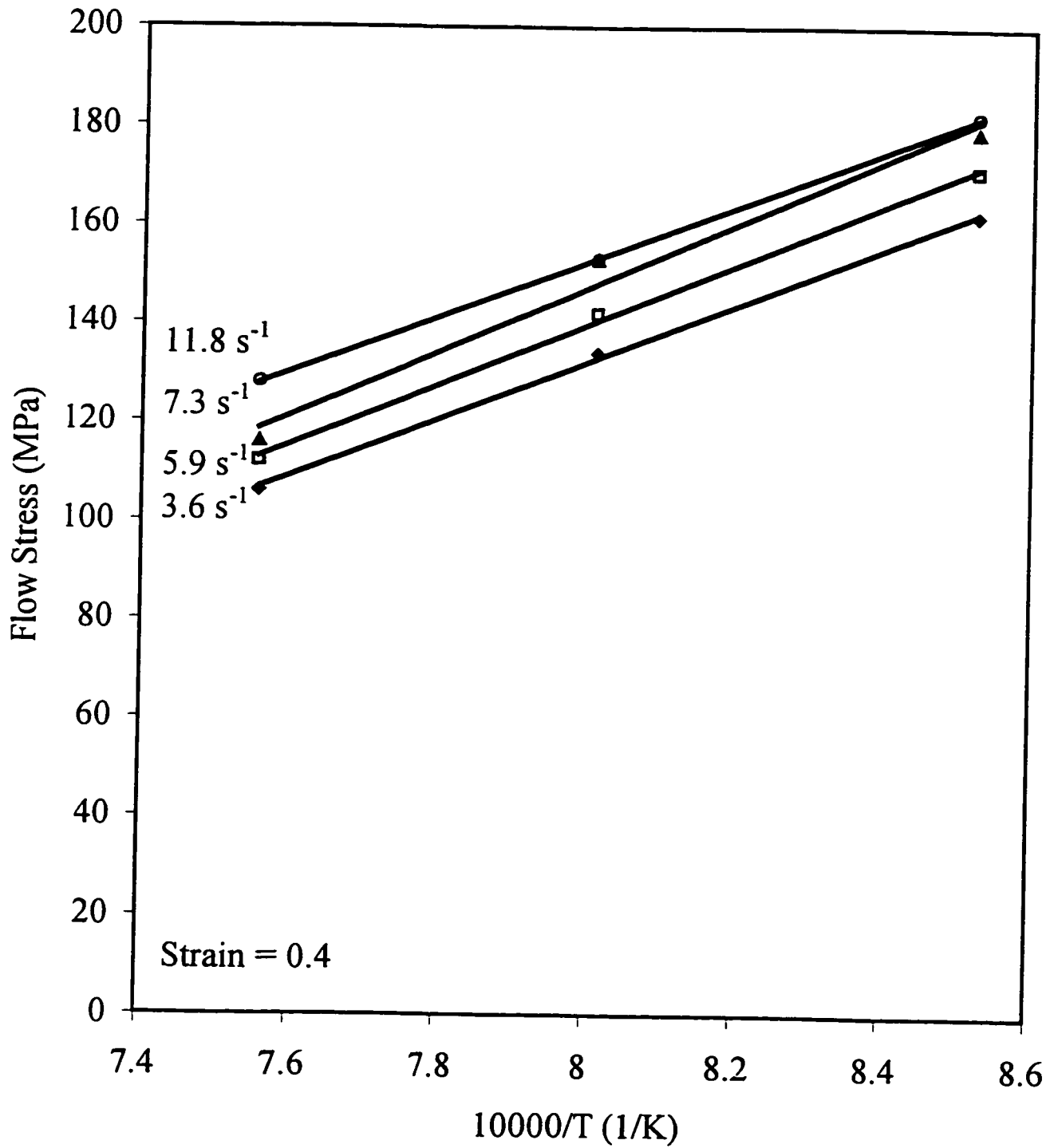
$$C_{eq} = C + A(C) \left(\frac{Si}{24} + \frac{Mn}{6} + \frac{Cu}{15} + \frac{Ni}{20} + \frac{Cr + Mo + V + Nb}{5} + 5B \right) \quad (5.21)$$

where $A(C) = 0.75 + 0.25 \tanh[20(C - 0.12)]$. This multiplier lessens the effects of the other alloying elements for low carbon contents.

5.2.2 Results and Discussion

The experimental flow stress for AISI 1018 can be seen in Figure 5.9. The figure shows the flow stress at a strain of 0.4, corresponding to the greatest reduction seen in the laboratory, for strain-rates ($3.6 - 11.8 \text{ s}^{-1}$) and temperatures ($900-1050^\circ\text{C}$). The material

Figure 5.9 Experimental Flow Stress for AISI 1018



behaviour is as can be expected: the flow stress increases with increasing strain-rate and decreasing temperature. A strain-rate of 3.6 s^{-1} and a temperature of 1050°C result in a flow stress of 106 MPa, whereas 11.8 s^{-1} and 900°C result in a flow stress of 182 MPa.

The flow stress for the HSLA grade can be seen in Figure 5.10, albeit for different strain-rates ($0.2 - 4.0 \text{ s}^{-1}$). A similar behaviour with regards to strain-rate and temperature is displayed. The 4.0 s^{-1} curve for the HSLA grade is close to the 3.6 s^{-1} curve for the AISI 1018 grade in Figure 5.9. Apparently, there is little difference in flow stress behaviour among the two steels.

Comparing the experimental data to Shida's formulas leads to a carbon equivalency of 0.3 for the AISI 1018 grade. This is consistent with equation 5.21. For the micro-alloyed steel, the same equation gives a number of 0.21, whereas equation 5.20 gives a number of 0.29. The best fit to the experimental data is obtained by including Nb in the last term of equation 5.20. This results in a carbon equivalency of 0.30, i.e. identical to the low carbon steel's. Figure 5.11 illustrates experimental versus calculated flow stress for both steels. This figure might be seen as an indication of the accuracy of Shida's model. The error of $\pm 10\%$ is within the margin of error of Shida's original data (1974a, 1974b).

Finally, Figure 5.12 depicts the expected flow stress for some laboratory hot rolling conditions of AISI 1018, as calculated according to Shida's formulas. For the highest anticipated reduction (33%, $\epsilon = 0.4$), the flow stress is expected to increase from a low of about 100 MPa at 10 rpm and 1050°C to a high of above 300 MPa at 160 rpm and 825°C . The strain-rates correspond to those presented in Figure 5.9. These were calculated assuming sliding friction, i.e. according to equation (2.8), and a deformed roll radius according to equation (2.6). Lower reductions result in lower flow stresses.

Figure 5.10 Experimental Flow Stress for Nb-HSLA

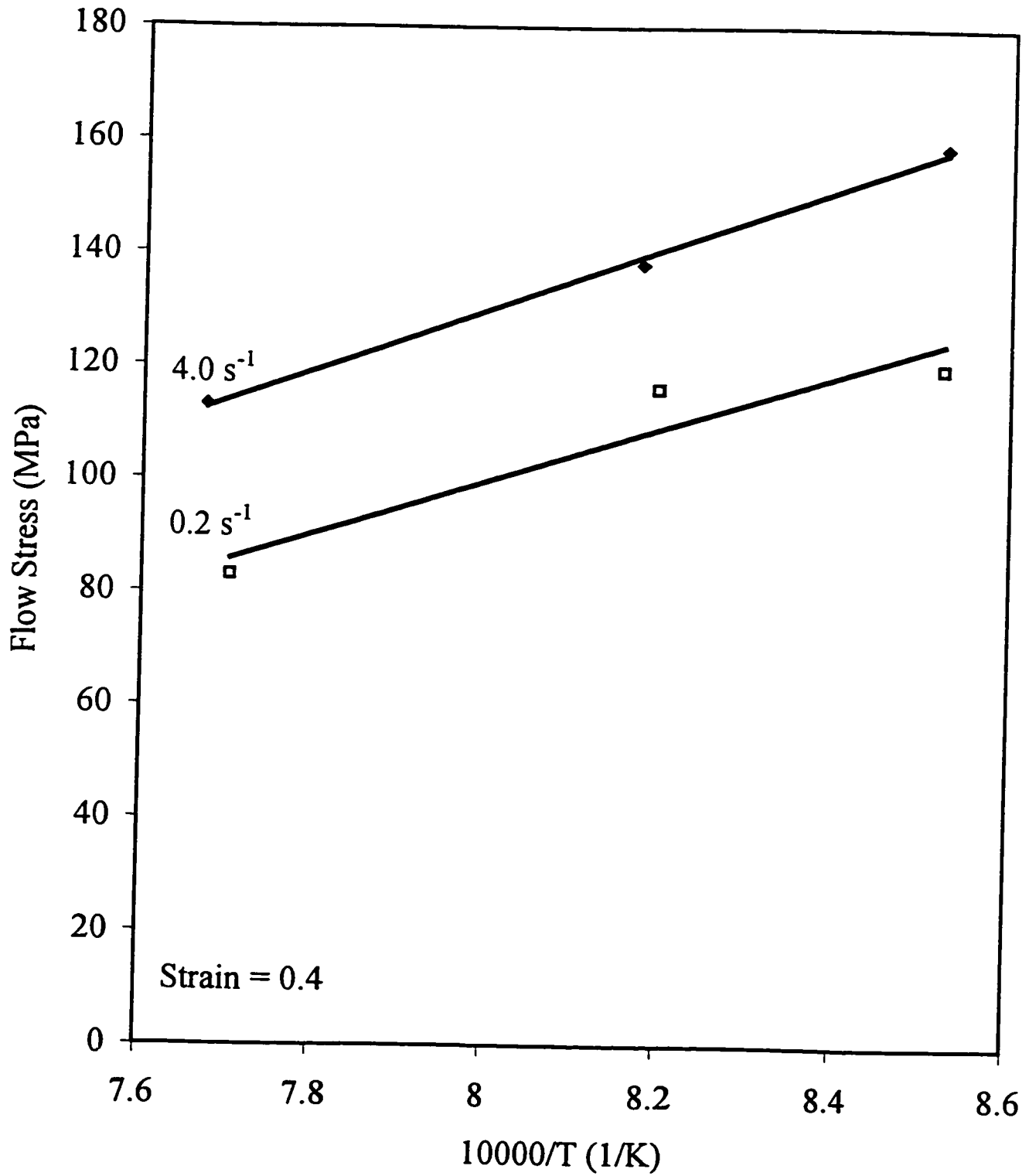


Figure 5.11 Experimental and Calculated Flow Stresses

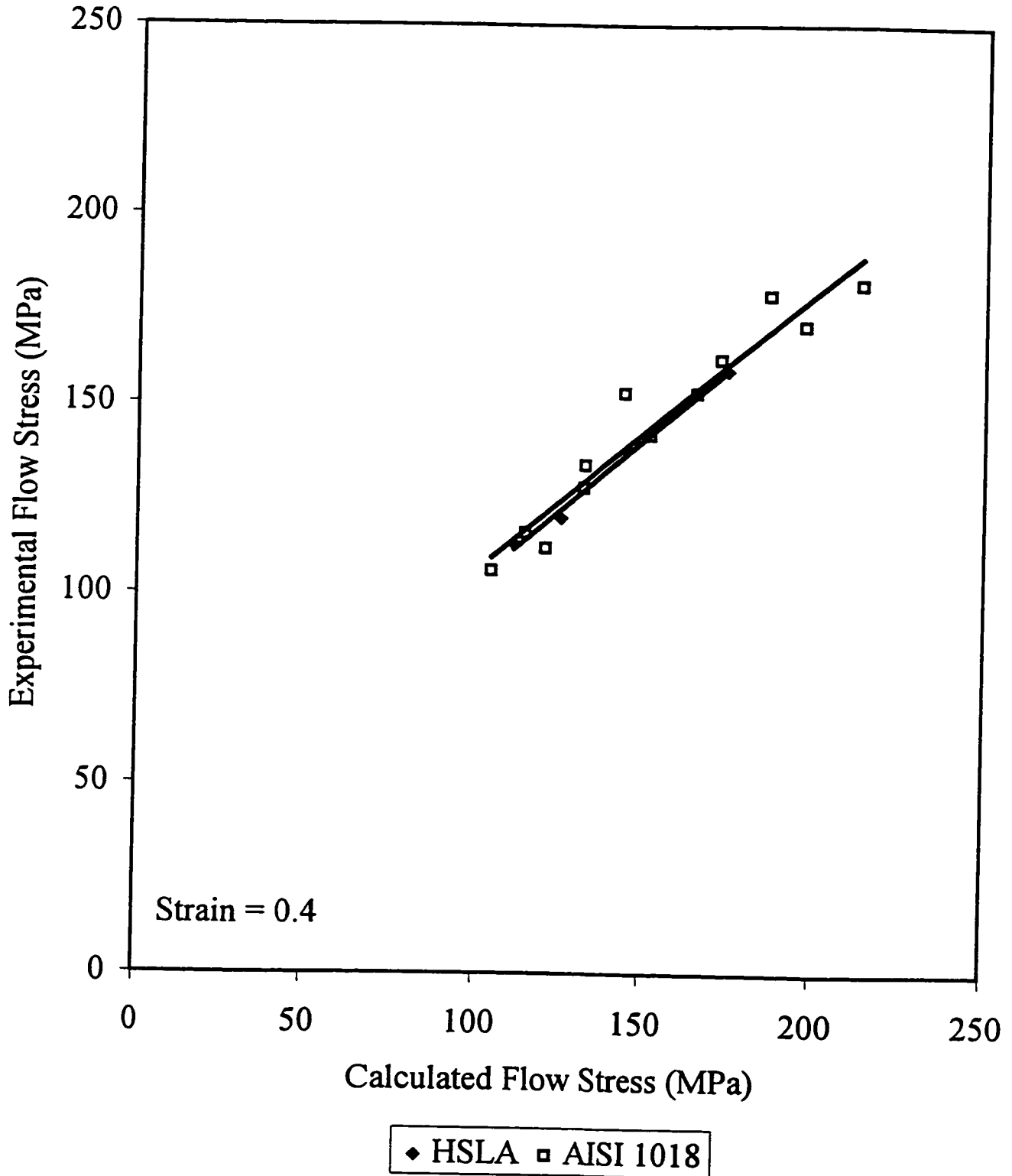
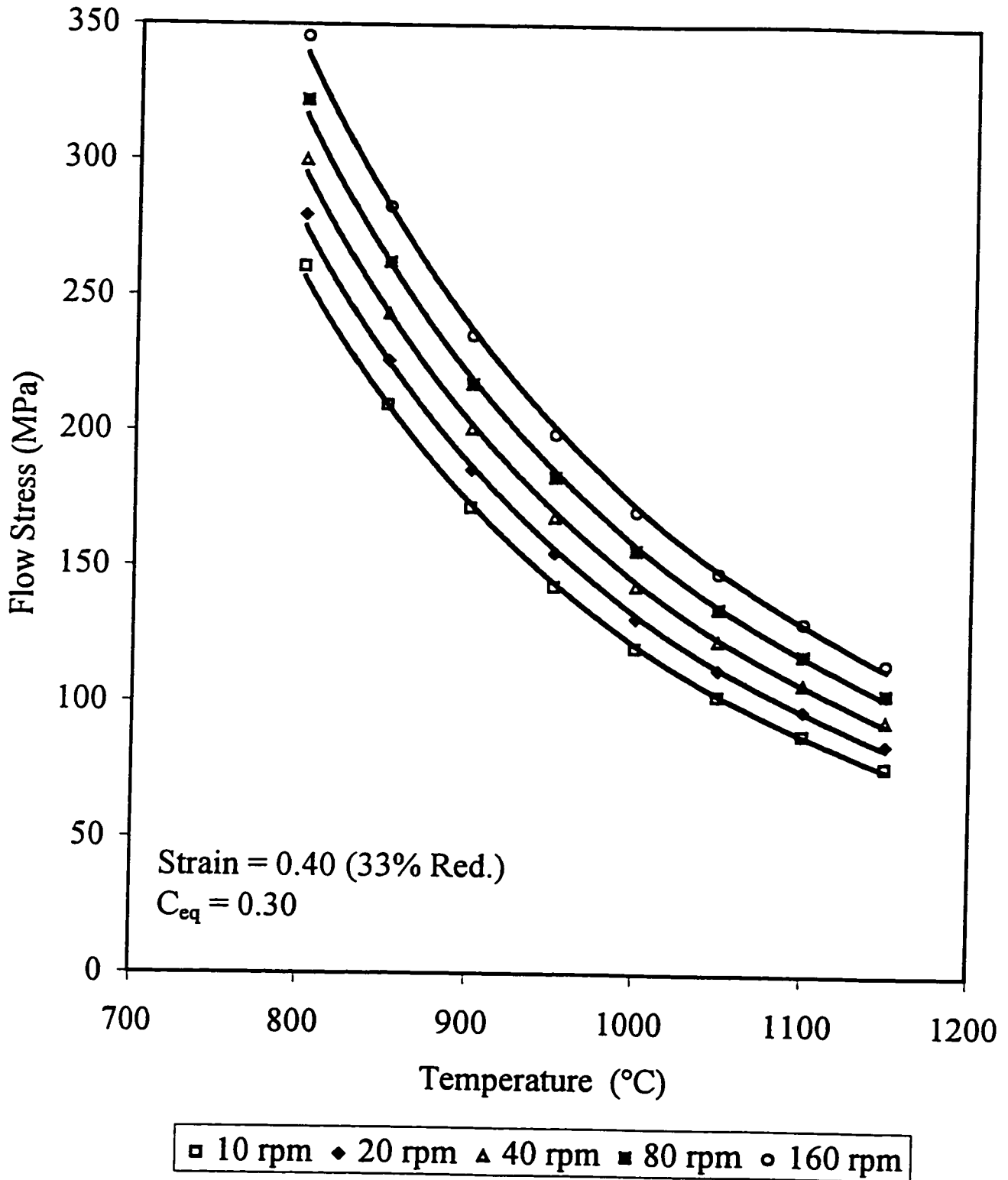


Figure 5.12 Modelling Flow Stress According to Shida



5.3 Conclusions

It can be concluded from the hot oxidation investigations presented in this chapter that:

1. Scale growth is parabolic with time and exponential with temperature, as monitored in terms of weight increase per unit surface area.
2. There is little difference in scale growth kinetics between low carbon and HSLA steels.
3. The amounts of magnetite and haematite are small for the laboratory conditions described.
4. Purging with oxygen-free nitrogen results in a drastically reduced scale growth, making it a useful tool in controlling scale growth prior to rolling.
5. A simple model based on mass balance may be used to predict the scale thickness.

The hot compression tests and the analysis of the results lead to the following conclusions:

1. Due to differences in initial microstructure, the two steels display similar flow stress behaviour.
2. Shida's formulas may effectively be used to describe the flow stress behaviour of both steels, in which case a carbon equivalence of 0.3 is used.

Chapter 6

Hot Rolling - Laboratory

Laboratory hot rolling experiments were carried out under controlled conditions in which one process parameter at a time was varied. Two grades of steel, one low carbon and one micro-alloyed were rolled at temperatures between 825 and 1050°C. The velocity ranged from a low of 140 mm/s to a high of 699 mm/s, whereas the reduction was increased from 12.5 to 32%. The effect of a variation in the scale thickness was also investigated, as scale thicknesses ranging from 0.015 to 1.59 mm were produced on the samples before rolling. The roll separating force, roll torque, and forward slip were measured along with the roll velocity and the surface temperature. These were used as inputs in the analysis of the results.

A commercial finite-element code, Elroll, previously described, is used in the analysis of the results. Two parameters - the coefficients of heat transfer and friction - may be chosen at will. The heat transfer coefficient has been determined in previous experiments and a value of 10 - 30 kW/m²K has been established, depending mainly on pressure, as proposed by Wankhede *et al.* (1997). The constants in their proposed equation were modified to agree with experimentally measured numbers of the coefficient of heat transfer. This resulted in an equation that described the conditions in the Manufacturing Laboratory at the University of Waterloo:

$$h = \frac{P}{3} - 40 \text{ (kW / m}^2\text{K)} \quad (6.1)$$

where p is the roll pressure in MPa. This equation is limited to roll pressures greater than 120 MPa. The coefficient of friction is then chosen such that the calculated and measured values of the roll force, the roll torque and the forward slip agree as closely as possible.

The scale growth was modelled according to the kinetics of oxidation. The difference in scale thickness resulted in different initial sample thickness, depending on soaking time and furnace environment, as described in Chapter 5. The sample thickness was therefore corrected by calculating the thickness increase due to scale formation and the thickness decrease due to material loss of the substrate for the various soaking times, assuming 100% wüstite.

Although the finite-element calculations provide some results on the thermal events at the interface, it is more convenient to monitor these with closed form equations, which indicate the prevailing trends.

Adiabatic temperature rise due to deformation and temperature drop due to conduction to the rolls was approximated along with the instantaneous contact temperature in order to gain insight in possible contributions of roll chilling on sample flow stress. The adiabatic temperature rise, ΔT_D , in the stock was modelled according to the following equation (Richardson *et al.*, 1985):

$$\Delta T_D = \frac{w_D t_c}{V \rho_s C_p} \quad (6.2)$$

where w_D is total power required for plastic deformation calculated from roll torque in W, t_c is the contact time given by the contact angle, V is the volume, ρ_s is the steel sample's density (7550 kg/m³), and C_p is its specific heat (656 J/kg°C).

The temperature drop due to conduction, ΔT_K , can, under assumptions of perfect contact between the rolls and the sample be described by (Richardson *et al.*, 1985):

$$\Delta T_K = \frac{2A(T_S - T_C)}{V\rho_S s_S} \sqrt{\frac{\rho_S s_S K_S t_c}{\pi}} \quad (6.3)$$

where A is the contact area, V is the volume of metal under deformation, K_S is the thermal conductivity of the sample (27.45 W/m°C), T_S is the sample temperature, and T_C is the instantaneous contact temperature:

$$T_C = \frac{T_S \sqrt{K_S \rho_S s_S} + T_R \sqrt{K_R \rho_R s_R}}{\sqrt{K_S \rho_S s_S} + \sqrt{K_R \rho_R s_R}} \quad (6.4)$$

where subscripts R refer to the roll material, for which the density is taken as 7840 kg/m³, specific heat as 481.3 J/kg°C, and the thermal conductivity as 48.13 W/m°C.

Since an infinite heat transfer was assumed in the initial approximation, the true temperature drop due to conduction is exaggerated. Due to the insulating nature of the scale layer, and according to Hollander's comparison of theoretical and experimental findings (1970) the true temperature drop due to conduction shall be taken as $0.6\Delta T_K$.

An important indication of the number of adhesive bonds between the rolls and the steel sample is the ratio between real area (A_r) and apparent area (A_a) of contact. In cases when the real area approaches that of the apparent area, a maximum number of adhesive bonds may be found. This can potentially result in a high value of the coefficient of friction, since more energy is needed to break these bonds.

Bay and Wanheim (1976) and Wanheim and Bay (1978) proposed the following relationship between the coefficient of friction, the friction factor, m , the tool pressure, p ,

and shear flow strength of the softer material, k :

$$\mu = \frac{mk}{p} \frac{A_r}{A_a} \quad (6.5)$$

Wanheim and Bay (1978) also plotted the coefficient of friction as a function of the friction factor. Regression analysis of their data allows the friction factor to be described in terms of the coefficient of friction, as $m = f(\mu)$. The ratio between the real and apparent contact area can thus be calculated from the experimentally found coefficient of friction and roll pressure as:

$$\frac{A_r}{A_a} = \frac{p}{k} f(\mu) \quad (6.6)$$

Apparently, a high pressure or low shear flow strength provides a greater real contact area between the rolls and sample. The apparent contact area becomes the real contact area when the ratio approaches unity. Regression analysis of Wanheim and Bay's data results in the following relationship between the friction factor and the coefficient of friction:

$$m = 4.3923\mu - 4.1402\mu^2 - 1.4522\mu^3 \quad (6.7)$$

which together with equation (6.6) enables the calculation of the ratio between the real area and apparent area of contact.

Table 6.1 illustrates the typical procedure in analysing an experiment. A best match is sought in as many parameters as possible. The roll separating force is always of the highest priority, since it is measured with the greatest accuracy. In this case, the best match is obtained for $\mu = 0.31$, as both the calculated roll separating force and forward slip match the measured closely. Apparently, a 10 % difference in μ causes a 4 %

difference in roll separating force and forward slip.

μ	P_{measured} (kN/mm)	M_{measured} (Nm/mm)	$S_{f,\text{measured}}$ (%)	$P_{\text{calculated}}$ (kN/mm)	$M_{\text{calculated}}$ (Nm/mm)	$S_{f,\text{calculated}}$ (%)	Note
	3.70	32.0	7.35				Expmnt
0.33				3.83	32.87	7.40	Elroll
0.31				3.70	32.29	7.32	Elroll
0.30				3.67	32.26	7.14	Elroll

Table 6.1 Typical Procedure of Determining the Coefficient of Friction (LC1312, 910°C, 32% reduction, 21 rpm, 0.29 mm scale thickness)

6.1 The Effect of the Temperature on the Coefficient of Friction

After being soaked at 1200°C for 20 minutes, two different entry heights are rolled at various temperatures ranging from 820 to 1050°C while maintaining the velocity constant at 175 mm/s. One set of data is for an initial height of 6.21 mm and the other is for an initial height of 12.65 mm. A reduction of 32% is achieved in both cases. Figures 6.1-6.3 illustrate the effect of the temperature on the roll separating force, roll torque, and forward slip. It can be seen that the roll separating force decreases with increasing temperature, because of decreasing flow stress. The same goes for both roll torque, and forward slip. This may be seen as indicative of the trends in the coefficient of friction. The forward slip ranges from a high of 9% and a low of 7%. This is well within the data presented by Wallquist (1955, 1960, 1962) for similar conditions. Due to the increased amount work that is associated with the thicker sample, both roll torque and roll separating force are greater for this geometry.

The experimental data on the roll separating force, roll torque, and forward slip were used to calculate the coefficient of friction presented in Figure 6.4. In the case of the lower thickness, the coefficient of friction reaches a maximum of 0.39 at the lowest temperature (820°C) and a minimum of 0.2 at the highest temperature (1050°C). In the case of the thicker samples of 12.65 mm, the coefficient of friction approaches a maximum of 0.39 at 878°C and a minimum of 0.33 at the highest temperature (1006°C). The coefficient of friction reaches a value of 0.38 at the lowest temperature (836°C) for this series. Nevertheless, the effect of temperature is clear since an increase lowers the coefficient of friction in both cases, in a fairly linear fashion.

The change in the coefficient of friction can be explained by two phenomena. The first concerns the adhesive bonds that form between the sample and the rolls upon contact, which are harder to separate as the temperature drops. The required shear stresses increase, thereby increasing the frictional forces. Furthermore, the material's flow stress

Figure 6.1. Roll Separating Force as a Function of Temperature

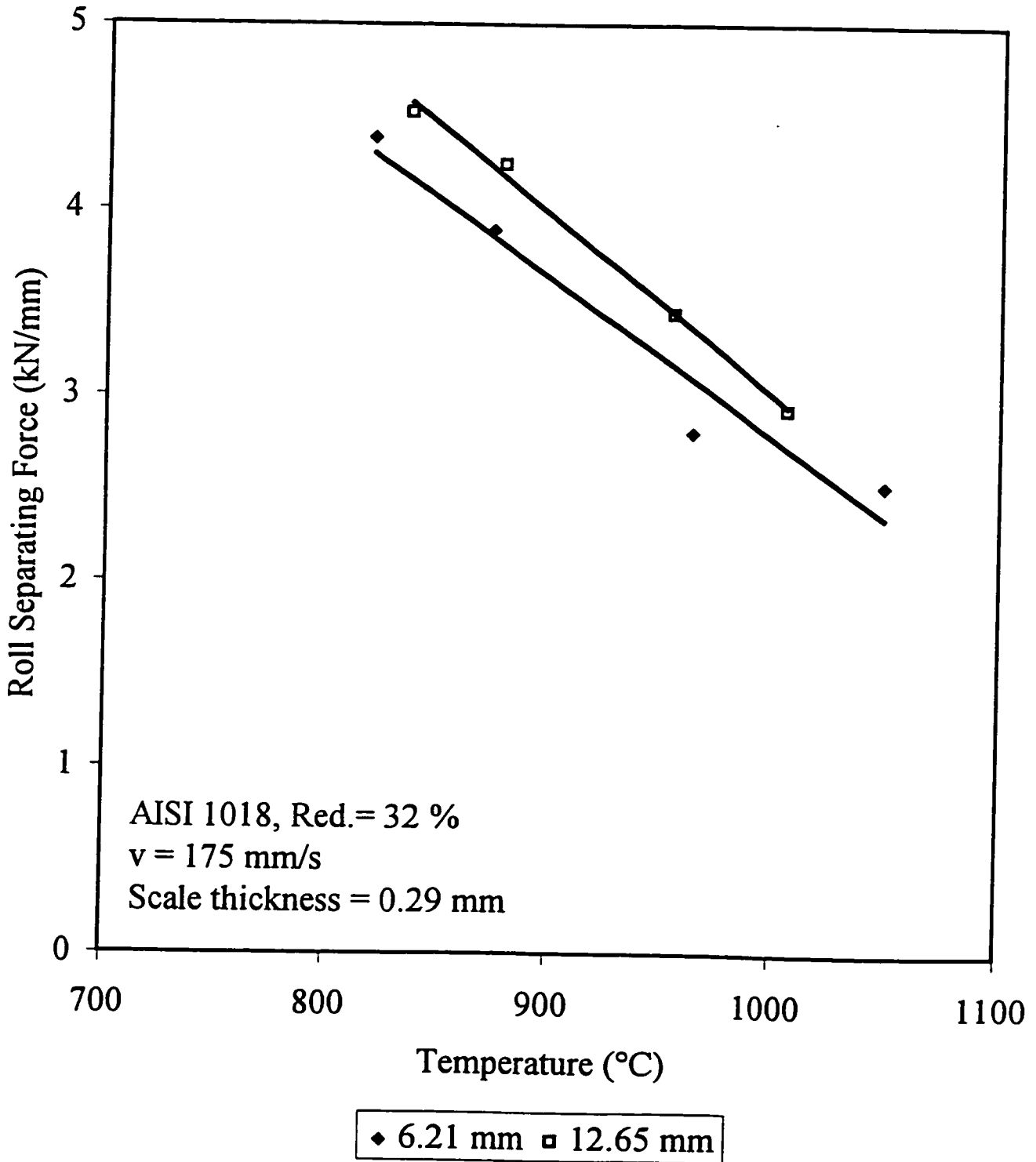


Figure 6.2. Roll Torque as a Function of Temperature

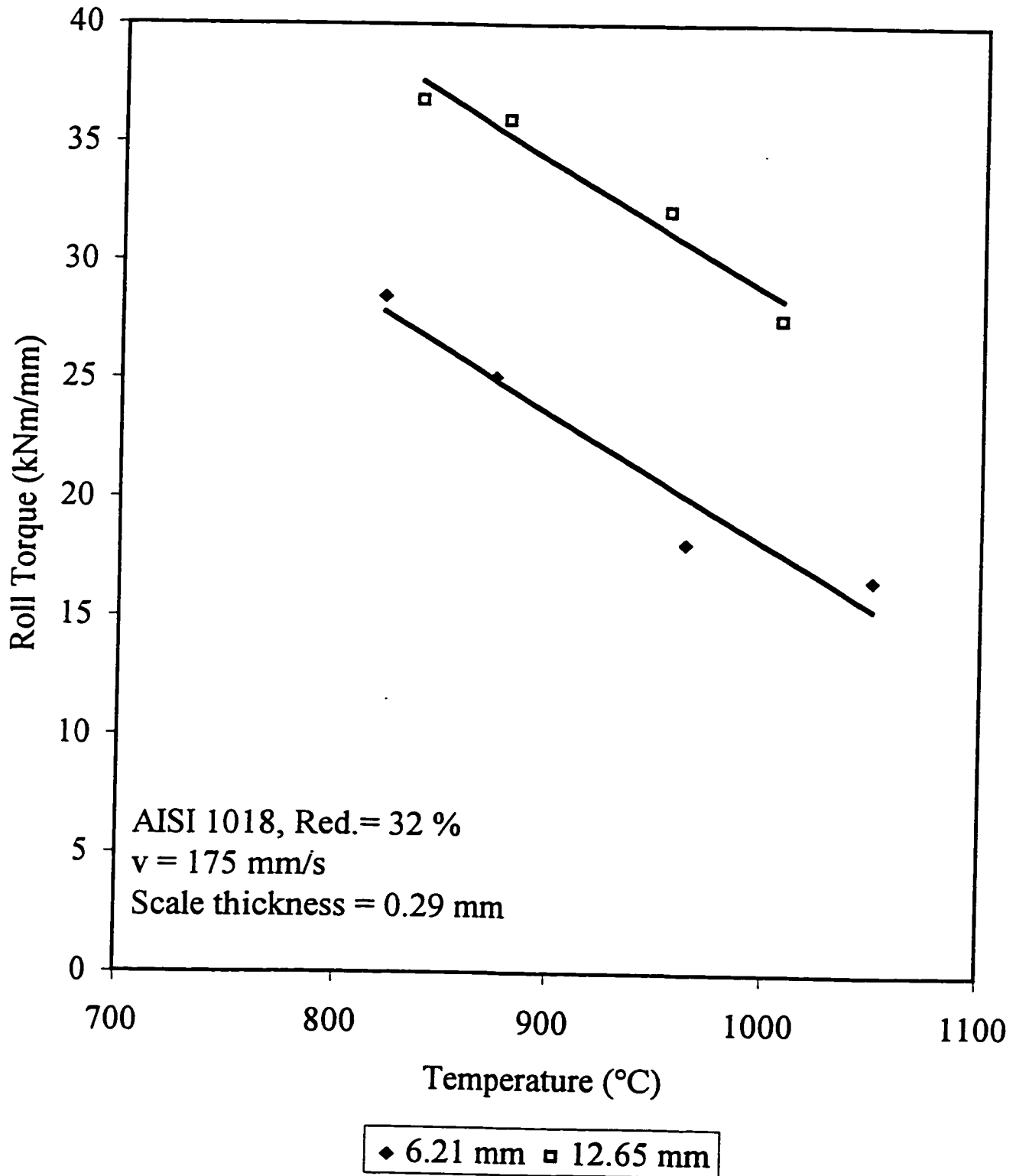


Figure 6.3. Forward Slip as a Function of Temperature

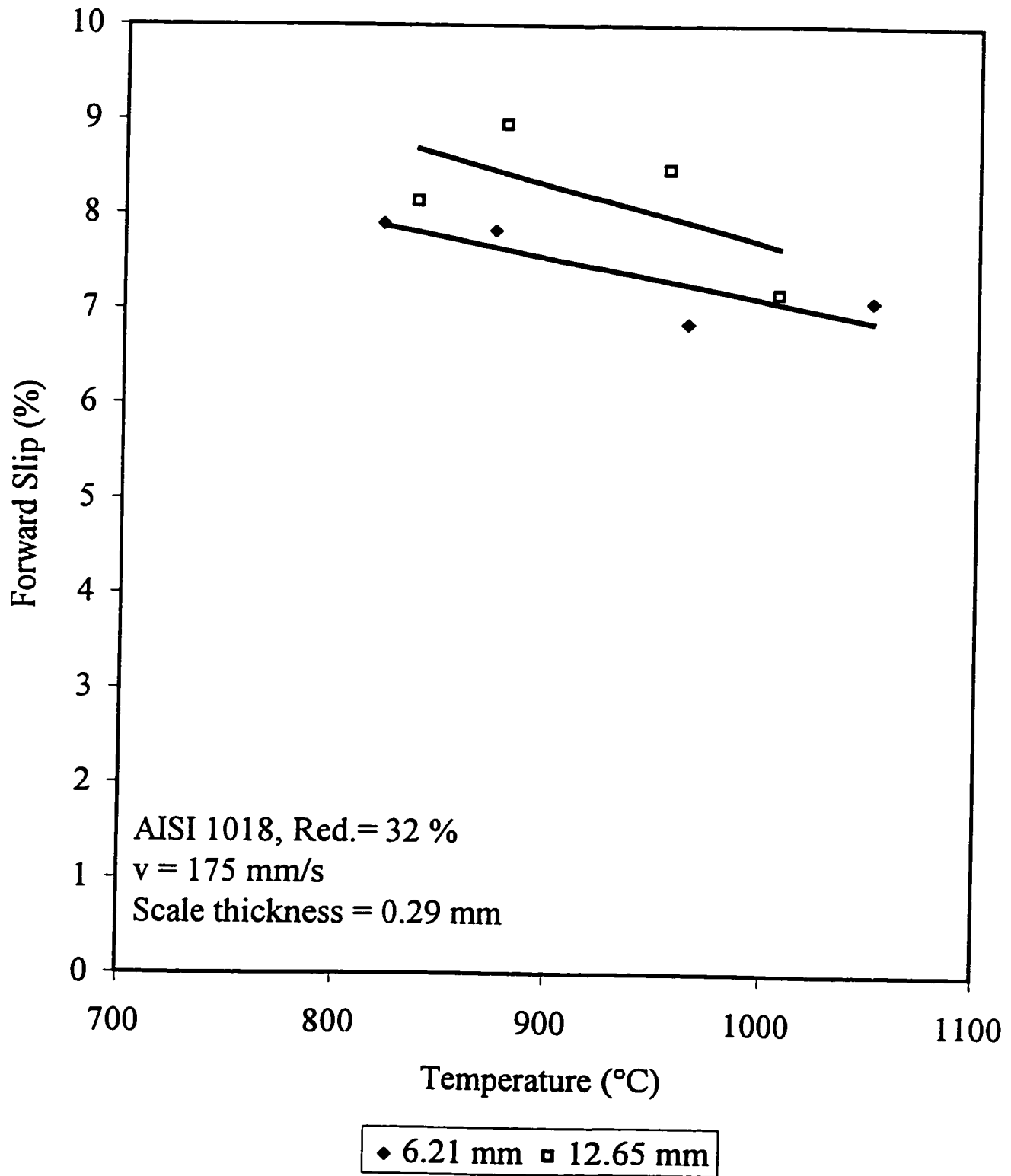
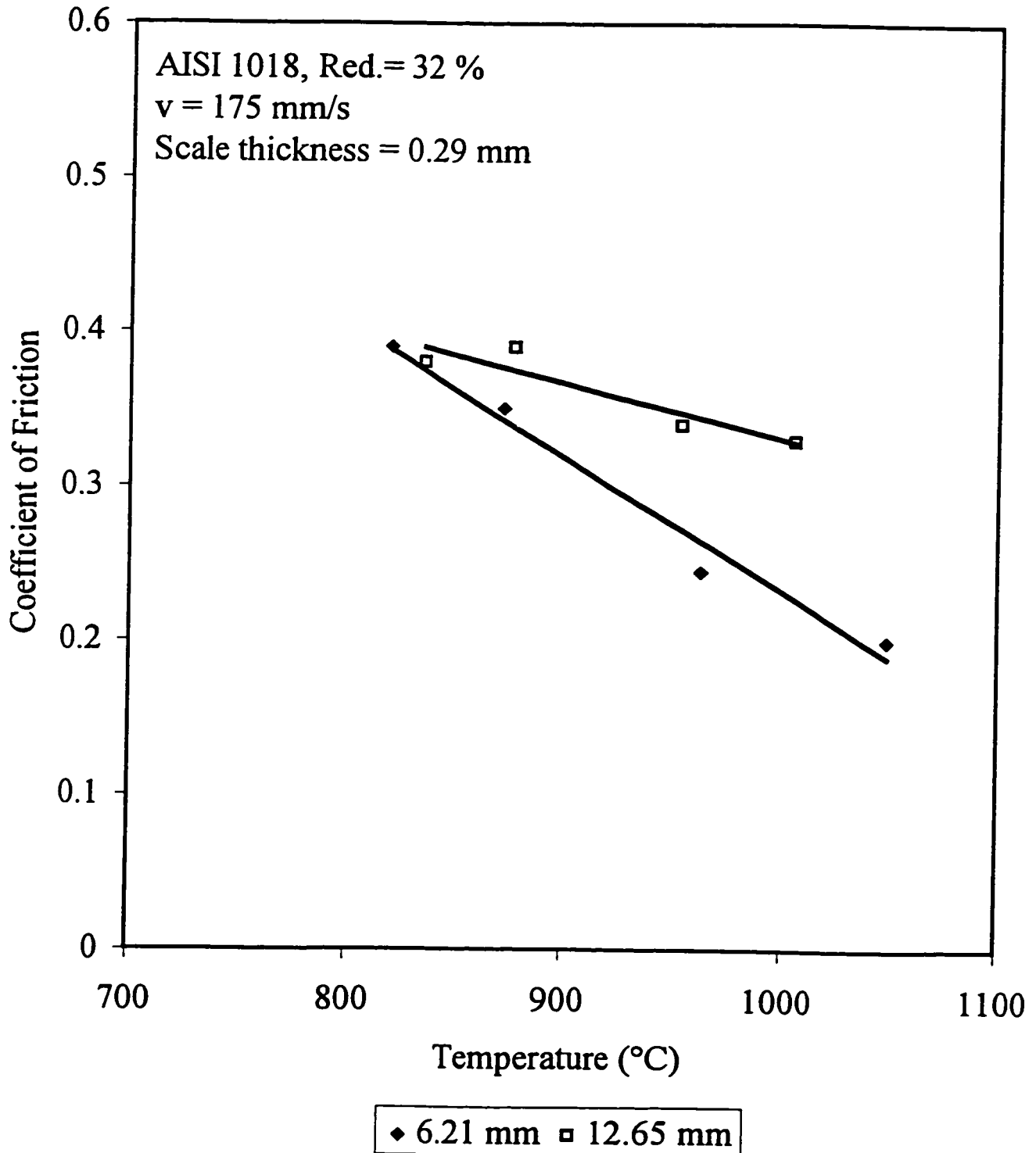


Figure 6.4. The Coefficient of Friction as a Function of Temperature



increases with decreasing temperature because of the strengthening mechanisms described earlier. The asperities on the surface become harder to deform, resulting in an increased friction.

The chemical composition of the scale is temperature dependent. A greater amount of hard oxide, such as haematite, would in such a case also increase the coefficient of friction. However, the scale on these samples were all of the same composition, mainly wüstite, since they were all soaked at the same temperature for the same amount of time. The chemical composition of the scale was probably not affected by the temperature. Nevertheless, it was noted that the amount red oxide left on the sample upon cooling was indeed affected by the temperature and the pressure, as a lower temperature and a higher pressure left more on the surface. This, however, appeared to be the effect of the breaking of the scale and powdering some of the wüstite, which, in the absence of iron ions becomes free to oxidise further to become haematite. It was also noted that the scale broke up from the edge and growing towards the centre of the sample. The cracks were initiated as the sample entered the deformation zone and grew continuously until exit, a result of the sample expanding in and perpendicular to the rolling direction. This often resulted in cracked edges and a centre section that blistered up. The greatest red oxide amount was found where the pressure was highest, i.e. in the centre of the sample.

The approximations of the temperature rise, due to deformation, and temperature drop, due to conduction, indicated that the overall sample temperature dropped more at high temperatures than at low (32° compared to 19°C). Sample size played a significant role, as the thin samples experienced a greater temperature drop than the thick samples (54° compared to 43°C).

6.2 The Effect of the Velocity on the Coefficient of Friction

Figures 6.5-6.7 illustrate the effect of roll velocity on roll separating force, roll torque, and forward slip. AISI 1018 samples, 12.65 mm thick, were soaked at 1200°C for 20 minutes and were rolled at various velocities ranging from a low of 140 mm/s to a high of 699 mm/s. It can be seen that the roll separating force increases with roll velocity. This is due to strain-rate sensitivity of the metal substrate, an effect that gets more pronounced at lower temperatures. The measured roll torque does not display a similar effect, as the numbers in two out of four cases appear to decrease slightly with increasing roll velocity. One very possible explanation is the contribution of frictional effects, which indicate that the coefficient of friction might decrease with increased velocity. The effect on forward slip shown in Figure 6.7 indicates a dramatic drop from about 7 to 2%, as the roll velocity is increased from 170 to 700 mm/s. This trend in the forward slip is a clear indication of what the effect will be on the coefficient of friction, as rolling theory says that a decrease in forward slip results from a lower coefficient of friction. This, in turn, reduces the roll torque. In other words, the trend in the forward slip corroborates the trend found in the roll torque, both indicating that the coefficient of friction will decrease with roll velocity. It was also visually observed that roll velocity affected the break-up of the scale, as a lower roll velocity resulted in a greater amount red oxide on the surface. This may be attributed to the fact that a lower velocity causes greater chilling of the sample's surface, which in turn causes the scale to expand and then break up.

The effect of the velocity on the coefficient of friction is given in Figure 6.8. The figure shows that the coefficient of friction drops from a high of 0.36 at a velocity of 140 mm/s and a temperature of 825°C to a low of 0.17 at a velocity of 699 mm/s and a temperature of 1050°C. The trend is clear, showing that an increase in the velocity results in decreasing coefficients of friction.

Figure 6.5. Roll Separating Force as a Function of Velocity

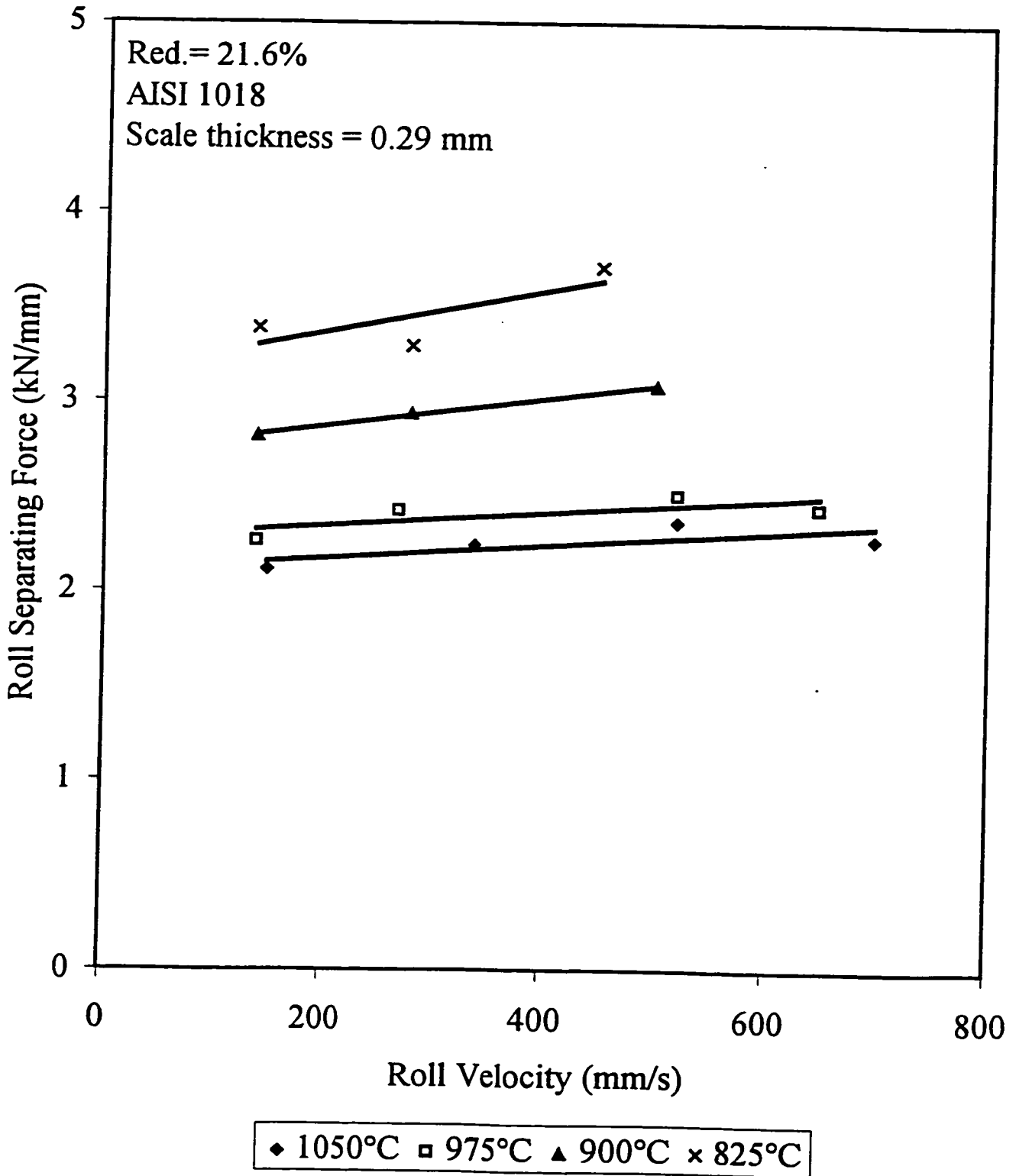
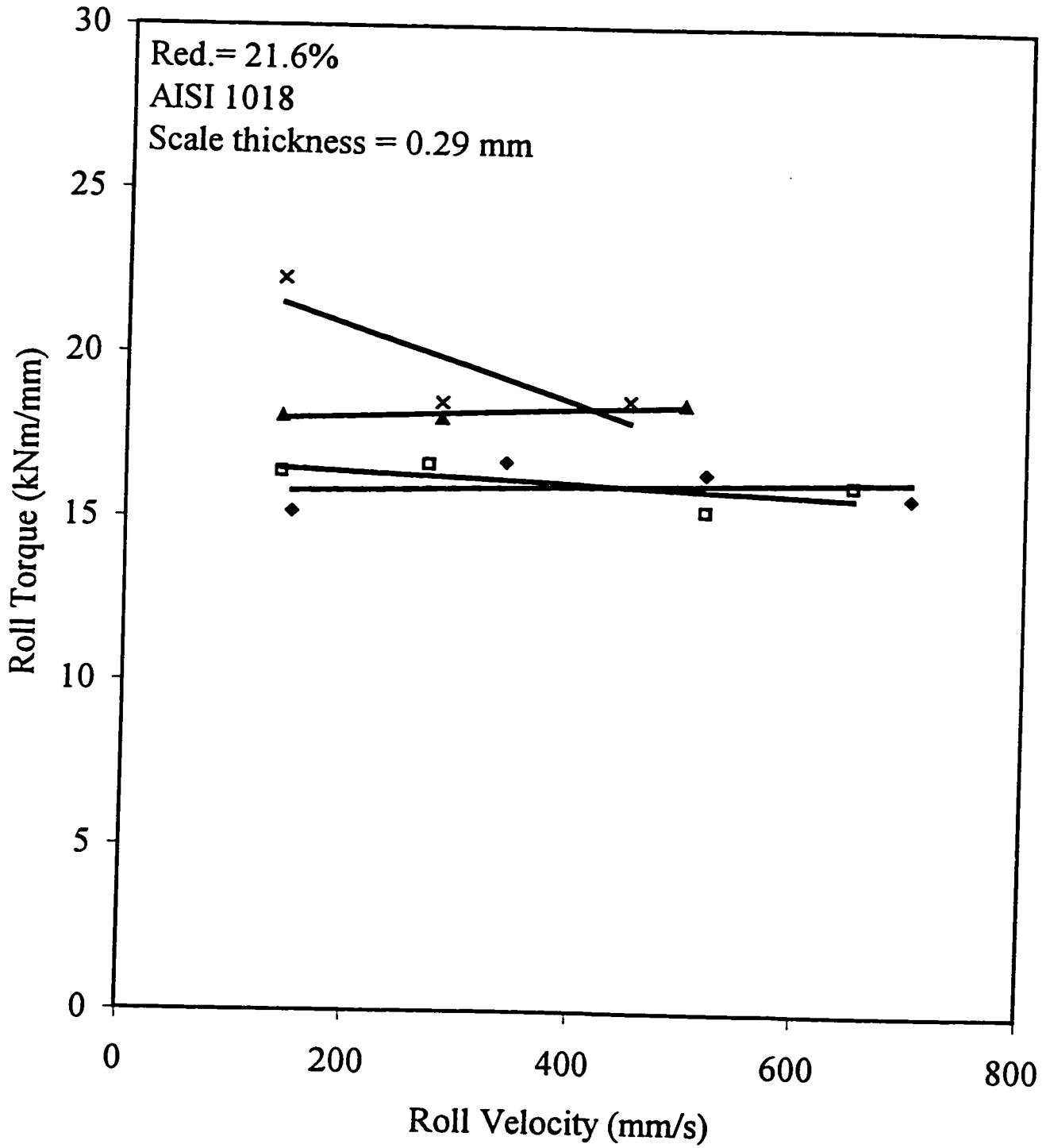


Figure 6.6. Roll Torque as a Function of Velocity



◆ 1050°C □ 975°C ▲ 900°C × 825°C

Figure 6.7. Forward Slip as a Function of Velocity

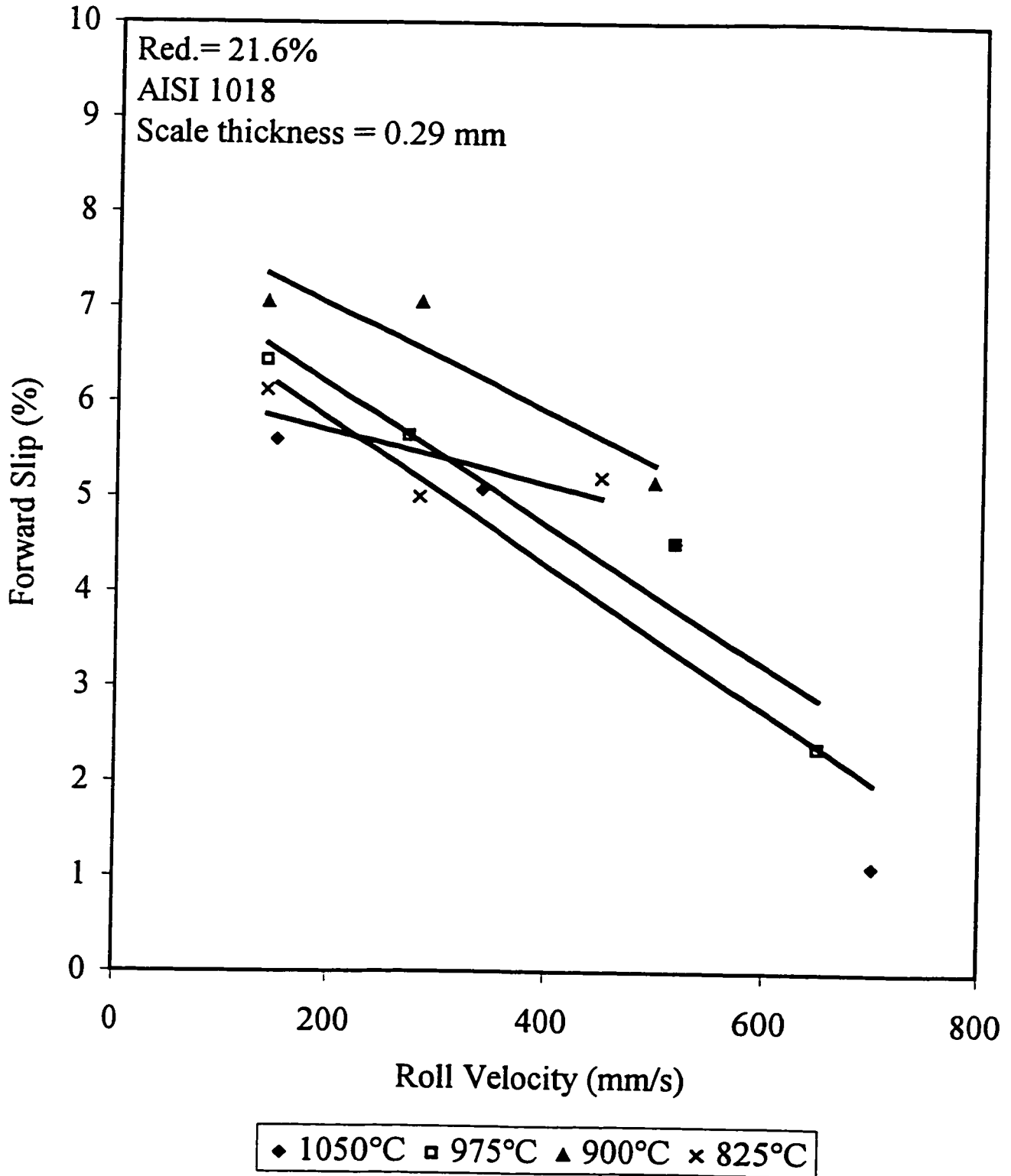
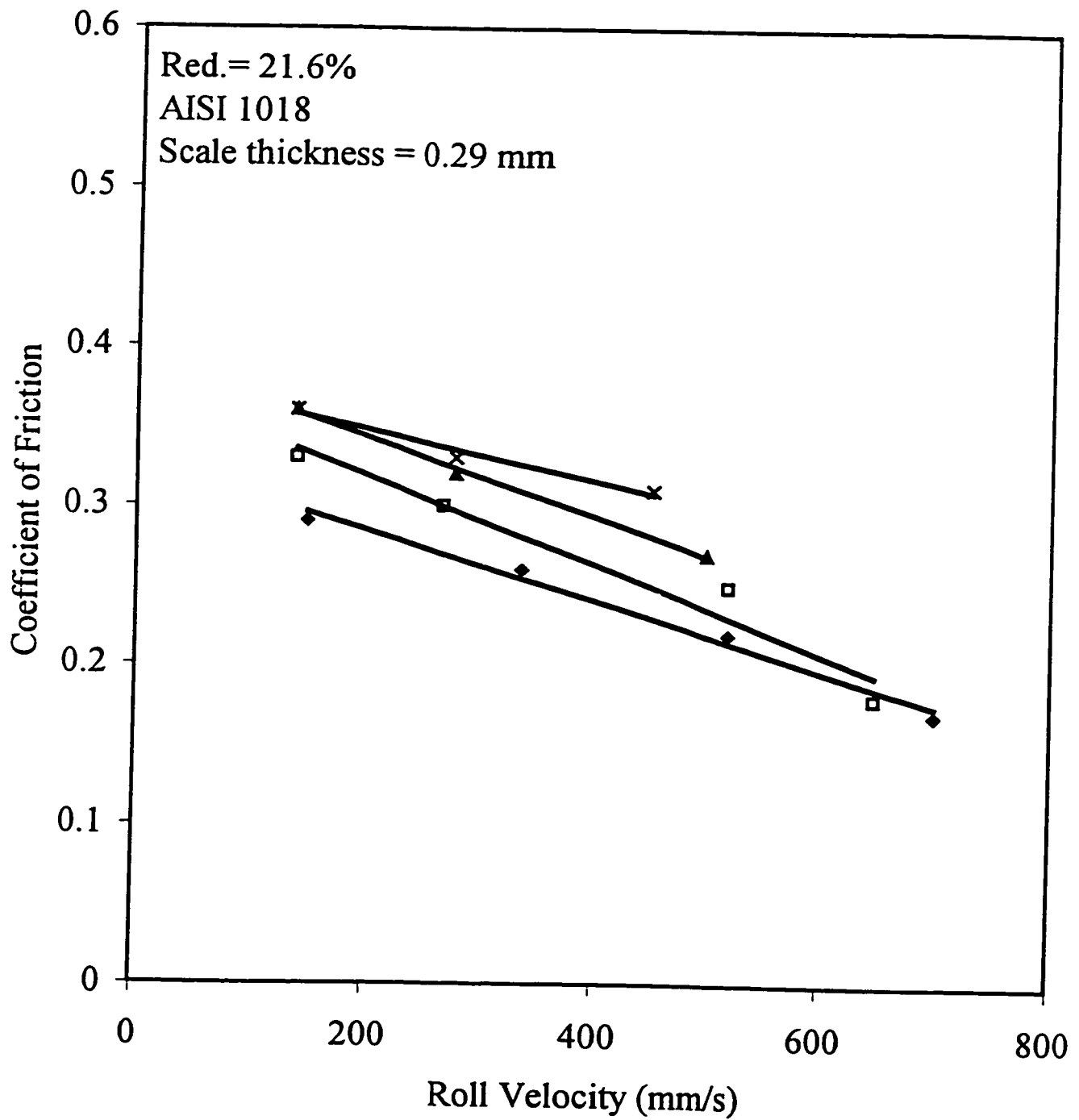


Figure 6.8. The Coefficient of Friction as a Function of Velocity



◆ 1050°C ◻ 975°C ▲ 900°C × 825°C

The investigated conditions resulted in strain rates ranging from 1.8 to 32.8 s⁻¹. An increase in material flow stress from 96 to 152 MPa caused by the higher strain-rates seems to have little influence on the frictional conditions. However, the local increase in flow stress caused by heavier chilling at lower velocities is likely to contribute to an increase in the coefficient of friction. The role of the velocity on the chilling effects was estimated to be around 12°C for the higher velocities compared to 37°C for the lowest velocity. Undoubtedly, this effects the material's flow stress strongly. This corresponds to an increase in average flow stress from 127 to 144 MPa at 1000°C or from 166 to 192 MPa at 900°C. The effects of an increase in actual flow stress on the surface and in the subsurface are expected to be far more severe.

The reason for the decrease in the coefficient of friction with increasing velocities is also explained by the adhesion theory. High velocities mean shorter roll/sample contact times. The higher velocities leave less time for adhesive bonds to form between the rolls and the sample, resulting in fewer bonds to be broken. The shorter contact leaves less time for chilling of the surface and subsurface, making it easier to break the adhesive bonds. It was also noted that the ratio between real and apparent contact area approached unity for the lower velocities whereas a ratio of 0.6 was common for the higher velocities. This means that there is a probability of a higher number of adhesive bonds at lower temperatures.

The pioneering findings by Tafel and Schneider (1924) may be seen as corroborative, since they found that the minimum angle of bite was strongly affected by rolling speed. Ekelund (1927) later derived an equation from roll gap geometry which shows that the minimum angle of bite increases as friction increases ($\mu > \tan\alpha_{\min}$). However, this relationship is insensitive to all but geometry and greatly underestimates the coefficient of friction. Wusatowski (1969) quoted Pavlov and Kuprin's findings on the effect of rolling speed for a Ni-Cr micro-alloyed steel. Although their numbers on μ are greater, the trend is similar to the one presented in Figure 6.8.

6.3 The Effect of the Reduction on the Coefficient of Friction

The effect of reduction on roll separating velocity, roll torque, and forward slip can be seen in Figures 6.9 - 6.11. These all increase as the reduction is increased from 12.5 to 32%. As well, lower temperatures produce higher forces and torques. The most severe effect of the increase in reduction is on the roll torque, which increases one order of magnitude, while the roll separating force triples - a result of increased work. The numbers on the forward slip, shown in Figure 6.11, increase from a low of about 4% to a high of just below 10%. These numbers are close to those presented by Wallquist (1955) for similar conditions. It was noted that the amount red oxide was greater for the higher reductions. Once again, the amount red oxide increased with increasing pressure.

Figure 6.12 shows that the coefficient of friction increases with increasing reduction. The coefficient of friction has a value of 0.24 at a reduction of 12.5 % and a temperature of 975°C. This increases as the temperature decreases at the same reduction. The coefficient of friction reaches a maximum of 0.34 at this reduction for a temperature of 825°C. The coefficient of friction gradually increases as the reduction is increased, first to 21.6 % and then to 30.7 %, reaching its maximum of 0.39 at 900°C. Its value is 0.38 at 825°C, a difference that is insignificant.

As the reduction is increased the deformation zone and the contact time increase. As above, these increase the number of adhesive bonds, resulting in higher frictional resistance. These phenomena lead to an increase in the coefficient of friction. In fact, a reduction of 12.5% produced a real/apparent contact area ratio of 0.73 at temperature of 900°C and a velocity of 280 mm/s. A reduction of 21.6% for the same conditions resulted in a contact area ratio of 0.8, which grew to 0.87 for a 30.7% reduction. This behaviour was common at other temperatures and velocities as well and clearly corroborates the hypothesis that more adhesive bonds form at higher reductions.

Figure 6.9. Roll Separating Force as a Function of Reduction

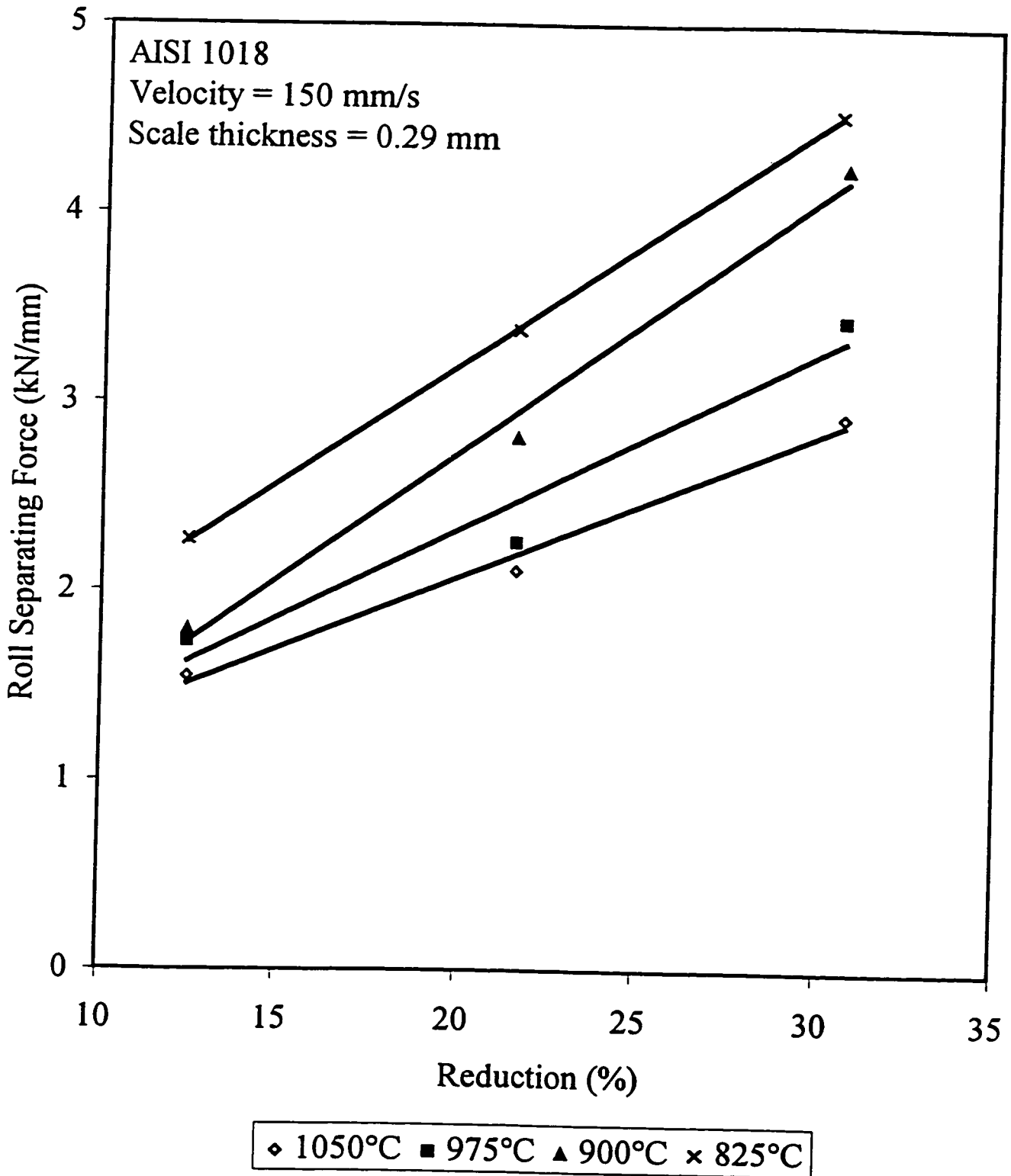


Figure 6.10. Roll Torque as a Function of Reduction

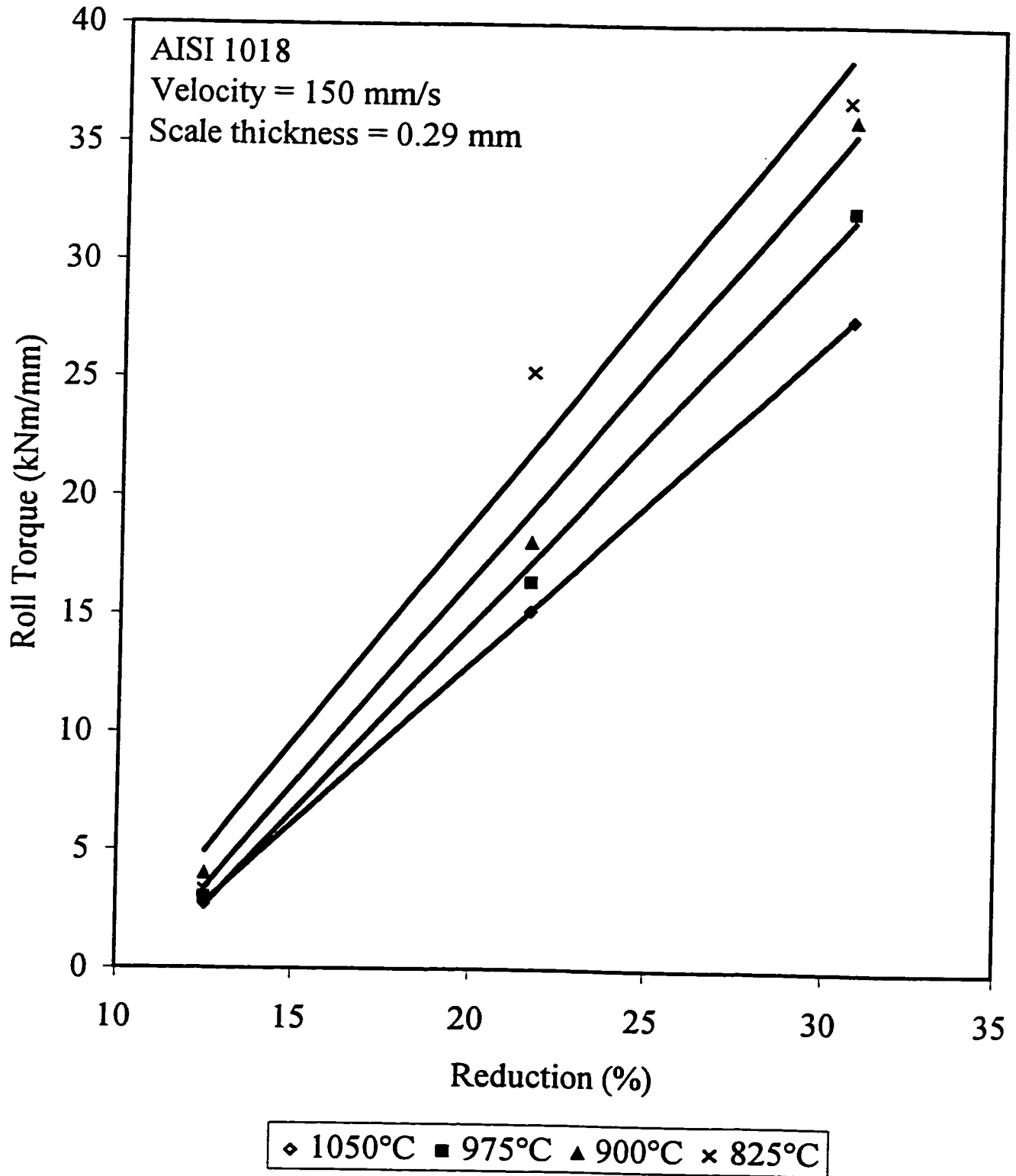


Figure 6.11. Forward Slip as a Function of Reduction

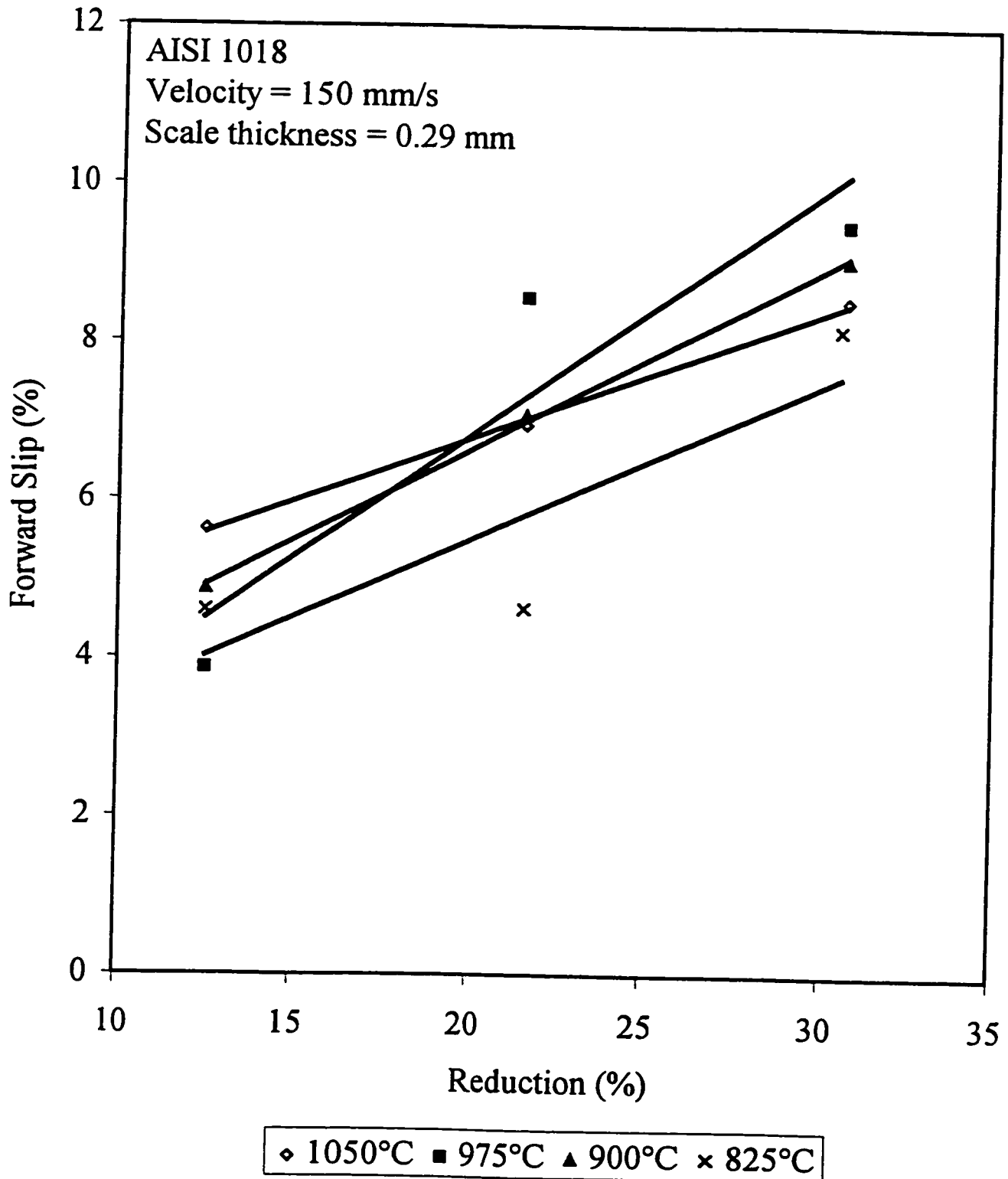
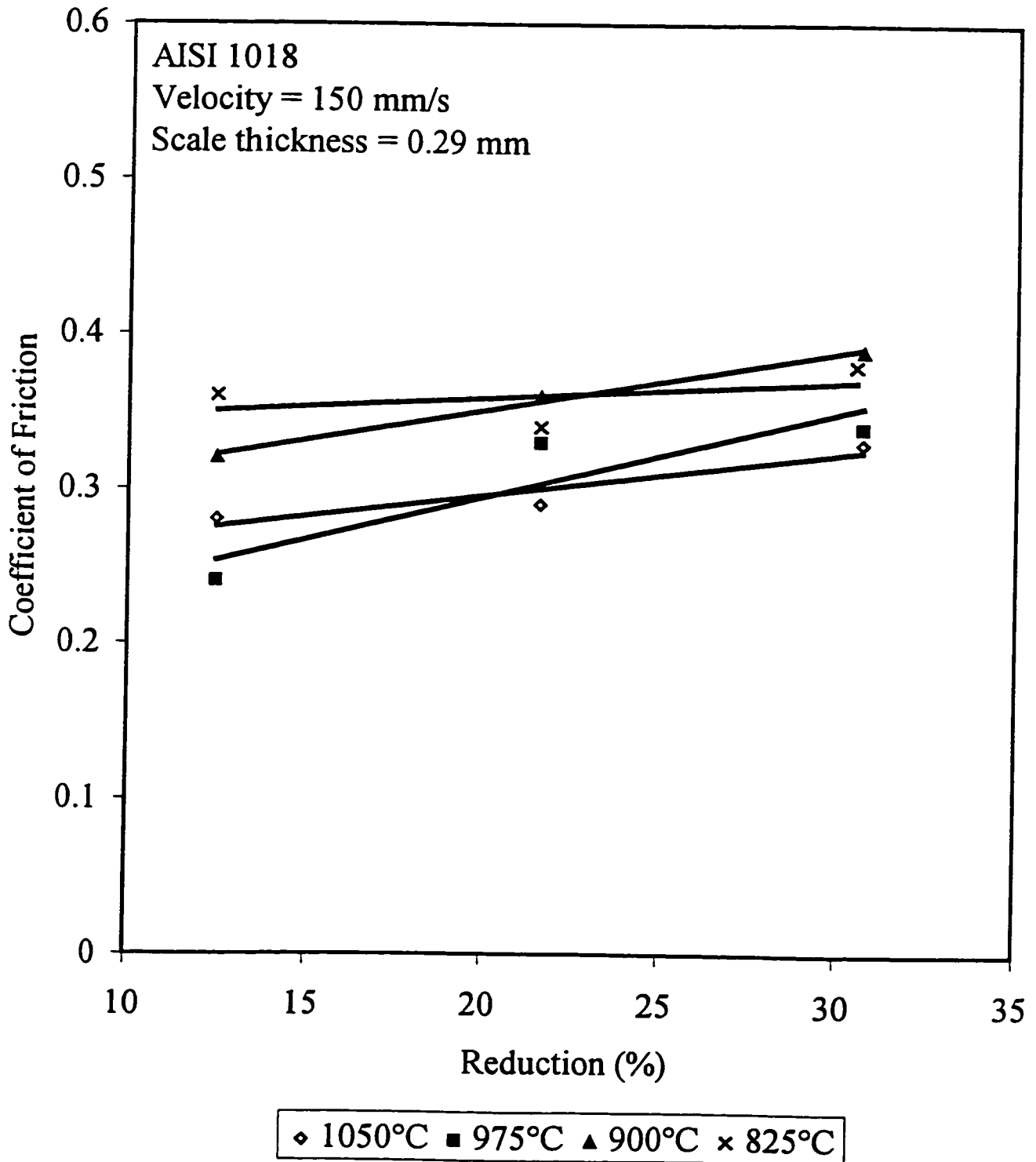


Figure 6.12. The Coefficient of Friction as a Function of Reduction



The higher pressures present at greater reductions also increase the overall flow stress. Furthermore, the potential for scale breakage increases as the normal pressures grow, leaving progressively more metal-to-metal contact, and even more resistance to relative motion of the contacting surfaces. In spite of these events, which appear to reinforce one-another, the rate of increase of μ with reduction is not very large. The reason is best understood when the effects of chilling of the surface are studied. A change in reduction from 12.5 to 30.6% only resulted in a 4.5°C difference in temperature. This corresponds to a 4 MPa change from 200 MPa in average flow stress at a temperature of 900°C and roll velocity of 280 mm/s. This difference of mere 2% can hardly be expected to affect the frictional stresses and the coefficient of friction, since there is at least a 2% error margin in match between measured and calculated roll separating force.

6.4 The Effect of the Steels' Chemical Composition on the Coefficient of Friction

The effect of the steels' chemical composition on the roll separating force, roll torque, and forward slip is illustrated in Figures 6.13-6.15, where the two different grades are rolled to a reduction of 21.6 % at a target temperature of 1050°C. The velocity is gradually increased from a low of about 150 mm/s to a high of 699 mm/s. Evidently, the low carbon steel produces higher forces, but lower torques than the micro-alloyed steel, with similar hot strength. The effect on the forward slip indicates that higher numbers on the coefficient of friction may be expected for the HSLA grade. The highest values for both grades are produced at the lowest velocity. However, the HSLA grade demonstrates a value that is about 20% greater than the low carbon grade's. This difference decreases gradually as the velocity increases, and culminates in a similar value at the highest velocity.

The higher roll separating forces seen by AISI 1018 are due to lower temperatures. The target temperature was in both cases 1050°C. However, the real temperature was in the region 1007 - 1025°C for the AISI 1018 grade, whereas it ranged between 1034 to 1064°C for the HSLA grade. This is enough to cause the measured 10% difference in roll separating force. The higher roll torques for the HSLA grade, along with the trends in forward slip, are an indication of the frictional conditions, which presumably will produce a higher coefficient of friction.

A noticeable difference in the break-up of the scale was observed upon inspection after rolling. The scale on the HSLA grade broke off easier upon rolling than it did on the AISI 1018, and resulted in a greater amount of red oxide on the surface. This may be inferred from the higher roll torque values for the HSLA grade.

Figure 6.13. Roll Separating Force as a Function of Velocity for Two Different Steels

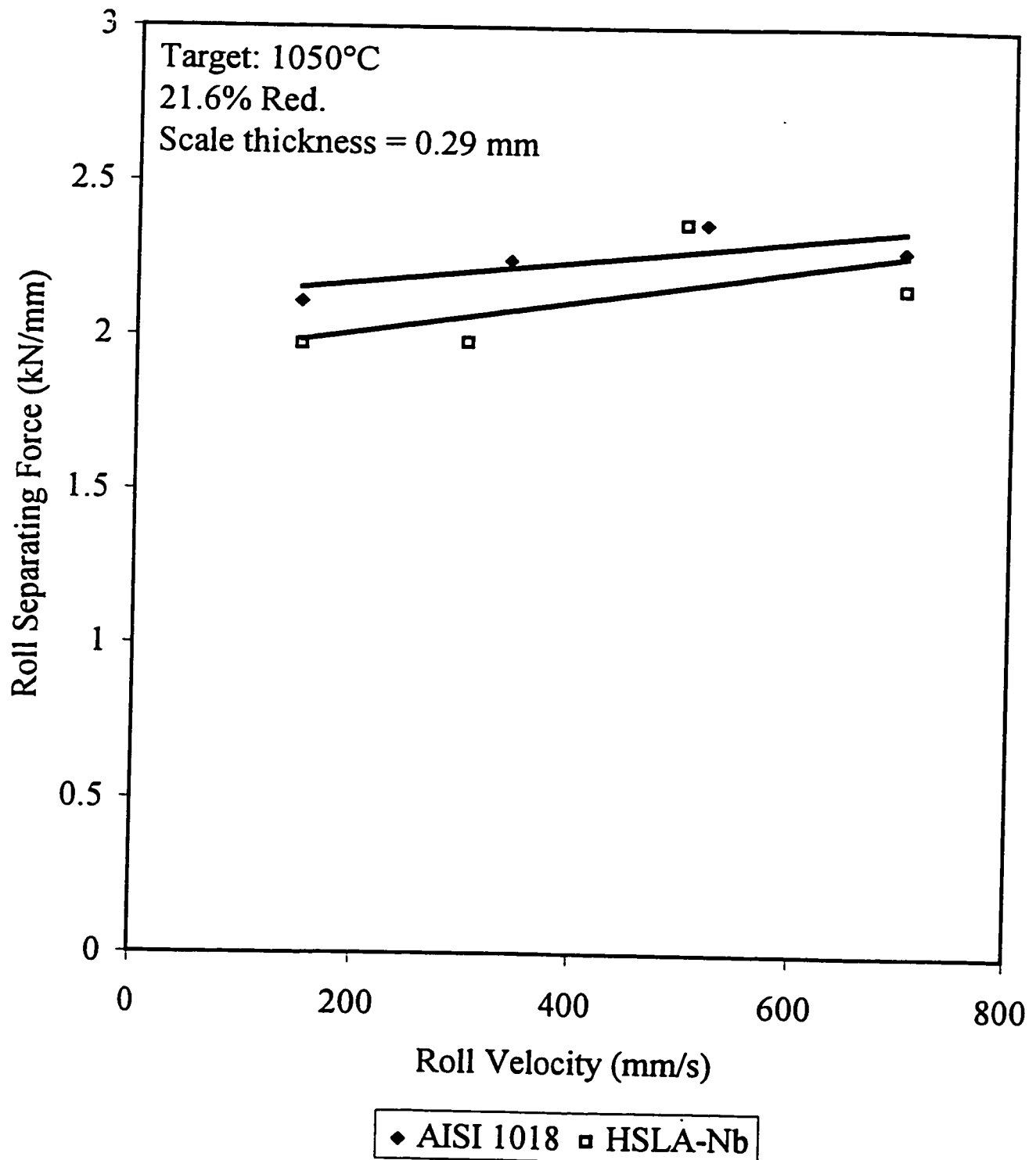


Figure 6.14. Roll Torque as a Function of Velocity for Two Different Steels

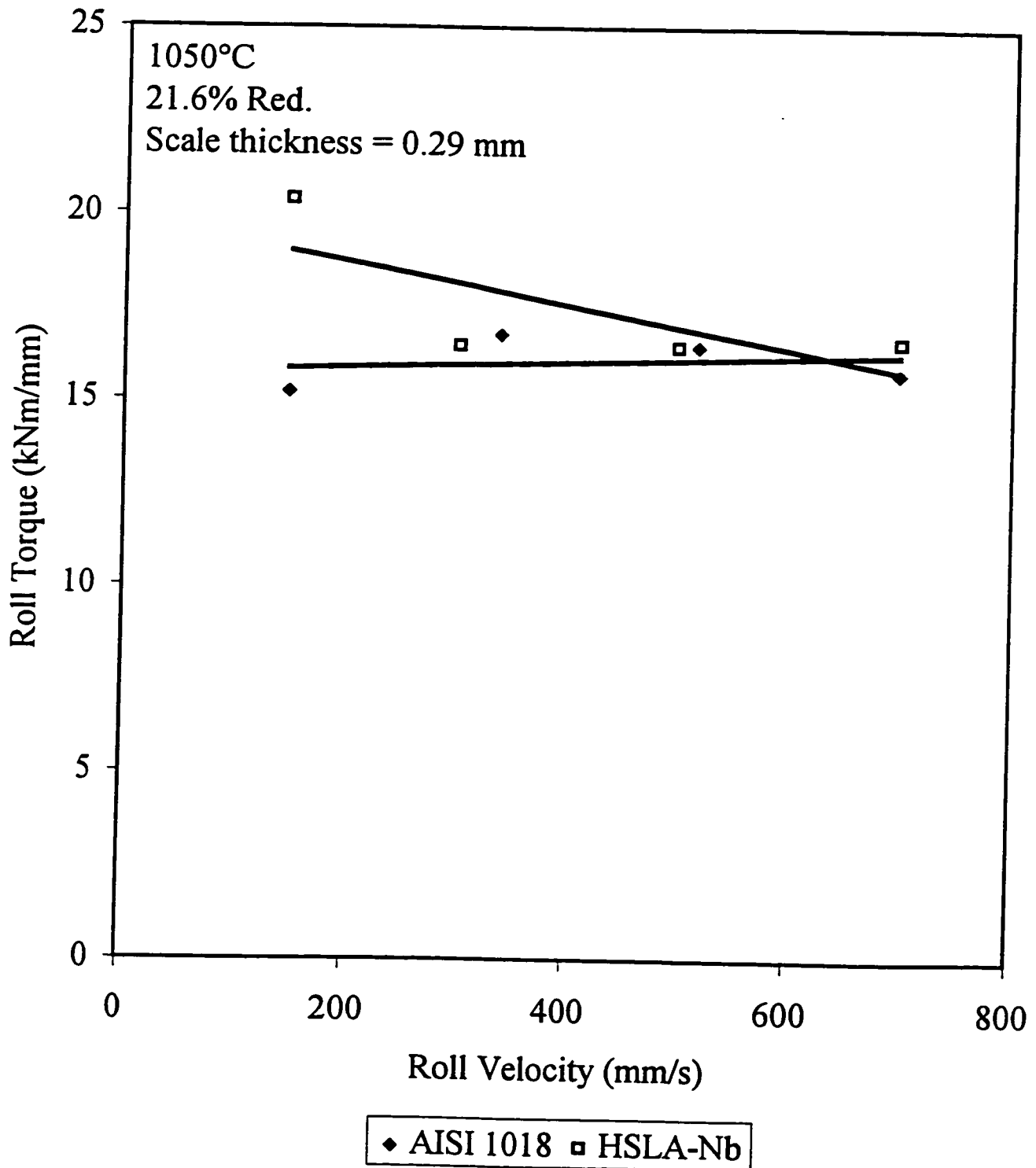
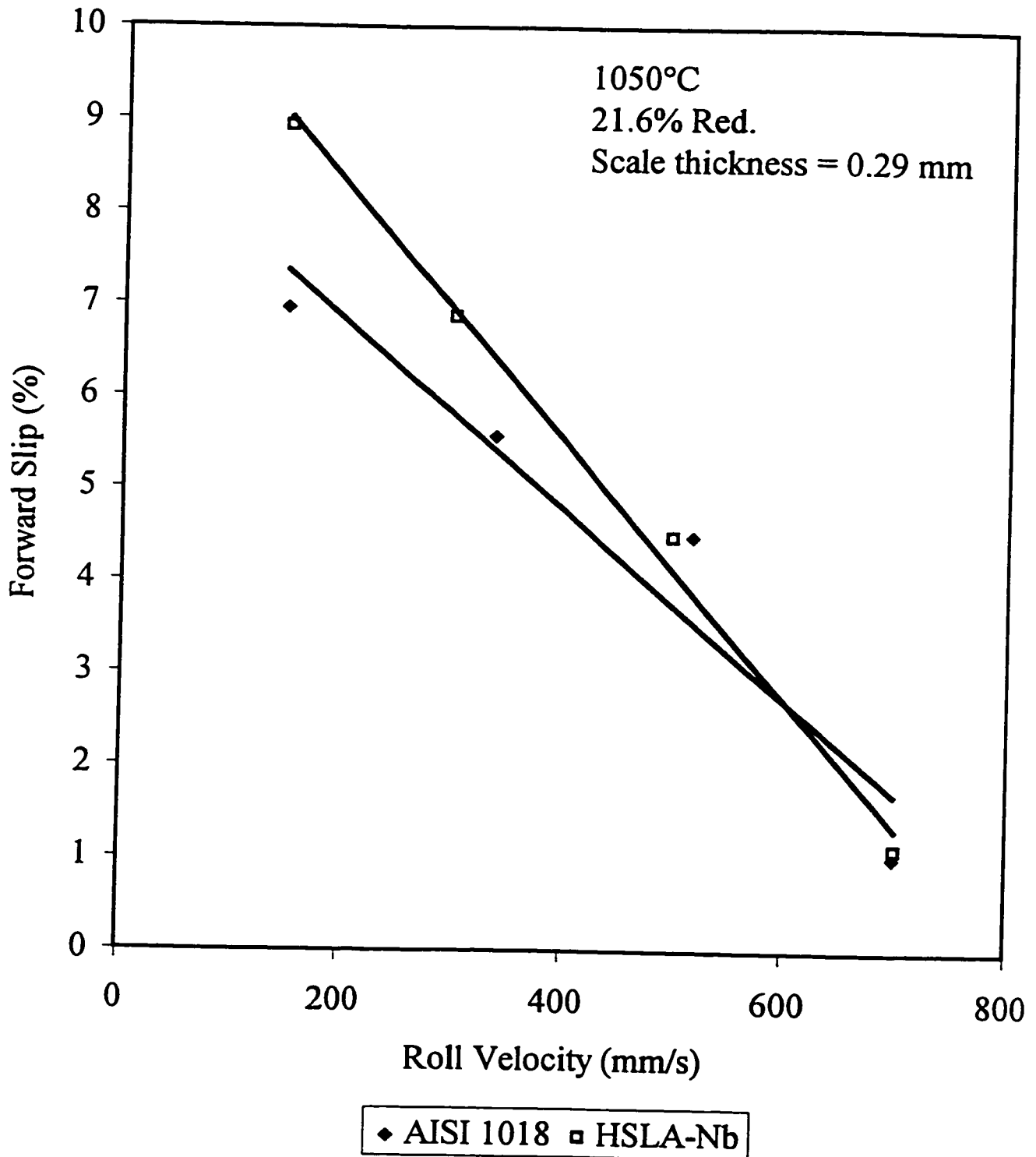


Figure 6.15. Forward Slip as a Function of Velocity for Two Different Steels

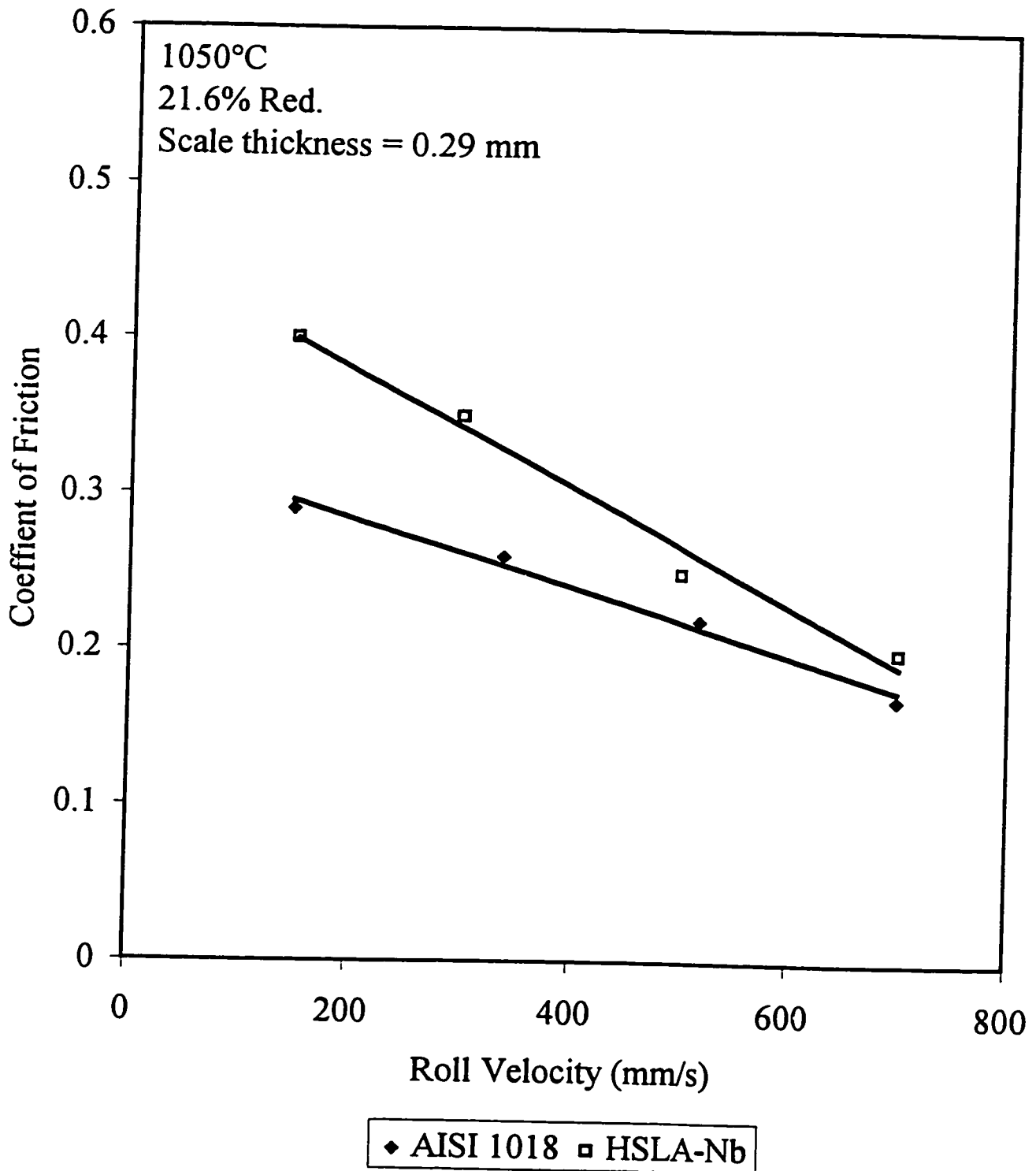


The effect on the coefficient of friction is illustrated in Figure 6.16. The coefficient of friction reaches its highest value of 0.4 for the HSLA grade at the lowest reduction. The value for the low carbon grade is 0.29 at the same velocity. The coefficient of friction then progressively drops off as the velocity is increased, to 0.2 for the HSLA grade and 0.17 for the low carbon grade. The coefficient of friction for the HSLA grade is higher than the coefficient of friction for the low carbon grade at all velocities. Wusatowski (1969) quoted findings by Pavlov and Kuprin, who investigated the effects of chemical composition on the coefficient of friction. Although there is a large scatter amongst the various groups of steels for some process parameters (i.e. relative velocities and temperature), the coefficient of friction is constantly greater for a micro-alloyed steel (St20) when compared to a low carbon steel (A20). This is also evident by Wallquist's (1955, 1960, 1962) data, which corroborates the trends in forward slip and by mill investigations by Munther *et al.* (1996), which corroborate the trends in the coefficient of friction.

The alloy contents, shown in Table 4.3, indicate that the differences may not be great enough to produce different scales under the same soaking conditions. This was corroborated by the kinetics study in Chapter 5. In addition, the scale thickness for the two grades was also comparable. Since the scales do not differ, the increase in the coefficient of friction with alloy content can possibly be explained by considering the crushing of asperities and the large deformation of the subsurface that causes a greater local flow stress for the HSLA grade, a result from the associated differences in physical metallurgy, i.e. the temperature sensitivity.

It is likely that the chilling effect of the work rolls plays a significant role as well. This is due to the fact that HSLA and low carbon grades differ greatly in temperature sensitivity. Migaud (1979) showed that for certain conditions HSLA grades increase in flow stress with 0.7-0.9 MPa/°C, whereas a similar temperature drop for a low carbon

Figure 6.16. The Coefficient of Friction as a Function of Velocity for Two Different Steels



grade only produces a flow stress increase of 0.2-0.4 MPa/°C. Judging from the approximations of the instantaneous contact temperature, temperature drops between 400 and 500°C may have been experienced by both grades. This corresponds to a local increase in flow stress on the surface between 280 and 410 MPa for the HSLA grade and 80 and 200 MPa for the low carbon grade. It is therefore likely quite that local chilling by the rolls affects the local flow stress on the surface and in the subsurface in such a way that the HSLA grade's local flow stress exceeds the low carbon grade's to such an extent that the frictional conditions are altered. Meanwhile, the HSLA grade has an average flow stress that does not exceed the low carbon grade's.

As far as the adhesion theory goes, the two steels produced numbers on the ratio between true and apparent contact area that were close for similar conditions on the process parameters. The ratio ranged in these cases from a low of 0.6 up to unity, depending on temperature, velocity, and reduction.

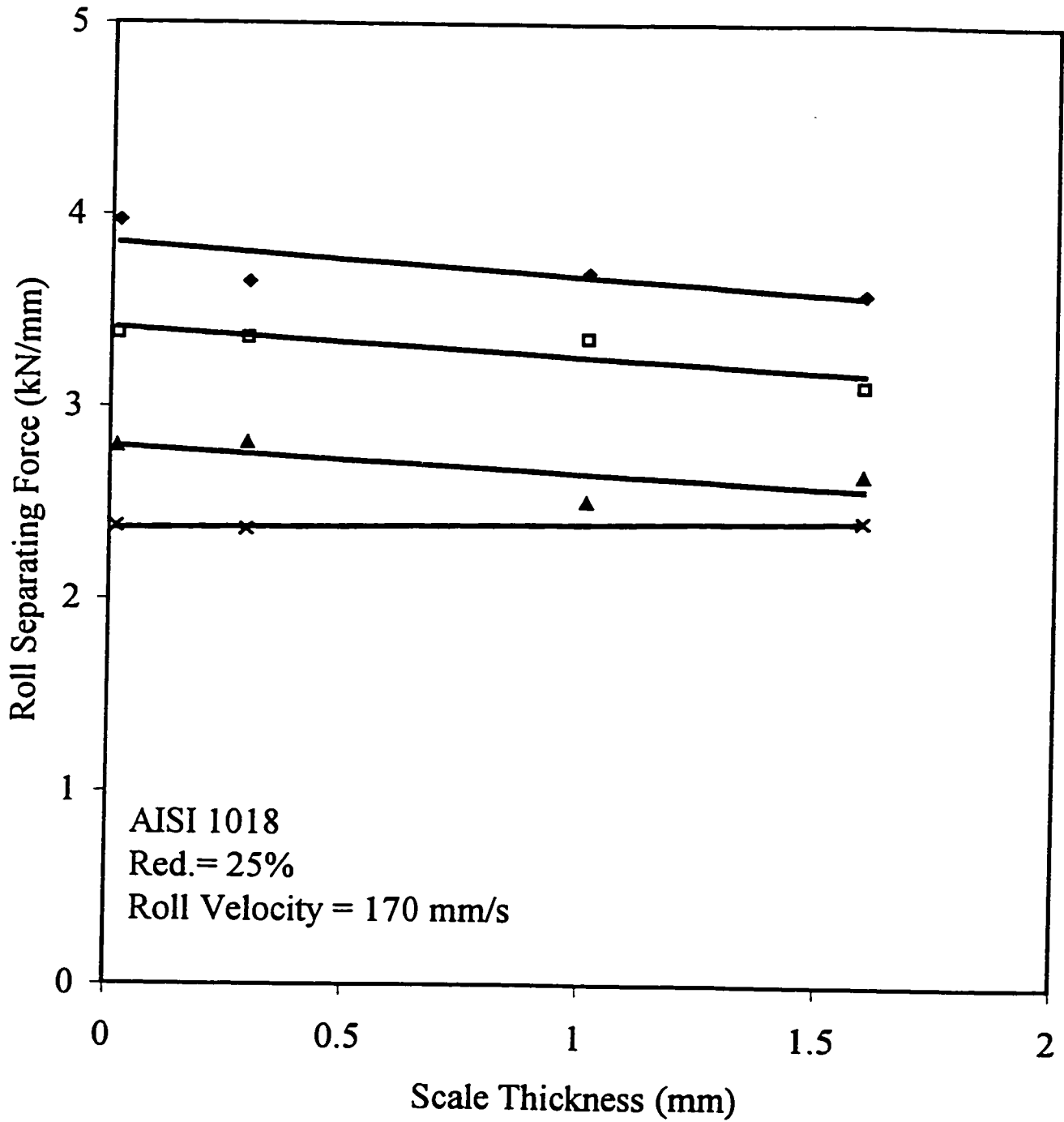
6.5 The Effect of the Scale Thickness on the Coefficient of Friction

For experiments in which the effect of scale thickness was investigated the reduction and the velocity were kept constant at 25 % and 170 mm/s, respectively. As has been mentioned previously, the oxide interface can be described in terms of the scale thickness or the scale index. Figures 6.17-6.19, show the effect of the scale thickness on the roll separating force, roll torque, and forward slip.

The effect of the temperature and the scale thickness can be seen in Figures 6.21-6.23. Figures 6.25-6.27 illustrate the same information as Figures 6.17-6.19. However, the data is plotted versus the ratio of the scale index and roll roughness. This enables cross-referencing the scale thickness to the scale index. Figures 6.17 and 6.25 show that an increase in scale thickness has a slight effect of lowering the roll separating force. On the other hand, it also raises the roll torque slightly, as indicated in Figures 6.18 and 6.26. The most severe effect is that on the forward slip that drops from about 7% to a low of about 1% as the scale thickness is increased from 0.015 to 1.590 mm. This is also visible in Figure 6.23, where the coefficient of friction is plotted versus the temperature for the various scale thicknesses. Here, lower numbers than those presented by Wallquist are produced. This is a consequence of investigating scale thicknesses beyond those produced by his experimental conditions. Surprisingly, the thickest scale produces the highest roll torque (Figure 6.22) when the overall effect of temperature is studied. However, this is not the case when the roll separating force is considered (Figure 6.21). The high torque values are explained by the fact that this scenario is also that of the thickest sample and thus correspondent with a greater contact length, an effect that was seen in Figure 6.2, where two sample sizes were compared.

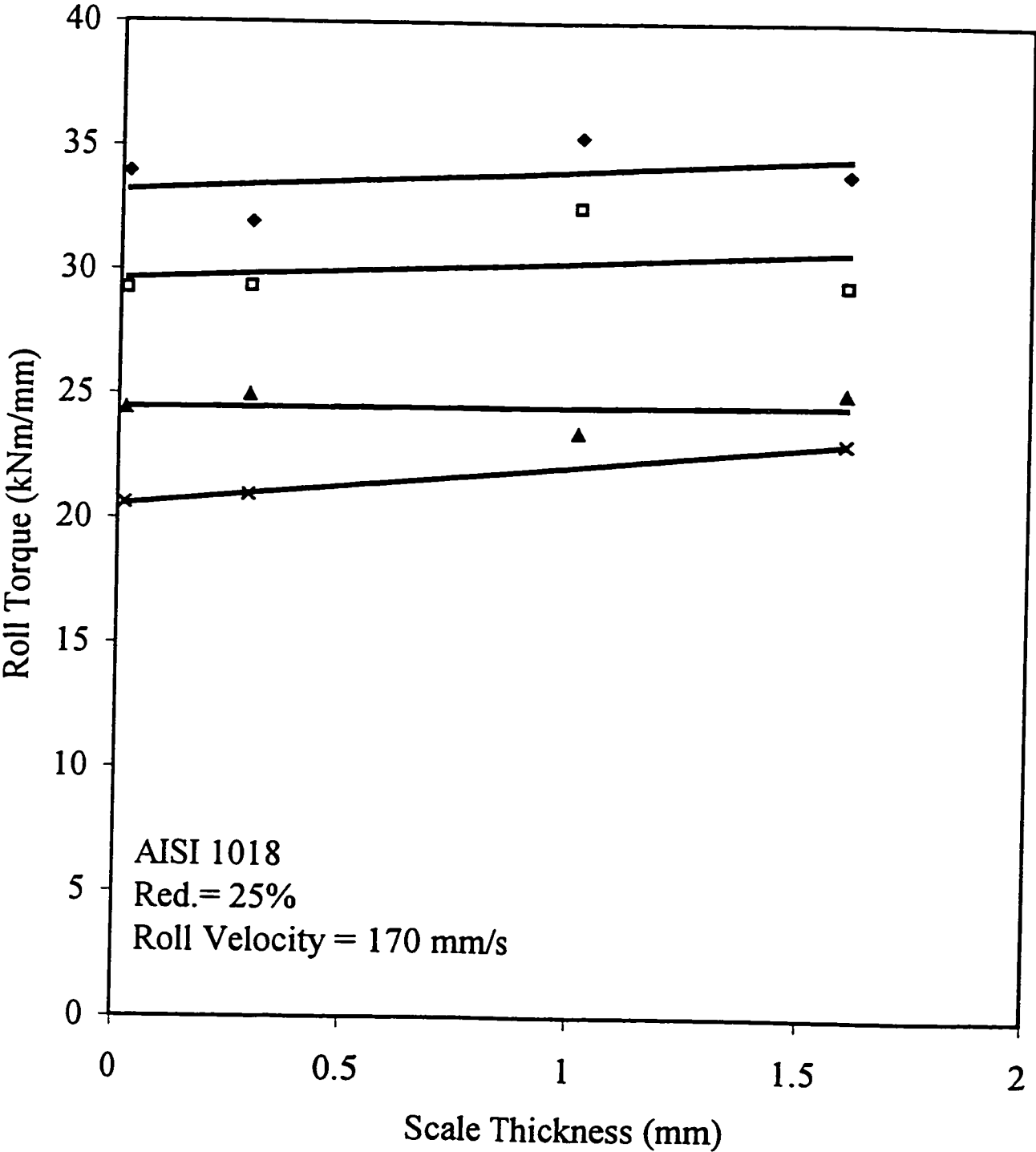
The effect of scale thickness on the frictional conditions can be seen in Figure 6.20. It is evident that the coefficient of friction has its highest value for the thinnest scale

Figure 6.17. Roll Separating Force as a Function of Scale Thickness



◆ 825°C □ 900°C ▲ 975°C × 1050°C

Figure 6.18. Roll Torque as a Function of Scale Thickness



◆ 825°C □ 900°C ▲ 975°C × 1050°C

Figure 6.19. Forward Slip as a Function of Scale Thickness

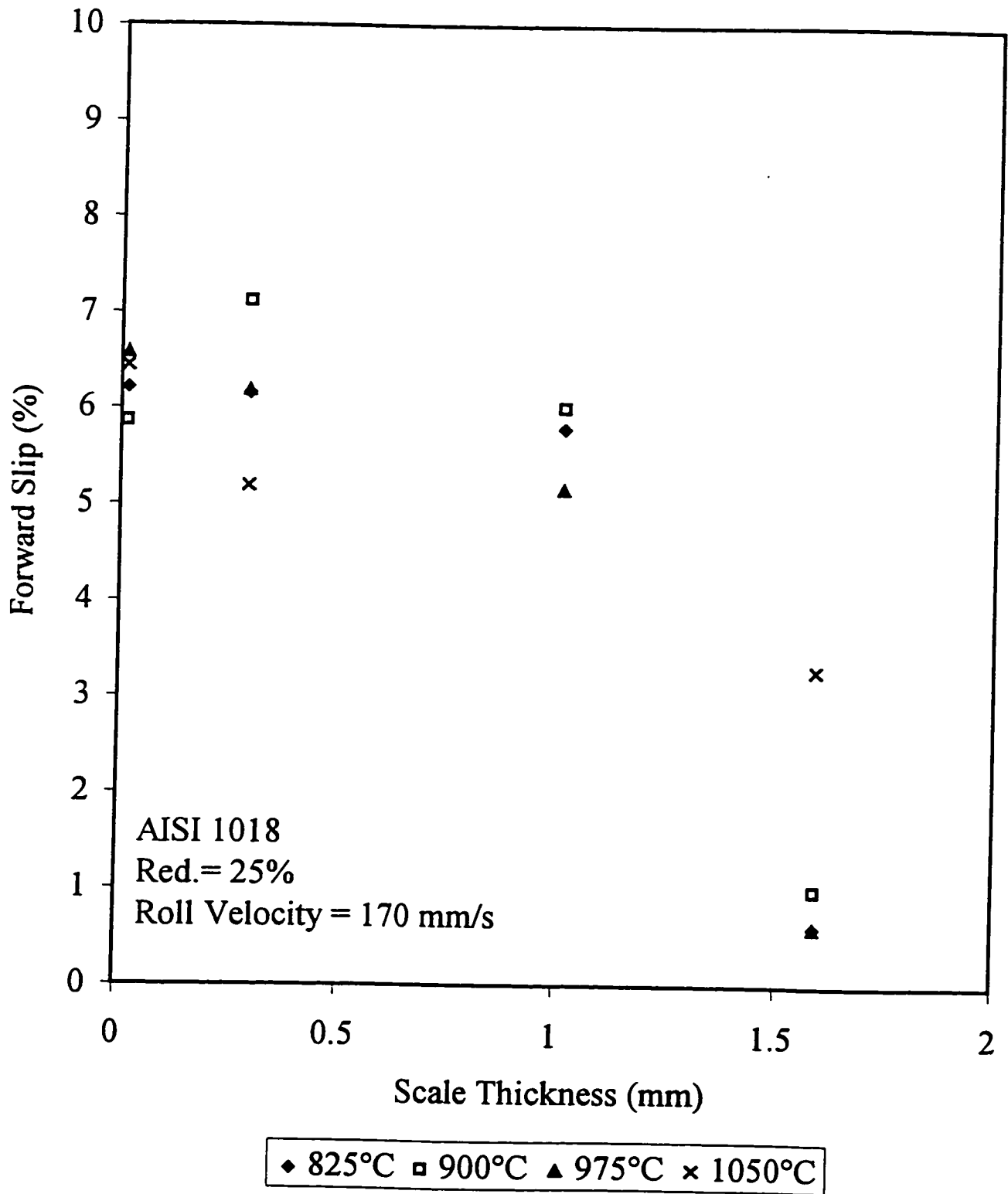
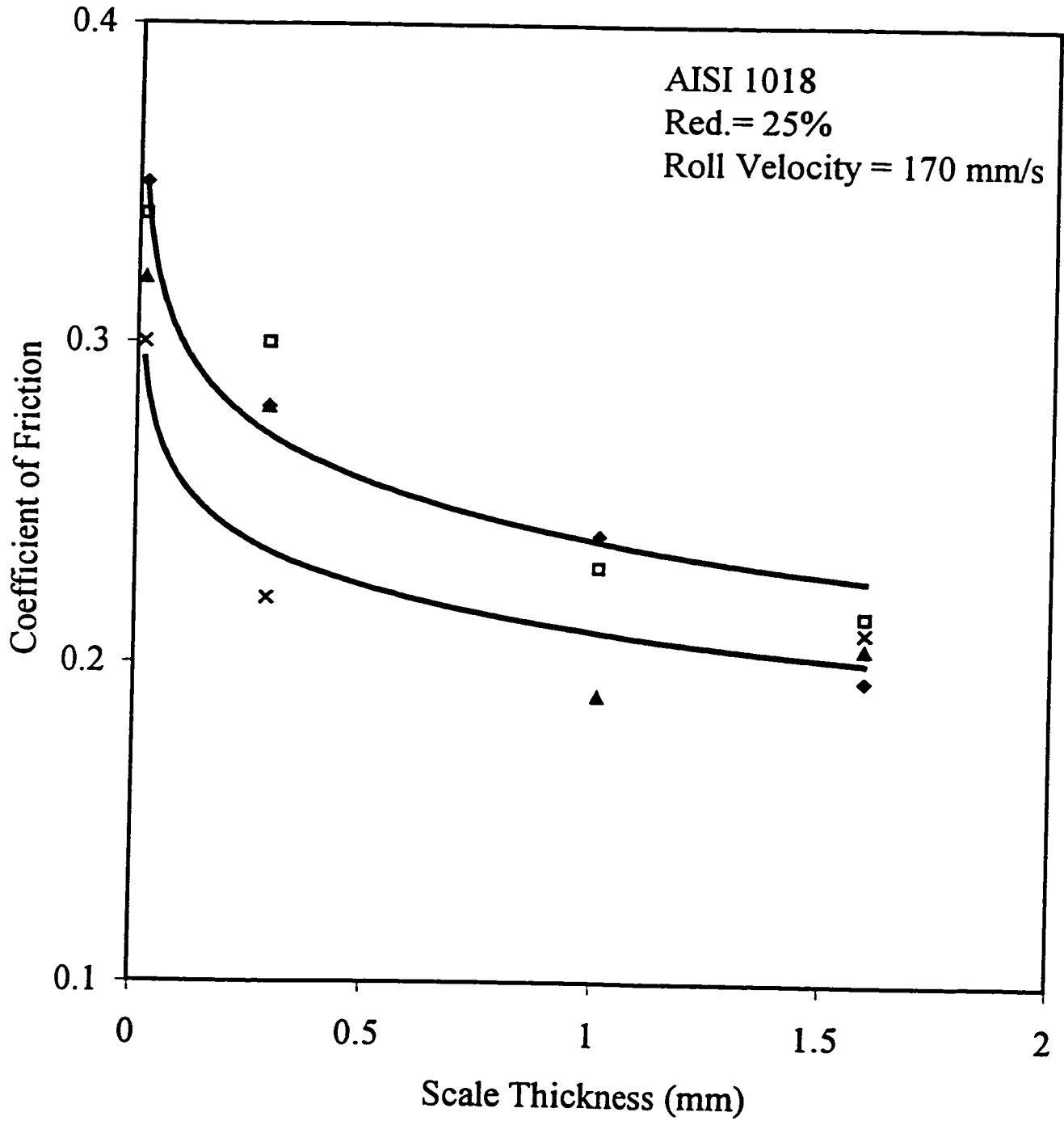


Figure 6.20. The Coefficient of Friction as a Function of Scale Thickness



♦ 825°C □ 900°C ▲ 975°C × 1050°C

Figure 6.21. Roll Separating Force as a Function of Temperature for Various Scale Thickness

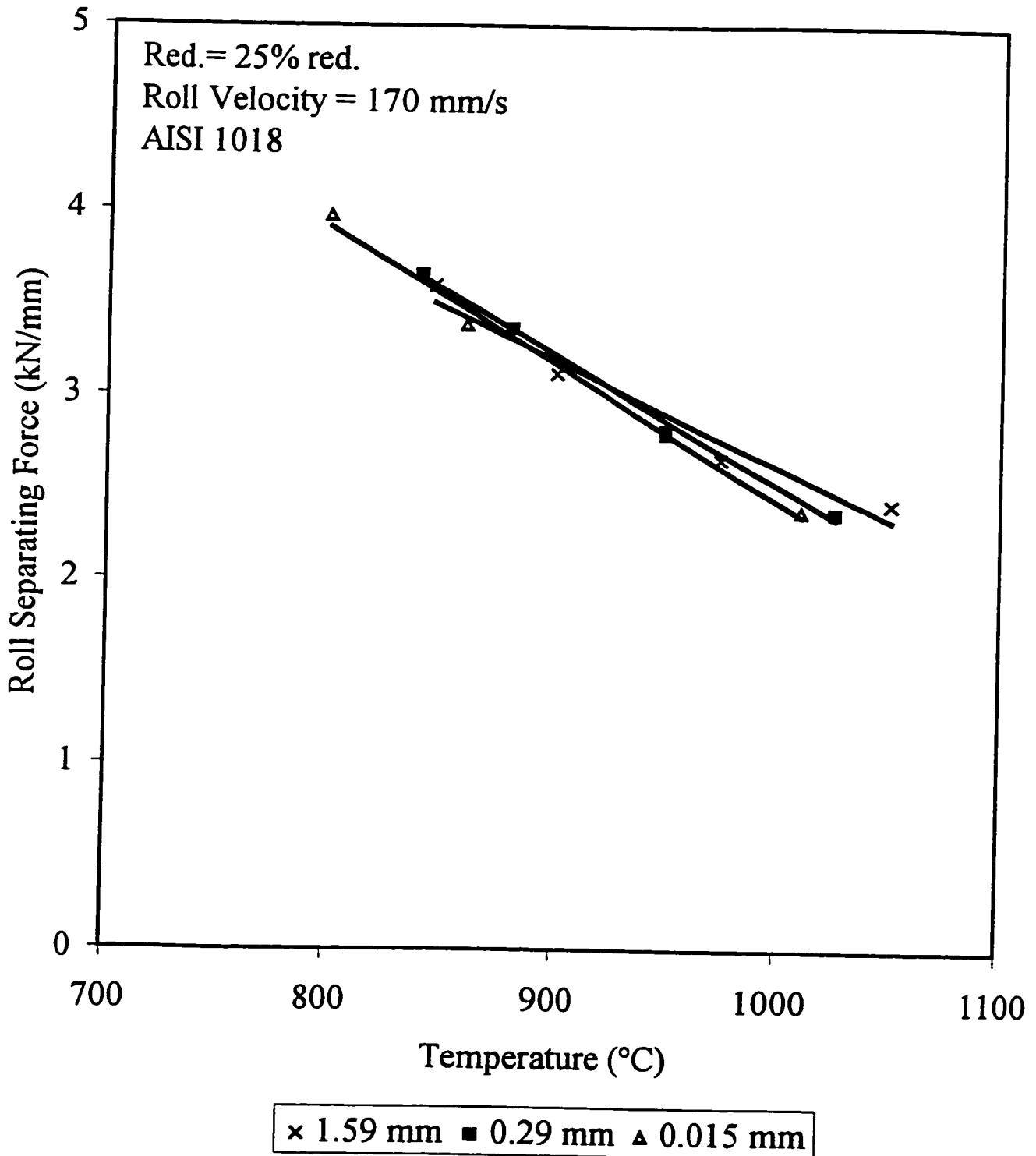


Figure 6.22. Roll Torque as a Function of Temperature for Various Scale Thickness

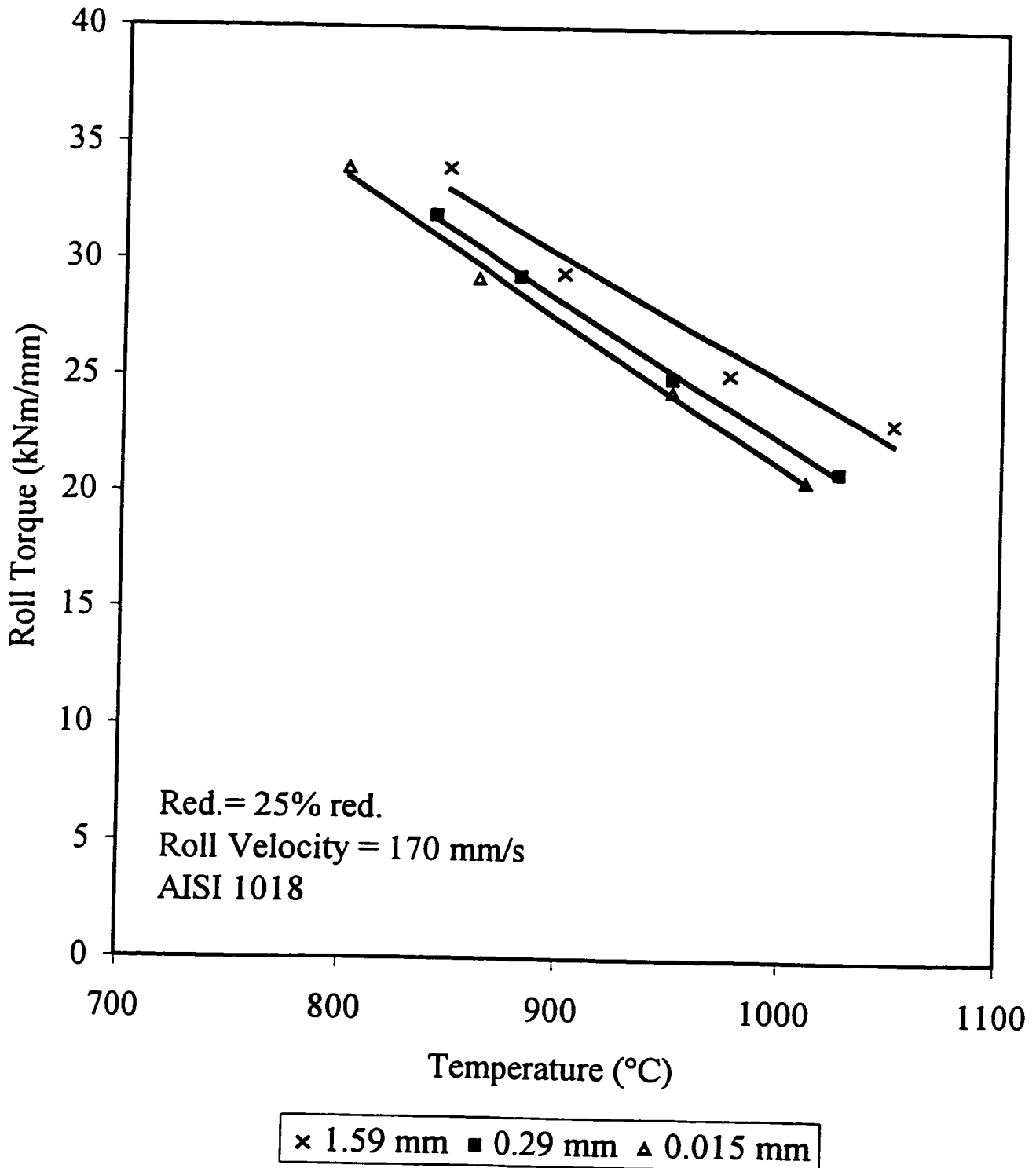
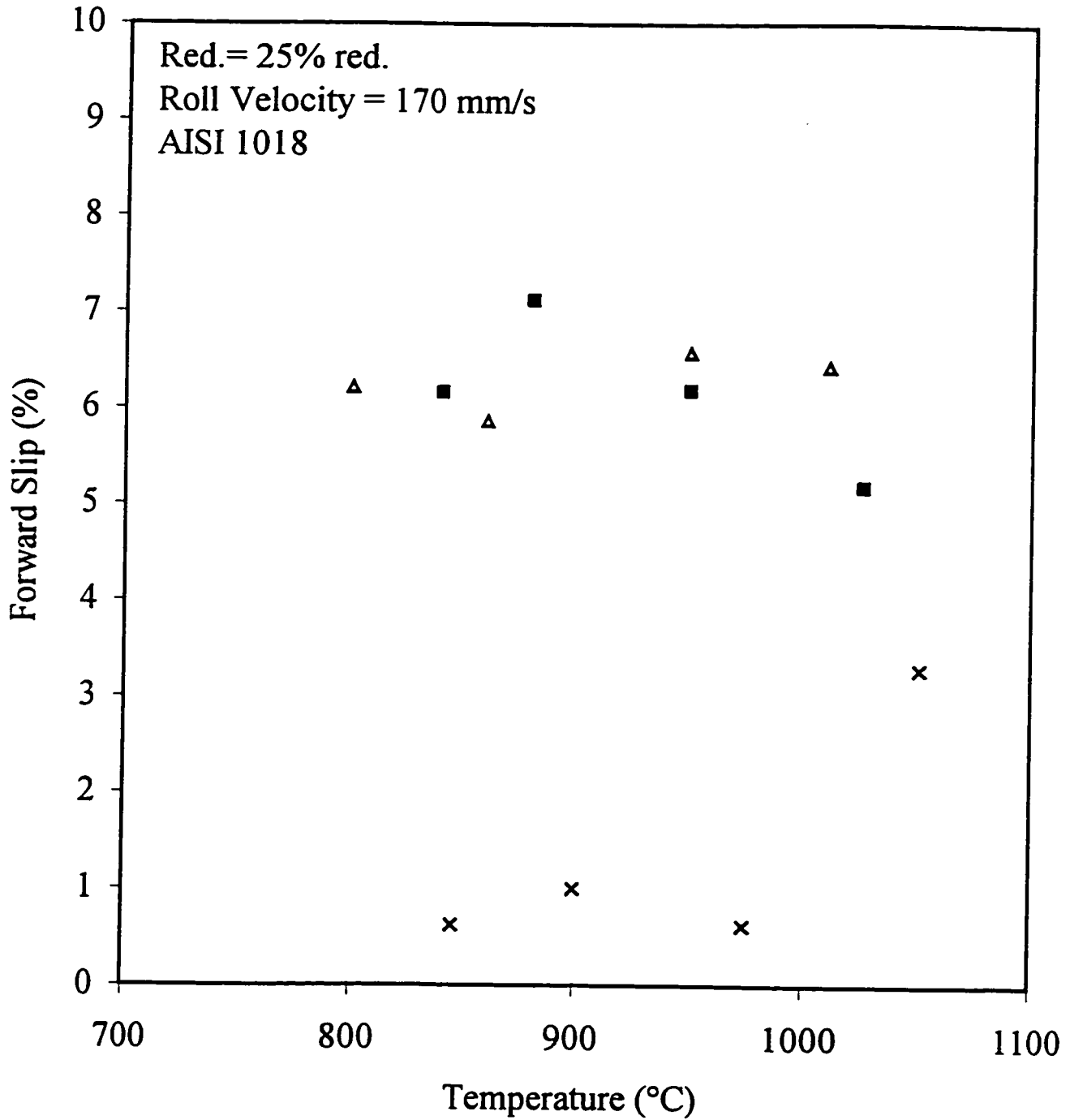


Figure 6.23. Forward Slip as a Function of Temperature for Various Scale Thickness



× 1.59 mm ■ 0.29 mm △ 0.015 mm

Figure 6.24. The Coefficient of Friction as a Function of Temperature for Various Scale Thickness

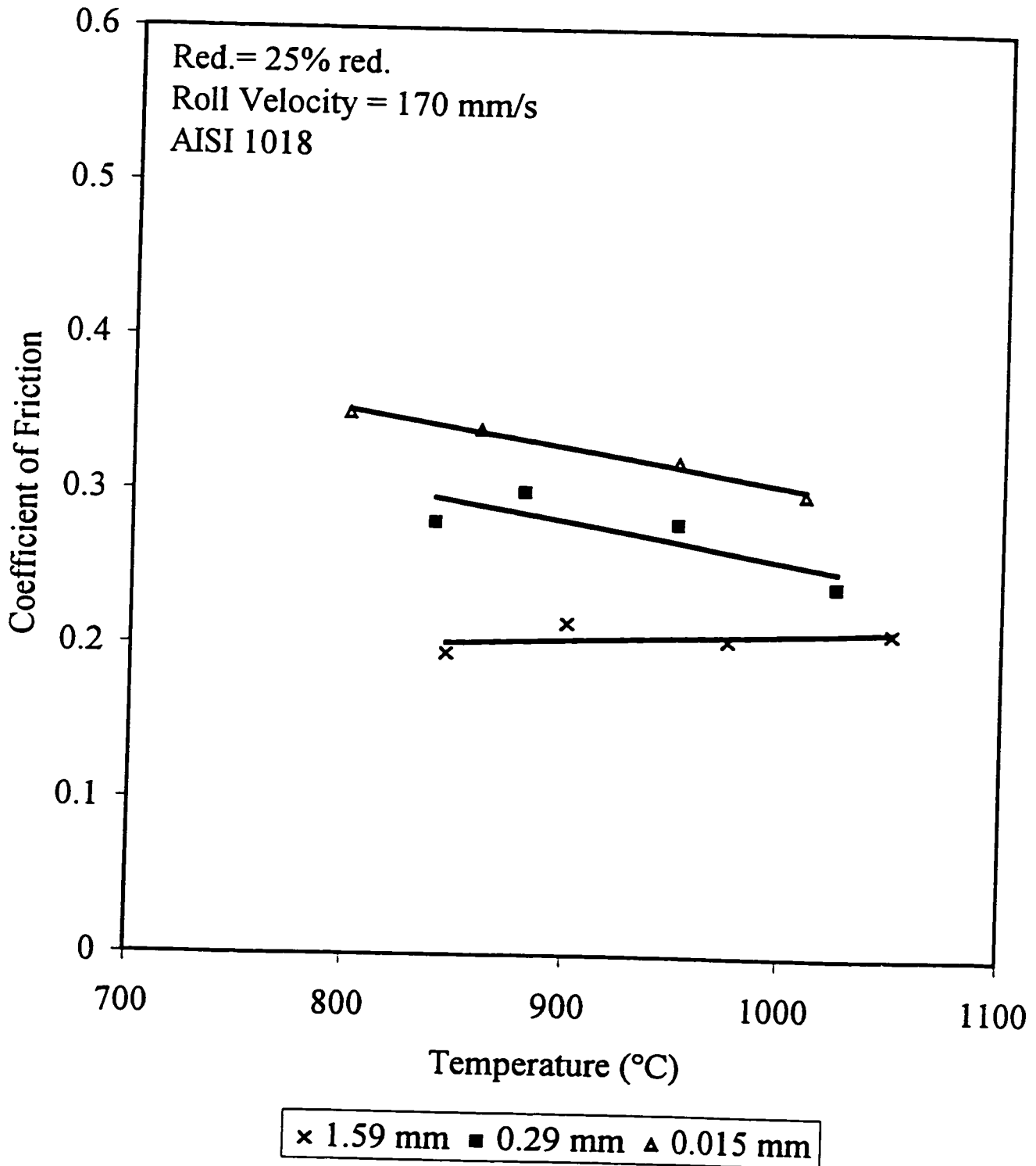


Figure 6.25. Roll Separating Force as a Function of Scale Index and Roll Roughness

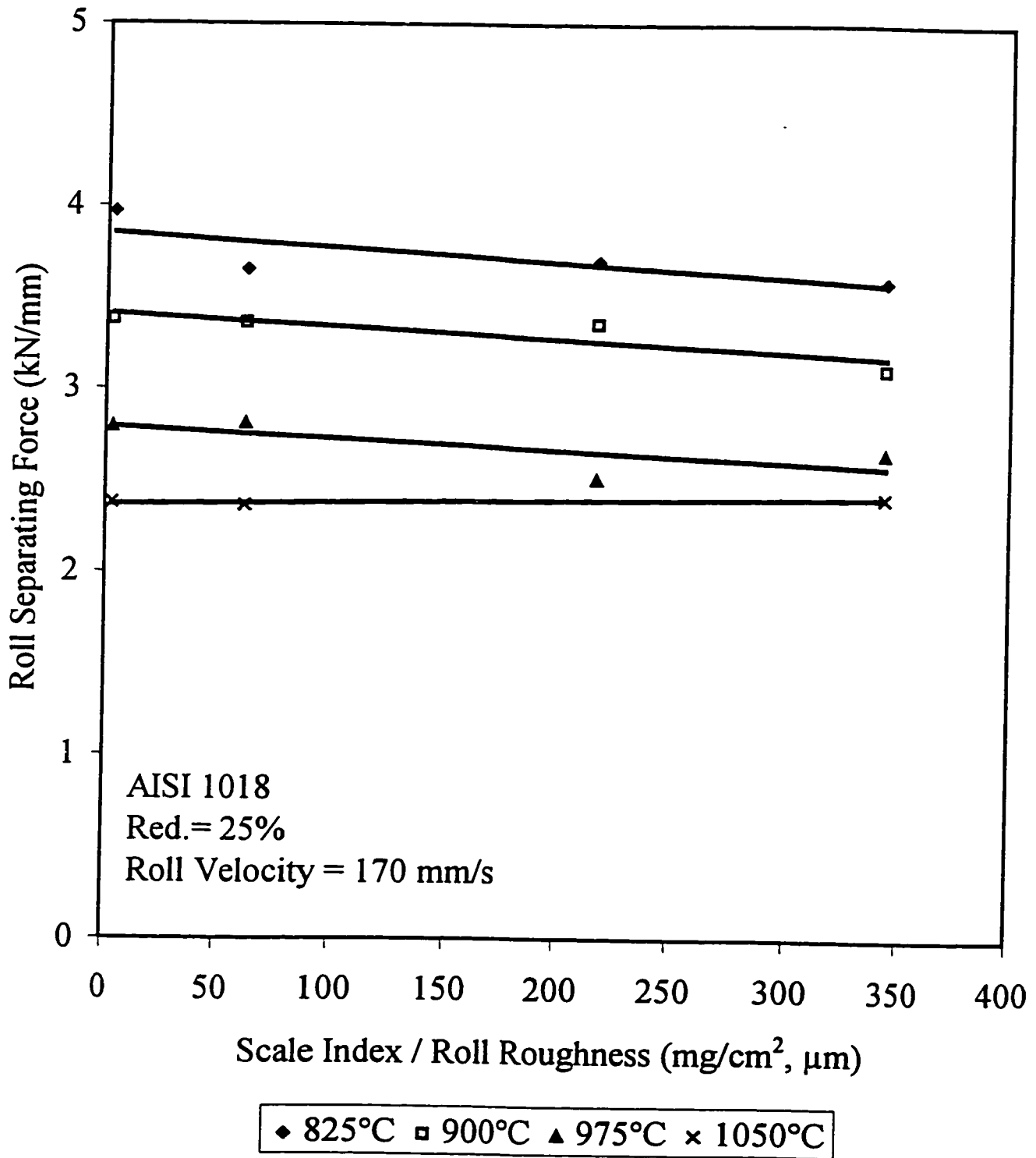


Figure 6.26. Roll Torque as a Function of Scale Index and Roll Roughness

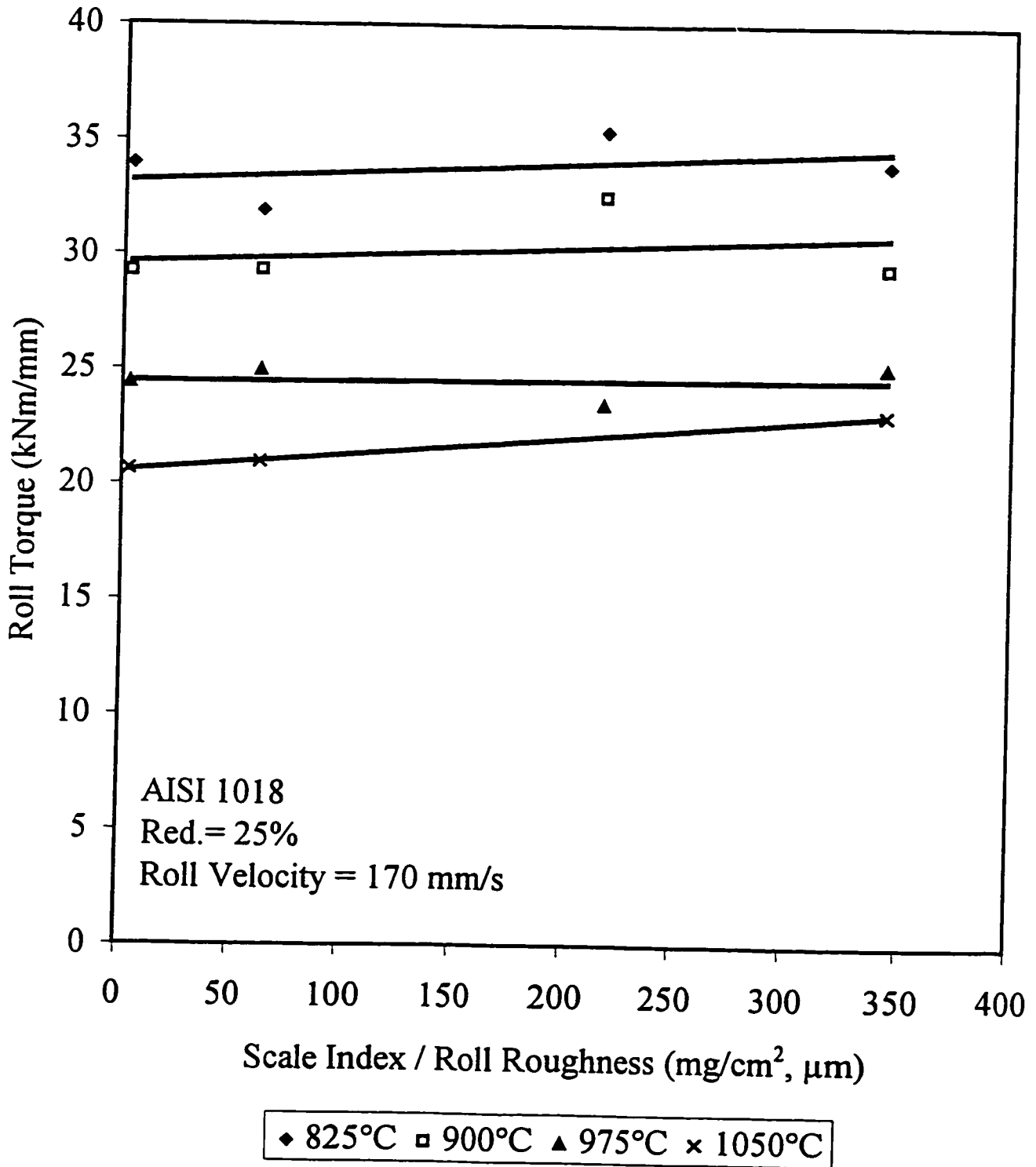
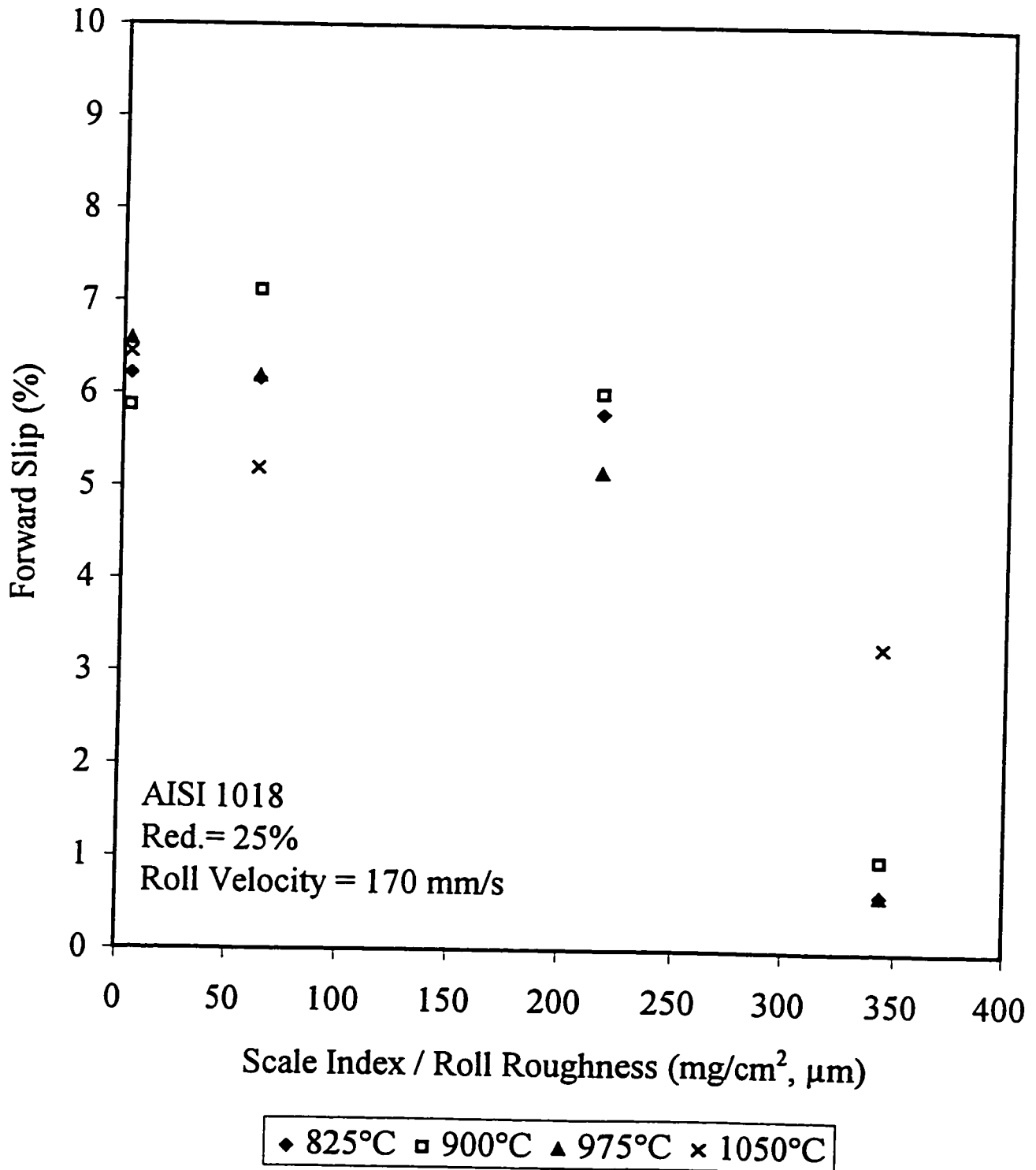


Figure 6.27. Forward Slip as a Function of Scale Index and Roll Roughness

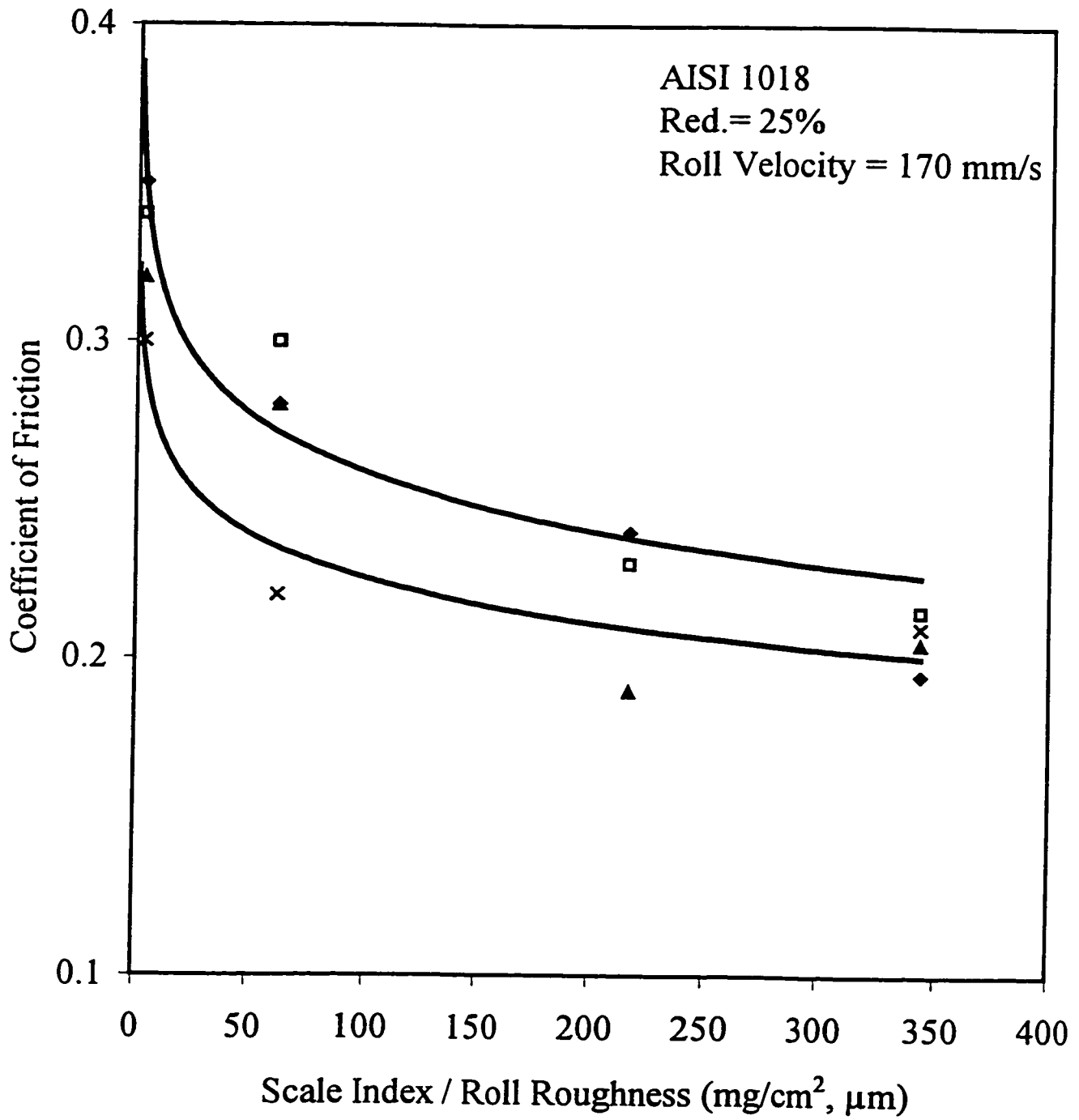


layer of 0.015 mm, varying from a high of 0.35 at 825°C and a low of 0.30 at 1050°C. The soaking time and hence, the scale thickness, is then increased, first to 0.29 mm, then to 1.01 mm followed by 1.59 mm. This results in a reduction in the coefficient of friction at all temperatures, giving values ranging from 0.22 to 0.30 for a scale thickness of 0.29 mm. A scale thickness of 1.01 mm results in a variation in the coefficient of friction from 0.19 to 0.24. The lowest values are seen for the thickest scale. This gives a coefficient of friction between 0.195 and 0.215. This general trend is corroborated by the information seen in Figure 6.24, in which the coefficient of friction is plotted versus temperature for three different scale thickness. The highest values of the coefficient of friction, ranging from 0.30 to 0.35, are obtained when the samples have been soaked in an environment of oxygen-free nitrogen gas, producing a scale 0.015 mm thin. A scale thickness of 0.29 mm resulted in values of the coefficient of friction that ranged from 0.24 to 0.30 for the same conditions. An increase in scale thickness to 1.59 mm lowers the coefficient of friction further, reaching a low of 0.195 and a high of 0.215.

The scale thickness appears to have the most significant effect on the frictional conditions. In analysing the experimental data, the gain in thickness was taken into account along with changes in the heat transfer coefficient due to the insulating effect the scale provides. Figure 6.20 indicates that a scale thickness 0.015 mm thick produced a coefficient of friction double that of 1.59 mm scale, corroborating the results of el-Kalay and Sparling (1968) and of Roberts (1983) and confirming that under certain conditions the scale has a lubricating effect.

The scale thickness can also be described by a scale index which, in weight gain per unit surface area (mg/cm^2), is shown in Figure 6.28, where the roll roughness is also taken into account. Visual observations of the samples indicated a certain amount of break-up of the scale. A thinner scale was more adherent and did not break up to the same extent as a thicker scale. This resulted in lesser red oxide on the surface of cooled samples, confirming Blazevic's (1996) findings.

Figure 6.28. The Coefficient of Friction as a Function of Scale Index and Roll Roughness

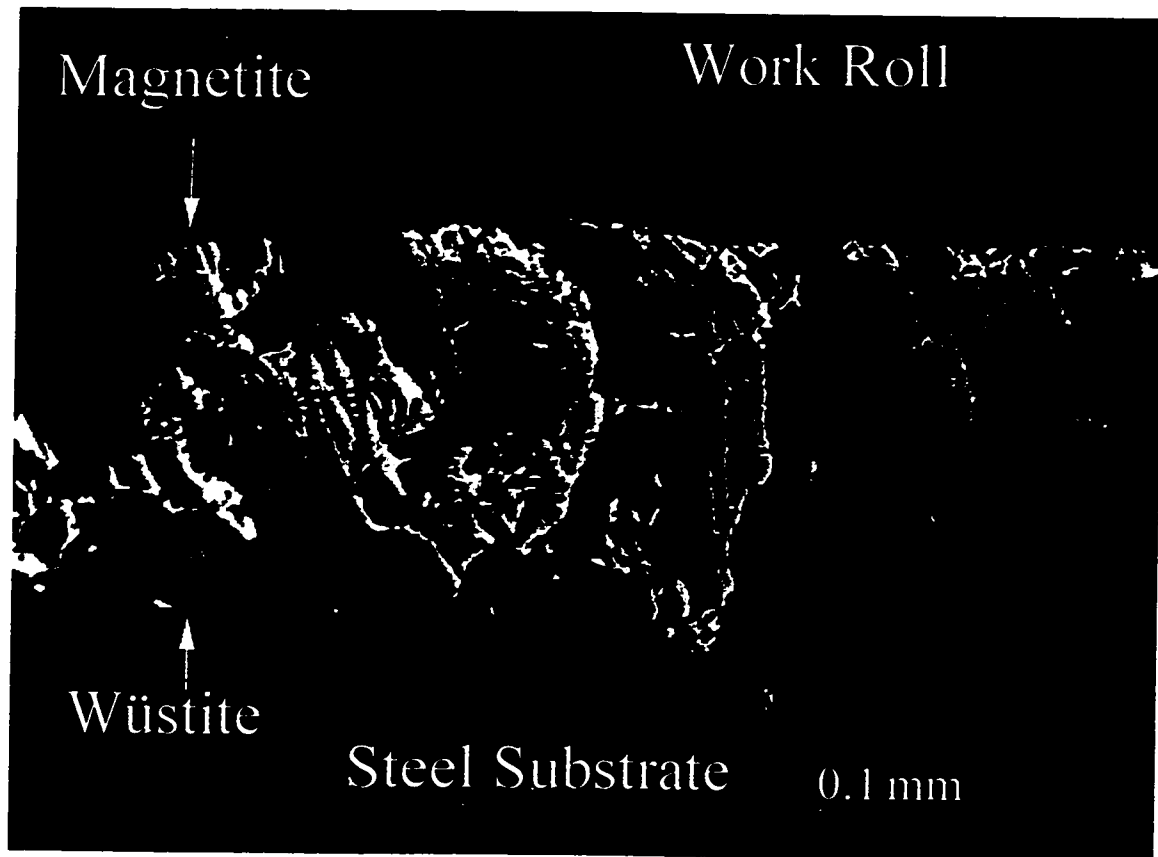


A number of samples stalled in the roll gap, as a result of overloading the mill. Observations of the partially rolled surfaces indicated that the scale appeared to have a certain degree of ductility resulting in a visco-plastic wave, pushing the scale out of the roll gap towards the entry side. It can therefore be argued that the break-up itself provides a certain degree of lubricity. It was also seen that the scale commonly cracked at the edges. The size and orientation of the cracks appeared to be a function of roll pressure, as higher pressures led to longer cracks that deviated from the direction perpendicular to rolling, observed at lower pressures. One can only speculate on the insulating effect of the scale layer. However, the calculated numbers on real and apparent contact area indicate that the true contact area is greater when a thin scale is present.

Depending on the process parameters, the ratio for a scale thickness of 0.015 mm ranges from 0.81 to unity, whereas the ratio for the thickest scale, 1.59 mm, ranges from 0.55 to 0.77. An intermediate scale thickness of 0.29 mm results in real and apparent contact area ratios between 0.60 and unity. This may be seen as an indication of the lubricating effect that the scale might have. One hypothesis is that the scale upon roll gap entry fills the asperity valleys of the rolls, thus effectively minimising the metal to metal contact and the resulting adhesive bonds. Consequently, this influences the heat transfer between sample and rolls, and thereby the chilling effect the rolls have on the surface flow stress. The change in the heat transfer coefficient ought to be proportional to the area of the points of contact, i.e. the ratio between real and apparent contact area.

Figure 6.29 depicts an initial 0.29 mm thick scale layer on the AISI 1018 steel, sectioned in the rolling direction after the pass. The scale layer has two constituents: a darker wüstite layer located closest to the steel substrate and a lighter coloured magnetite layer located towards the surface of the scale layer and around some voids in the centre. Cracks caused by the deformation run from the top to the bottom of the two-layered scale. It can also be seen that particles have spalled from the surface of the scale layer where a

Figure 6.29. Scale Layer after Deformation

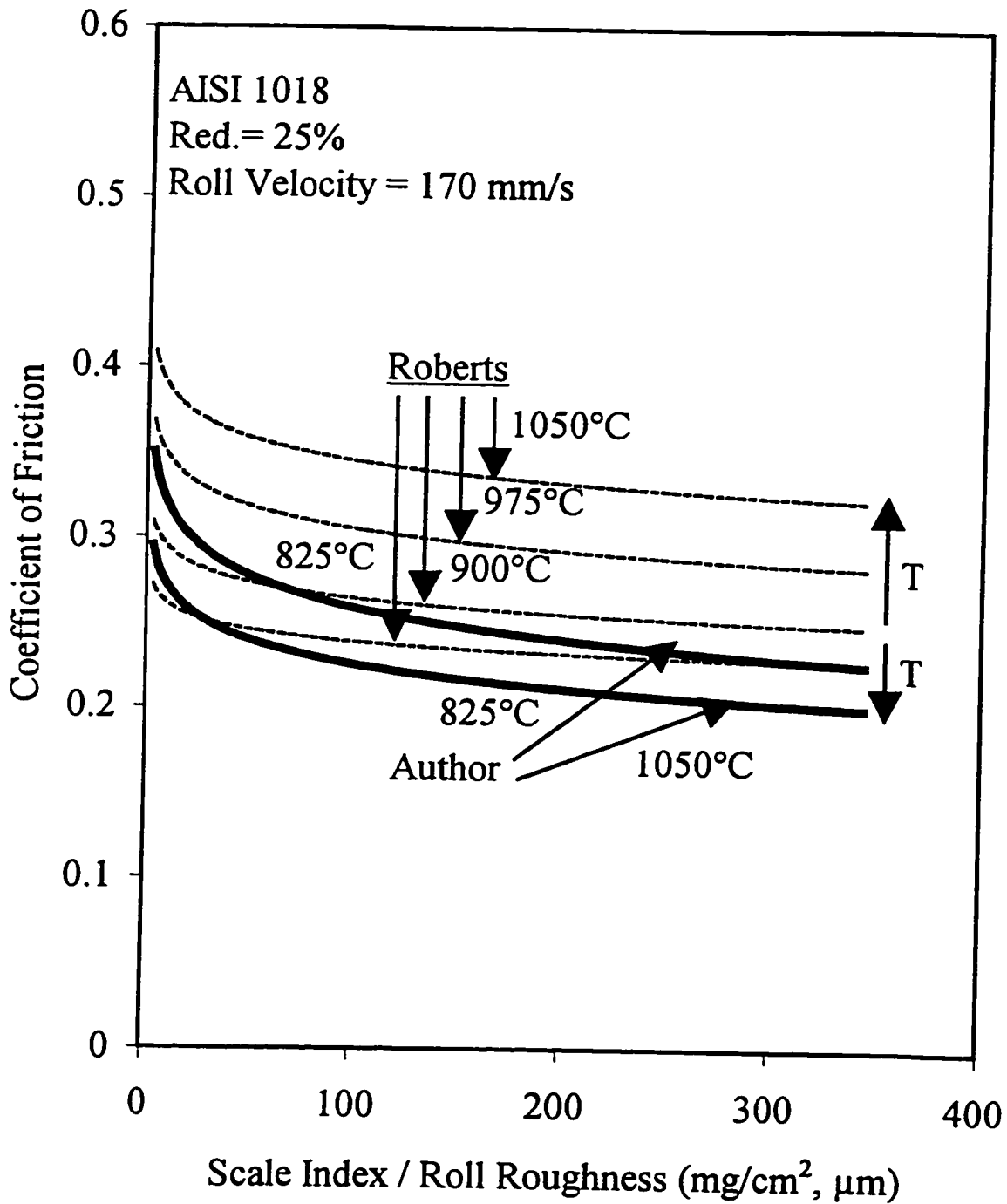


Reduction = 32%
Temperature = 900°C
Velocity = 170 mm/s

chilling effect from the work roll has caused a reduced ductility of the already hard magnetite.

Roberts (1977, 1983) has published data on the coefficient of friction as a function of scaling. Since he based his calculations on the laboratory results by el-Kalay and Sparling (1968), and proposed that the coefficient of friction increase with increasing temperature, one might doubt the validity of his model. Roberts proposed that equation 2.14 describe the frictional conditions in hot rolling. In this model, only the temperature and the scale index - surface roughness ratio describe the frictional conditions. Contributions from other process and material parameters are not taken into account. However, the present investigations have clarified the fact that there are contributions by the roll velocity, reduction, and the steel's chemical composition each of which affect the frictional conditions as well. Figure 6.30 shows a comparison of Roberts' model and this author's work. Evidently, the effect of the temperature on the coefficient of friction is opposite to Roberts' findings when it is plotted versus the ratio of scale index and roll roughness. Furthermore, the variation in the coefficient of friction concerning the temperature is far less than suggested.

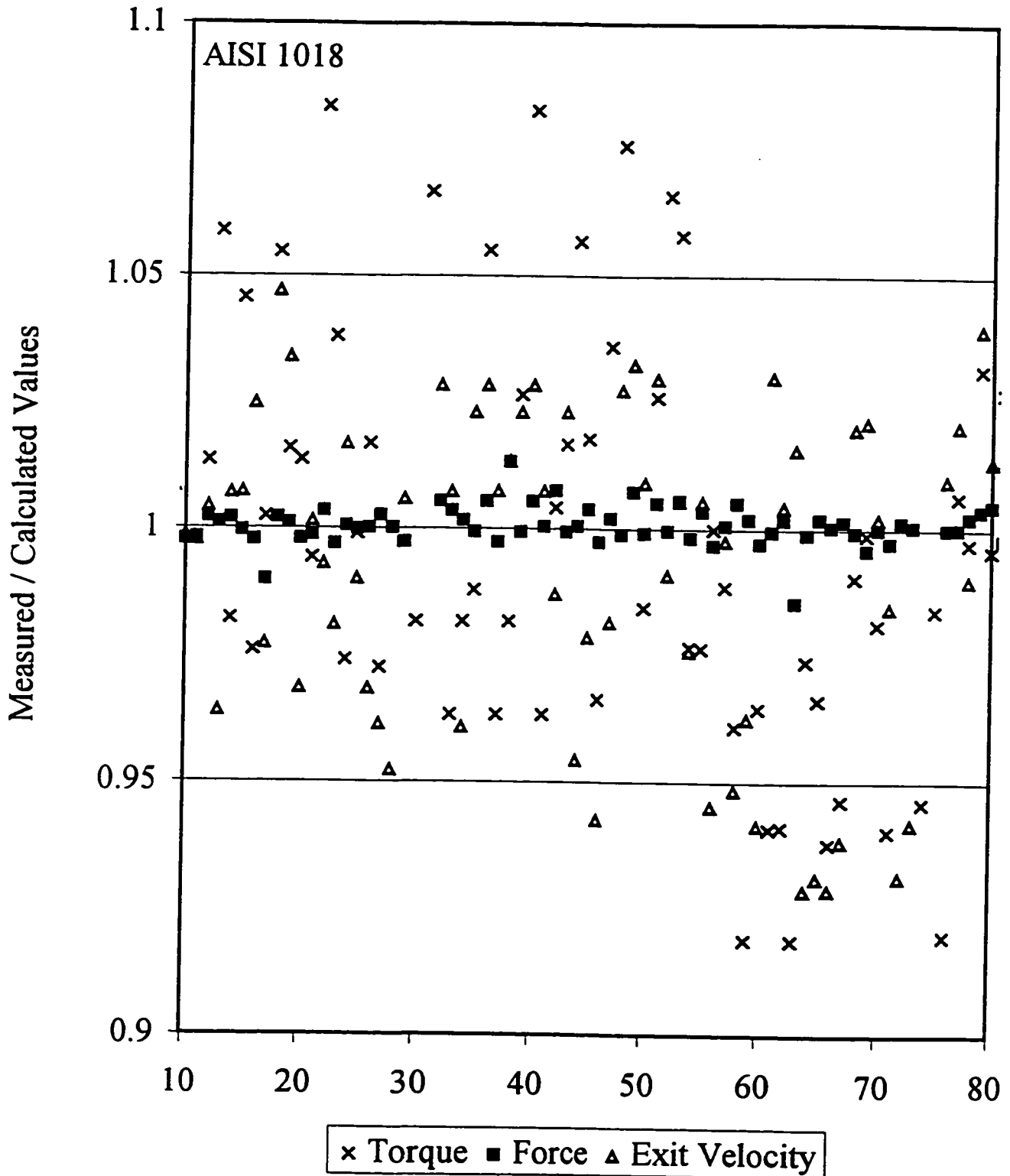
Figure 6.30. A Comparison on the Effect of Scale on Frictional Behaviour



6.6 Experimental Error

As mentioned above, the magnitude of the coefficient of friction was inferred by matching the measured and computed roll force, torque and forward slip. The accuracy of the calculations is of some importance. Figure 6.31 shows the differences in terms of ratios of measured and calculated numbers on the roll separating force, roll torque, and exit velocity, obtained with the carbon steel. The lowest scatter is exhibited by the roll separating forces. The error in this case ranges no more than $\pm 2\%$. The experimental error in the exit velocity is $\pm 7\%$. The match of the measured and calculated torque is the worst fit giving an experimental error ranging $\pm 8\%$ after friction losses of 15% in bearings, etc. were deduced from the measured values.

Figure 6.31. Experimental Errors



6.7 Conclusions

An investigation was undertaken in order to determine the effects of some process and materials parameters on frictional conditions during hot rolling of steels. Samples of AISI 1018 and HSLA steels were rolled at different reductions, velocities, temperatures, and with different interfaces, using a laboratory rolling mill. It can be concluded that the coefficient of friction is strongly influenced by the rolling temperature, the roll velocity, the roll/metal interface, and to a certain degree, the reduction:

1. The coefficient of friction increases with decreasing temperature as a result of increased material flow stress and increased adhesive bond strength.
2. An increase in velocity decreases the coefficient of friction as less time is made available to form adhesive bonds between the rolls and the metal/scale. The local increase in flow stress caused by heavier chilling at lower velocities is also likely to contribute to an increase in the coefficient of friction.
3. A greater reduction increases the coefficient of friction slightly since an increase in flow stress is seen due to larger deformation along with a longer arc of contact, resulting in longer times to form adhesive bonds.
4. The scale thickness affects the coefficient of friction the most along with sample temperature. A thick scale produces a lower coefficient of friction as it provides a certain degree of lubricity. A thin scale is more adherent to the metal substrate and is therefore harder to remove or break up.
5. An HSLA grade produces a higher coefficient of friction than a low carbon grade. This is attributed to differences in physical metallurgy and a variance in how the scale layers on the two steels break up.
6. The model proposed by Roberts indicates that the coefficient of friction increases with decreasing scale thickness and increasing temperature. The effect of scale thickness can be corroborated. However, the effect of temperature on the frictional

Chapter 7

Hot Rolling - Industry

Data obtained from Dofasco's hot strip mill logbooks was analysed in order to determine the effect of the various process parameters on the coefficient of friction as well as the break-in time of freshly ground high-speed steel work rolls. Several steels varying in chemical composition from low carbon to high-strength low-alloy grades were analysed using Elroll and, in some cases, Ekelund's formula. In both cases, a match in roll separating force was sought.

Some of the data presented in this chapter was previously analysed using Ekelund's equation for calculation of roll separating force and was published in (Munther and Lenard, 1996). Just like Sims' equation, Ekelund's consists of two distinguished parts, one defining the material and its properties and the other defining the geometry. The major difference between the two is that Ekelund's equation includes the frictional conditions. The roll separating force, P , may according to this equation, be calculated as:

$$P = wL \left[1 + \frac{1.6\mu L - 1.2\Delta h}{h_0 + h_1} \right] \sigma_{fm} \quad (7.1)$$

Note: σ_{fm} here substitutes for an original expression that describes the material flow stress in terms of the chemical composition, temperature, roll velocity, and geometry. The term in the parentheses describes homogeneity of deformation along with the frictional conditions. The coefficient of friction is obtained by solving the equation.

However, Wusatowski (1969) showed that Ekelund's equation has its limitations when it comes to heavy reductions. It is not clear whether that is due to the fact that Wusatowski used the original description of the material behaviour. Today, this description may seem outdated and the use of more accurate flow stress models may increase the performance of the model. Nevertheless, since the accuracy of the coefficient of friction and not computation time is the determining factor in these investigations, the finite-element code, Elroll, is used unless indicated.

The heat transfer coefficient was determined according to the model similar to the one that was used in Chapter 6, depending mainly on pressure, which originally was proposed by Wankhede *et al.* (1997). For industrial conditions, the heat transfer coefficient is much greater than in the laboratory, and may be described by their original model:

$$h = 0.695p - 34.4 \text{ (kW / m}^2\text{K)} \quad (7.2)$$

The coefficient of heat transfer in a hot strip mill typically ranges from 60 to 100 kW/m²K. However, when this model is used as proposed, the coefficient of heat transfer will range from well over 100 to about 500 kW/m²K. It is believed that the mill logbook flow stress originally was used when this model was derived, since substitution of the pressure with the predicted flow stress gives more reasonable numbers.

Just like in the laboratory experiments, the coefficient of friction is chosen so that the calculated and measured values of the roll force match as closely as possible. Data on F7 was left out, as the finite-element calculations indicated that sticking friction ($\mu > 0.5$) occurred at all times in this stand. Elroll does not permit an input on the coefficient of friction that exceeds 0.5.

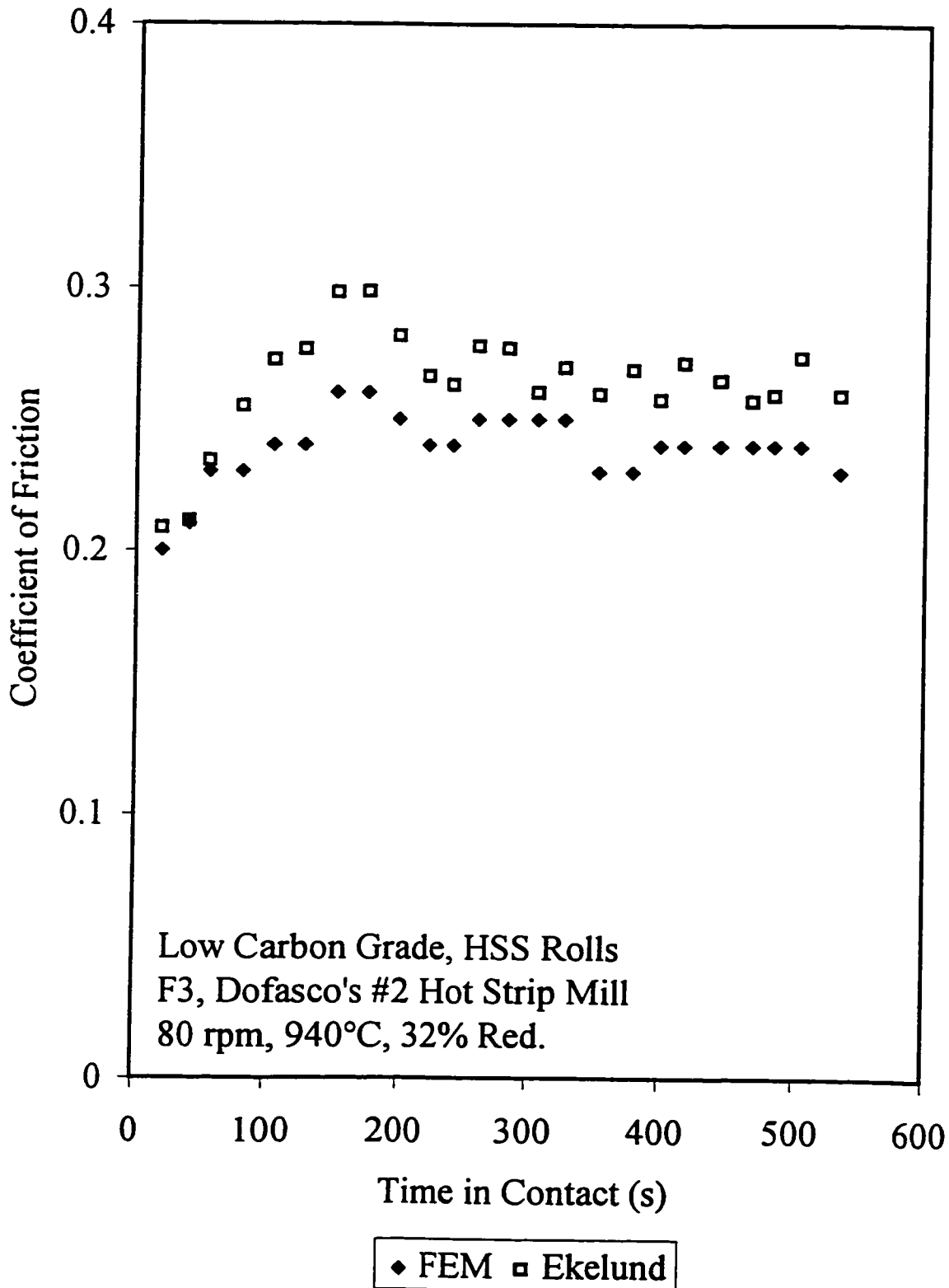
7.1 Break-in Time of Freshly Ground Rolls

It was concluded that deterioration of the rolls caused by thermal cracking cannot be measured in terms of an increase in the coefficient of friction. Build-up of black/grey oxide, on the other hand, can be detected. In most cases, the coefficient of friction is low immediately after a roll change; however, it increases until a steady state is reached.

The time for break-in of freshly ground HSS work rolls is shown in Figure 7.1 where time in contact is plotted versus the coefficient of friction for a part of one campaign of low carbon steel. Every point on the curve also represents one bar being rolled. It can be seen that a peak in the coefficient of friction is reached after about 160 seconds. The steady state is then reached after about 200 seconds in contact. All bars in this investigation were low carbon grades. It can be seen that a freshly-ground and oxide-free HSS work roll produces a low number on the coefficient of friction initially as it rises from 0.2 to the peak of 0.26 to then drops to the steady-state value of 0.24. This is a direct result of the build-up of the protective black/grey oxide on the roll surface. The fact that the coefficient of friction increases with the build-up of this oxide is due to the increase in work that is associated with the additional deformation work of the visco-plastic oxide layer. Average instantaneous contact temperatures were consistently around 450°C in F3. This enables the build-up of the oxide layer, while it makes it ductile.

The rolls appear to be broken in after 200 seconds in contact. This corresponds to a rolled length of 1500 m or 10 to 12 bars. The analysis reported in (Munther and Lenard, 1996) concluded the same, the only difference being a slight difference in the magnitude of the coefficient of friction. Ekelund's model predicted a coefficient of friction that was consistently 0.02 to 0.04 higher than the finite-element model. The consistency of Ekelund's simple model makes it suitable for on-line monitoring of changes in the coefficient of friction.

Figure 7.1. Break-in time of Freshly Ground HSS Rolls

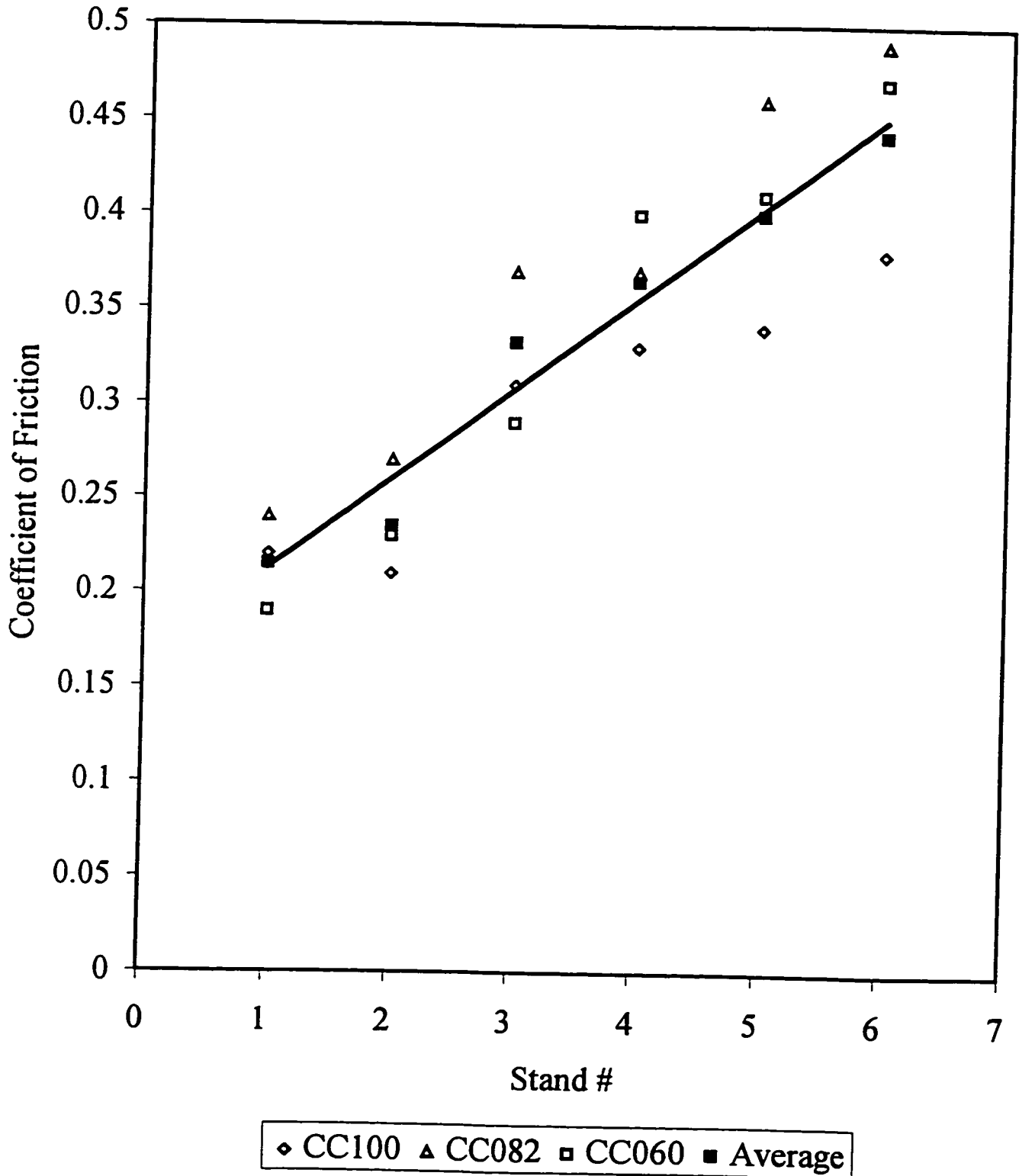


7.2 The Coefficient of Friction at the Various Stands

Figure 7.2 illustrates the average coefficient of friction for stands F1-F6. Several campaigns of 1006, 1008, and 1010 were analysed. Average numbers on entry, and exit thickness, temperature, velocity, roll force, torque, and power consumption were calculated for each grade at each stand. It can be seen that the lowest numbers on the coefficient of friction are produced at the first stand. As mentioned previously, F7 has been left out of the plot as the analysis showed that sticking frictional conditions prevailed for all grades. Interestingly, the steel with the highest carbon content and thus strength produced the lowest numbers on the coefficient of friction at the later stands. This is caused by a difference in process parameters, in particular the reduction. However, the general trend is obvious when the average amongst the three is studied: the coefficient of friction increases from a low of 0.22 in F1 to a high of 0.44 in F6 and there is little deviation from the linear trend line. It is believed that the variation in the different process parameters explains the deviation. The laboratory experiments, presented in Chapter 6, showed that the coefficient of friction increases with decreasing velocity, decreasing temperature, increasing amount alloying elements, and, to a certain degree, increasing reduction. The relatively high numbers on the coefficient of friction in the latter stands are an indication of abrasive wear. These trends are confirmed by surface roughness measurements carried out at Dofasco, which indicate that the roll roughness is between 0.07 and 0.43 μm for freshly ground rolls and between 0.75 and 2.0 μm for worn rolls, with the roll roughness increasing at the higher stands (Webber, 1997). Moreover, the coefficient of friction was always greater than 0.5 in F7. This corroborates the findings by Caillaud and Delaitre (1994).

Table 7.1 summarises the average interface conditions in the finishing train. The instantaneous contact temperature ranges from a high of 489°C in F1 to a low of 428°C in F6. The contact times are meanwhile 27.5 times greater in F1. The heat flux is, if there were to be perfect contact between the rolls and the strip, up to 27.5 times greater in F1.

Figure 7.2. Frictional Conditions in F1-F6



Consequently, thermal fatigue is more of a problem in the early stands of the finishing train. The approximate ratio of the real and apparent contact areas is 0.72 in F1, which increases and approaches unity by stand F3. This is an indication that there is more metal-metal contact in the middle stands than in the early stands. Finally, the high flow stresses and the high velocities in the higher stands cause abrasive wear to be the predominant mechanism, as shown by the measured wear rates, presented in Section 7.8. The increase in the overall temperature rise in the higher stands is explained by the higher flow stresses at lower temperatures, which increases the work term in the adiabatic heat equation.

The smaller numbers on the real and apparent area ratios may be explained by the behaviour of the tertiary scale layer on the bar surface. The transfer bar is fully covered in an approximate 0.019 mm thick scale upon entry in F1. This hinders direct metal-to-metal contact. However, the elongation that takes place as the bar is reduced in thickness exposes fresh, virgin material. Although this material is oxidised immediately, the lower temperatures at the higher stands in conjunction with the shorter interpass times allow less and less oxide to grow. After all, the kinetics study in Chapter 5 reconfirmed the steels' parabolic oxidation sensitivity with regards to time and exponential with regards to temperature. In addition, the higher roll pressures permit a greater deformation of the asperities, thereby causing the real contact area to approach the apparent.

Stand #	μ	t_c (s)	T_C (°C)	p (MPa)	A_r/A_a	ΔT (°C)	x (μm)
1	0.22	0.03849	489	210	0.72	16.6	18.66
2	0.24	0.01637	463	280	0.91	20.0	5.98
3	0.33	0.00826	448	362	~1	26.8	3.29
4	0.36	0.00398	437	493	~1	32.6	1.82
5	0.40	0.00219	432	627	~1	33.2	1.01
6	0.44	0.00140	428	659	~1	36.3	0.57

Table 7.1 Average Interface Conditions including Roll Pressure and Scale Thickness

7.3 The Effect of the Temperature on the Coefficient of Friction

The bars enter the finishing train at temperatures in excess of 1000°C. Figure 7.3 shows the effect of entry temperatures on the coefficient of friction. The presented numbers on the coefficient of friction have been corrected by means of regression analysis for flow stress, velocity, and reduction effects and represent average conditions in F2 concerning the velocity and the reduction. The regression analysis of the data was carried out in terms of the temperature, velocity, flow stress, and mean thickness - arc of contact ratio, as:

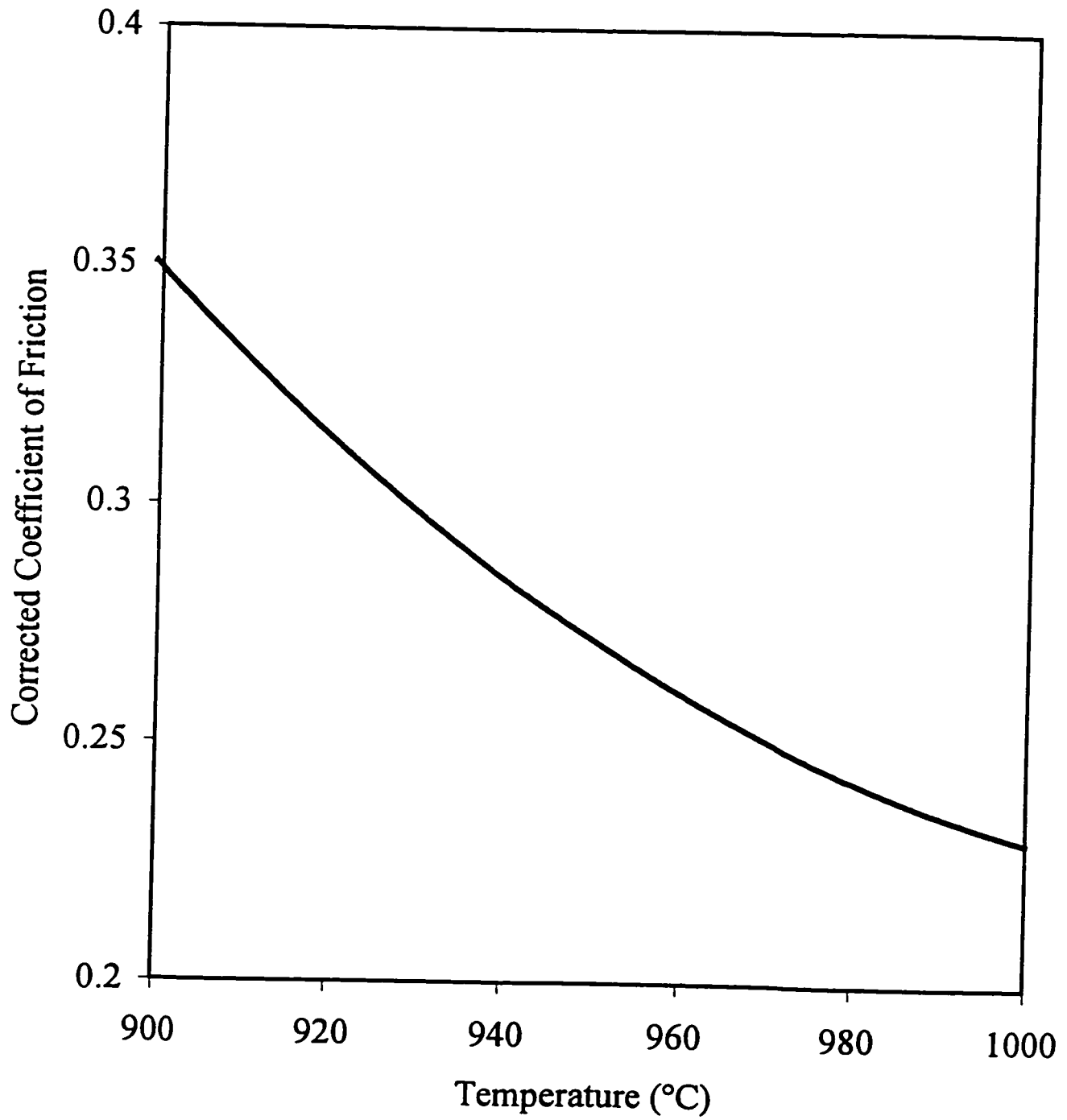
$$\mu = f\left(\sigma_{fm}, \frac{h_m}{L}, v, T\right) \quad (7.3)$$

The velocity in F2 is about 2 m/s and the reduction is roughly 30%. Typically, the entry temperature ranges between 960 and 980°C in this stand. This is enough for a change in the coefficient of friction from 0.24 at 980°C to 0.27 at 960°C.

It is worthwhile mentioning that the trend in these findings is opposite to the trend proposed by Roberts (1977, 1983), but consistent with the laboratory findings presented in Chapter 6 and with the information reported by Pavlov and Kuprin as quoted by Wusatowski (1969). The numbers found here are lower than the findings quoted by Wusatowski, which reported numbers ranging from 0.32 to 0.34 for a steel with slightly higher carbon content.

As discussed in Chapter 6, a decrease in temperature has two effects that may affect the frictional conditions. Firstly, a lower temperature results in a higher material strength of the workpiece and of the scale interface. This means that it gets harder to crush the asperities, while the shear stresses on the steel surface increase with lower temperatures and in order to overcome the gained strength, cause an increase in abrasive wear. Secondly, the adhesive bonds that form between the rolls and the bar become

Figure 7.3. The Effect of Temperature on the Coefficient of Friction



2.0 m/s, 30% Red

harder to break at lower temperatures. This also causes the shear stresses to increase.

Due to the interactions of the other process parameters, the overall temperature effects in the whole finishing train are best studied in conjunction with velocity, heat transfer, and material flow stress. This is done as dimensionless groups are introduced, in Chapter 7.6.

7.4 The Effect of the Steels' Chemical Composition on the Coefficient of Friction

The effect of the steels' chemical composition is shown in Figure 7.4. Three different groups of steels were investigated in this set of data, which consisted of averages for up to 100 bars: (1) low carbon grades (2) medium carbon grades and (3) high-strength low-alloy grades. It is evident that the coefficient of friction increases as the amount of alloying elements is increased. An increase in the amount of alloying elements results in increased temperature sensitivity, which causes the hot strength to increase locally. This is according to the hypothesis, presented in Chapter 6.

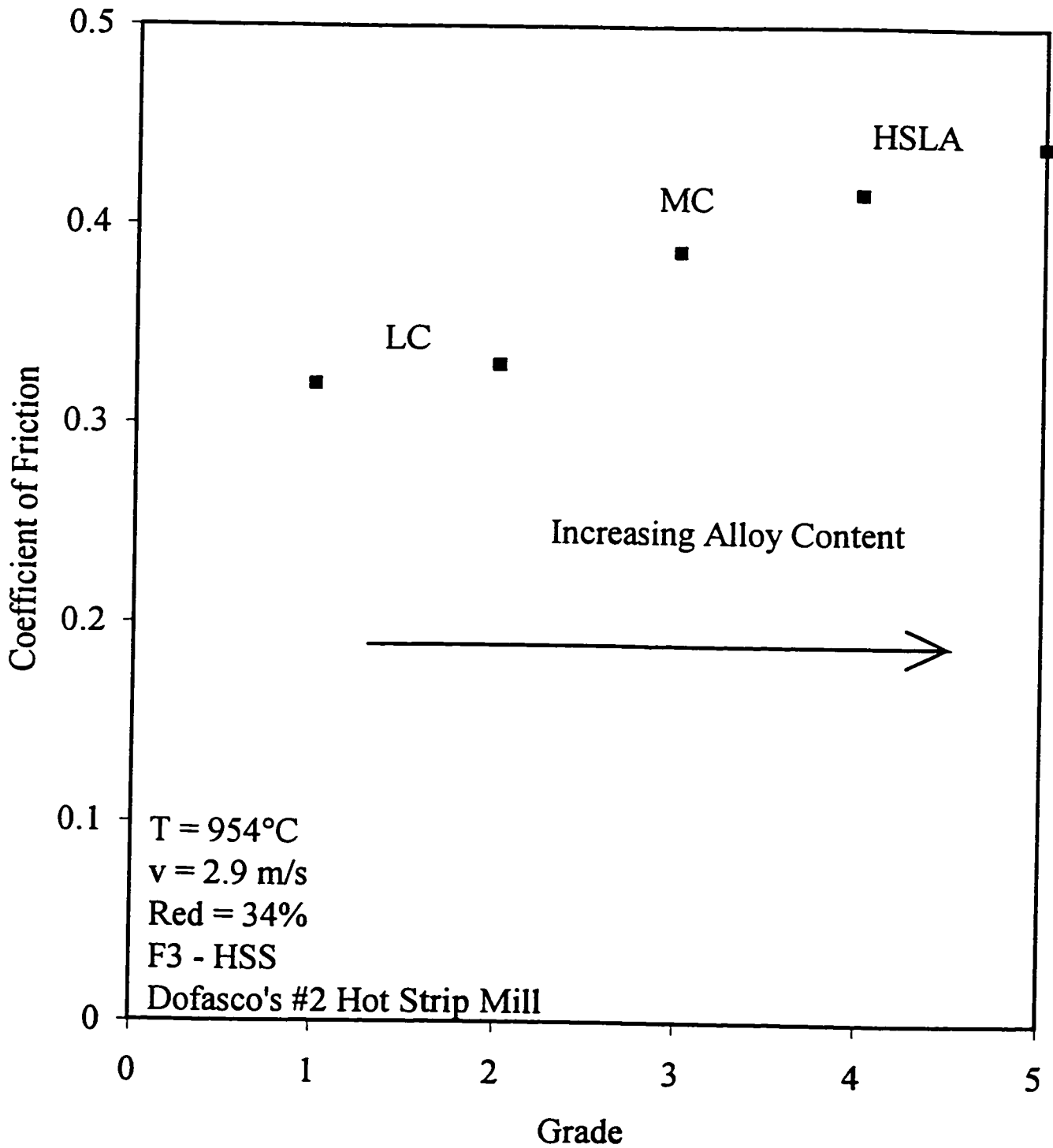
In stand F3, low carbon (LC) grades (0.04 - 0.10 %C) yielded a number on the coefficient of friction that ranged from 0.31 to 0.33, depending on the process parameters, which can be seen in Table 7.2, below. Medium carbon (MC) grades (0.21 - 0.35 %C) give numbers on μ ranging from 0.33 to 0.38.

Grade	T (°C)	Red. (%)	v (m/s)	σ_{fm} (MPa)	M (Nm/mm)	P (kN/mm)	μ
LC	956	34.4	3.04	196.3	0.465	12.70	0.32
MC	961	32.5	2.97	180.6	0.503	12.99	0.37
HSLA	947	35.9	2.92	174.8	0.491	15.00	0.42

Table 7.2 Average Conditions for Analysis of Various Grades in F3

Despite the lowest estimated flow stress, the highest numbers on the coefficient of friction are shown by the high-strength low-alloy (HSLA) grades, which give numbers on μ that range from 0.36 to 0.47. This behaviour can be directly related to the chilling of the surface and subsurface, which in turn increases the various steel grades' hot strength differently.

Figure 7.4. The Effect of the Steels' Chemical Composition on the Frictional Conditions



As discussed in Chapter 6, HSLA grades are more sensitive towards fluctuations in temperature. A chilling of the surface on these would therefore result in a local flow stress that exceeds the others' flow stress by far. However, this does not explain the fact that the highest total roll separating force is seen by the high-strength low-alloy grades. The high roll separating force can be explained by the deviation in process parameters. Here, the temperature is 15° less than for the MC grade, as it drops from 961 to 947°C, while the reduction is increased from 32.5 to 35.9%. The velocity is also slightly lower than for the other two groups.

7.5 The Effect of the Velocity on the Coefficient of Friction

Figure 7.5 illustrates the effect of roll velocity on the frictional conditions in F3 for rolling of a campaign of low carbon grade. The roll velocity in F3 typically varies between 2.7 and 3.4 m/s. Although the roll velocity increases ten folds throughout the finishing train, the strong interactions of the other process parameters, together with the fact that different roll materials are used in the different stands, makes it hard to study the effect of the roll velocity by considering the whole mill. Unless the interactions are corrected for or are studied in conjunction with one another, the effect of roll velocity is best studied in one stand only, where the interactions are relatively small.

The coefficient of friction was, at first, calculated using Ekelund's roll force formula. It can be seen in Figure 7.5 that the coefficient of friction decreases with increasing velocity, as it drops from a high of 0.33 to a low of 0.28. The scatter in the data is caused by the interactions of the other process parameters. The temperature ranged from 917 to 951°C and the reduction varied from a low of 32 to a high of 40 %. The strongest interaction is that of the temperature. The points beneath the trend line in the figure correspond to higher temperatures than those above.

The scatter was brought down substantially by dividing the data into groups of averages. The temperature then instead ranged from 927 to 943°C, whereas the reduction was between 34 and 38%. These results can be seen in Figure 7.6, where the original information was also used to back calculate the coefficient of friction using the finite-element code. Ekelund's formula resulted in numbers on the coefficient of friction that ranged between 0.30 and 0.32, whereas the finite-element code gave results between 0.24 and 0.26. These two methods resulted in similar trends although the magnitude of the coefficient of friction is different. This is consistent with the results on the break-in time of freshly ground work rolls that were presented in Section 7.1. The trends are consistent with those found in the laboratory that were presented in Chapter 6. Apparently, the

Figure 7.5. The Effect of Roll Velocity on the Coefficient of Friction

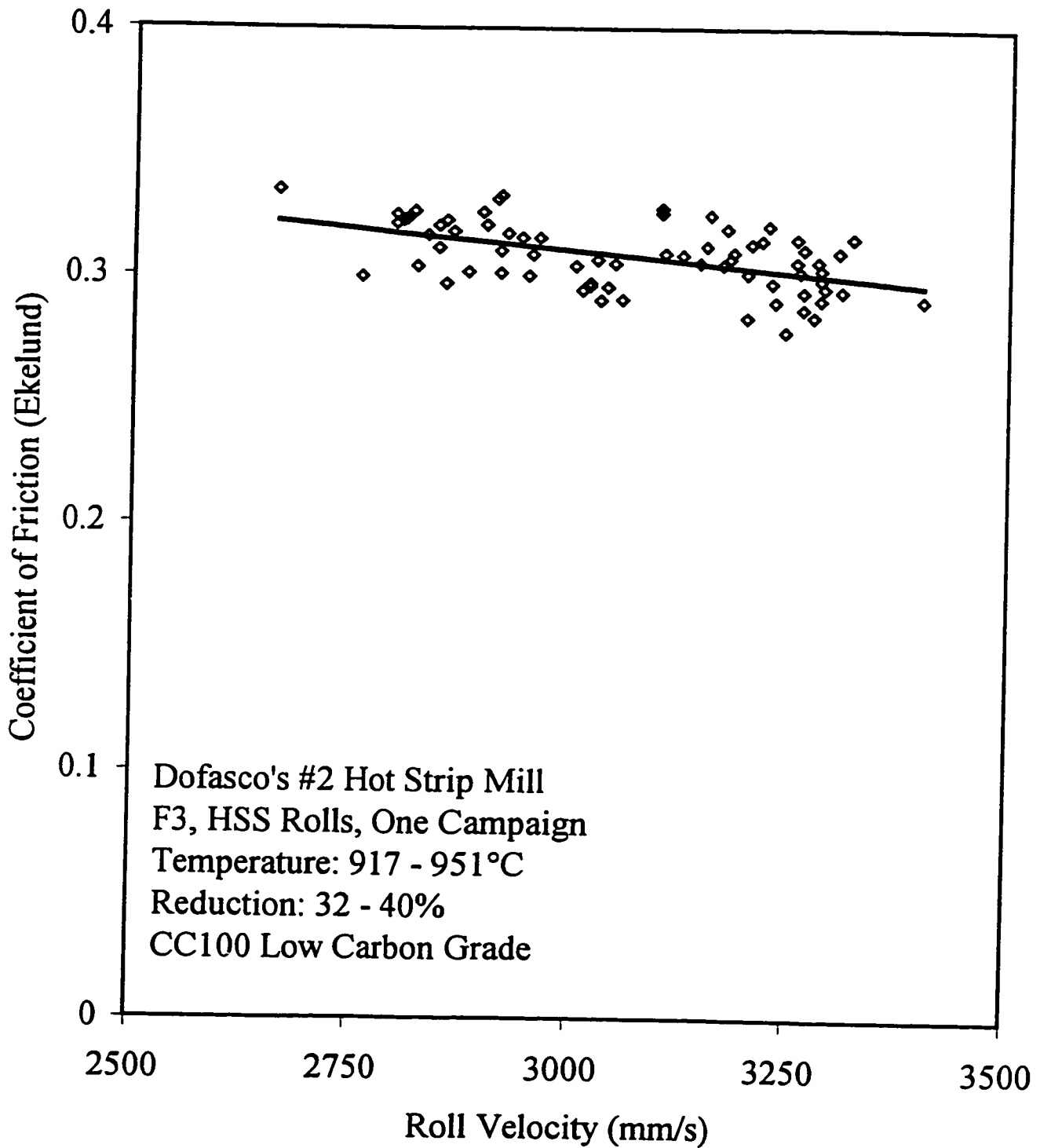
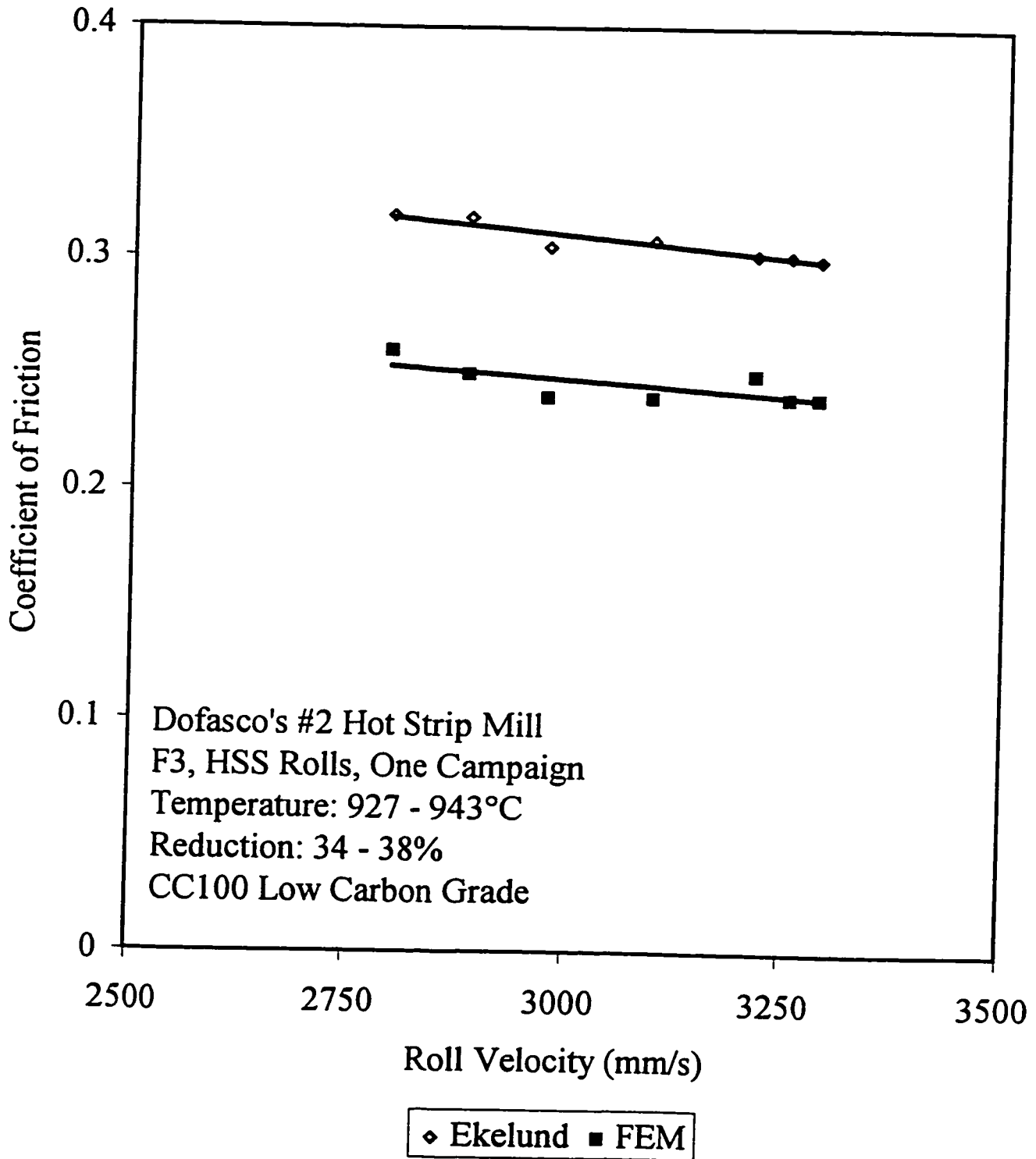


Figure 7.6. The Effect of Roll Velocity on the Coefficient of Friction - A Comparison of Methods of Solution



approach of dividing the data into average groups caused the effect of the roll velocity to be more modest.

The effect of the roll velocity on the coefficient of friction in this stand can be explained by the fact that lower velocities lead to an increased undercooling of the strip's surface. This results in an increased local flow stress, which in turn, causes the rise in the coefficient of friction, as the asperities become harder to deform.

However, the frictional conditions change from stand to stand, when the whole finishing train is considered. The fact remains that the coefficient of friction is increasing throughout the mill. This might even be the case when the effects of the temperature and the reduction are taken into account. A simple regression analysis of the mill results, similar to the one presented in Section 7.3 which takes the temperature and reduction effects into account, indicates that the coefficient of friction increases from 0.25 in F1, where the roll velocity is about 1 m/s, to 0.30 in F6, where the velocity is in excess of 6 m/s. This is indicative of that different wear modes reign in the different stands. After all, thermal fatigue was expected to be the prevailing wear mechanism in the early stands, whereas abrasive wear was expected to dominate in the higher stands. The oversimplified regression model (equation 7.3) may not be a suitable method of analysis. The interactions are best studied in terms of more complex dimensionless groups. These are introduced in Section 7.6.

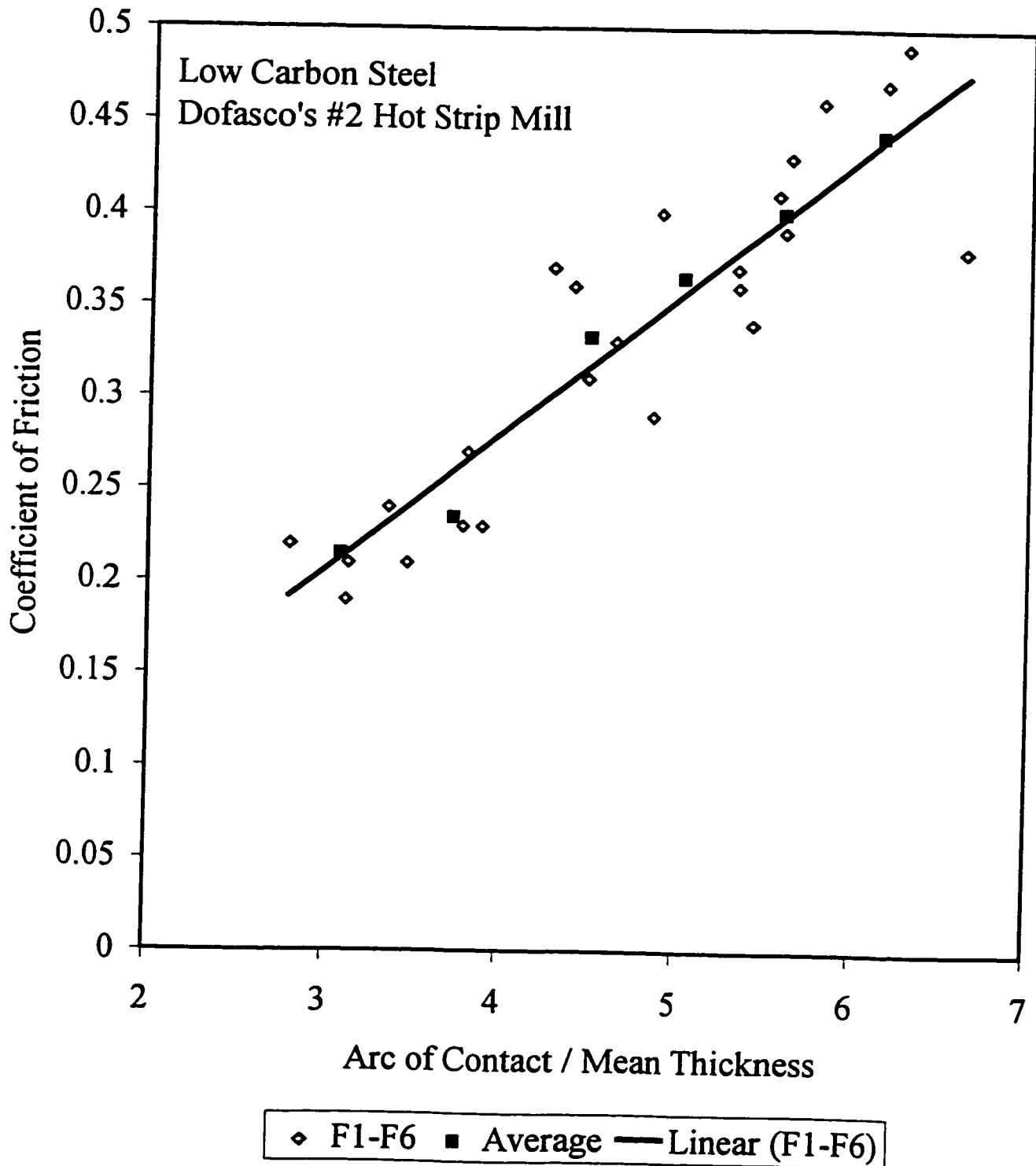
7.6 Introducing Dimensionless Groups

Due to the interactions between many process and materials parameters, comprehending the effects of geometry, velocity, reduction, material strength, and heat transfer is easiest understood when dimensionless groups are observed. Two dimensionless groups are of immediate interest. One is the arc of contact - mean thickness ratio, known as the shape factor, and the other combines the effects of heat transfer, temperature, material strength, and the relative velocity between the rolls and the bar.

Figure 7.7 illustrates the effect of the arc of contact - mean thickness ratio. This dimensionless group is generally considered an indication of the homogeneity of deformation. However, it is also associated with longer contact times, which may result in either an increased cooling of the strip surface or the possibility of forming more adhesive bonds between the work rolls and the strip. An increased cooling of the strip surface causes the flow stress to increase locally and results in a rise in the coefficient of friction. A greater amount adhesive bonds between the rolls and the strip would also increase the coefficient of friction, as more energy is needed to break the bonds. A greater reduction would also result in a smaller mean thickness as well as a longer arc of contact, and would thereby increase the overall material strength and thus the friction. It can be seen in Figure 7.7 that the coefficient of friction more than doubles from a number of 0.2 at a L/h ratio of 3 to a number of above 0.4 at a L/h ratio of 6.

When the ratio between the real and apparent contact areas is considered, a L/h ratio of 3 gives an area ratio of about 0.7. This increases with the arc of contact - mean thickness ratio, and unity on the area ratio is approached at an L/h ratio of about 4. Furthermore, the chilling effects of the work rolls also increase with the L/h ratio, as a ratio of 3 sees a temperature drop of 13°C , whereas an L/h ratio of 6 sees a drop by 23°C .

Figure 7.7. The Effect of the Arc of Contact - Mean Thickness Ratio on the Coefficient of Friction



It is therefore quite likely that a local increase in the flow stress also plays a role in the increased coefficient of friction.

The second dimensionless group, combining the effects of heat transfer, temperature, material strength, and the relative velocity is defined as:

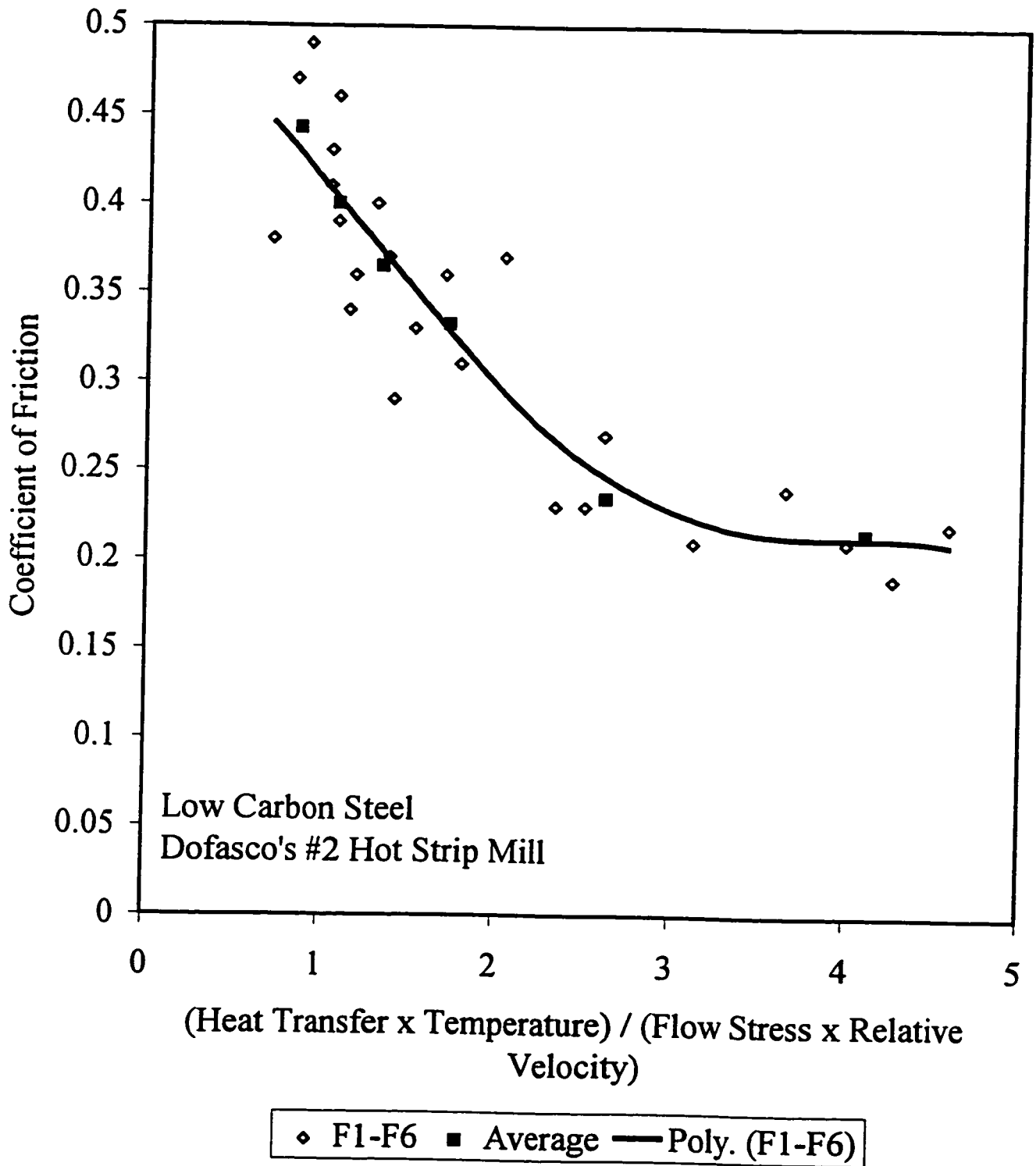
$$X = \frac{hT}{\sigma_{fm} \Delta v} \quad (7.4)$$

where h is the coefficient of heat transfer in $\text{kW/m}^2\text{K}$ as predicted by the formula proposed by Wankhede *et al.* (1997), T is the estimated entry temperature in K as obtained from the mill logs, σ_{fm} is material mean flow stress as obtained from the mill logs and Δv is the relative velocity obtained from the finite-element code.

It is evident from Figure 7.8 that the temperature effect is not the only cause of the changing coefficient of friction. A decrease in heat flux or an increase in flow stress would have the same effect as well as an increase in relative velocity. A number of 1 on the dimensionless group results in a coefficient of friction of 0.4. The coefficient of friction appears to reach a steady state of 0.2 at numbers on the dimensional group that exceed 3. It is conceivable that other parameters such as geometry or amount of scaling may affect the frictional conditions beyond this point. Material strength and adhesion are two predominant factors in this case as well. However, abrasion taken into account in the relative velocity component has a significant contribution since a doubled relative velocity (i.e. increased forward slip) could increase the coefficient of friction by 40%.

Considering the conditions in the finishing train at Dofasco and following the same dimensional approach as Farkas and Lenard (1994), regression analysis of the data permits the roll separating force per unit width to be described as:

Figure 7.8. The Combined Effect of Various Parameters on the Coefficient of Friction



$$P = 14.5(h_0 - h_1)\sigma_m \xi \left(\frac{h_0}{R}\right)^{-0.97} \frac{X^{0.1}}{\sqrt{L/h_m}} \mu^{0.281} \quad (7.5)$$

where X is the dimensionless parameter given by equation (7.4). Equation (7.5) is an extension of Farkas and Lenard's original expression considers roll material, for which the roll material constant, ξ , is defined as:

$$\xi = 0.9 \quad \text{for Hi-Cr rolls}$$

$$\xi = 1.1 \quad \text{for HSS rolls}$$

$$\xi = 1.0 \quad \text{for ICDP rolls}$$

While HSS rolls are associated with infinitesimal wear rates, they apparently produce a higher coefficient of friction than the other roll materials. The low wear rates are a reflection of the high compressive and tensile strengths. There is no information available on why the HSS rolls produce a higher number on the coefficient of friction. However, this has frequently been observed in industry, where they initially caused some off-gauge problems, especially in cases when they were used in the higher stands (Webber, 1994). Due to the higher thermal conductivity the HSS rolls possess, it is reasonable to believe that the local chilling effect by the rolls is increased and indeed causes the higher coefficient of friction. It is also conceivable that the hard carbides in the rolls increase the abrasive wear of the strip somewhat, but cause the coefficient of friction to be higher.

Although the dimensionless group, X , clarified some of the interactions, the question of how the relative velocity affects the frictional conditions still remains. It is therefore necessary to introduce another more complex dimensionless group, λ , which takes into account not only the effect of the temperature, heat transfer coefficient, material flow stress, and relative velocity, but also the mean strain rate, roll pressure, roll roughness, and material properties of the interface including its viscosity.

Starting with the viscosity, η , of the interface in Pas, which, assuming that the scale behaves as a Newtonian fluid, is defined as:

$$\eta = \tau \frac{x}{\Delta v} \quad (7.6)$$

where x is the thickness of the interface, i.e. the scale thickness as calculated from equation (5.14). This allows for plotting of the viscosity versus the coefficient of friction, see Figure 7.9. It becomes apparent that the coefficient of friction decreases with increasing viscosity, as it approaches a low of 0.2 at a viscosity greater than 0.014. Meanwhile, when the viscosity approaches zero, the coefficient of friction approaches a value of 0.5, indicating sticking friction. This trend is consistent with the theory of lubrication in cold rolling, where the coefficient of friction decreases with the viscosity in the boundary and mixed lubrication regimes.

The dimensionless group, λ , that describes the interface between the rolls and the strip may now be defined as:

$$\lambda = \frac{\eta \Delta v' h T}{p \dot{\epsilon} R_s \sigma_{yss}} \quad (7.7)$$

where $\Delta v'$ is the relative velocity in s^{-1} , p is the roll pressure in MPa, h is the coefficient of heat transfer in kW/m^2K , T is the predicted temperature in K, $\dot{\epsilon}$ is the mean strain rate in s^{-1} , R_s is the roll roughness in mm, and σ_{yss} is the yield strength of the scale layer in MPa, which may be inferred from the results found by Jarl (1990).

Figure 7.10 illustrates the dimensionless group, λ , versus the coefficient of friction. It can be seen that the coefficient follows the same general trend when plotted versus the viscosity. Since the relative velocity term in equation (7.7) is eliminated by the

Figure 7.9. The Effect of the Viscosity of the Interface on the Coefficient of Friction

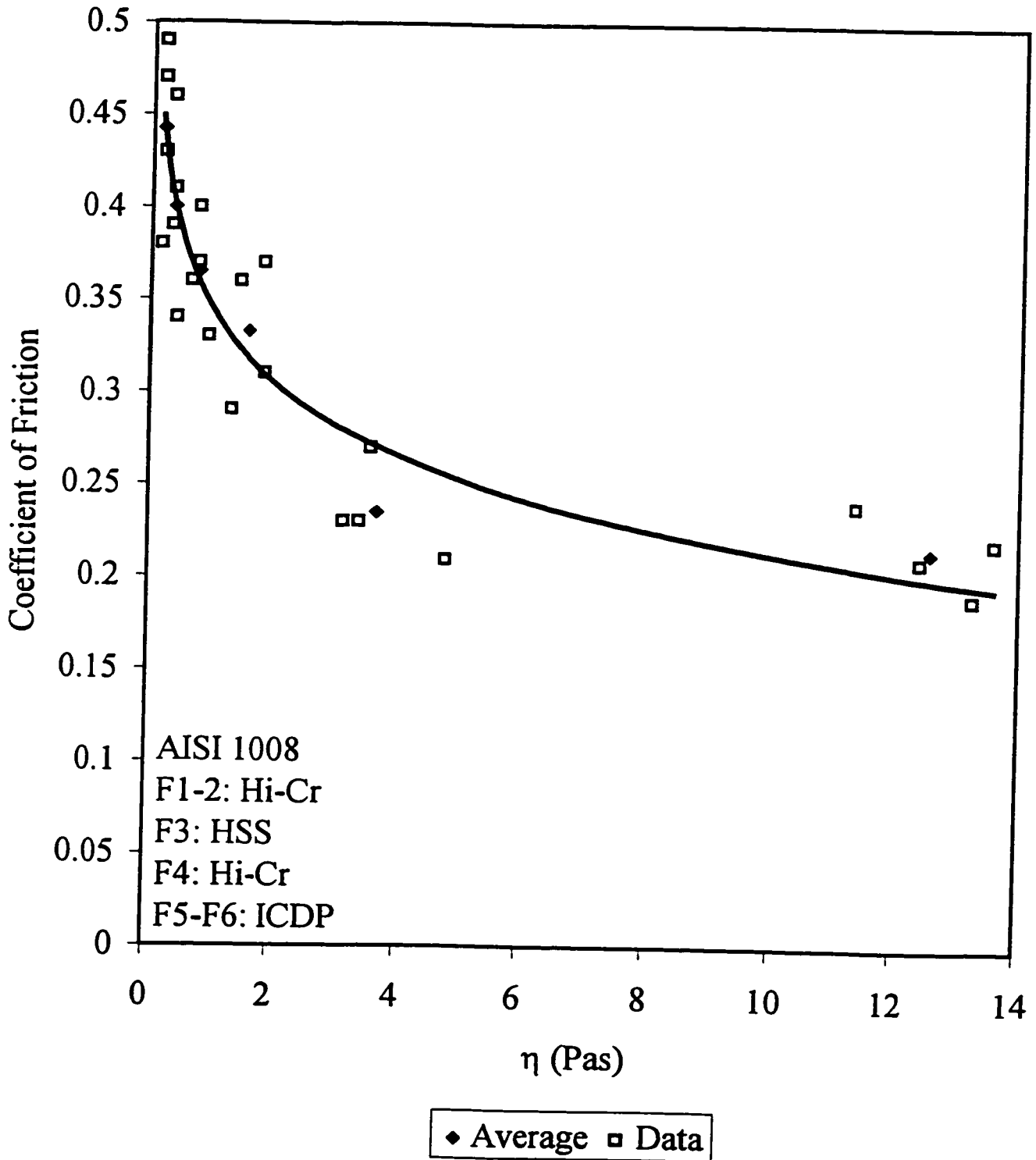
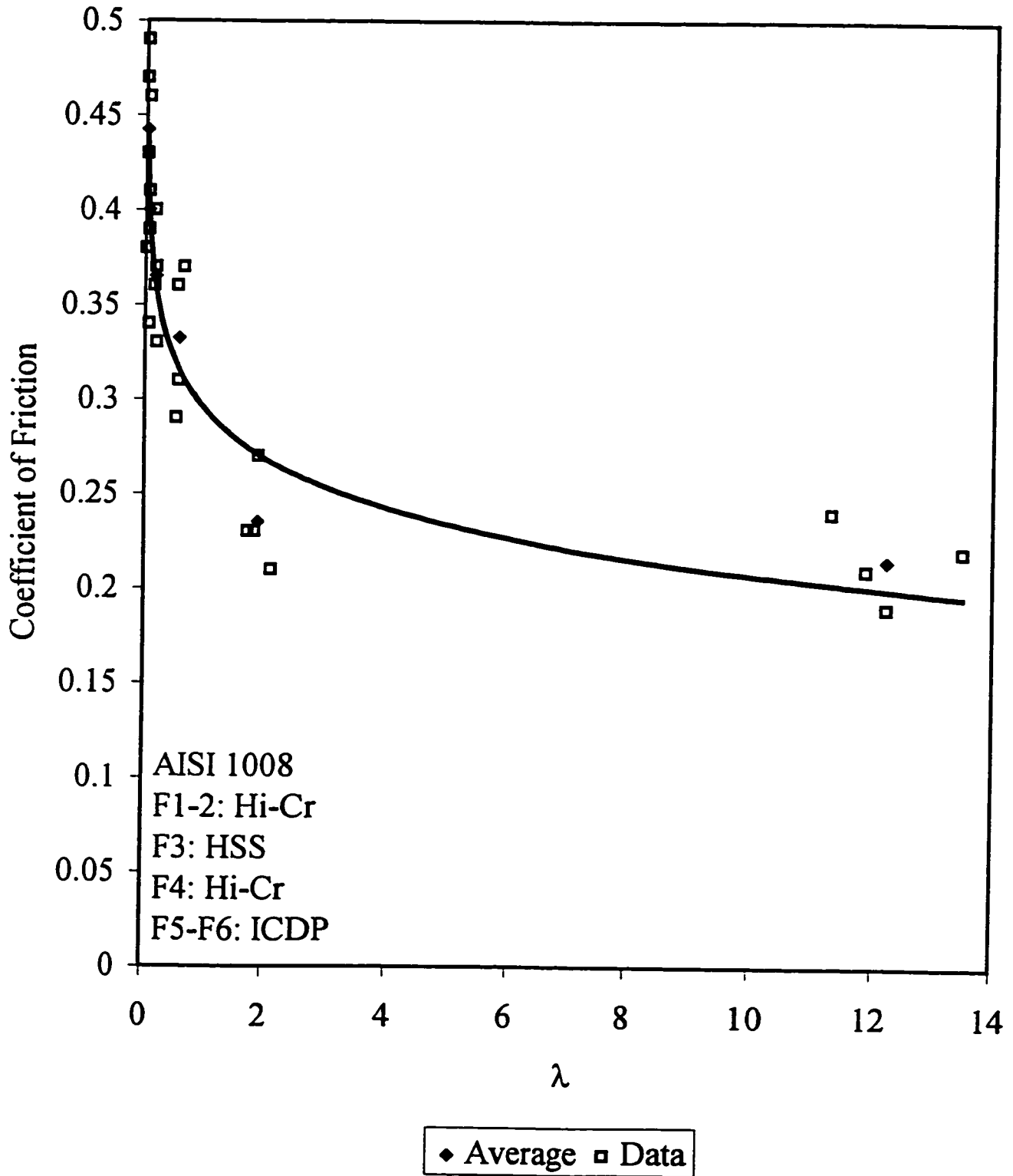


Figure 7.10. The Coefficient of Friction as a Function of λ



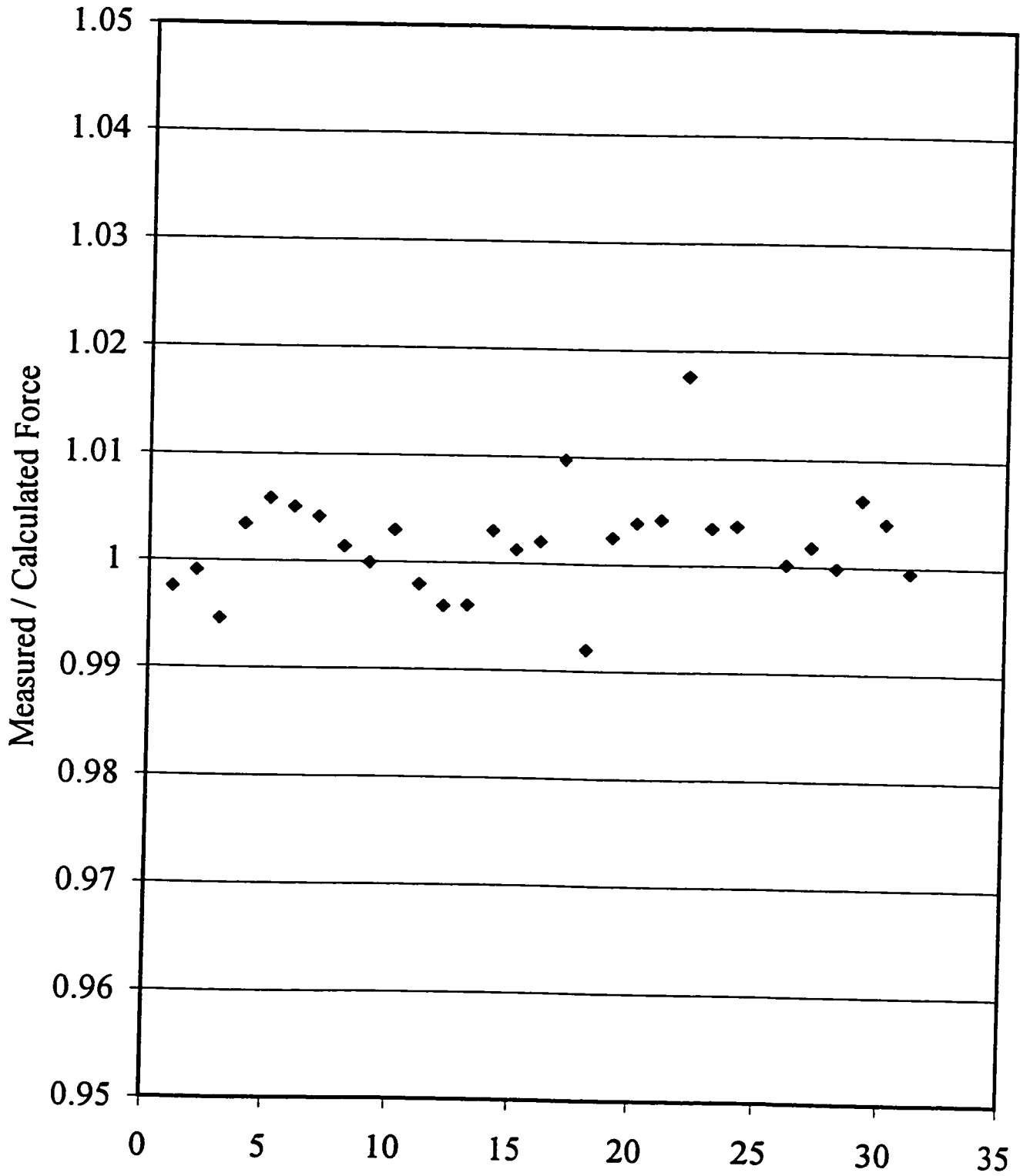
relative velocity term in the definition of the viscosity, only one term containing the velocity in one form still remains and that is the strain-rate. It must therefore be concluded that the coefficient of friction throughout the mill increases with increasing relative velocity, indicating a greater amount abrasive wear at the higher stands. This is contrary to the findings by Pavlov and Kuprin and quoted by Wusatowski (1969), who rolled between velocities of 1 and 4 m/s. Although this author corroborated their findings in the laboratory (see Chapter 6), the industry data includes velocities that are beyond the scope of Pavlov and Kuprin's investigation. The industry data also includes the use of different work roll materials. However, if one stand at the time is considered, the range in velocity becomes smaller, resulting in that an increase in the velocity decreases the coefficient of friction (see Figure 7.4 where F3 is investigated). This corroborates the laboratory findings and indicates that adhesion also plays a certain role on the frictional conditions. It can thus be concluded that while adhesive wear is present, thermal fatigue prevails at the early stands whereas abrasive wear dominates at the higher stands. Since thermal fatigue does not alter the surface of the roll to the same extent as abrasive wear, adhesion is therefore the friction, but not wear controlling mechanism at the early stands.

The dimensionless group further corroborates the influence of the temperature on the coefficient of friction, as an increase in temperature and thus λ results in a decrease in μ . It can also be noted that an increase in the strain rate, which increases the flow stress of the material, causes λ to decrease, which in turn increases the coefficient of friction. The effect of the roll roughness is as can be expected, as it lowers λ , which increases the coefficient of friction. Furthermore, an increase in the yield strength of the scale layer decreases λ and increases the coefficient of friction.

7.7 Experimental Error

As mentioned previously, the magnitude of the coefficient of friction was inferred by matching the measured and computed roll separating force. The accuracy of the calculations is of some importance. Figure 7.11 shows the experimental errors in terms of ratios of measured and calculated numbers on roll separating force, for 100 bars of tinplate grades. It is evident that the error is no larger than $\pm 2\%$. It can thus be concluded that a good match was made.

Figure 7.11. Experimental Error - Dofasco Data

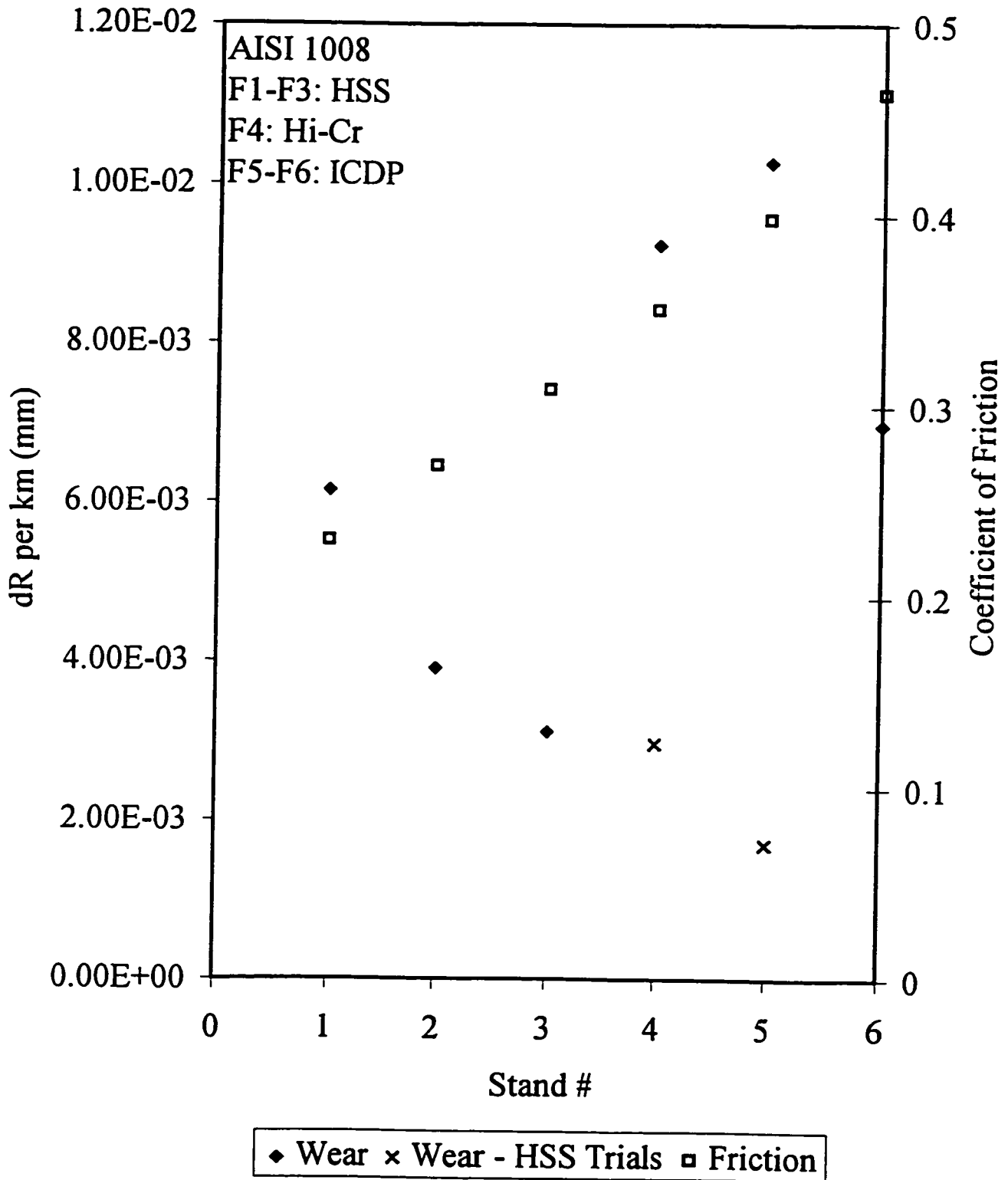


7.8 Relating the Coefficient of Friction to Roll Wear

The numbers on the coefficient of friction for the various stands, as presented in Figure 7.1 indicate that abrasive wear is of considerable significance for F4 and up. It is therefore of interest to model the abrasive wear and its dependency on the coefficient of friction. Abrasive wear effectively removes material from the rolls. Following Archard (1953), this volume was defined in Chapter 2 as a function of a wear constant, depending on the hard asperity angle and roll material, the coefficient of friction, the total roll separating force in N/mm, the compressive strength of the roll material in MPa, and the sliding length in mm, which was defined in terms of the arc of contact in mm, the rolled length in mm, the work roll diameter in mm, and the reduction as decimal fraction. The removed volume was also described in terms of unit width as a function of the roll diameter and the decrease in roll radius caused by the abrasive wear in mm. This set of equations resulted in equation 2.15, which may be used to determine the wear constant from industrial measurements.

The measured wear in the finishing train as of July 1997 is shown in Figure 7.12, in which the decrease in roll radius is plotted versus stand number. At this time, HSS rolls substituted Hi-Cr rolls in F1-F4. Mill trials in F5 indicate a dramatic change in wear as a result of the use of HSS rolls. The hypothesis that thermal fatigue prevails in the first stands and abrasive wear in the latter stands is corroborated by these findings as well. It is noteworthy that the measured wear in F4 is down by a factor 3 and in F5 by a factor 5 as a result of the change in roll material. The measured wear rates resulted in calculated modified wear constants that were 10^{-4} in F1-F3 (HSS), 3.5×10^{-4} in F4 (Hi-Cr), 5.5×10^{-4} in F5 (ICDP), and 4.5×10^{-4} in F6 (ICDP).

Figure 7.12. The Roll Wear in F1-F6



7.9 Conclusions

It has been shown that the finite-element code can be used successfully to analyse mill logbooks and it can be concluded from these investigations that:

1. Freshly ground HSS work rolls produce a low coefficient of friction. As a thin chromium oxide layer develops on the surface, the coefficient of friction increases, reaches a plateau, and then drops to a steady-state value, provided the process and material parameters remain the same. This steady-state value is reached after a contact time of 200 s.
2. The coefficient of friction is dependent on temperature, steel chemical composition, relative velocity, and flow stress. It increases with decreasing temperature, increasing amounts of alloying elements, increasing relative velocity, as well as increasing material flow stress.
3. Generally, the coefficient of friction is low in the first stands. It then increases stand by stand, and results in sticking friction in F7.
4. The predominant wear mechanism in the first 4 stands is thermal fatigue, whereas abrasive wear is more severe in the last 3 stands of a 7 stand finishing train.

Chapter 8

Tribology in Hot Rolling - A Comparison between Laboratory and Industry

The results on the frictional conditions of hot rolling in the laboratory and the industry presented in Chapters 6 and 7 are compared in an attempt to ascertain the usefulness of laboratory experiments. Relationships that permit a comparison of the results obtained in the laboratory and in the industry are presented. The comparison of the results is made in terms of both traditional and newly derived dimensionless groups.

8.1 Relating Results from Laboratory to Conditions in Industry

When comparing the geometry and power consumption for conditions concerning plane strain flow it is useful to plot the arc of contact - mean thickness ratio versus the roll pressure - shear strength ratio. The resulting curve is traditionally referred to as the Pawelski curve, in which an arc of contact - mean thickness ratio of less than unity indicates excessive inhomogeneous deformation. A ratio near unity indicates optimum conditions from a power consumption point of view. Ratios of far greater than unity are common for conditions of hot rolling in industry, as the contribution of the friction term increases with an increasing arc of contact, as a result of the use of large roll diameters.

Figure 8.1 illustrates the Pawelski curve for hot rolling of low carbon steels. It can be seen that the laboratory experiments, consisting of samples with a scale thickness of 0.015 mm, are grouped where the arc of contact - mean thickness ratio is slightly greater than unity. This indicates that inhomogeneous deformation is of little concern for this set of data. The points representing the results from industry have been corrected for the use of different roll materials in the various stands by multiplication of the inverse of the roll material constants, ξ , defined in Chapter 6. The roll material constant for the HSS rolls is kept as a reference since tool steel rolls were used in the laboratory experiments. The large roll diameters used in industry lead to greater numbers on the arc of contact - mean thickness ratio, resulting in increasing roll pressure - shear strength ratio due to the increased work necessary to overcome the frictional work. There is a trend in the laboratory and industry data, as they fall into line and can be connected by a trend line, see Figure 8.1. Consequently, it can be concluded that the laboratory and industry results can be compared in terms of the effects of geometry on the frictional behaviour.

Figure 8.2 depicts the effect of the draft, i.e. the reduction, and the material flow stress on the coefficient of friction. Although the trends are similar, there is a large difference in the magnitude of the laboratory and industry data because the numbers produced in the laboratory are at least 50% greater for similar conditions. However, the coefficient of friction can be corrected for the most obvious difference in geometry by multiplying the laboratory data by the square root of the different roll radii as:

$$\mu_{\text{corrected}} = \mu \sqrt{\frac{R_{\text{lab}}}{R_{\text{ind}}}} \quad (8.1)$$

Although the scatter in the laboratory data is brought down substantially, the most essential outcome is that the corrected laboratory data now overlaps the data from industry with a common trend line. Consequently, it can be concluded that for similar

Figure 8.1. The Pawelski Curve

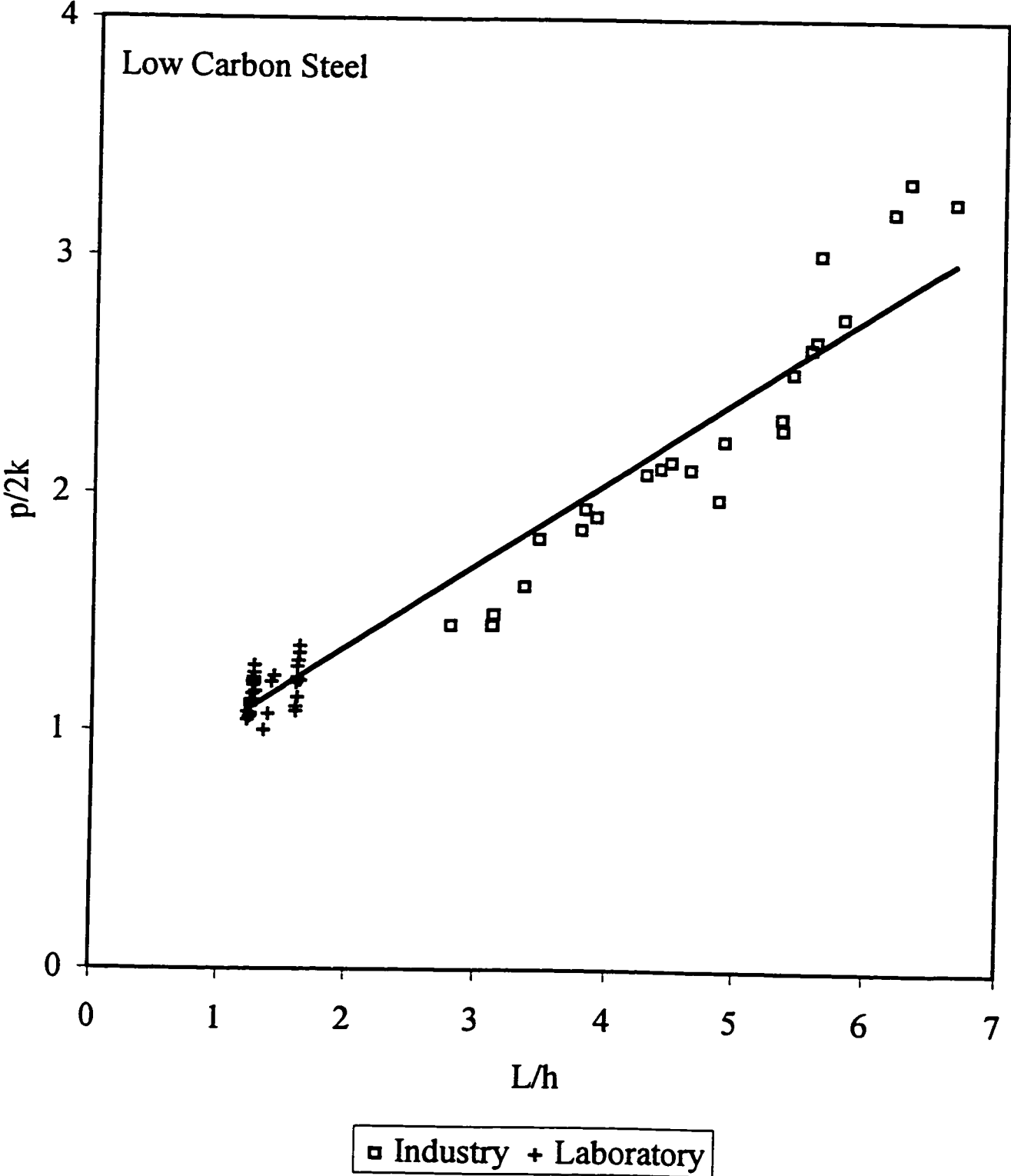
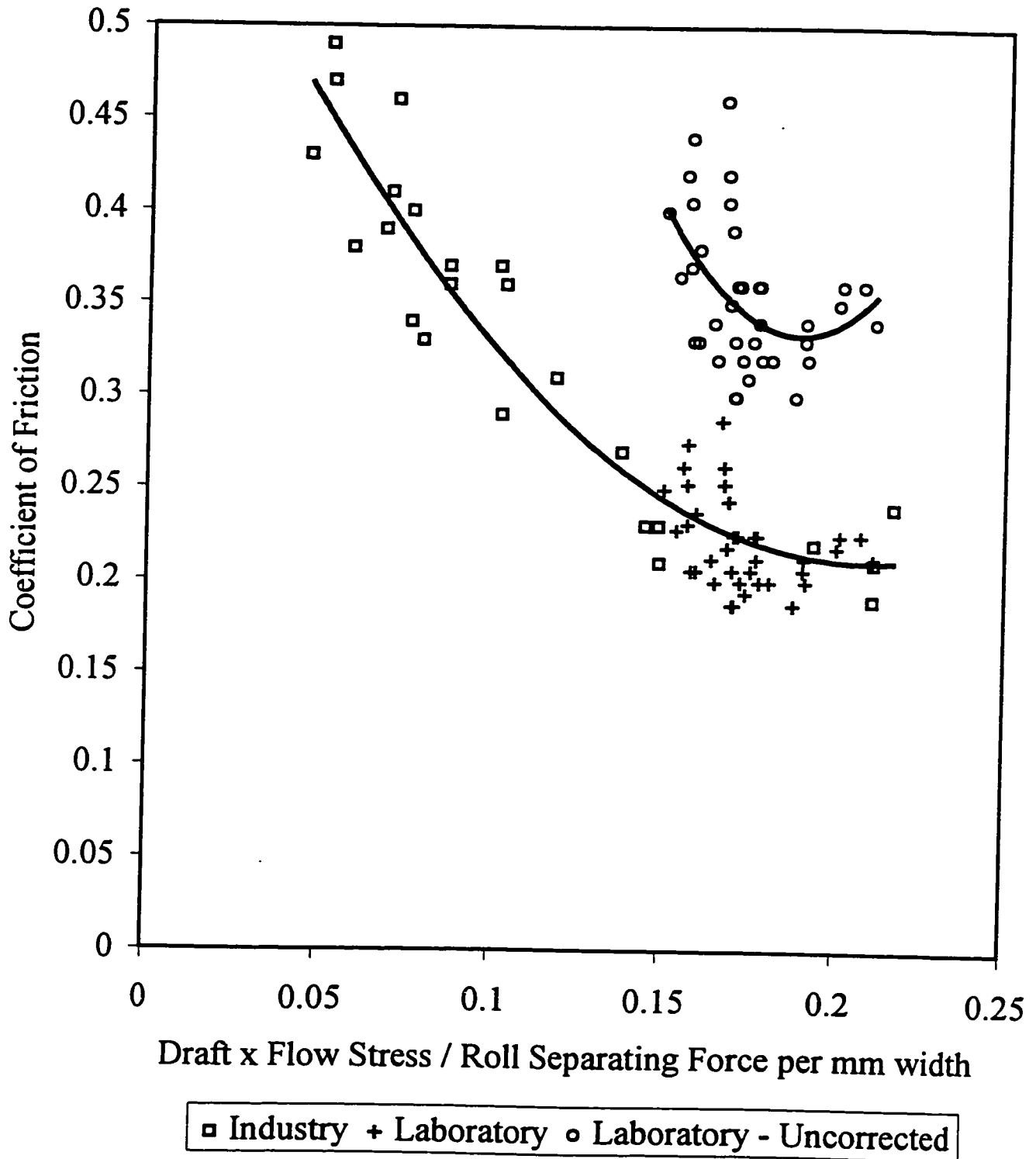


Figure 8.2 The Effect of Draft and Flow Stress on the Coefficient of Friction



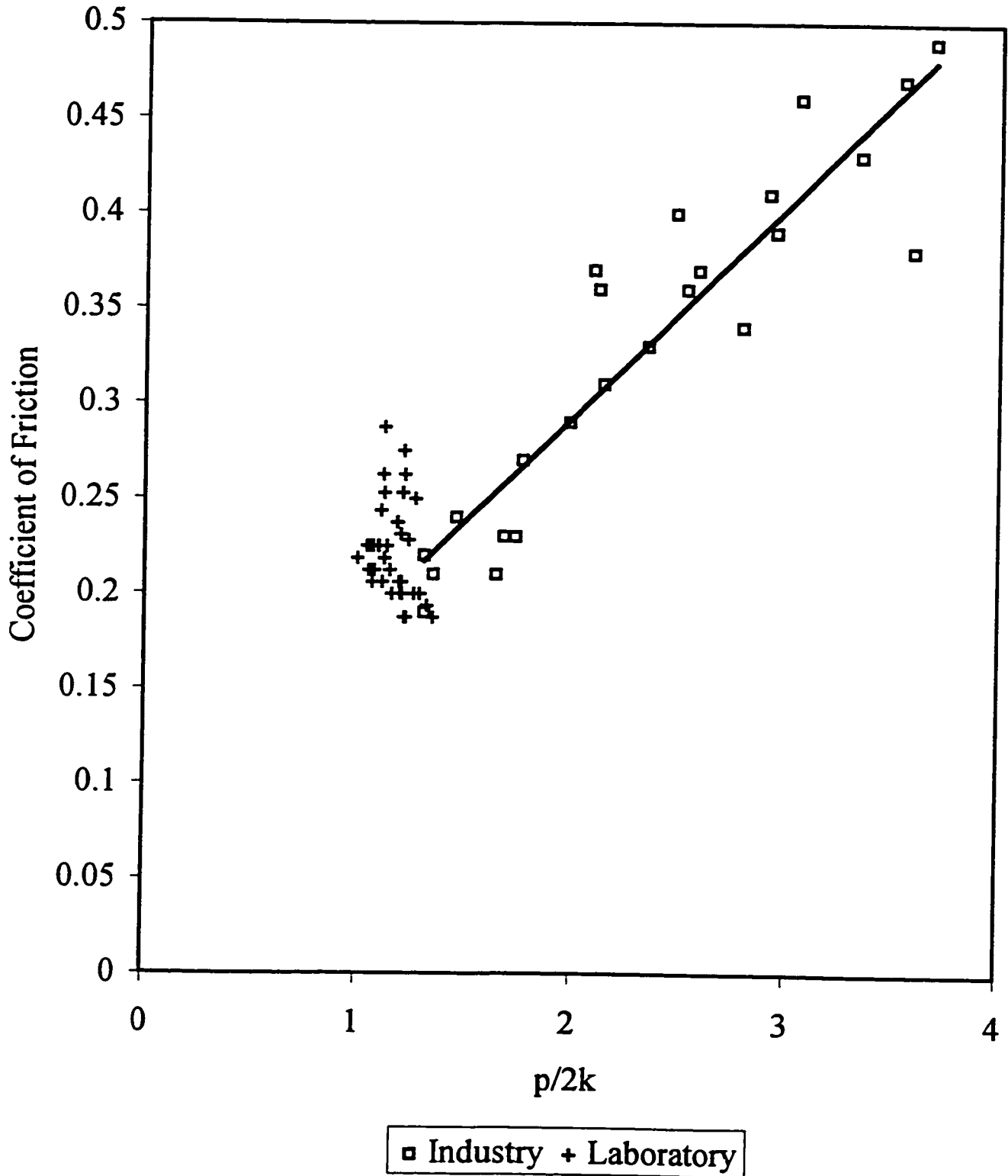
conditions regarding the process and material parameters, the coefficient of friction in the laboratory can be related to the coefficient of friction in the industry using the following relationship:

$$\mu_{\text{lab}} \sqrt{R_{\text{lab}}} = \mu_{\text{ind}} \sqrt{R_{\text{ind}}} \quad (8.2)$$

The implication is that, provided common dimensionless groups that define the process and the materials parameters are found, the results from the laboratory can be directly applied to the hot rolling conditions in a full scale hot strip mill.

Small numbers on the x-axis in Figure 8.2 correspond to large numbers of the roll pressure - shear strength ratio, allowing this curve to be seen in the same context as the Pawelski curve, presented in Figure 8.1. This is illustrated in Figure 8.3, in which it can be seen that the coefficient of friction increases linearly with the roll pressure - shear strength ratio. However, relationships defining the process and material parameters must still be found.

Figure 8.3. The Effect of $p/2k$ on the Coefficient of Friction



8.2 Interpreting Results from Laboratory and Industry

The introduction of the modified Stribeck curve in Chapter 7 showed that similar modes of lubrication can commonly be found in cold rolling could also be found in hot rolling. It was stated that, for hot rolling in industry, boundary and mixed lubrication is probably due to the behaviour of the interface, and in particular the behaviour of the scale.

Figure 8.4 illustrates the traditional Stribeck curve, in which the dimensional Sommerfeld number ($\eta\Delta v/p$) is plotted versus the coefficient of friction. When the corrected laboratory data is added to the industry data previously analysed, see Figure 8.4, it becomes obvious that some form of quasi-hydrodynamic lubrication may occur for the laboratory conditions including F1. This phenomenon is due to the break up of the scale, which acts as a Newtonian fluid, completely separating the asperities of the rolls from the asperities of the strip. The scale is thereby lubricating the process, but is at the same time also insulating heat transfer from the strip to the roll, which in turn also affects the frictional behaviour since it reduces the chilling effect of the rolls. The scatter in the laboratory data is due to the extremes in the process parameters, i.e. very low velocities and temperatures. The Sommerfeld number may be expanded into the λ -parameter (Figure 8.5). This is done in order to include the effects of the strain-rate, temperature, coefficient of heat transfer, roll roughness, and the strength of the scale. Evidently, the effects are limited in that they have little influence on the magnitude of the coefficient of friction. Their primary influence is that they directly affect the roll pressure, which itself is a constituent of the Sommerfeld number. A higher roll pressure causes a lower Sommerfeld number, which, in turn, causes a higher coefficient of friction. Nevertheless, the λ -parameter affects only the x-axis. Its usefulness lies in that it provides convenient numbers on the x-axis.

Figure 8.4. The Stribeck Curve

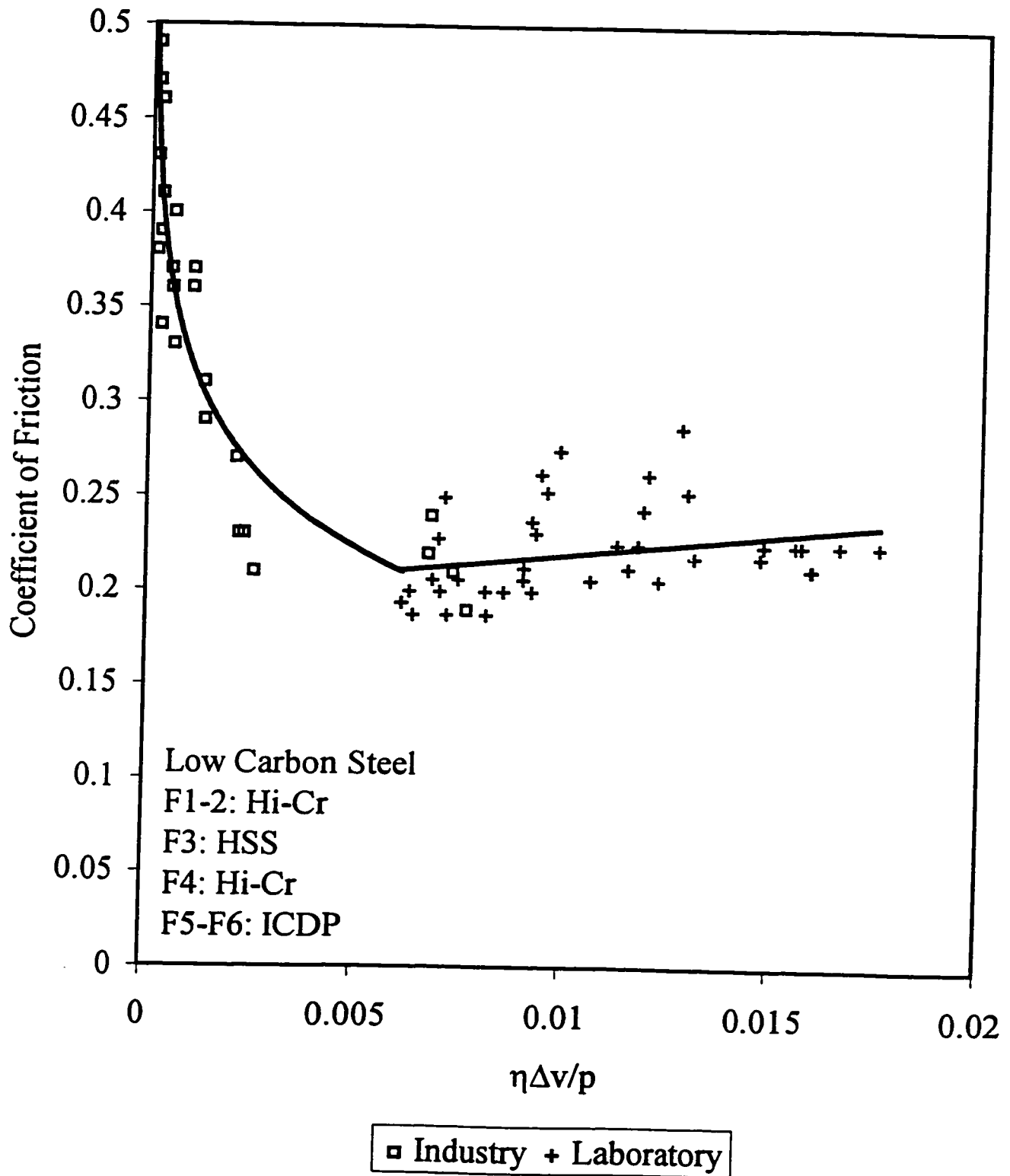
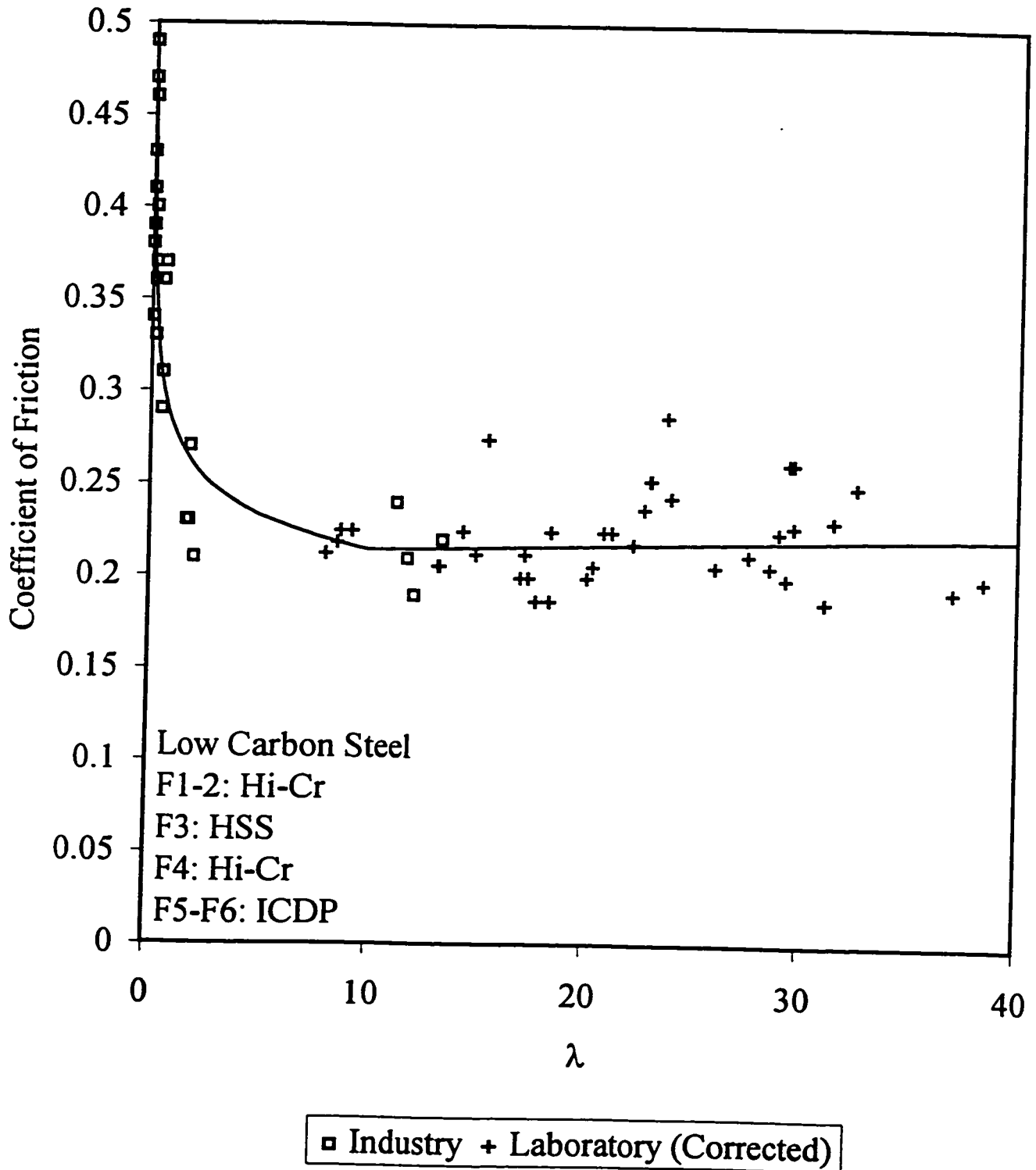


Figure 8.5. The Coefficient of Friction in Industry and Laboratory as a Function of the λ - Parameter



A λ - parameter greater than 10 appears to be the transition point between the mixed and quasi-hydrodynamic lubrication regions. The laboratory data in the graph is represented by the experiments with a scale thickness of approximately 0.015 mm, which is comparable to the scale thickness that forms on the strip after the scale breaking operation and is thereby the scale thickness present in the roll gap of F1. The velocity, temperature and reduction in F1 are also similar to the conditions in the laboratory. Consequently, a λ - parameter of about 10 will produce the same value on the coefficient of friction for both the conditions in the industry and the laboratory, provided that the latter is corrected for its smaller roll radius, which makes it possible to infer results found in the laboratory to industry. In the quasi-hydrodynamic region, the coefficient of friction may be described in terms of the λ - parameter or the Sommerfeld number as:

$$\mu = 0.22 + 0.0001\lambda \quad (8.3)$$

$$\mu = 0.20 + 2.13 \frac{\eta \Delta v}{p} \quad (8.4)$$

In stand F2 and beyond, where the λ - parameter is about two and descending, hot rolling is carried out in the mixed lubrication regime. A λ - parameter of less than ten is mainly characterised by a thin scale thickness as well as a high relative velocity. The behaviour of the interface is therefore different than what it is when the λ - parameter has a value of 10 or more. Rolling in the mixed lubrication regime means that the film, which in the case of hot rolling may be seen as a quasi-film, consisting of the protective oxides on the rolls, the scale on the strip, its debris, and water from the roll cooling and scale breaking operations, is sometimes penetrated by the asperities of the rolls and the strip. This causes metal to metal contact and this becomes more apparent as the λ - parameter descends further at the higher stands, where it causes an increase in abrasive wear. Accordingly, the coefficient of friction increases. This was also corroborated by the ratios of real and apparent contact areas throughout the mill, indicative of greater metal to metal

contact. The coefficient of friction can, in the mixed lubrication region, be related to the λ - parameter or the Sommerfeld number by the following relationships:

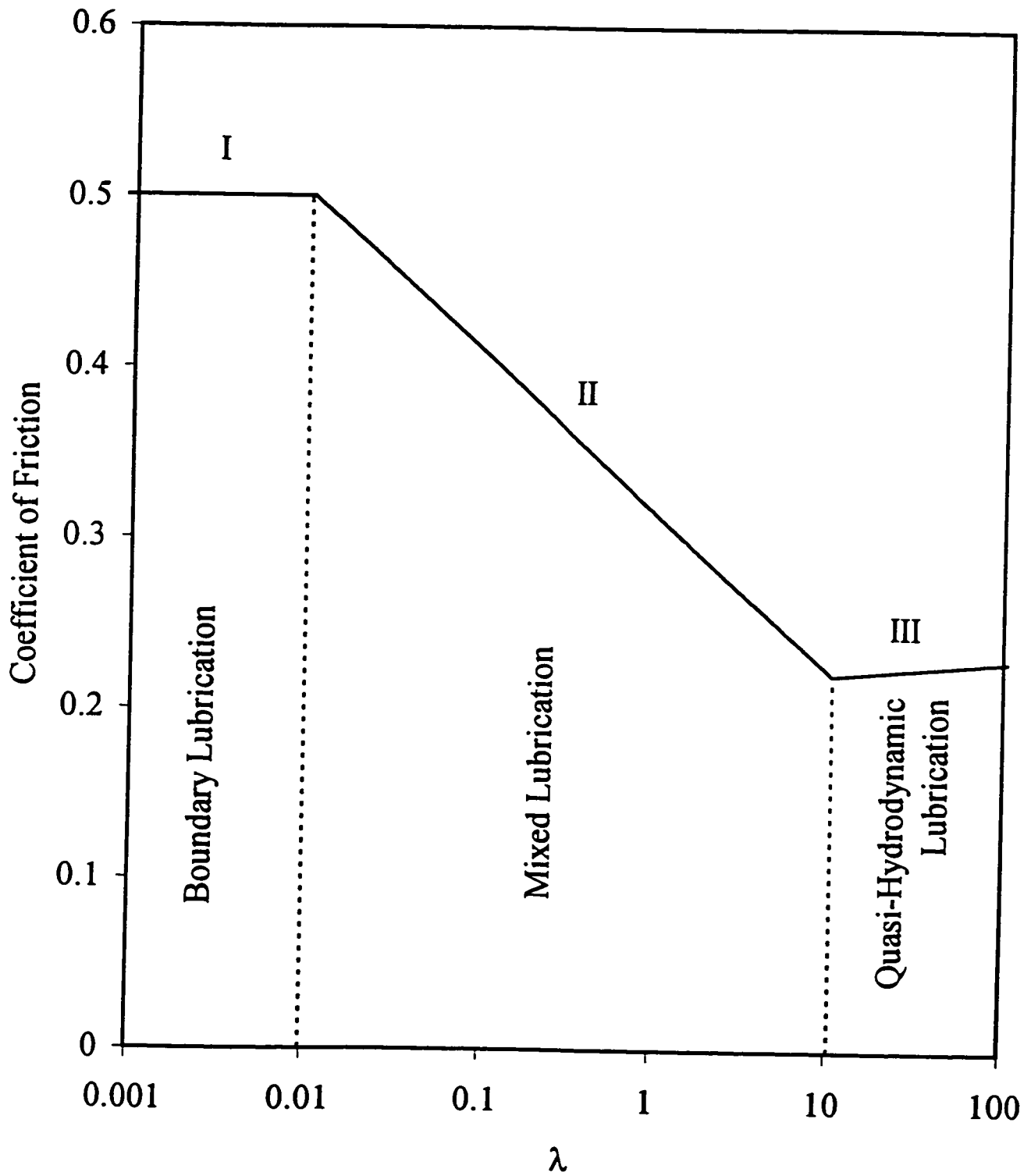
$$\mu = 0.28\lambda^{-0.1215} \quad (8.5)$$

$$\mu = 0.09 \left(\frac{\eta \Delta v}{p} \right)^{-1.859} \quad (8.6)$$

In F7, the coefficient of friction can be so high that problems with the strip sticking to the rolls have been reported (Lait, 1997). This was corroborated early on in the analysis of the industry data, which indicated that the coefficient of friction was greater than 0.5. It can be seen in Figure 8.5 that for even smaller values on the λ - parameter, the coefficient of friction approaches a value of 0.5, as the λ - parameter approaches zero. A coefficient of friction of 0.5 is indicative of conditions of sticking friction. It is therefore reasonable to believe that F7, if not completely in the boundary lubrication region, characterised by full metal to metal contact, might be at least in the stage of transition from the mixed to the boundary lubrication region.

The information presented in Figure 8.5 can be used as a basis when constructing a general map for the frictional conditions in hot rolling. Resulting from this map, the three regions of lubrication are revealed, see Figure 8.6. Region I, boundary lubrication, is characterised by nearly full metal to metal contact, caused by a very thin scale thickness (less than 1 μm) and/or a very high relative velocity (over 750 mm/s) often seen in the last stand. This results in a coefficient of friction that has the maximum theoretical value, i.e. $\mu = 0.5$.

Figure 8.6. The Three Lubrication Modes in Hot Rolling



A transition into Region II, mixed lubrication, occurs at a λ - parameter of 0.01. The scale is here slightly thicker and the relative velocities are somewhat lower. An increasing λ - parameter causes less and less metal to metal contact, resulting in a drop in the coefficient of friction, which decreases steadily until the asperities of the rolls and strip are completely separated. Initially, abrasive wear is the controlling wear mode. However, its role decreases as the relative velocity drops. At a λ - parameter of 0.1, thermal fatigue becomes the rate controlling mode.

The transition into region III, quasi-hydrodynamic lubrication, which takes place at a λ - parameter of 10, occurs when there is no contact between the asperities of the rolls and the strip. The coefficient of friction appears, at the same time, to be at its lowest point ($\mu \approx 0.2$), and is thereafter increasing slightly, as the relative velocity becomes so low that adhesion is the wear controlling mode.

Due to the low relative velocities, high temperatures, and thick scale, extrapolation makes it reasonable to believe that plate and rough rolling occur in region III.

8.3 Conclusions

This chapter has shown that laboratory experiments can be compared successfully to the conditions of hot rolling in industry. As a result, the following conclusions may be drawn:

1. Laboratory hot rolling experiments may be compared to data from industry by correcting for the most obvious difference in geometry - the roll radius.
2. The tribology of hot rolling can be considered in terms of regions of different modes of lubrication. Previously, this theory has been limited to the tribology of cold rolling.
3. Although the temperature has an effect, two parameters, the scale thickness and the relative velocity, appear to control the mode of lubrication.
4. The quasi-hydrodynamic region can be described by a linear relationship between the coefficient of friction and the λ - parameter.
5. A λ - parameter of 10 marks the transition from the quasi-hydrodynamic to the mixed lubrication region.
6. The mixed lubrication region is best described in terms of a power law, whereas the boundary region, if present, is characterised by that the coefficient of friction approaches 0.5 as the λ - parameter approaches zero.

Chapter 9

Summary

The presented research project was undertaken since the available information of the effects of process and material parameters on the conditions at the interface was found to be inconclusive, outdated or filled with contradictions and inconsistencies. For instance, Roberts proposed an equation, in which the predicted coefficient of friction increases with increasing temperature, despite the fact that the material hot strength drops as the temperature increases. In this equation, only the temperature and the scaling affect the coefficient of friction. Wallquist presented information on forward slip, roll separating force, roll torque, power consumption, and spread. However, he did not use his experimental data to calculate the coefficient of friction, since he was mainly preoccupied with power consumption and shape. The same goes for el-Kalay and Sparling. Their work resulted in the derivation of new roll force and torque formulae, which did not include the coefficient of friction itself. Although Ekelund and others have derived relationships between forward slip and the coefficient of friction, these are of little practical use as they often result in unrealistic predictions. The same may be said about the use of traditional roll separating force formulas, like the ones proposed by Sims, Green-Wallace, Bland-Ford, Ford-Alexander, Ekelund, and others, which, for those that contain the coefficient of friction, also often result in values of μ that exceed what is theoretically possible.

9.1 Summary and Conclusions

There is little information available on the effects of the process parameters, much of which dates back 30-50 years. This information was often produced using methods that have limited accuracy. In industry, inaccurate roll forces may be predicted, since the coefficient of friction is not an input in the General Electric control algorithm, which is based on Sims' roll separating force equation and is used in most hot strip mills. Since numbers on μ are missing, it is common to assume that the coefficient of friction is 0.4. Most researchers who have investigated the effect of oxides on the frictional conditions have done so for processes other than hot rolling in attempts to simulate the hot rolling process. Others have investigated metals other than steel. Blazevic investigated the behaviour of the scale layer in terms of surface defects, but not the contributions of the coefficient of friction. No researcher has tried to reproduce the scale thickness in a laboratory that is seen in industrial hot rolling. Researchers that indeed have worked on the effects of scale on friction have not modelled the kinetics of scale formation in terms of scale thickness in order to control their laboratory experiments in an effort to reproduce the actual mill conditions.

As a result, a number of questions that had to be answered arose. These were:

1. *What are the effects of process parameters such as temperature, velocity, and reduction on the frictional conditions in laboratory and industry?*
2. *What are the effects of material parameters such as steel chemical composition and scale thickness on the frictional conditions?*
3. *What is the break in time of freshly ground high-speed steel work rolls?*
4. *Can relationships be found between laboratory and industry results?*

As a consequence, the investigations were divided into four separate parts:

The first part (A) dealt with the material behaviour in terms of scale growth kinetics and modelling of flow stress. The scale growth kinetics experiments enabled modelling of the scale thickness as well as the reproduction of preferred scale thicknesses later in the hot rolling experiments. The modelling of the flow stress ensured that the best possible flow stress description was made when the coefficient of friction in the laboratory hot rolling experiments was calculated.

The second part (B) dealt with laboratory hot rolling experiments which were carried out under controlled conditions in which one parameter at a time was varied. Two grades of steel, one low carbon and one micro-alloyed were rolled, using a Stanat laboratory rolling mill, at different temperatures, velocities, and reductions. The effect of a variation in scale thickness on these conditions was investigated since different scale thicknesses were produced on the samples prior to rolling. The roll separating force, roll torque, and the forward slip were measured along with the roll velocity and surface temperature. These were used as inputs in the analysis of the results, in which a simultaneous match in roll separating force, roll torque, and the forward slip was sought.

Hot rolling data from Dofasco's mill logbooks was analysed in the third part (C) of the investigations. This was carried out in an effort to determine the effect of the various process parameters on the coefficient of friction as well as the break-in time of freshly ground high-speed steel work rolls for conditions in industry. Several different steel grades were analysed. A match in roll separating force was sought.

The laboratory and industry results were compared in the fourth and last part of the investigations (D). The two sets of results were compared in an attempt to ascertain the usefulness of laboratory experiments. Relationships that permit a comparison of the results obtained in the laboratory and in the industry were presented in form of equations

and a map that illustrates that different modes of lubrication do exist in hot rolling. The comparison was made in terms of both traditional and newly derived dimensionless groups.

A. Conclusions regarding the material behaviour

Scale growth kinetics investigations were undertaken in order to enable modelling of scale thickness and reproduction thereof. It was concluded from the scale growth kinetics investigations presented in Chapter 5 that:

1. Scale growth is parabolic with time and exponential with temperature, as monitored in terms of weight increase per unit surface area.
2. There is little difference in scale growth kinetics between low carbon and HSLA steels.
3. The amounts of magnetite and haematite are small for the laboratory conditions described.
4. Purging with oxygen-free nitrogen results in a drastically reduced scale growth, making it a useful tool in controlling scale growth prior to rolling.
5. A simple model based on mass balance may be used to predict the scale thickness.

Hot compression tests were carried out on AISI 1018 and HSLA steels in order to enable modelling of the material flow stress behaviour during laboratory hot rolling. The hot compression tests and the analysis of the results in Chapter 5 lead to the following conclusions:

1. Due to differences in initial microstructure, the two grades of steel display similar flow stress behaviour.
2. Shida's formulae may effectively be used to describe the flow stress behaviour of both grades, in which case a carbon equivalence of 0.3 is used.

B. Conclusions from the laboratory hot rolling analysis

Hot rolling investigations was undertaken in order to determine the effects of some process and materials parameters on frictional conditions during hot rolling of steels. Samples of AISI 1018 and HSLA steels were rolled for different process parameters, and with different interfaces. Chapter 6 concluded that the coefficient of friction is strongly influenced by the rolling temperature, the roll velocity, the roll/metal interface, and to a lesser degree, the reduction:

1. The coefficient of friction increases with decreasing temperature as a result of increased material flow stress and increased adhesive bond strength.
2. An increase in velocity decreases the coefficient of friction as less time is made available to form adhesive bonds between the rolls and the metal/scale. The local increase in flow stress caused by heavier chilling at lower velocities is also likely to contribute to an increase in the coefficient of friction.
3. A greater reduction increases the coefficient of friction slightly since an increase in flow stress is seen due to larger deformation along with a longer arc of contact, resulting in longer times to form adhesive bonds.
4. The scale thickness affects the coefficient of friction the most, along with sample temperature. A thick scale produces a lower coefficient of friction since it provides a certain degree of lubricity. A thin scale is more adherent to the metal substrate and is therefore harder to remove or break up.
5. An HSLA grade produces a higher coefficient of friction than a low carbon grade. This is attributed to differences in physical metallurgy and a variance in how the scale layers on the two steels break up.
6. The model proposed by Roberts indicates that the coefficient of friction increases with decreasing scale thickness and increasing temperature. The effect of scale thickness can be corroborated. However, the effect of temperature on the frictional conditions is the opposite since it increases with decreasing temperature.

C. Conclusions from the analysis of industry mill logbooks

Mill logbook data obtained from Dofasco was analysed in Chapter 7. It was shown that the finite-element code can be used successfully to analyse mill logbooks. It was concluded that the coefficient of friction in full scale hot rolling is strongly influenced by the rolling temperature, the roll velocity, the roll/metal interface, and to a certain degree, the reduction:

1. Freshly ground HSS work rolls produce a low coefficient of friction. As a thin chromium oxide layer develops on the surface, the coefficient of friction increases, reaches a plateau, and then drops to a steady-state value, provided the process and material parameters remain the same. This steady-state value is reached after a contact time of 200 s.
2. The coefficient of friction is dependent on temperature, steel chemical composition, relative velocity, and flow stress. It increases with decreasing temperature, increasing amount of alloying elements, increasing relative velocity, as well as increasing material flow stress.
3. Generally, the coefficient of friction is low in the first stands. It then increases stand by stand, and results in sticking friction in F7.
4. The predominant wear mechanism in the first 4 stands is thermal fatigue, whereas abrasive wear is more severe in the last 3 stands of a 7 stand finishing train.
5. The introduction of a dimensionless parameter, λ , successfully describes the general frictional conditions throughout the finishing train.

D. Conclusions on the comparison between laboratory and industry analyses

It was shown in Chapter 8 that laboratory experiments can successfully be compared to the conditions of hot rolling in industry. Furthermore, the λ - parameter successfully describes the frictional conditions, both in the laboratory and in industry. The following conclusions was, as a result, drawn from the comparison:

1. Laboratory hot rolling experiments may be compared to data from industry by correcting for the most obvious difference in geometry - the roll radius.
2. The tribology of hot rolling can be considered in terms of regions of different modes of lubrication. These are boundary, mixed, and hydrodynamic lubrication. Previously, this theory has been limited to the tribology of cold rolling.
3. Although the temperature has an effect, two parameters, the scale thickness and the relative velocity, appear to control the mode of lubrication.
4. The quasi-hydrodynamic region can be described by a linear relationship between the coefficient of friction and the λ - parameter.
5. A λ - parameter of 10 marks the transition from the quasi-hydrodynamic to the mixed lubrication region.
6. The mixed lubrication region is best described in terms of a power law, whereas the boundary region, if present, is characterised by the approach of the coefficient of friction to 0.5 as the λ - parameter approaches zero.

9.2 Recommendations for Future Work

As this work has shown, tribology in hot rolling is multidisciplinary and spans over several traditional fields of engineering, ranging from heat transfer to metallurgy. Its implications concerning common hot rolling problems such as roll wear and surface issues are significant. Much work must be completed until the frictional behaviour in hot rolling is fully understood. In this author's opinion, future fields of interests in the topic of hot rolling tribology should include the following.

Other steels and metals

The current work was restricted to low-carbon and micro-alloyed steels. The frictional conditions associated with hot rolling of other grades such as stainless, extra low carbon (ELC), and interstitial free (IF) steels, etc. have yet to be explored. These are likely to differ in frictional behaviour in comparison to the investigated steels. Recently, there have been indications from the industry that, in rolling of ELC steels, the coefficient of friction is extremely high, almost causing the strip to wrap around the rolls. It is also of interest to investigate other metals, like aluminium, in a similar manner.

Additional process parameters

Due to the limitations in equipment, temperatures below 825°C were left out of the experimental matrix. Today some hot strip mills roll in the intercritical austenite-ferrite two-phase region. In the pursuit of desired mechanical properties, warm rolling in the upper ferrite region is also getting more common. Some trends found in the literature indicate that the coefficient of friction decreases with decreasing temperature below 800°C. This needs to be addressed since an increased understanding would be beneficial in predicting roll separating forces, as well as wear behaviour.

Break-up behaviour of the scale layer

Scale was shown to have a great effect on the overall frictional conditions. Moreover, the effect of scaling on the surface quality was not investigated in this work. It is well known that the role of the scale breakers prior to the finishing train is important. Its effectiveness and its placement affect the surface quality of the final product. It is therefore important to study how the scale behaves in the roll gap, how it adheres to the strip, and how it breaks up.

Several questions might be answered when some of these events are studied in detail: Firstly, how does the scale act under deformation in terms of flow behaviour and what are the effects of the various material process parameters thereon? Secondly, what is the effect of the initial scale thickness on the final surface quality? This question applies to the optimum placement of the scale breakers, which is an important consideration in the design of new mills and in the modernisation of older mills. Consequently, the relationship between the adherence of the scale and its thickness should be studied.

Friction in rolling of long products

Although smaller in volume than flat products, rolling of long products is an important bulk deformation process. This, in combination with the elevated complexity of analysing the process, has left much work undone. Increased understanding of the frictional conditions in rolling of long products would potentially increase work roll life, which, in turn, would decrease the shape problems associated with uneven wear of the rolls due to the non-uniform pressure distribution, as well as result in considerable financial savings.

Rolling with emulsions

Hot rolling emulsions have been used in hot rolling for a long time. However, the use of the recently introduced HSS rolls has indicated that traditional hot rolling emulsions are of little benefit, at least as far as power consumption is concerned. The work presented here showed that the different modes of lubrication common in cold rolling were also found in hot rolling. The use of functioning lubricating emulsions will shift the transition point from one region to another, thereby reducing the friction and wear resulting in lower force requirements and power consumption. Moreover, functioning emulsions may also help to insulate the work rolls from the hot strip, thereby reducing the thermal fatigue problem in the early stands. The implications are multifaceted, as roll life, profile, gauge consistency, and power consumption will all be improved provided suitable rolling emulsions are developed and applied in the best possible way.

References

- Archard, J.F. (1953). *Contact and Rubbing of Flat Surfaces*. J. Appl. Phys., Vol. 24, pp981-988
- Arnaud, J.C. (1996). *Trials of High Speed Steel Rolls in Sollac Hot Strip Mills*. 37th MWSP Conf. Proc., ISS Vol. XXXIII, pp261-265
- Askeland, D.R. (1996). *The Science and Engineering of Materials*. 3rd SI Edition, Chapman and Hall, London
- Ball, J., Treverton, J.A., and Thornton, M.C., (1993). *Evaluation of the Effects of Stresses in Hot Rolling Mills on Oxide Films on Aluminum*. Lubr. Eng., Vol. 50, pp89-93
- Barzan, D.R. (1996). *The Use and Performance of HSS Rolls at Inland's 50" Hot Strip Mill*. 37th MWSP Conf. Proc., ISS Vol. XXXIII, pp271-273
- Bay, N. and Wanheim, T. (1976). *Real Area of Contact and Friction Stress at High Pressure Sliding Contact*. Wear, Vol 38, pp201-209
- Birks, N. and Meier, G.H. (1983). *Introduction to High Temperature Oxidation of Metals*. Edward Arnold, London
- Bland, D.R. and Ford, H. (1948). *The Calculation of Roll Force and Torque in Cold Strip Rolling with Tensions*. Proc. Inst. Mech. Eng., Vol. 159, pp144-153
- Blau, P.J. (1989). *Friction and Wear Transitions of Materials*. Noyes Publishers, Park Ridge, New Jersey
- Blazevic, D.T. (1983a). *Rolled in Scale: the Continual Problem, Part I - Scale Formation and Rolling Characteristics*. Hot Rolling Consultants, Homewood, Ill, Feb
- Blazevic, D.T. (1983b). *Rolled in Scale: the Continual Problem, Part II - Rolled in Scale Descriptions, Causes, and Cures*. Hot Rolling Consultants, Homewood, Ill, Feb
- Blazevic, D.T. (1985). *Rolled in Scale: the Continual Problem, Part IV - Red Oxide Scale*. Hot Rolling Consultants, Olympia Fields, Ill, July
- Blazevic, D.T. (1996). *Tertiary Rolled in Scale - the Hot Strip Mill Problem of the 1990's*. 37th MWSP Conf Proc, ISS-AIME, Vol. XXXIII, pp33-38

- Caillaud, J.C. and Delaitre, L. (1994). *Metallurgy of HSS Roll Materials*. 35th MWSP Conf. Proc., ISS-AIME, Vol. XXXI, pp27-31
- Callister, W.D. (1996). *Materials Science and Engineering - An Introduction*. John Wiley and Sons, New York, New York
- Chen, B.K., Thomson, D.F., Choi, S.K. (1992). *Temperature Distribution in the Roll Gap During Hot Flat Rolling*. J. Mater. Process. Technol., Vol. 30, pp115-130
- Chen, W.C., Samarasekera, I.V., and Hawbolt, E.B. (1993). *Fundamental Phenomena Governing Heat Transfer During Rolling*. Met. Trans. A, Vol. 24A, pp1307-1320
- Collins, D.B. (1994). *Factors Affecting the use of HSS Rolls in the Hot Strip Mill*. 35th MWSP Conf. Proc., ISS-AIME, Vol. XXXI, pp33-36
- Ekelund, S. (1927). *Några Dynamiska Förhållanden vid Valsning (Some Dynamic Relationships in Rolling)*. Jernkont. Ann., Vol. 111, pp39-97
- el-Kalay, A.K.E.H.A. and Sparling, L.G.M. (1968). *Factors Affecting Friction and Their Effect upon Load, Torque, and Spread in Hot Flat Rolling*. J. Iron Steel Inst., Vol. 43, pp152-168
- Farkas, K. and Lenard, J.G. (1994). *New Method of Deriving Formulae for Modelling Metal Rolling Processes*. GÉP, Vol. XLVI, pp30-33
- Fukagawa, T., Okada, H. Maehara, Y. (1994). *Mechanism of Red Scale Defect Formation in Si - Added Hot-Rolled Steel Sheets*. Trans. ISIJ, 34, pp906-911
- Funke, P., Holland, J., and Kulbrok, R. (1978). *Einfluss unterschiedlicher Warmwalzbedingungen beim Bandwalzen auf die Walzoberfläche und deren Auswirkung auf das Walzgut*. Stahl u. Eisen, Vol. 98, pp403-409
- Ginzburg, V.B. (1989). *Steel Rolling Technology*. Marcel Dekker Inc., New York, New York
- Goto, K., Matsuda, Y., Sakamoto, K., and Sagimoto, Y. (1992). *Basic Characteristics and Microstructure of High-Carbon High Speed Steel Rolls for Hot Rolling Mills*. Trans. ISIJ, Vol. 32, 1992, pp1184-1189
- Hashimoto, M., Otomo, S., Yoshida, K., Kimura, K., Kurahashi, R., Kawakami, T., and Kouga, T. (1992). *Development of High Performance Roll by Continuous Pouring Process for Cladding*. Trans. ISIJ, Vol. 32, pp1202-1210

- Hashimoto, M., Kawakami, T., and Kurahashi, R. (1994). *Characteristics and Application of High-Speed Tool Steel (HSS) Rolls in Hot Strip Rolling*. 35th MWSP Conf. Proc., ISS-AIME, Vol. XXXI, pp55-64
- Hashimoto, M., Takigawa, H., and Kawakami, T. (1996). *Development and Application of High-Speed Tool Steel (HSS) Rolls in Hot Strip Rolling*. 37th MWSP Conf. Proc., ISS Vol. XXXIII, pp275-282
- Hill, W. and Kerr, E. (1996). *Tool Steel Work Roll Maintenance at Dofasco*. 37th MWSP Conf. Proc., ISS Vol. XXXIII, pp283-286
- Hirano, F. and Ura, A. (1970). *Effect of Difference in Hardness of Rubbing Surfaces on Abrasive Wear*. Faculty of Engineering, Kyushu University, Fakoda, Japan, pp164-216
- Hollander, F. (1970). *A Model to Calculate the Complete Temperature Distribution in Steel during Hot Rolling*, in Mathematical Models in Metallurgical Process Development. The Iron and Steel Institute, London, Publication No. 123, p46-78
- Innse Cilindri Catalogue (1995). Technical Specifications: Rolls for Flat Products (Hot and Cold Rolling). Brescia, Italy
- Jarl, M. (1990). *Friktion vid valsning - en litteraturstudie (Friction in rolling - literature survey)*. BTF 89050, Metalworking Research Plant, Luleå (1989), revised (1990), Internal Research Plant Report
- Jarl, M. (1988). *Friction and Forward Slip in Hot Rolling*. Scand. J. Metallurgy, Vol. 17., pp2-7
- Kato, K. (1997). *Abrasive Wear of Metals*. Tribology International, Vol. 30, pp333-338
- Kiessling, R. and Lange, N. (1964). *Non-metallic inclusions in steel - part 1*. The Iron and Steel Institute, Special Report 90, Stockholm
- Kortzfleisch, B., Pawelski, O., and Krause, U. (1967). *Untersuchung des Temperatureinflusses auf das Greifen und Durchziehen beim Warmwalzen*. Stahl u. Eisen, Vol. 87, pp588-597
- Kudo, T., Kawashima, S., and Kurahashi, R. (1992). *Development of Monobloc Type High-Carbon High-Alloyed Rolls for Hot Rolling Mills*. Trans. ISIJ, Vol. 32, pp1190-1193
- Kurahashi, R., Waseda, T., Nashiyama, Y., Kouga, T., and Hashimoto, M. (1991). *Basic Design of Hot Strip Mill with Extremely small Work Roll and Its Application to Production Mill*. J. JSTP, Vol. 32, pp1238-1243

- Kurahashi, R., Kawakami, T., Suruwatari, Y., and Hashimoto, M. (1992). *The Application of High Speed Steel Rolls in Hot Rolling Strip Mill at NSC Hirohata Works*. ISI Committee on Technology, 24th Regular Meeting, Madrid, pp31-47
- Laasraoui, A., and Jonas, J.J. (1991). *Prediction of Steel Flow Stresses at High Temperatures and Strain Rates*. Met. Trans. A., Vol. 22A, pp1545-1558
- Lait, J. (1997). *Private Communication*
- Lenard, J.G. and Pietrzyk, M. (1990). *The Effect of Temperature Rise of the Roll on the Simulation of the Flat Rolling Process*. J. Mat. Process. Technol., Vol. 22, pp177-190
- Lenard, J.G., Malinowski, Z., and Pietrzyk, M. (1992). *Comparison of the Predictive Capabilities of Mathematical Models of the Flat Rolling Process*. J. Mater. Process. Technol., Vol. 34, pp85-92
- Li, Y.H., and Sellars, C.M. (1996). *Evaluation of Interfacial Heat Transfer and Friction Conditions and Their Effects on Hot Forming Processes*. 37th MWSP Conf Proc, ISS-AIME, Vol. XXXIII
- Loung, L.H.S., and Heijkoop, T. (1981). *The Influence of Scale on Friction in Hot Metalworking*. Wear, Vol. 71, pp93-102
- Lundberg, S.-E. and Waldén, B. (1992). *Evaluation of Friction under Hot Working Conditions in a High Temperature Test Rig*. Steel Res., Vol. 63, pp304-308
- Lundberg, S.-E. (1993). *A New High Temperature Test Rig for Optimization of Materials for Hot Rolling Rolls*. J. Mater. Process. Technol., Vol. 36, pp273-301
- Lundberg, S.-E. and Gustafsson, T. (1994). *The Influence of Rolling Temperature on Roll Wear, Investigated in a New High Temperature Test Rig*. J. Mater. Process. Technol., Vol. 42, pp239-291
- Majta, J., Lenard, J.G., and Pietrzyk, M. (1996). *Modelling the Evolution of the Microstructure of a Nb Steel*. Trans. ISIJ, Vol. 36, pp1094-1102
- Matsuno, F. (1980). *Blistering and Hydraulic Removal of Scale Films of Rimmed Steel at High Temperature*. Trans. ISIJ, Vol. 20, pp413-421
- Mielnik, E.M. (1991). *Metalworking Science and Engineering*. McGraw Hill, New York, New York
- Migaud, B. (1979). *Simulation by Hot Torsion Testing of Hot Strip Mill Rolling for Low-Carbon and Nb-Microalloyed Steels*. Proc. Int. Conf. on Hot Working and Forming Processes, Sheffield, pp67-76

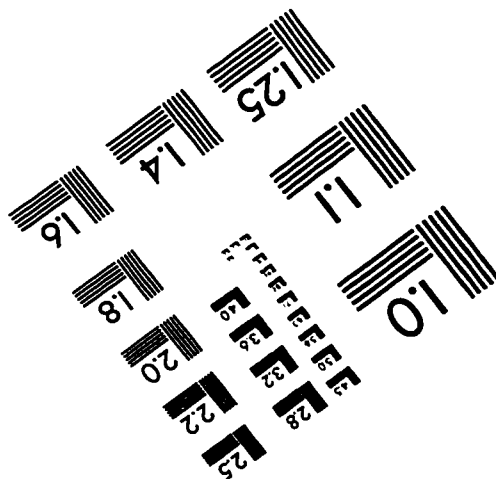
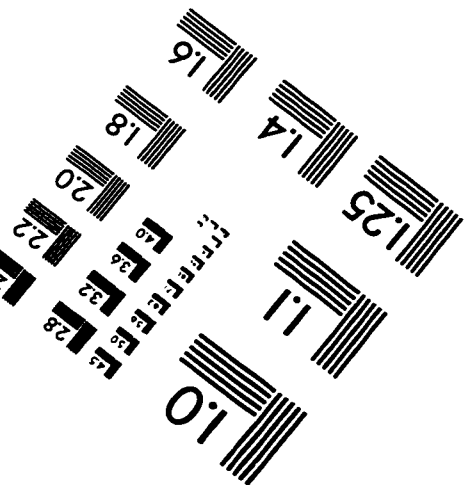
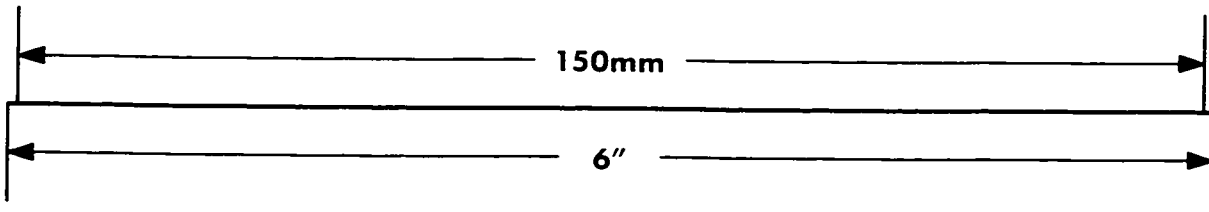
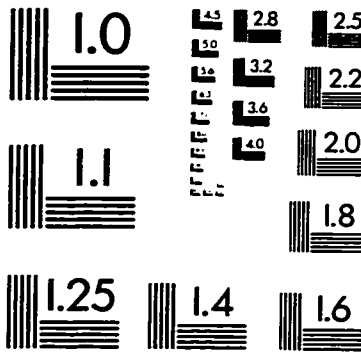
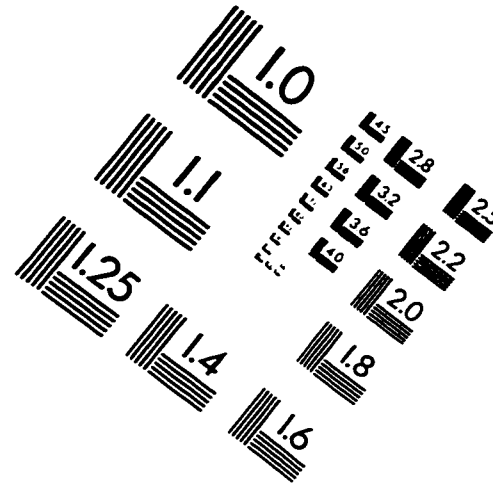
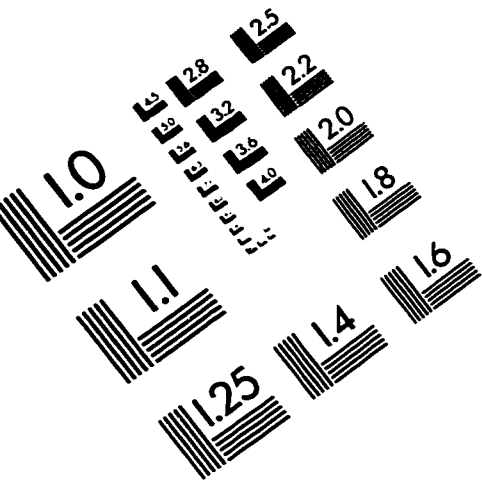
- Munther, P.A. and Lenard, J.G. (1995a). *The Hot Strip Mill as a Metalforming System - the Metal, the Mill, and the Interface*. 36th MWSP Conf. Proc., ISS Vol. XXXII, pp357-365
- Munther, P.A. and Lenard, J.G. (1995b). *Tribology during Hot Flat Rolling of Steels*. Annals of the CIRP, Vol. 44, pp213-216
- Munther, P.A., Webber, R., Lenard, J.G. (1996). *Evaluation of the Coefficient of Friction for HSS Rolls from Hot Strip Mill Logbook Data*. 37th MWSP Conf. Proc., ISS Vol. XXXIII, pp39-45
- Murata, K., Morise, H., Mitsutsuka, M., Naito, H., Kumatsu, T., and Shida, S. (1984). *Heat Transfer Between Metals in Contact and its Application to Protection of Rolls*. Trans. ISIJ, Vol. 24, B-309
- Pietrzyk, M. and Lenard, J.G. (1988). *Experimental Substantiation of Modelling Heat Transfer in Hot Flat Rolling*. Proc. Nat. Heat Transfer Conf., Houston, pp47-52.
- Pietrzyk, M. and Lenard, J.G. (1990). *A Study of Heat Transfer During Flat Rolling*. special issue of JNME, Vol. 30, pp1459-1469
- Pietrzyk, M. and Lenard, J.G. (1991). *Thermal-Mechanical Modelling of the Flat Rolling Process*. Springer-Verlag, Berlin
- Pietrzyk, M. and Lenard, J.G. (1992). *Experimental Substantiation of a Finite Element Model of the Evolution of Structure in Hot Forming Processes*. 33rd MWSP Conf. Proc., ISS-AIME, Vol. XXIX, pp423-426
- Pietrzyk, M., Kusiak, J., and Cierniak, M. (1992). *Computer Program for the Thermal-Mechanical Finite Element Simulation of the Flat Rolling Process*. Elroll Software Manual, Krakow, 1992
- Price, R., Gisborne, H.T., Hanlon, D.N., Rainforth, W.M., and Sellars, C.M. (1996). *Enhanced Roll Materials for Forged Steel Work Rolls*. 37th MWSP Conf. Proc., ISS Vol. XXXIII, pp213-219
- Rabinowicz, E. (1965). *Friction and Wear of Materials*. John Wiley & Sons Inc., New York, New York
- Richardson, G.J, Hawkins, D.N., and Sellars, C.M. (1985). *Worked Examples in Metalworking*. The Institute of Metals, London
- Roberts, G.A. and Cary, R.A. (1980). *Tool Steels, 4th Edition*. ASM, Metals Park, Ohio

- Roberts, W.L. (1977). *Tribological Considerations in Hot Rolling of Low-Carbon Steels*. Lubrication Engineering, Vol. 33, pp575-580
- Roberts, W.L. (1983). *Hot Rolling of Steel*. Marcel Dekker Inc., New York, New York
- Robertson, J. and Manning M.I. (1988). *Criteria for Formation of Single Layer, Duplex, and Breakaway Scales on Steels*. Mat. Sci. Technol., Vol. 4, pp 1064-1071
- Sachs, K and Tuck, C.W. (1968). *Surface Oxidation of Steel in Industrial Furnaces, in Reheating for Hot Working*. The Iron and Steel Institute, London, Publication No. 111, pp1-17
- Samsonov, G.V. (1973). *The Oxide Handbook*. IFI/Plenum, New York, 1973
- Sander, Å. (1995). *Progress in Hot Rolled Flat Product Technology for Demanding Customers*. Iron & Steelmaker, Vol. 22, 2, pp21-23
- Sano, Y., Hattori, T., Haga, M. (1992). *Characteristics of High-Carbon High Speed Steel rolls for Hot Strip Mill*. Trans. ISIJ, Vol. 32, pp1194-1201
- Savage, G., Boelen, R., Horti, A., Morikawa, H., and Tsujimoto, Y. (1996). *Hot Wear Testing of Roll Alloys*. 37th MWSP Conf Proc, ISS-AIME, Vol. XXXIII
- Schey, J. (1983). *Tribology in Metalworking*. ASM, Metals Park, Ohio
- Schunke, J.N., Sudarshan, T.S., and Srivatsan, T.S. (1988). *Effects of Oxygen in Influencing Friction Characteristics of Metals*. Wear. Vol. 128, pp211-221
- Schurmann, E., Beck, H., and Brand, W.D. (1973). *On the Scaling of Unalloyed Steels*. Arch. Eisenhüttenwes., Vol. 44, pp927-934
- Shaesby, J.S., Boggs, W.E., and Turkdogan, E.T. (1984). *Scale Growth on Steels at 1200°C: Rationale of Rate and Morphology*. Met. Sci., Vol. 18, 1984, pp127-136
- Shaw, L., Miracle, D., and Abbaschian, R. (1995). *Microstructure and Mechanical Properties of Metal/Oxide and Metal/Silicide Interfaces*. Acta Metall. Mater., Vol. 43, pp4267-4279
- Shida, S. (1974a). *Effect of Carbon Content, Temperature, and Strain Rate on Compressive Flow Stress of Carbon Steels (Resistance to Deformation of Carbon Steels at Elevated Temperatures, 1st Report)*. Hitachi Research Report, Hitachi Metals Ltd., pp1-4

- Shida, S. (1974b). *Empirical Formula of Flow Stress of Carbon Steels (Resistance to Deformation of Carbon Steels at Elevated Temperatures, 2nd Report)*. Hitachi Research Report, Hitachi Metals Ltd., pp1-7
- Sims, R.B. (1954). *The Calculation of Roll Force and Torque in Hot Rolling Mills*. Proc. Inst. Mech. Eng., Vol. 168, pp191-200
- Smith, W.F. (1990). *Principles of Materials Science and Engineering*. 2nd Edition, McGraw-Hill, New York, New York
- Sørensen, O.T. (1981). *Nonstoichiometric Oxides*. Academic Press, New York, New York
- Sparling, L.G.M. (1977). *Load and Torque Determination for Hot Flat Rolling with Variable Frictional Conditions*. Met. Tech., Vol. 11, 301-306
- Stevens, P.G., Iven, K.P., and Harper, P. (1971). *Increased Work-roll Life by Improved Roll-cooling Practice*. J. Iron Steel Inst., Vol. 209, pp1-11
- Tafel, W., and Schneider, E. (1924). *Das Greifen von Walzen bei Veränderlicher Walzgeschwindigkeit*. Stahl u. Eisen, Vol 44, pp305-309
- Tamura, I., Sekine, H., Tanaka, T., and Ouchi, C. (1988). *Thermomechanical Processing of High-Strength Low-Alloy Steels*. Butterworths, London, 1988
- Tiley, J. (1997). *Private Communication*
- Torres, M. and Colas, R. (1994a). *Modelling Heat Conduction through an Oxide Layer During Hot Rolling of Steel*. Manuf. Sci. Eng., Vol. 2, pp577-582
- Torres, M. and Colas, R. (1994b). *Modelling the Behaviour of the Oxide Layer During Hot Rolling of Steel*. 7th Intl. Symp. on Transport Phenomena in Manufacturing Processes, Pacific Center of Thermal-Fluids Engineering, pp122-125
- Troeder, C., Spielvogel, A., and Xu, J.-W. (1985). *Temperature and Thermal Stresses in Work Rolls During the Hot Rolling of Strips*. Steel Res., Vol. 56, pp379-384
- Tselikov, A.I., Nikitin, G.S., Rokotyan, S.E. (1981). *The Theory of Lengthwise Rolling*. MIR Publishers, Moscow
- Underwood, L.R. (1950). *The Rolling of Metals, Vol. 1*. John Wiley & Sons Inc., New York, New York

- Wallquist, G. (1955). *Investigations of the Influence of Different Factors on Roll Pressure, Energy Consumption, Spread, and Forward Slip in Hot Rolling*. Jernkont. Ann., Vol. 139, pp923-1030
- Wallquist, G. (1960). *Investigations of the Influence of Different Factors on Roll Pressure, Energy Consumption, Spread, and Forward Slip in Hot Rolling: Part II*. Jernkont. Ann., Vol. 144, pp193-257
- Wallquist, G. (1962). *Investigations of the Influence of Different Factors on Roll Pressure, Energy Consumption, Spread, and Forward Slip in Hot Rolling: Part III*. Jernkont. Ann., Vol. 146, pp681-716
- Wanheim, T. and Bay, N. (1978). *A Model for Friction in Metal Forming Processes*. Annals of the CIRP Vol. 27, pp189-194
- Wankhede, U. and Samarasekera, I.V. (1997). *Thermal Behavior of High Speed Steel Work Rolls in the Finishing Train of a Hot Strip Mill*. Iron and Steelmaker, Vol. 24, 5, pp55-60
- Webber, R. (1994). *Private Communication*
- Webber, R. (1996). *The Performance of High Speed Steel Rolls At Dofasco*. 37th MWSP Conf. Proc., ISS Vol. XXXIII, pp267-269
- Webber, R. (1997). *Private Communication*
- Werquin, J.C. and Bocquet, J. (1994). *The New Generation of Spun Cast High Speed Steels for Hot Strip Mills*. 34th MWSP Conf. Proc., ISS-AIME, Vol. XXXI, pp135-151
- Williams, R.V. and Boxall, G. (1965) *Roll Surface Deterioration in Hot Strip Mills*. J. Iron Steel Inst., Vol. 203, pp369-377
- Wood, W.E. (1971). *Fundamental Factors Determining the Mode of Scaling of Heat Resistant Alloys*. Werkst. u. Korros., Vol. 22, pp491-503
- Wusatowski, Z. (1969). *Fundamentals of Rolling*. Pergamon Press, Oxford
- Yurioka, N., Okumura, M., Kasuya, T., and Cotton, H.J.U. (1987). *Met. Constr.*, Vol. 19, p217R
- Zum Gahr, K.-H. (1987). *Microstructure and Wear of Metals*. Elsevier, Amsterdam

IMAGE EVALUATION TEST TARGET (QA-3)



APPLIED IMAGE, Inc
 1653 East Main Street
 Rochester, NY 14609 USA
 Phone: 716/482-0300
 Fax: 716/288-5989

© 1993, Applied Image, Inc., All Rights Reserved